EVALUATION OF THE MD SHEAR TEST METHOD AS A CRITERION FOR PREDICTING BOX COMPRESSIVE STRENGTH

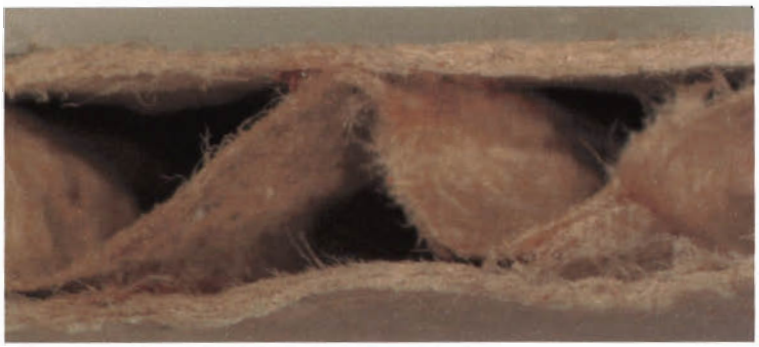

By

John David Jones

A thesis submitted to the faculty of Engineering and the Built Environment of the University of Cape Town in fulfilment of the requirements for the degree of MSc(Eng) in Materials Engineering

Centre for Materials Engineering

Department of Mechanical Engineering

University of Cape Town

September 2004

I would like to thank my father, mother and sister for their help and encouragement throughout this thesis. Without them, it would not have been completed.

I would like to express my appreciation to the following:

- **My supervisor, Dr. K Marcus, for his enthusiasm and encouragement throughout this project.**
- **Jacques Haarhoff for his continued help and support.**
- **Nampak Corrugated for sponsoring this thesis.**
- **The staff at Nampak R&D for putting up with me.**
- **Glen Newins and the workshop staff for manufacturing my fixtures.**
- **Sam Ginsberg for his electronics wizardry.**
- **Norma Africa for putting up with my constant nagging and fulfilling my financial needs.**
- **The NRF for their financial assistance.**
- **The students and staff at the Centre for Materials Engineering for their continued encouragement.**

"I am the vine, you are the branches. If a man remains in me and I in him, he will bear much fruit. Apart from Me you can do nothing."

John 15:5

ABSTRACT

Corrugated board is a composite sandwich type material used in the packaging industry worldwide. In the design of corrugated boxes, the stacking strength is an important design parameter. Current research shows that box failure is influenced by the flexural rigidities of the panel and its transverse shear rigidities. McKinlay proposed a new method to measure the MD transverse shear stiffness of corrugated board. This research was aimed at designing a fixture to perform the MD shear test and to evaluate its performance. In addition, the properties that influence box strength were to be investigated. These properties were then to be used in improved box strength predictions.

It was found that the designed MD shear fixture was able to measure the transverse shear stiffness of corrugated board in the MD direction with a high degree of accuracy and reproducibility. This method was much easier to perform than the standard block shear test method and also much quicker. This was a very important factor considering the application of this testing method in a research and development environment. In addition, the stiffness test exhibited good possibilities for use as a quality control tool.

Extensive testing showed that the material used in the manufacture of corrugated board had a strong influence on board and box strength. In addition, it was found that the separation of the faces in a corrugated board structure had an influence on the strength and stability of the box. Factors such as the manufacturing process and board structure were also found to have an effect on box strength.

Box strength predictions were performed using the methods available in the literature. These predictions had good correlation with the experimental box compression values. It was shown that box strength can be accurately predicted from liner and fluting properties and this capability is an important tool in box strength design.

RSC box	***Regular slotted container box***
Liner	***Sheet of paper glued to the fluting***
Fluting	***Sheet of paper formed into a waved shape, also known as the medium, separates the two liners in a corrugated board structure***
Pulping	***The process by which wood is reduced to pulp through the use of chemicals***
Kraft	***Term referring to paper made from 75% virgin fibre using a sulphate process***
MD	***Machine direction***
CD	***Cross-machine direction***
ZD	***Z direction***
Single-wall board	***Corrugated board consisting of one liner glued to the fluting***
Double-wall board	***Corrugated board consisting of two liners separated by the fluting***
Triple-wall board	***Corrugated board consisting of three liners and two corrugated mediums of different height and pitches***
Flute height	***Height of fluted paper***
Flute pitch	***Distance between two troughs in the wave shape of the corrugated medium***
Flute A,B,C,E	***Referring to flutes of different heights and pitches***
Corrugator	***Set of machines in-line used to produce corrugated board***
Single-facer	***Part of the Corrugator that produces single faced board***
Double-backer	***Part of the Corrugator that produces double-wall board***
Curl	***When board deforms in a buckling type shape due to the manufacturing process***
RH	***Relative humidity***
Anisotropic material	***A term relating to a material with properties that are inhomogeneous i.e. different in all directions***
Slenderness ratio	***Ratio of panel width over thickness***
Orthotropic	***Material with elastic properties different in three perpendicular planes***
Homogeneous	***Of the same composition throughout***
E_{11}, E_{22}, E_{33}	***Elastic modulus in MD, CD, ZD respectively***
$\nu_{12}, \nu_{13}, \nu_{23}$	***Poisson's ratio in 1-2, 1-3 and 2-3 planes respectively***
G_{12}, G_{13}, G_{23}	***Shear moduli in 1-2, 1-3 and 2-3 planes respectively***
D_{11}, D_{22}, D_{12}	***Bending stiffness in MD, CD and 1-2 plane***
D_{66}	***Bend-twist couple***
A_y, c_2	***Slope of stress strain curve***
Poisson's Ratio	***Ratio of transverse strain to longitudinal strain***

Plane stress	***Based on the assumption of an infinitely thin object resulting in the stress components σ_x, σ_y and τ_{xy} being zero***
Composite sandwich	***Composite material consisting of two skins separated by a lightweight core***
τ_{i3}	***Shear stress***
γ_{i3}	***Shear strain***
Δ	***Slope of load displacement curve***
W	***Width***
L	***Length***
K	$\frac{4a^3}{3L}$
a	$\frac{W}{2}$
M	***Applied moment***
S	***MD shear stiffness***
ϑ	***Angle of rotation***
D	***Bending stiffness***
I	***Second moment of inertia***
I_l	***Second moment of inertia of the liner***
Caliper	***Thickness***
C	***Core caliper***
T_l	***Liner caliper***
e	***Distance between centre lines of liner***
A	***Area of the face***
J	***Distance from the neutral axis of the corrugated board to the neutral axis of the face***
I_f	***Inertia of the flute***
T_b	***Board caliper***
R	***Tip radius***
TF	***Take-up factor***
P	***Flute pitch***

H	*Flute height*
Θ	*Angle of wrap*
B	$\frac{\theta}{2}$
E_l	*Modulus of the liner*
E_f	*Modulus of the flute*
ECT	*Edge compression test*
ECS	*Edge compression strength*
BCS	*Box compression strength*
FEFCO	*European Federation of Corrugated Board Manufacturers*
SCT	*Short span compression Test*
BCT	*Box compression test*
N_{cr}	*Critical buckling load per unit width*
P_{col}	*Collapse load of plate*
P_{cr}	*Critical buckling load*
Z	*Box perimeter*
E	*Box depth*
P_m	*Edgewise compression load*
a,b,c	*Constants*
k_{cr}	*Buckling coefficient*
n	*Number of half-waves in buckled panel in direction of applied load*
K	*Plate parameter*
d	*Panel depth*
α	*Empirical parameter*
α,η	*Postbuckling constants*
S	*Normalised plate stiffness*
l	*Flute wavelength*
λ	*Half buckling wavelength*
μ	*Indication of nodal lines*
ζ	*Shear Load*
χ	*CD load*
α	*MD load*
POT	*Potentiometer*
LVDT	*Linear variable displacement transducer*

R	***Edgewise crush resistance in kN/m***
F_{max}	***Maximum applied load in newtons***
X	***Applied 3-point bend load***
Δ	***Centre span deflection during 3-point bend***
o	***Displacement of one plate relative to the other***
SD	***Standard deviation***

TABLE OF CONTENTS

CHAPTER 1

INTRODUCTION

1.1 The Packaging Industry in South Africa

The term packaging refers to any material that is used for the containment of another product. In our everyday life we interact with packaging on a regular basis. In many situations the packaging of a consumable good can influence the consumer to acquire goods that he or she had not originally planned to. The relationship between the packaging and consumer, and the packaging and the product can be summed up in the following statement:

"The packaging must protect what it sells and sell what it protects" [1].

The family of packaging materials can be divided into six main groups, namely: wood, polymeric, glass, metal, paper and composite materials [**1**]. In 2003 South Africa was ranked fifth in the world by the World Packaging Organisation (WPO) in terms of packaging standards and quality of packaging [**2**]. In 2000 the worldwide packaging industry was valued at US$ 500 billion and of this amount South Africa contributed US$ 2.5 billion i.e. 0.5% of the total packaging industry [**3**]. In 2003 the South African packaging industry was estimated at US$ 2.12 billion (ex factory), which translates to 2.4 million tons of packaging material produced [**2**]. Figure 1.1 shows that the paper industry in 2003 contributed 36.3% of the total packaging material produced in South Africa, which is equivalent to 903 000 tons of paper and paper products valued at US$ 0.77 billion.

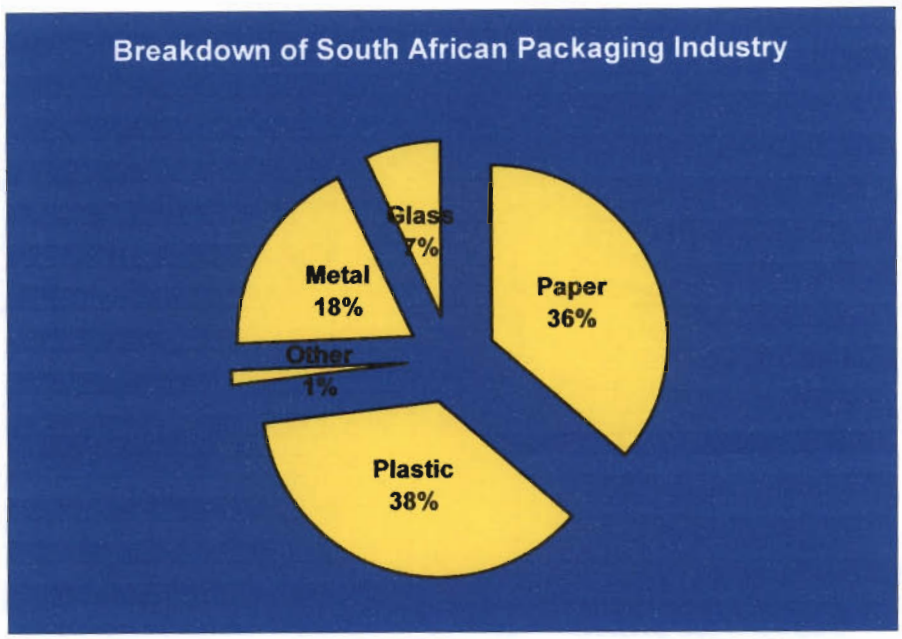

Figure 1.1: A breakdown of the packaging materials produced by the South African packaging industries in 2003 [2].

Figure 1.2 shows that the total amount of material converted into paper and paperboard packaging, in 1984, amounted to 672 000 tons. This figure has grown by 196 000 tons with a total of 868 000 tons being converted in 2000. This is an increase in yearly conversion of 29.2% over a period of 16 years. Even though this is a fairly low increase, considering the time span, it does show that the paper and paperboard packaging industry is growing. In 1998, 24% of the total paper consumed was due to the corrugated board industry. The corrugated board industry was the primary area of growth of the paper packaging industry in 2002. This was primarily due to the favourable export market of wine and fruit. It is forecasted that the continual demand in the export market, particularly the wine export market, will favourably impact on the South African corrugated board industry, resulting in the increased growth of this industry [**2**].

In 1999 the global production of corrugated board was 91 million tons. Figure 1.3 shows that North America, Asia and Europe produce 94% of all the corrugated board in the world. Africa and Oceania produce only 2% of the world's corrugated board [**4**]. Due to the low cost of labour in South Africa and the relatively lower production costs, as compared to other nations, South Africa is in an ideal situation to break into

the overseas packaging market with a competitively priced product that can compete favourably with overseas corrugated packaging in terms of mechanical properties, cost and environmental considerations.

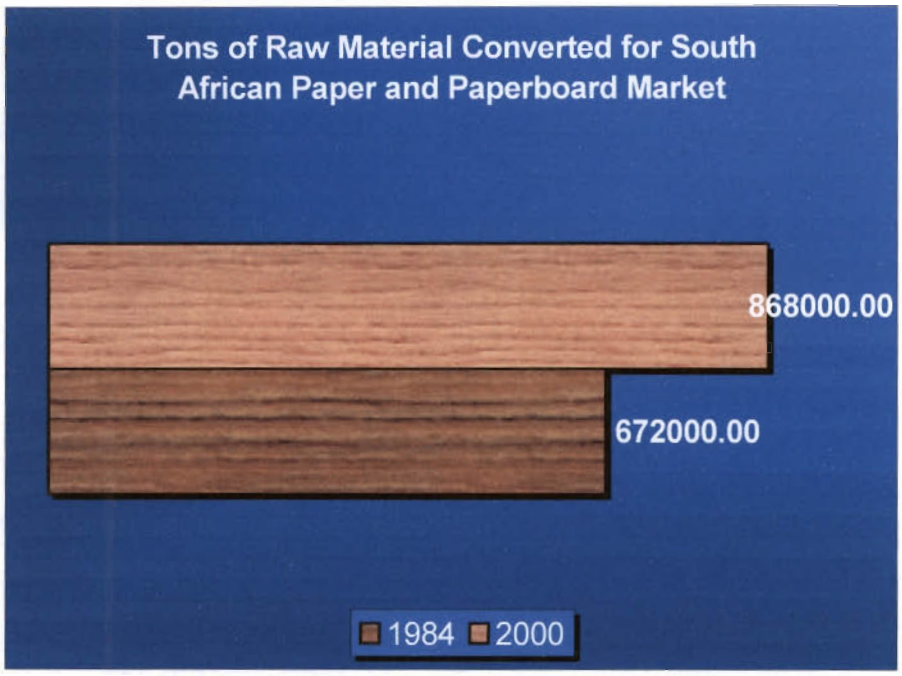

Figure 1.2: A comparison of the total tonnage of material converted into paper and paperboard packaging in 1984 and 2000 [2].

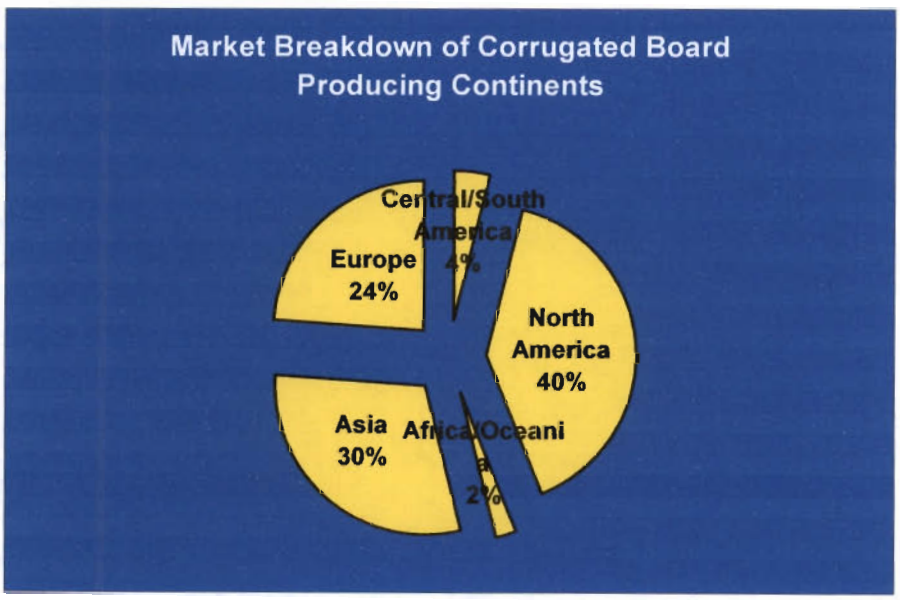

Figure 1.3: The percentage of total corrugated board produced in 1999 [4].

1.2 Project Motivation

Currently there is an increasing focus on recycling and the environmental impact of packaging materials, both nationally and internationally. This is particularly evident in the paper and paperboard industry. Figure 1.4 shows the increase in material recycled from the paper and paperboard industry. The total tonnage of paper and paperboard recycled in 2000 amounted to 770 000 tons. This is an increase of 405 000 tons over 16 years. Today, almost every type of paper produced in South Africa has a recycled content [**2**]. Corrugated board is almost completely recyclable. The fact that recycled board can be used to manufacture more corrugated board means that the amount of corrugated board produced could be doubled without further endangering South Africa's ecology [**4**].

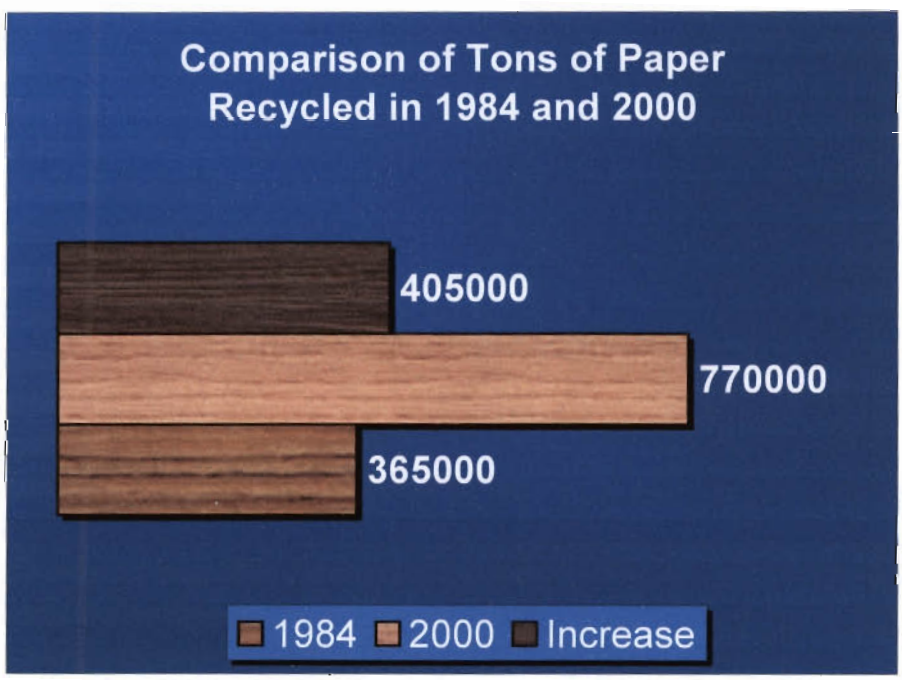

Figure 1.4: A comparison of the paper tonnage recycled in 1984 and 2000 [2].

Due to environmental issues and the competitiveness of the corrugated board industry, the global trend is for corrugated board to be made from recycled material and to have as low a grammage as possible without sacrificing the mechanical properties of the board. Figure 1.5 shows that the grammage of corrugated board manufactured has

decreased since 1992. Since 1997 there has been a 7g/m² decrease in corrugated board grammage, which is significant considering the affect on box weight. The same trend of decreasing corrugated board grammage and thus box weight is also seen in the South African boxboard market. Figure 1.6 shows that the average box weight in 2000 was 530g, while the average box weight in 1975 was 559g which equates into a decrease of 29g over 25 years. In 1999 the average corrugated board grammage in Europe was 551g/m², while in the UK it was 471g/m². In 1999 Europe was producing 22.1 million tons of corrugated board. If Europe had reduced their average board grammage to that of the UK's, they would have reduced their production to 18.9 Million tons which is effectively a 14% reduction in material used [**4**]. The only way that this could have been achieved would be through developing tools, not based on empirical relationships, to evaluate and optimise their packaging.

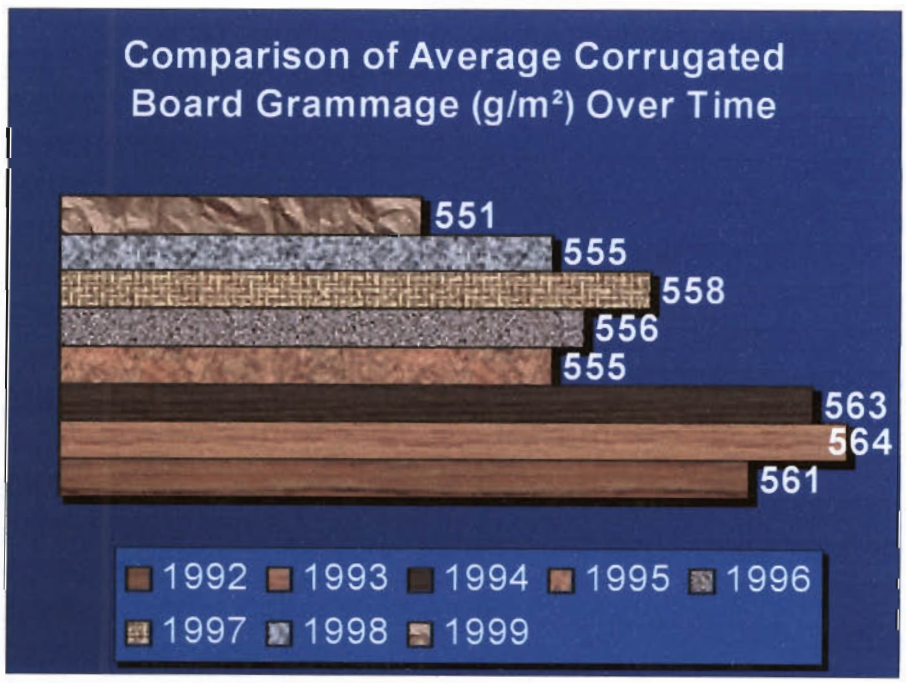

Figure 1.5: A comparison of the annual average corrugated board grammage manufactured in Europe [4].

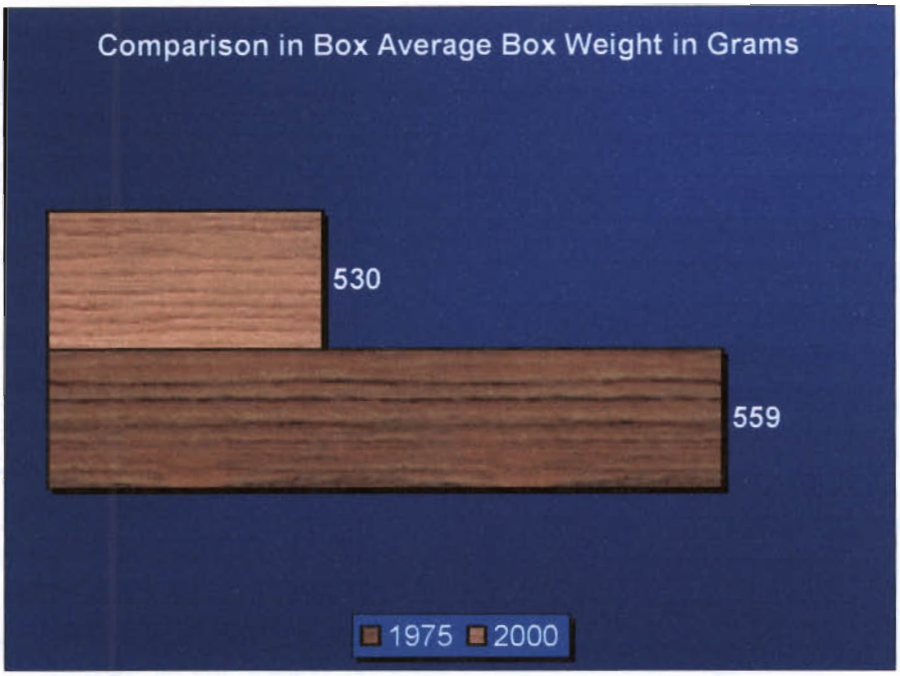

Figure 1.6: A comparison of the average box weights produced in South Africa between 1975 and 2000 [2].

Nampak has recently invested millions in upgrading existing corrugating machinery and purchasing new technology. The Nampak Group is the largest packaging group in South Africa. This is evident by the fact that in 2000 Nampak had a 43% share in the South African packaging market [**3**]. Nampak's increasing corrugated board research approach resulted in Nampak Research and Development (R&D) and Nampak Corrugated approaching the Centre for Materials Engineering, University of Cape Town to perform an investigation into box strength prediction methods and to evaluate a new test method, namely the MD shear test.

Nampak Corrugated currently uses a simplified version of the McKee formula for its box strength predictions, which is empirically based. This formula predicts the maximum load that a box can sustain in compression. The literature available on this box strength prediction method highlights its shortcomings. In order to remain competitive and reduce production cost, Nampak is particularly interested in accurately predicting box strength values in order to optimise their products. In this regard Nampak became aware of a new test method, namely the MD shear test, which they believe will be beneficial for use in box strength predictions. Nampak

Corrugated believes that this test method will improve their box strength prediction capabilities and also provide a useful quality control method for evaluating various board combinations.

1.3 Aims of the Project

The aims of this project were:

- Design and build a test facility to perform the MD shear test.
- Evaluate the performance of the MD shear test with regard to the accuracy of the results and ease of use in an R&D environment.
- Establish how the MD transverse shear stiffness and bending properties of corrugated board relate to the strength of a standard rectangular box.
- Perform box strength predictions using methods available in the literature to establish the most reliable method. In addition, to use predicted board properties as well as experimental values for box strength prediction and evaluate their correlation.
- To evaluate test methods used to describe the mechanical properties of corrugated board for use in an R&D environment.

1.4 Limitations of this Thesis

The limitations of this thesis are:

- This project is mainly experimentally based. In this regard no modelling software has been used.
- Only analytical models, available in the literature, have been considered for box compression prediction.
- Only regular slotted container (RSC) style boxes have been analysed.

1.5 Outline of this Thesis

The thesis begins with a literature review, *Chapter 2*. The literature review discusses the history, manufacturing route and properties of corrugated board and the relevant terminology. It also investigates the work done in characterising the compressive properties of corrugated boxes and board. *Chapter 3* describes all the test fixtures that were designed by the author to carry out the experiments of this project. *Chapter 4* discusses all the experimental techniques used in this thesis. All results are shown in *Chapter 5* and discussed in *Chapter 6*. The conclusions that can be drawn from *Chapters 5* and *6* are then stated in *Chapter 7*. Recommendations for future work are listed in *Chapter 8*.

CHAPTER 2

LITERATURE REVIEW

2.1 Corrugated Board

2.1.1 The History of Corrugated Board

Healey and Allen obtained the first recorded patent of corrugated paper in 1856 [**5**,**6**]. The paper was fed through a simple hand machine consisting of two fluted rolls. Once corrugated the paper was used as hat linings. In 1871 Albert L Jones patented the first use of corrugated paper as a packaging material. The corrugated paper was used to insulate bottles and other fragile items [**5**,**6**]. Jones is also recorded as patenting the idea of using heat to corrugate paper and for patenting an unlined corrugated box with folded ends, in 1873 [**5**,**7**]. The first corrugated board was a single faced board manufactured by Oliver Long in 1874. He glued a sheet of paper to the fluted paper to protect the fluted paper from flattening [**5**,**6**,**7**]. The manufacture of corrugated board then steadily evolved with Robert H Thompson patenting double faced corrugated board in 1882 [**8**]. This was followed by the invention of the corrugated cardboard box, in 1890, by Robert Gair [**9**].

2.1.2 Manufacture of Corrugated Board

Corrugated board is made from two distinct paper elements: the liner and the medium, often referred to as the fluting. The process of pulping the paper usually involves chemicals such as sulphates or sulphites. Due to the nature of wood there can be a variance of up to 8% in the strength characteristics of paper manufactured from the

same batch of raw material [**10**]. Kraft paper is typically used for the liners whereas the fluting is usually made from 100% recycled fibre. The term Kraft is of German origin and refers to paper made from at least 75% virgin fibre via the sulfate process [**10,11**]. During the corrugating process the fluting is corrugated and is glued to the liner through the use of a starch adhesive. Figure 2.1 shows a typical corrugated board structure. Due to the manufacturing process, the fibres are aligned in the machine direction (MD) [**12,13**].

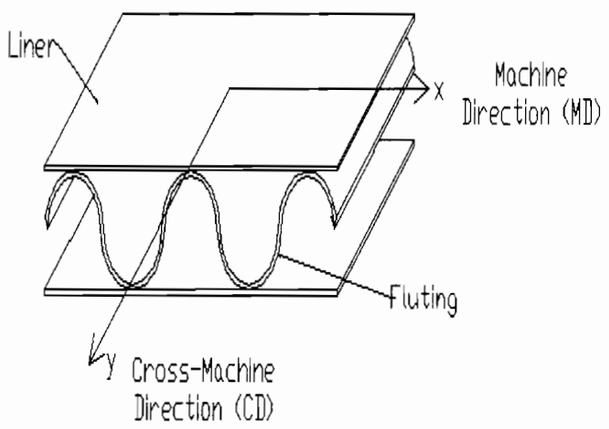

Figure 2.1: A typical corrugated board structure.

Board that consists of two faces and fluting is known as double-wall board as seen in Figure 2.2a [**14**]. Similarly board with a single-wall and fluting is known as single-face board as shown in Figure 2.2b. Single-wall board can be used as an insulating material within a container to cushion the content of the container from damage [**10**]. In the manufacture of corrugated board four flute heights are generally used. These are notated A, B, C, E. These flute types have different heights and pitches as shown in Figure 2.3 [**15**]. Commercial board can often be a combination of a large flute shape and a small flute shape to optimise design and have a board with good stacking strength and puncture resistance [**16**]. This type of board consists of three walls and two flutes and is known as triple-wall board as shown in Figure 2.4.

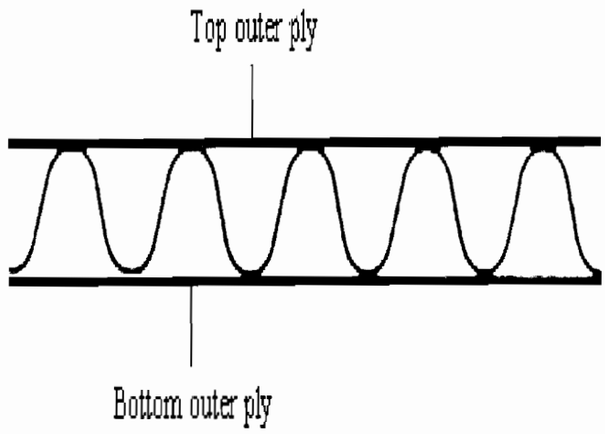

Figure 2.2a: Double-wall board [14].

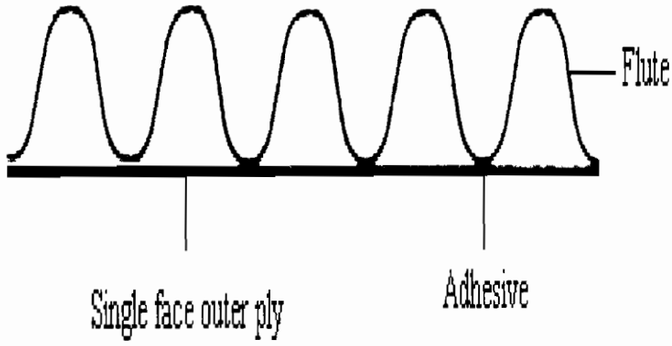

Figure 2.2b: Single-wall board [14].

Flute Shape	Flute Pitch	Flute Height
Coarse Flute (**A** Flute)	8.0 - 9.5 mm	4.0 - 4.9 mm
Medium Flute (**C** Flute)	6.8 - 8 mm	3.2 - 4.0 mm
Fine Flute (**B** Flute)	5.5 - 6.5 mm	2.2 - 3.0 mm
Micro Flute (**E** Flute)	3.0 - 3.5 mm	1.0 - 1.8 mm

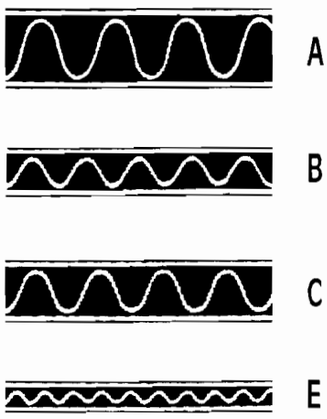

Figure 2.3: A comparison of the different flute heights and pitches associated with various flute notations [14,15,16].

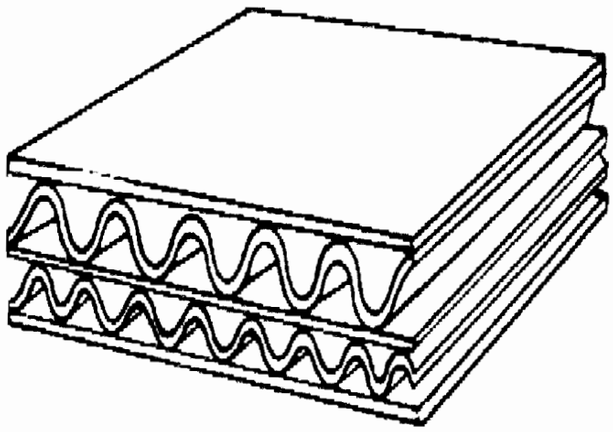

Figure 2.4: A typical triple-wall board structure [15].

Corrugated board is manufactured on a set of machines in-line, commonly referred to as a Corrugator. It is capable of manufacturing single, double or triple-wall board in a continuous process [**6**]. The major components that make up the Corrugator are discussed in the paragraphs below.

2.1.2.1 The Single Facer Component of the Corrugator

In this part of the Corrugator the fluting is glued onto the top liner. The fluting and liner are first fed into the Single Facer from unwinds. The fluting and liner are then fed onto heated drums to heat the paper before being glued together. During this process steam is often applied to the paper to increase its flexibility. This is particularly important for the fluting. The fluting is then passed between two rolls with corrugated surfaces, as seen in Figure 2.5. This process forces the fluting into the corrugated shape. The corrugated rolls are heated to dry the fluting and ensure that it holds its shape. As the medium leaves this section, the fluted tips are coated with a starch adhesive and glued to the facing [**6**]. The complete process of manufacturing single faced board that occurs in the Single Facer is shown in Figure 2.6 [**17**].

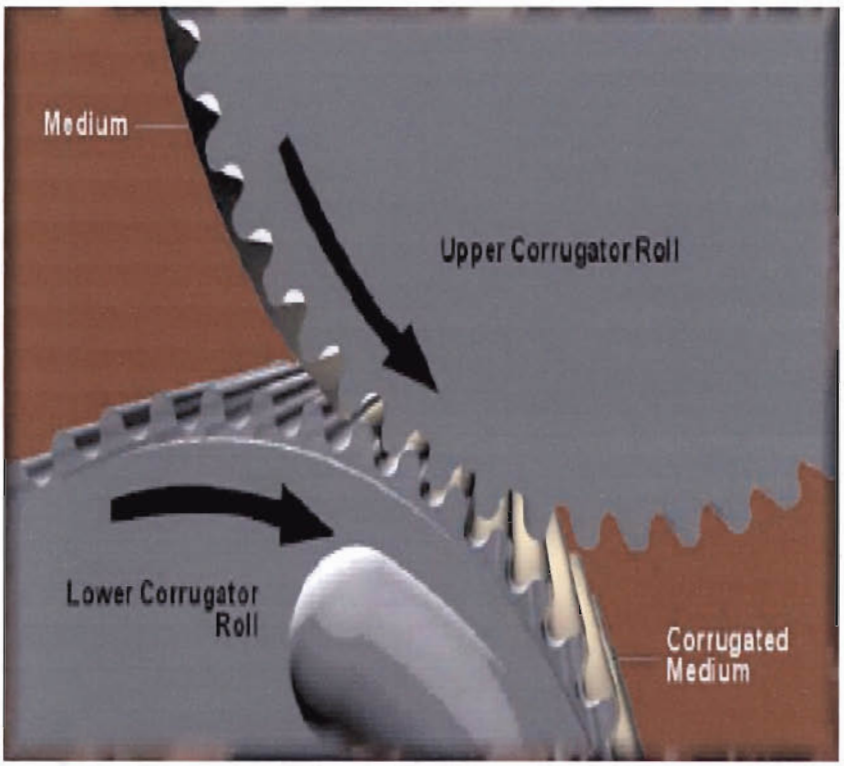

Figure 2.5: The process of forming the fluting between the corrugated rolls [17].

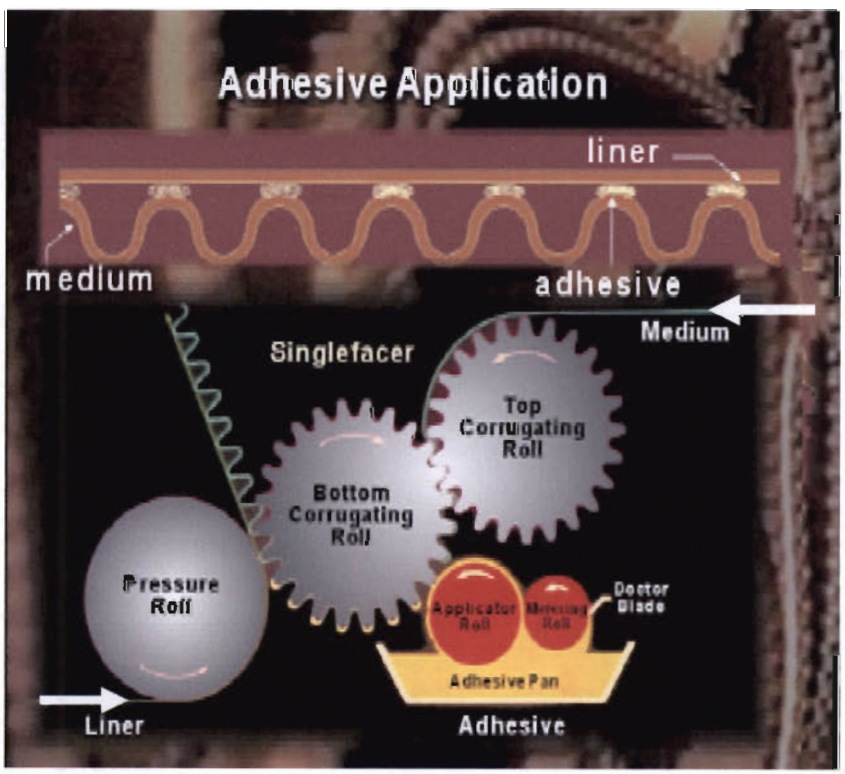

Figure 2.6: The complete operation occurring in the Single Facer component of the Corrugator [17].

2.1.2.2 The Double Backer Component of the Corrugator

To create double-wall board the single-wall board created in the Single Facer must be fed into the Double Backer and have the second liner glued to the fluting. The bottom liner is fed into the Double Backer and sprayed with steam to increase its similarity with the single-wall board. This is important to prevent curl. The single-wall board is then fed into the Double Backer and coated with a starch adhesive. The bottom liner is then brought into contact with the single-wall board and the two are then fed into steam chests. In the steam chests the bottom liner and the single-wall board are held together under pressure and temperature to dry and cure the glue. In this operation it is important that the pressure is not too high so that the flutes are not crushed [**16**,**18**]. In addition, the corrugating process can cause delamination damage to the flutings, due to large bending and shear deformations that can occur during manufacturing. This will result in a decrease in the transverse shear stiffness of the corrugated board which will affect the stability of the board [**19**]. Figure 2.7 shows the complete corrugated board manufacturing process that occurs in the Corrugator.

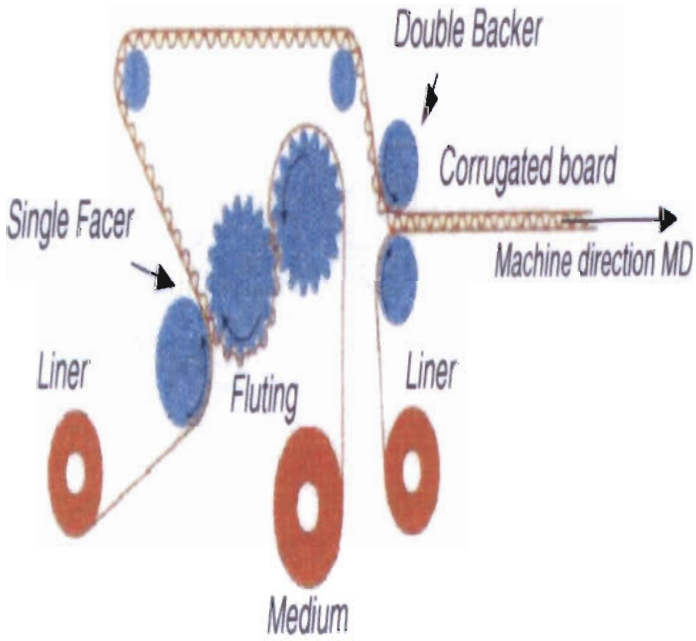

Figure 2.7: The complete manufacturing process of corrugated board that is performed by the Corrugator [5].

2.1.3 Advantages of Corrugated Board

The major advantage of corrugated board is that it is a low density structure. This is particularly important in the transporting industry as the lighter the package, the lower the transport costs. Another major advantage of corrugated board is that it can support up to 500 times its own weight under a stacking type load **[9]**. Typically corrugated board has high strength to weight and stiffness to weight ratios [**4**,**13**,**20**]. Corrugated board also has good tearing and puncture resistance. This provides rough handling resistance during transportation. Due to the fluted structure, corrugated board provides cushioning for the content of a corrugated container and reduces shock and vibration effects that could damage the content **[10]**. Corrugated containers can be printed in any design or colour desired, adding to the attractiveness of the container. They can be treated to provide protection against water, grease, oil, static electricity and abrasion. In addition, corrugated board containers use only 20% of wood, if wood pulp Kraft paper is used, and uses no wood if the container is made out of Kraft paper using agricultural residues or other non-conventional raw materials **[21]**. Corrugated board can be recycled and used to make new boxes **[1]**. As shown in Figure 2.8, 70% to 80% of all board manufactured is made from recycled fibre. In the production of corrugated board 50% of the total cost is due of the cost of the raw material used in the manufacturing process. In Europe the use of 70% recycled fibre has helped to reduce these costs **[4]**. In Sweden 98% of corrugated board is recycled **[5]**. Therefore the increased use of recycled fibre and alternative raw materials can limit the damage caused to our environment by using raw material for corrugated board manufacturing. This makes corrugated packaging more eco-friendly **[21].**

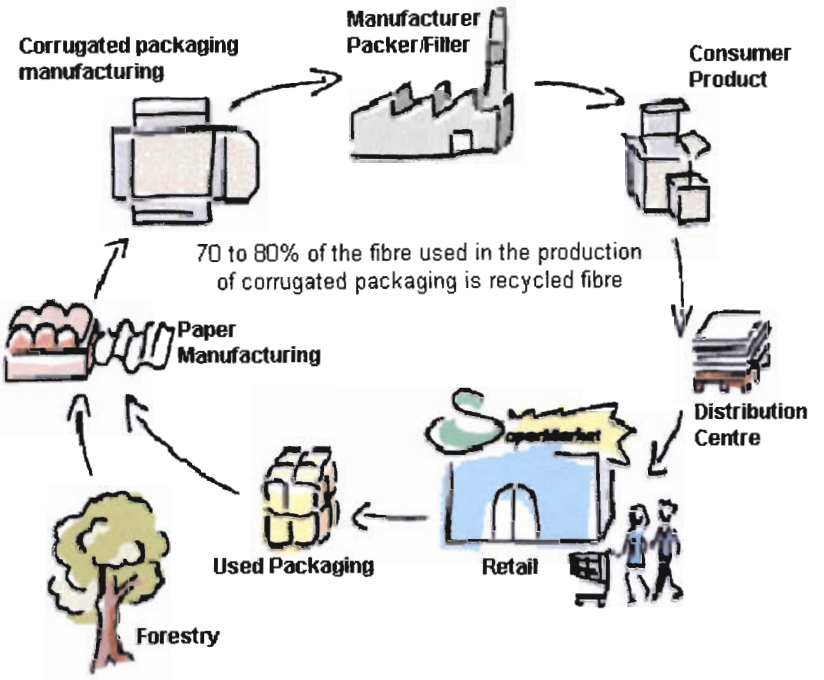

Figure 2.8: The lifecycle of a corrugated container from raw material to the consumer to the recycling for the manufacture of further containers [4].

2.1.4 Disadvantages of Corrugated Board

The major disadvantage of corrugated board is that it is sensitive to moisture. As the water content increases the board will swell. Moisture also affects the stiffness properties of the board. This leads to a decrease in board stiffness and results in premature box failure that is very costly to the corrugated fibreboard shipping industry [**22**,**23**]. At 85% relative humidity (RH) the board will have about half the stiffness it would have had at standard testing conditions of 50% RH. Corrugated board also tends to creep under stacking load. It has been shown that after one year of storage the stacking strength of the board is about one half the original stacking strength [**10**].

2.2 The Manufacture of Corrugated Boxes

After the corrugated board has been manufactured, it is cut into blanks. The blanks are then converted into corrugated containers. The process of converting a blank into a container involves cutting, scoring and printing. The design of the box required by the customer determines the complexity of the operation required to make the box. The simplest box to manufacture is an RSC box. These boxes are normally manufactured in a single process on an in-line flexographic Printer / Slotter / Folder / Gluer. This machine combines all the operations of printing, cutting, folding and gluing into a single operation. During these operations the corrugated board is subjected to large multi-axial stresses that can result in plastic deformation and localised damage. These effects can affect the corrugated board's mechanical properties, particularly the MD shear stiffness [**18**,**24**]. The RSC box is the simplest and most economical box to manufacture. The main feature of this style of box design is that the box flaps meet in the centre when folded [**25**].

2.3 The Mechanical Properties of Corrugated Board

Corrugated cardboard can be considered an orthotropic composite sandwich type material due to the mechanical properties of the paper used in the construction of the board. Corrugated board has high stiffness and strength per unit weight due to the structure and mechanical properties of the board. In addition it has an excellent strength to cost value. This results in corrugated board finding important applications in the packaging industry worldwide [**26**,**27**,**28**].

2.3.1 The Mechanical Properties of Paper

Paper is manufactured from cellulose wood fibres. As these fibres are orientated, paper has anisotropic properties. The fibres tend to be orientated in 3 principal directions which result in the assumption that paper is an orthotropic material i.e. having elastic properties that are different in three mutually perpendicular directions namely the MD, CD, and ZD corresponding to the directions 1, 2 and 3 [**24,29,30,31,32,33**]. The stress strain relationship of an orthotropic material aligned in the principal material directions can be expressed by the following matrix [**24**]:

$$\begin{bmatrix} \varepsilon_{11} \\ \varepsilon_{22} \\ \varepsilon_{33} \\ \gamma_{12} \\ \gamma_{13} \\ \gamma_{23} \end{bmatrix} = \begin{bmatrix} \frac{1}{E_{11}} & -\frac{\nu_{21}}{E_{22}} & -\frac{\nu_{31}}{E_{33}} & 0 & 0 & 0 \\ -\frac{\nu_{12}}{E_{11}} & \frac{1}{E_{22}} & -\frac{\nu_{32}}{E_{33}} & 0 & 0 & 0 \\ -\frac{\nu_{13}}{E_{11}} & -\frac{\nu_{23}}{E_{22}} & \frac{1}{E_{33}} & 0 & 0 & 0 \\ 0 & 0 & 0 & \frac{1}{G_{23}} & 0 & 0 \\ 0 & 0 & 0 & 0 & \frac{1}{G_{31}} & 0 \\ 0 & 0 & 0 & 0 & 0 & \frac{1}{G_{12}} \end{bmatrix} \begin{bmatrix} \sigma_{11} \\ \sigma_{22} \\ \sigma_{33} \\ \tau_{12} \\ \tau_{13} \\ \tau_{23} \end{bmatrix}$$

where:

E_{11}, E_{22}, E_{33} = Young's modulus in the 1, 2 and 3 direction

ν_{ij} = Poisson's ratio for transverse strain in the *j*-direction when stressed in the *i*-direction

G_{23}, G_{31}, G_{12} = Shear moduli in 2-3, 3-1, and 1-2 planes

Due to symmetry [**5**,**34**]:

$$\frac{\nu_{12}}{E_{11}} = \frac{\nu_{21}}{E_{22}} \qquad \frac{\nu_{13}}{E_{11}} = \frac{\nu_{31}}{E_{33}} \qquad \frac{\nu_{23}}{E_{22}} = \frac{\nu_{32}}{E_{33}}$$

Therefore the only parameters that need to be measured for an orthotropic material are:

$E_{11}, E_{22}, E_{33}, \nu_{12}, \nu_{13}, \nu_{23}, G_{12}, G_{13}, G_{23}$ [**5**].

2.3.1.1 The Tensile Modulus of Paper

The tensile modulus of the liner and fluting are easily obtained through standard tensile tests. The ratio of the modulus in the MD to the modulus in the CD has been found to be roughly 1 to 6 [**24**,**31**]. The tensile modulus in the Z or 3 direction, E_{33}, can be approximated by dividing the MD modulus by 200 [**5**].

2.3.1.2 The Shear Modulus of Paper

The shear modulus in the 1-2 plane, G_{12}, can be approximated by Equation 2.1 [**30**].

$$G_{12} = 0.387\sqrt{E_{11}E_{22}} \qquad \textbf{2.1}$$

The transverse shear moduli G_{13} and G_{23} can be approximated by Equations 2.2 and 2.3 [**30**,**31**,**32**].

$$G_{13} = \frac{E_{11}}{55} \quad \textbf{2.2}$$

$$G_{23} = \frac{E_{22}}{35} \quad \textbf{2.3}$$

G_{12} can be calculated using the initial slope of the stress-strain curve (A_y) in the CD direction and Equation 2.4 **[35]**.

$$G_{12} = \frac{A_y \sqrt{\left(\frac{\nu_{11}}{\nu_{22}}\right)}}{2\left(1 + \sqrt{\nu_{11}\nu_{22}}\right)} \quad \textbf{2.4}$$

2.3.1.3 The Poisson's Ratio of Paper

Poisson's ratio ν_{ij} for transverse strain in the j direction when stressed in the i direction is defined as [**29**]:

$$\nu_{ij} = -\frac{\varepsilon_j}{\varepsilon_i} \quad \textbf{2.5}$$

The Poisson's ratio of corrugated board and paper is a difficult property to obtain. For paper, ultrasonic methods have been used involving expensive equipment and a degree of expertise. Nyman and Gustafsson use an approximate value of $\nu_{xy} = 0.2$ for an orthotropic material [**36**]. It has been stated that the ratio of the Poisson's ratio in the *xy* plane over the Poisson's ratio in *yx* plane is the same as the ratio of corrugated boards flexural rigidity in the MD over the flexural rigidity in the CD [**37**]. Nordstrand assumes the Poisson's ratio in the *xz* and *yz* to be small and equal to 0.01 due to the assumption of plane stress conditions **[38]**.

2.3.2 The Mechanical Properties of a Corrugated Board Composite Sandwich

A composite sandwich consists of two stiff faces separated by a low density core [**18**]. The main function of the faces is to carry the stresses applied to the sandwich due to in-plane deformation and curvature of the sandwich. The purpose of the core is to provide the sandwich with rigidity (keep the faces separated) and carry the shear stresses applied to the sandwich without adding too much weight [**34**]. As with all composite sandwich type materials the stiffness of the board is related to the structure of the board i.e. the separation of the faces due to the core.

2.3.2.1 The Tensile Modulus of Corrugated Board

The tensile modulus of corrugated board is usually predicted using laminate theory or other methods. Aboura *et al.* have proposed a novel way of measuring the tensile modulus of corrugated board in the MD and CD [**1**]. This method allows for the measurement of both the tensile modulus and the Poisson's ratios. The method involves designing typical dog bone tensile specimens in the MD and CD and then impregnating the grip ends in resin to provide the ends with rigidity. This prevents damage to the sample that may influence the tensile readings and result in premature failure.

2.3.2.2 The Shear Modulus of Corrugated Board

Research has shown that the out of plane shear stiffness (transverse) of corrugated board is much higher in the CD than in the MD [**39**]. The CD stiffness is directly related to the in-plane shear stiffness of the paper used to form the core. The MD is dependant on the shape of the fluting and its elastic properties. In addition, the transverse shear stiffness of corrugated board can be further decreased due to delamination damage caused to the corrugated medium during the manufacturing

process thus altering the MD stiffness properties [**18,19,39**]. Nordstrand *et al.* stated that the transverse shear rigidities of corrugated board would always be lower than a homogeneous material with the same flexural stiffness. This is due to the low density, flexible core used in the manufacture of corrugated board. Nordstrand *et al.* derived analytical expressions for the elastic constants of an equivalent homogeneous core material [**26**]. The in-plane modulus of the fluting was calculated using Baum's approximation [**5,19,30**]. The in-plane shear modulus can also be calculated by using the method advocated by Urbanik *et al.* [**35**].

By comparing the derived values of transverse shear to the values predicted using finite element analysis, Nordstrand *et al.* found that G_{13} is very sensitive to corrugation shape while G_{23} is less sensitive to the corrugated shape and generally higher than G_{23}. It was also noted that G_{13} is affected by core elastic moduli. Nordstrand and Carlsson compared the calculated transverse shear values to experimentally determined values using 3-point bend testing and block shear testing [**19**]. Their results indicated that the 3-point bend test was a factor of 2 lower than the block shear values. They explained this discrepancy through deformation of the facings and denting, due to the rollers, during the 3-point bend test. It was also noted that their predicted values were higher than the experimentally determined values. They determined that this was due to the fact that their calculations were based on material properties prior to corrugation, and that the flute stiffness is greatly reduced due to damage that occurs during the corrugation process. The discrepancy between the calculated and measured values could also be due to the buckling of the fluting during shear loading that had not been accounted for in the analytical model.

The standard methods for measuring the transverse shear stiffness of corrugated board in the CD and MD is to use the block shear method or the 3-point bend test method. McKinlay has developed a new method in which corrugated board specimens are subjected to torsion loading [**40**]. The MD transverse shear stiffness can then be calculated.

2.3.2.2.1 The Block Shear Test

According to ASTM C273-61 [**41**] the shear modulus of a sandwich construction can be calculated using Equation 2.6:

$$G_{i3} = \frac{\tau_{i3}}{\gamma_{i3}} = \frac{\delta T_b}{WL} \qquad \textbf{2.6}$$

where:

i = 1,2

τ_{i3} = Shear stress

γ_{i3} = Shear strain

δ = Slope of linear part of load-displacement curve

T_b = Total board thickness also known as board caliper

W = Specimen width

L = Specimen length

Aboura *et al.* report that during the course of a block shear test in the MD direction of corrugated board, four distinct stages are observed as shown in Figure 2.9 [**1**]. The first stage is characterized by the linear shape of the load displacement curve. This is typically referred to as the elastic phase. At the end of the elastic phase the load drops corresponding to the failure of the flutes. This is the beginning of the second stage. The flutes are then compressed until their minimal height is reached. This is the third stage. During this stage the load increases until failure occurs. This stage is characterised by the shear loading of the flute liner interface. The final stage is characterised by total board failure in shear with the starch adhesive failing and the detachment of the liners. The CD behaviour is different to the behaviour observed above with the latter stages being characterised by a second linear elastic stage prior to failure [**1**]. The block shear values measured by Nordstrand and Carlsson display

large amounts of scatter which is consistent with a composite material. It also depicts the variability of the material properties and the manufacturing process [**19**].

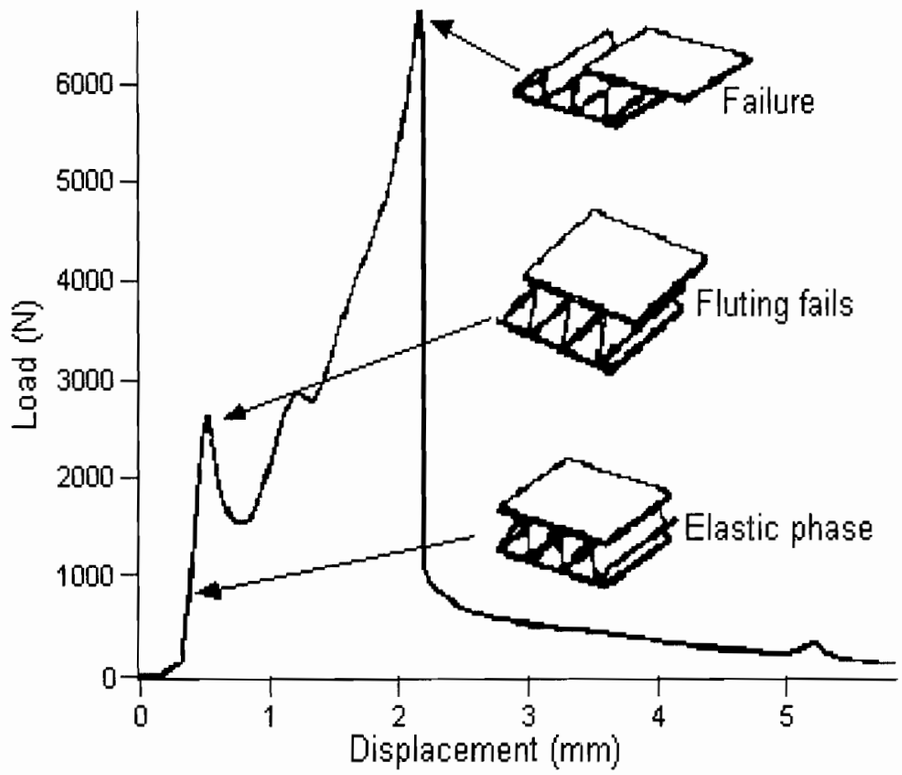

Figure 2.9: A typical block shear load displacement curve for a specimen tested in the MD [1].

2.3.2.2.2 The McKinlay Method for the Measurement of Transverse Shear Stiffness of Corrugated Board

The McKinlay test is only relevant for calculating the MD transverse shear stiffness. In this test a corrugated board specimen is subjected to a torsion load. Using Equation 2.7 the MD transverse shear stiffness can be calculated by:

$$M = K\vartheta S \qquad \textbf{2.7}$$

where:

K = $\frac{4a^3}{3L}$ where a is half the sample width and L the free length

M = Applied moment (Nm)

S = MD stiffness

ϑ = Angle of rotation

Hung and Suhling have devised a method for shear testing of paper and found that the shear modulus of paper increases with increasing strain rate. This result is similar to that found by Sawyer *et al.* who report that the stress strain properties of paper are highly rate dependant [**42**]. This is particularly important for the McKinlay method for which no reference to cross-head speeds and strain rates are available [**43**].

2.3.2.3 The Poisson's Ratio of Corrugated Board

Using the tensile test mentioned in section 2.3.2.1 Aboura *et al.* proposed a method for measuring the Poisson's ratio of corrugated board [**1**]. The tensile specimens mentioned were instrumented with bi-directional strain gauges. Using Equation 2.5, the Poisson's ratio of the board in the MD and CD were obtained. However, no reference was made to the manner in which the gauges were attached, or what types of gauges were used, leading to difficulties in repeating these experiments. Vorakunpinij *et al.* have measured the deformation of paper under creep loads using magnetic field changes. This method of displacement measurement could be used in the measurement of Poisson's ratio of corrugated board [**44**].

2.3.2.4 The Bending Stiffness of Corrugated Board

The bending stiffness of corrugated board can be defined as the measure of resistance of that board to a bending force [**45**]. The bending stiffness of a material is defined by Equation 2.8:

$$D = EI \qquad \textbf{2.8}$$

where:

D = Bending stiffness

E = Modulus of the material

I = Second moment of area, moment of inertia $= \frac{WT_b^3}{12}$

The bending stiffness of a material is dependent on the elastic properties of the constituents and the dimensions of the specimen. Therefore, if a corrugated board of high bending stiffness were required, the specimen would be manufactured out of liners that had a high elastic modulus and a high caliper [**45**,**46**,**47**]. The separation of the faces would also need to be optimised. It is important to note that the conversion operations of the corrugating process may lower the bending stiffness of the corrugated board. This is mainly due to the decrease in overall board caliper due to crushing during the process [**48**]. Research has shown that the bending stiffness of corrugated board is much higher in the MD, i.e. transverse to the corrugations, than in the CD [**19**]. This is largely due to the fact that paper fibres are aligned in the MD.

When bending in the MD occurs, the tensile modulus of the liners is much greater than the modulus in the CD, resulting in a higher bending stiffness even though the fluted medium gives the board more rigidity in the CD. In corrugated board the fluting does not contribute any additional stiffness to the board for bending in the MD. However, for bending in the CD the contribution of the core to the overall stiffness of the corrugated board cannot be neglected and is usually between 6% and 13% of the total sandwich stiffness [**49**,**50**,**51**]. When considering composite sandwich type materials, the calculation of bending stiffness becomes more complicated due to the fact that the composite sandwich is not homogeneous. Equation 2.9 is the standard equation for calculating the flexural rigidity of a composite sandwich material [**34**].

$$D = E_l \frac{WT_l^3}{6} + E_l \frac{WT_l e^2}{2} + E_f \frac{WC^3}{12} \quad \textbf{2.9}$$

where:

D = Flexural rigidity of the sandwich

E_l = Modulus of the liner

E_f = Modulus of the flute

W = Width of the sandwich

C = Thickness of the core

T_l = Caliper of the liner

e = Distance between the centre lines of liner

However, due to the nature of the fluted profile, Equation 2.9 cannot be used as it is based on a continuous core. A simple solution to this problem is to assume that the core does not contribute any stiffness to the sandwich. This results in the moment of inertia value being the same for both the MD and CD for a square beam. This simplification leads to Equation 2.10, which can be used to calculate the moment of inertia of both faces through the neutral axis of the core.

By the parallel axis theorem **[52]**:

$$I_{NA} = I_l + AJ^2 \quad \textbf{2.10}$$

where:

I_{NA} = Second moment of area of the face about the neutral axis

$I_l = \frac{WT_l^3}{12}$

A = Area of the face

J = Distance from the neutral axis of the corrugated board to the neutral axis of a face

Using the second moment of area, the flexural rigidity of the corrugated board can be determined using Equation 2.11, where the subscripts l and f stand for liner and fluting, respectively. When bending occurs in the MD the second term is omitted.

$$EI = E_l I_l + E_f I_f \qquad \textbf{2.11}$$

Urbanik [**50,51**] has derived expressions for calculating the moment of inertia of corrugated board. These expressions are shown in Figure 2.10. Koning and Moody predicted bending stiffness using board modulus and moments of inertia around the neutral axis and found that they could predict the stiffness with a maximum error of about 6% [**53**]. Reasonably good predictions of bending stiffness were also obtained by Koran using this method [**45**].

TABLE IV
NON-DIMENSIONAL MOMENT OF INERTIA COMPONENTS

Term	Equivalent expression
$\frac{I_l}{PT_l^3}$	$\frac{1}{2}\left(\frac{T_b}{T_l}-1\right)^2+\frac{1}{6}$
$\frac{I_f}{PT_m^3}$	$\frac{R}{P}\left(\left(4\left(\frac{R}{T_m}\right)^2+1\right)\frac{\sin\theta+\theta}{4}+\left(12\left(\frac{R}{T_m}\right)^2+1\right)\left(\frac{H}{R}-2\right)\frac{\sin\beta}{3}+\left(\frac{R}{T_m}\right)^2\left(\frac{H}{R}-2\right)^2\beta\right)$
X	$\frac{R}{T_m}\left(\frac{1}{2}\frac{P}{R}TF-\theta\right)$
$\frac{I_l}{PT_m^3}$	$\frac{1}{6}\frac{T_m}{P}(x^3\sin^2\beta+x\cos^2\beta)$
$\frac{I_m}{PT_m^3}$	$\frac{I_l}{PT_m^3}+\frac{I_f}{PT_m^3}$

Figure 2.10: Urbanik's inertia equations for calculating the flexural stiffness of corrugated board [50,51].

2.3.2.5 The Edge Compression Strength of Corrugated Board

The edge compression strength (ECS) of corrugated board is an important board property used in the strength design of corrugated board packages [**46,54**]. The edge compression strength of corrugated board is obtained by carrying out edge compression tests (ECT) and is generally known as the ECT value of the board. Due

to its relationship to box compression strength (BCS), industry is tending to characterize board combinations by ECT as a means of comparing different combinations for strength design. This results in the ECT being an important board property [**55**,**56**]. The ECS of corrugated board is determined by the compressive properties of the board constituents, namely the fluting and liners [**46**,**54**]. As these properties are affected by the manufacturing process i.e. wet pressing and refining, the ECS of corrugated board can give an indication of board quality [**46**,**54**,**57**]. ECT involves subjecting a specimen to a compressive load until failure occurs as shown in Figure 2.11. During testing the specimen fails in modes similar to that of a corrugated box. It will either fail in compression or localised buckling. There are a number of different test methods to measure ECS which try to eliminate the influence of edge effects on the corrugated board specimens. The reason for avoiding edge effects is that during the compression of a box, failure does not occur at an edge [**58**]. A badly cut edge can induce stress concentrations which will lead to an incorrect ECT value. Many of these methods involve necked down specimens or specimens with reinforced edges. The European Federation of Corrugated Board Manufacturers (FEFCO) method uses a specimen which is simply a piece of board without reinforcement or necked structure. This method does not try and avoid edge effects. It is carried out in a similar manner to that which the short span compression test (SCT) is carried out to obtain liner compression data. This makes SCT relevant for ECT predictions [**58**].

Westerlind and Carlsson investigated the prediction of edge compression strength through constituent compressive properties [**59**]. They found that boards with B flute failed in compression rather than localized buckling. It was postulated that this was probably due to the reduced wavelength of the B flute as opposed to that of C flute which failed in localised buckling. Westerlind and Carlsson proposed a new method for measuring ECT strength using a necked down specimen and an improved test method which they believe is more relative to panel compressive strength as it prohibits edge damage.

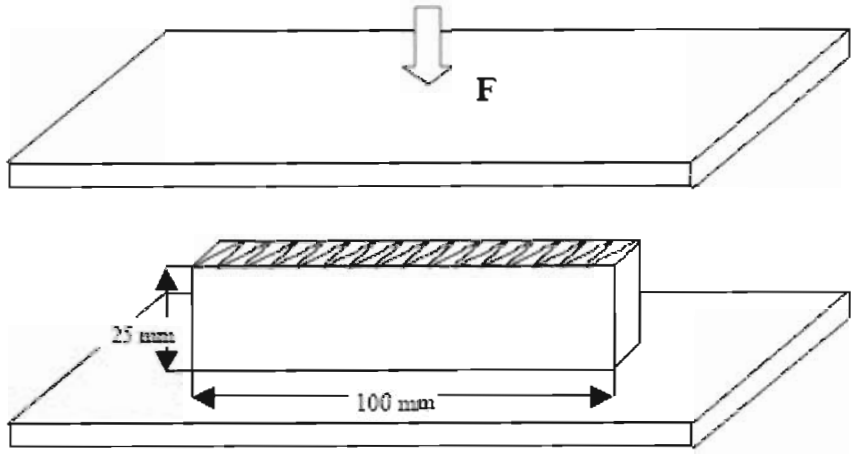

Figure 2.11: The FEFCO ECT testing procedure [56].

2.4 Corrugated Box Strength Design

Corrugated board boxes are one of the most common packaging materials used worldwide. During their service life they will usually be loaded in top-to-bottom compression as shown in Figure 2.12. BCS is the most common design parameter that is used for box characterisation and probably gives the best evaluation of how well a box will perform in a stacking situation [**26,46,54,60,61,62**].

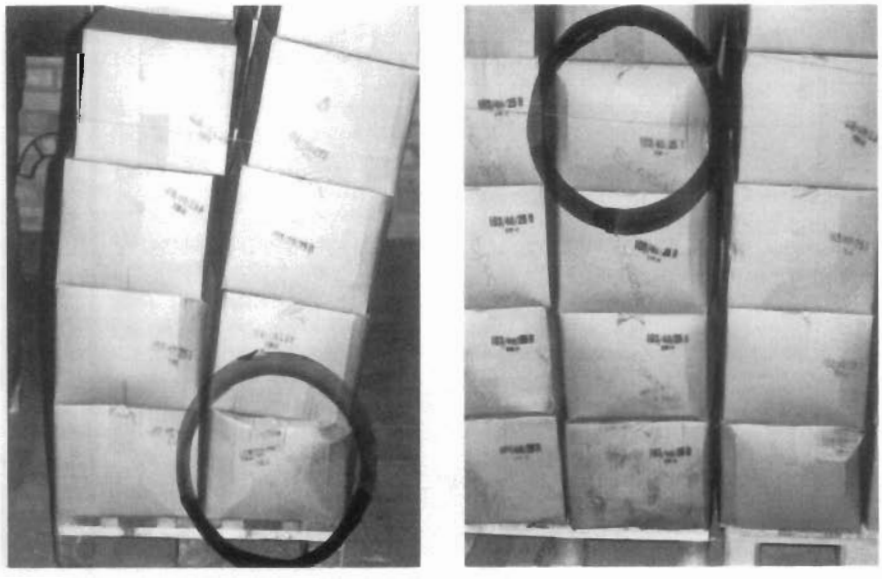

Figure 2.12: Box failure due to top-to-bottom compression during stacking [58].

2.4.1 Box Compression Strength

In the design of corrugated board boxes the boxes are generally designed for a specific load carrying level with an applied safety factor. Due to the nature of box construction, box compression strength is related to the CD compression strength of corrugated board. The safety factor is applied to compensate for the lack of knowledge regarding material properties and decrease in load carrying ability due to imperfections and eccentric loading induced by box creases and flaps **[62,63,64]**. The BCS value will also give manufacturers and idea of how the box will perform in service and the quality of the box **[54,65]**. The BCS value of a box is obtained by carrying out box compression tests (BCT).

2.4.1.1 The Box Compression Test

The BCT consists of compressing an unfilled corrugated board box between two parallel loading plates as seen in Figure 2.13.

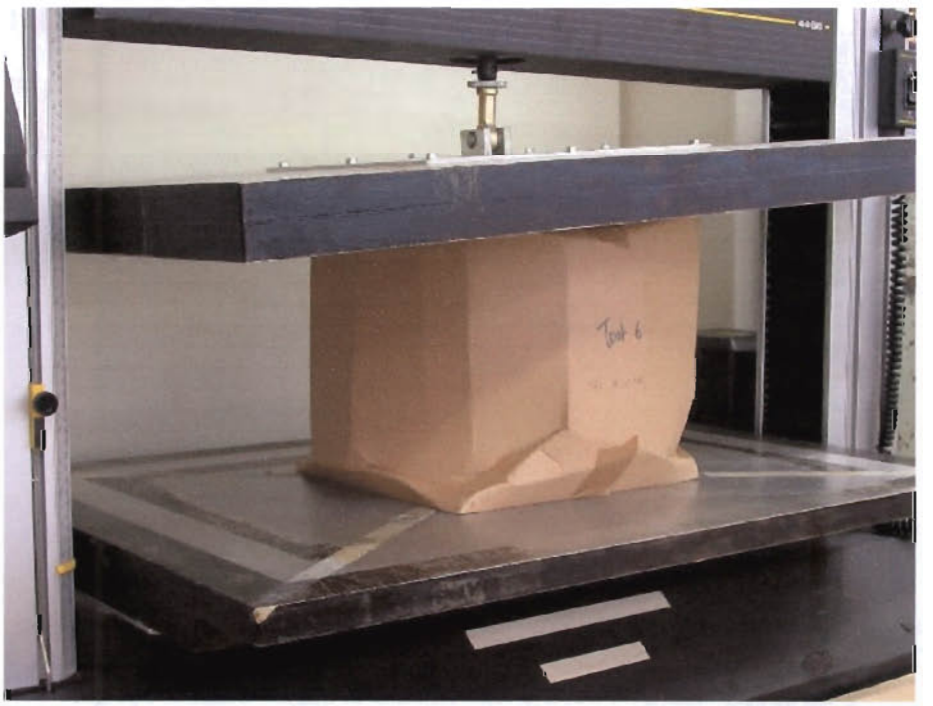

Figure 2.13: A box undergoing compression during a BCT.

As the load increases during a BCT, the box resists compression until a load is reached at which the board becomes unstable. This can be likened to the yield point in homogeneous materials. At the point where the panels become unstable they begin to buckle. The result of buckling is that the centre panels of the box are now unstable and cannot support further load. The load at which buckling begins is referred to as the critical buckling load. The deflection of the centre panels can be seen in Figure 2.13. This buckling does not coincide with the maximum BCS value of the box as the load is still supported by the combined board at the corners of the box. These vertical edges are constrained by the panels of the box and can therefore support substantially more load.

The box can support higher loads than the critical buckling load after the buckling of the sides, but at an increased deformation per unit load i.e. decrease in board stiffness. An idealised load distribution profile of a box during BCT is shown in Figure 2.14. The side panels of the box are elastically buckled, but the load is carried by the edges [**47**]. Box failure occurs when the combined board at the edges fails [**48**,**54**]. During failure the applied load is redistributed throughout the corrugated board structure. This process of load redistribution and eventual box collapse is governed by the boundary conditions of the panels, the flexural rigidities of the panels and the transverse shear rigidities of the panels [**26**].

In general the transverse shear stiffness in the MD of corrugated board is lower than that in the CD. The result is that the direction of high flexural stiffness, the MD, is also the direction of low transverse shear stiffness. This can result in large shear deformations and affect the overall structural stiffness and stability [**19**]. The low transverse shear stiffness in the MD will affect the critical buckling load of the panel [**26**].

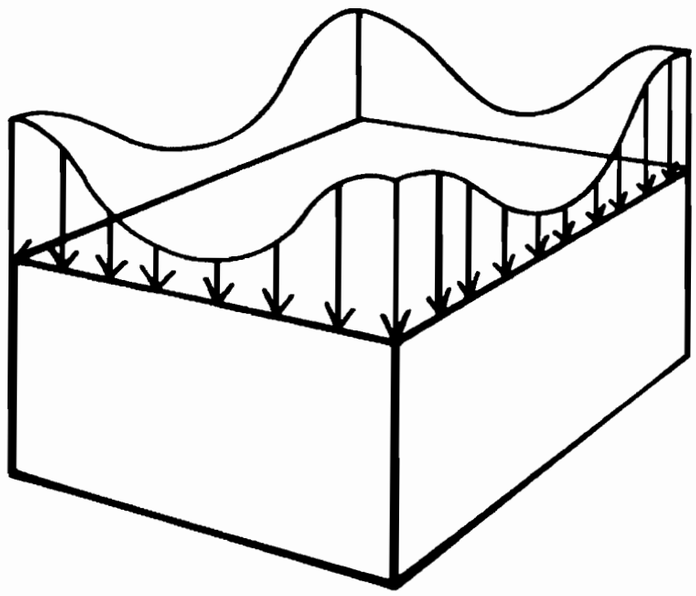

Figure 2.14: Distribution of the compression load around the perimeter of a box during a BCT [54].

2.4.1.2 Disadvantages of the BCT

Even though this method of box testing has been reported as being the best indication of box performance, it still has some limitations, namely [**54**]:

- The BCT is carried out at the end of the manufacturing process. This could mean that a number of boxes might have been manufactured before the box is found to be inadequate. This can result in large losses in material and manufacturing time.
- The BCT does not give the designer an indication of which factors of the corrugated board affect the BCS. When a box is found to be inadequate the designer will not know whether it is due to the liner, fluting, the manufacturing process or the conversion process.
- The BCT does not cover all the types of loading and environmental conditions that a box may be subjected to during its lifetime. The test is carried out on empty boxes, whereas boxes are normally filled. The filling can place internal forces on the box.

- A box may also experience different atmospheric conditions. Due to the hygroscopic nature of paper this can result in a change in the box's mechanical properties.
- The BCT does not take into account the fact that boxes will spend a long time stacked. Due to this continuously applied load, over a long period of time, the boxes' strength characteristics may change.
- The BCT does not compensate for vibrations and shock loading that may occur during transportation. A box may experience static loading due to internal and external pressure from surrounding boxes and dynamic loading due to vertical and horizontal accelerations [**66**].
- The BCT does not compensate for the fact that during testing the load is applied parallel to the box and that due to a swivel connection it can compensate for local failures and adjust accordingly. This is not true in service where the box will probably not be loaded in a perfect parallel manner. The load will not adjust itself to make sure it is uniformly applied as it would during a BCT.
- The BCT is carried out on boxes with the board loaded in the CD. However, during the service life of a box it may experience forces in the MD [**67**].

Research has shown that of the measured BCT value, only 20% – 34% of the measured BCT value can be relied upon. The result is that during box design safety factors within the order of 3 – 5 have to be used to account for factors such as [**58**]:

- Several re-loadings during transport
- Different climates
- Long storage times

Despite these disadvantages, the BCT is still the standard method used for measuring corrugated board box strength. In addition to carrying out BCT testing, box manufacturers have shown considerable interest in predicting the BCS value of boxes from known combined board properties. The ability to predict BCS allows for improved box design.

2.4.2 Box Failure

Corrugated board failure is dominated by material and structural failure. Material failure involves failure of the fibres or failure of the inter-fibre bond. Nordstrand conducted compression tests on panels and predicted the failure load using the Tsai-Wu failure criterion. A 6% difference between the analytically determined and experimentally determined failure load led him to conclude that collapse of corrugated panels was triggered by material failure of the inner liner [**63**]. Local instabilities of the facings and core can interact with the failure propagation [**68**]. Structural failure involves facing instability i.e. local buckling. Local buckling of the faces dominates corrugated board failure when the box experiences high transverse and normal shear stresses [**69**].

2.4.3 Factors Affecting Box Compression Strength

The BCS of a corrugated box is dependent on the ECT of the board and its flexural properties [**13,53,39,46,48,50,54,55,57,65**]. In addition, research has shown that the transverse shear stiffness and structure of the box, i.e. creases and flaps, affects the BCS of the box [**62,65,72**]. The quality of the paper used to construct the board and its structure, as well as the mechanical process of board manufacturing, affects the BCS of a box [**20,70,71**].

2.4.3.1 The ECS of Corrugated Board

Due to the nature of box failure, McKee stated that the material at the edge fails at a load intensity equal to the intrinsic corrugated board property. McKee stated that box failure is triggered by edge failure of the corrugated board. In addition, ECT data was relevant to total BCS as it reflected some of the effects of the manufacturing process and the inherent material properties of corrugated board [**54**]. Nordstrand *et al.* state that the edge stiffness influences box failure load as it affects the load distribution on the top and bottom edges of the box when the panels buckle [**72**]. Hahn *et al.* have

found that the most effective way of increasing the collapse load of corrugated board panels is by improving the compressive properties of the panels which means an increase in the ECT value [**68**].

2.4.3.2 The Flexural Stiffness of Corrugated Board

The flexural stiffness of the panel also contributes to the total BCS [**48**]. As with all composite sandwiches, the tensile modulus of the liners and the separation of the liners, i.e. the core height, influence the flexural rigidity of corrugated board. As the flexural rigidity of the panels plays a significant role in box failure, the design of the corrugated board used for box construction cannot be underestimated. The flexural rigidity of corrugated board in both the MD and the CD are of importance for box failure as the initial buckling of the box occurs in both the MD and CD. It is also important to note that the direction of high bending stiffness i.e. MD is also the direction of the low out-of-plane shear stiffness. This is important for box strength due to the fact that when a corrugated panel is loaded transversely, large shear deformation could occur. This means that the overall structural stability of a box could suffer due to low shear rigidity in the MD [**19**].

2.4.3.3 The Transverse Shear Stiffness of Corrugated Board

Before box failure occurs, the vertical panels of the box undergo large out-of-plane deformations. Nordstrand *et al.* stated that the final failure of the box is governed by the boundary conditions, the shear stiffness and bending stiffness of the panel [**26**]. The importance of paper shear properties on the compressive strength of corrugated containers has been highlighted by Hung and Suhling [**43**]. Low transverse shear stiffness in the MD of corrugated board will also tend to reduce the critical buckling load of corrugated board, thus affecting the BCS [**38**].

2.4.3.4 The Structure of Corrugated Boxes

McKee *et al.* found that 90% of box deformation, due to compression forces, occurs in the creases [**65**]. Nordstrand *et al.* found that the crushing strength of creased board is about 50% of the ECS [**69**]. The crease stiffness is an important property as it affects the load distribution of the top and bottom edges when the box panels buckle. In addition, the creases of the corrugated box result in eccentricity of the applied load, which reduces the load carrying ability of the panels. Nordstrand investigated the effect of load eccentricity and found that an eccentricity of 25% of the panel thickness results in a 15% reduction in panel compression load [**64**]. In addition, an imperfection of ten times the board thickness resulted in a 40% decrease in the panel collapse load. Nordstrand has also found that design parameters, such as the slenderness ratio and stiffness asymmetry, have an effect on the collapse load of corrugated board panels. The safest design was found to be a symmetrical board as this eases the buckling prediction calculations. The collapse load of corrugated panels was found to be very sensitive to changes in core thickness whilst it was insensitive to changes in panel size above a slenderness ratio of 40. His analysis found that panels of small slenderness ratio were more efficient in carrying compressive loads.

2.4.4 Box Strength Prediction Formulae

Box strength prediction is important due to the fact that today's consumers want an optimised product. The global trend of corrugated board grammage has steadily decreased from 1992 till 1999 [**4**]. This is due to the fact that consumers require lighter packaging materials. This results in box manufacturers needing to optimise their products and cut the cost of the packaging [**63**]. In addition, recent environmental concerns have also increased the pressure on manufacturers for better utilization of raw materials [**39**]. This requires a thorough knowledge of paper properties, their influence on board properties and their effect on corrugated box failure. Even though box strength is well characterized by BCT, the process of conducting extensive testing is costly and time consuming and therefore not practical. The result is the increased use of computer based models and prediction techniques,

based on board and paper mechanical properties as well as board geometry, to predict BCS [**60**].

Original corrugated board analysis was based on thin plate theory. Thin plate theory is based on the assumption that if the plate is assumed to be thin, a line originally straight and perpendicular to the middle surface of the laminated plate will remain so when the plate is extended and bent. This is equivalent to ignoring the shearing strains in the planes perpendicular to the middle surface of the laminated plate. This results in the assumption that $\gamma_{xz} = \gamma_{yz} = 0$, where Z is the direction normal to the middle surface [**29**,**73**]. Using thin plate theory Timoshenko derived an equation for the critical buckling load of a plate loaded in compression [**74**]. The critical buckling load of a plate can be defined as:

"A plate buckles when the in-plane load gets so large that the originally flat equilibrium state is no longer stable and the plate deflects into a nonflat configuration." [**29**].

After buckling the in-plane stiffness of the panel has been reduced. Corrugated board can either buckle globally, as seen in Figure 2.15, or locally, as seen in Figure 2.16. In this project global buckling will be referred to as buckling.

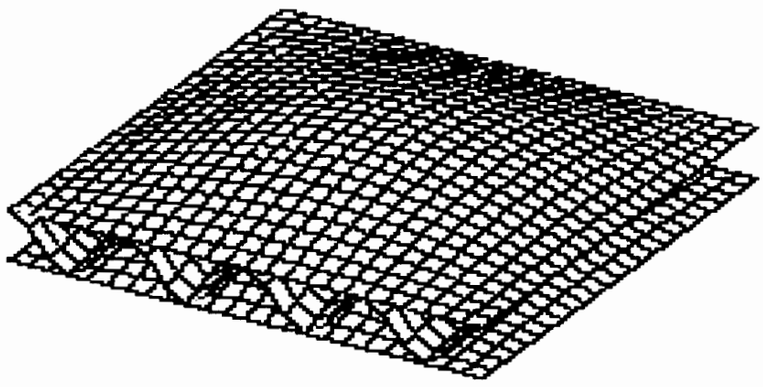

Figure 2.15: The global buckling of corrugated board [5].

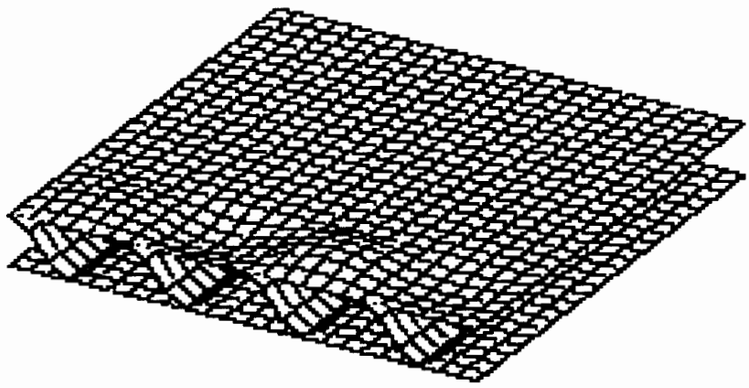

Figure 2.16: The localised buckling of corrugated board [5].

Timoshenko's equation for the critical buckling load of a thin plate states that:

$$N_{cr} = \frac{4\pi^2 D}{W^2} \qquad \textbf{2.12}$$

where:

N_{cr} = Critical buckling load per unit width

D = Flexural rigidity of the plate

W = Plate width

The stiffness of a plate has a large influence on the critical buckling load of the plate and therefore the importance of the elastic modulus of the material cannot be ignored [**57**]. Research has shown that the assumptions of thin plate theory lead to an overestimation of the critical buckling load of orthotropic plates. The result is that the transverse shear stresses cannot be ignored [**36**]. Recent research has focused on finite element codes for more theoretical corrugated board strength analysis [**27**]. In particular, researchers have attempted to incorporate the uncertainties of corrugated board into these models.

The uncertainties being [**27**]:

- Material properties
- Geometric properties including imperfections
- Loads, stack heights, duration of load and mishandling
- Environmental conditions

The other focus of the recent corrugated board research is to evaluate the risk of board buckling without excessive numerical calculation resulting in decreased analysis costs [**28**]. The use of computer based corrugated cardboard box models will result in improved product design and the reduction of costly mechanical testing. This will stem from a thorough understanding of box compression and corrugated board strength and will allow for either the reduction of material needed for a given box or for unique design innovations that will allow corrugated board to become more competitive with other packaging materials [**75**].

2.4.4.1 The Maltenfort Formula for Box Strength Prediction

One of the first empirical formulae to be used for predicting BCS was the Maltenfort formula that was published in 1956 [**27**]. Maltenfort's formula related BCS to box dimensions using statistical methods such as linear regression. His work was based on 14 800 tests on single-wall board boxes in top, side and end compression [**37**]. His formula can be written in the form:

$$P_{col} = 2090 + Z\left(\frac{350}{L/W + 1} + 328\right) - 237E \qquad \textbf{2.13}$$

where:

P_{col} = Collapse load of box

W = Panel width

L = Panel length

E = Box depth

Z = Box perimeter

The major limitation of this formula is that it does not take into account material effects i.e. board properties [**48**]. However, it does provide a useful formula for comparing the maximum load obtained for a square box against the maximum load obtained for a rectangular box. Urbanik has found that treating a rectangular box as a square induces a 7% strength error [**37**].

2.4.5 The McKee Formula for Box Strength Prediction

The McKee formula was based on the idea that the edge compression strength of corrugated board was the major property influencing the BCS. This is due to the fact that during a BCT, the box fails at the vertical edges and this triggers total box failure. However, McKee also stated the importance of flexural rigidity of the combined board in the MD and CD as contributing to the total BCS. The McKee formula is a semi-empirical post-buckling formula applicable to thin plates constructed from a linear material [**60**]. McKee initially related the compressive strength of a plate to its instability load and edgewise compression strength by means of a power function:

$$P_{col}/P_{cr} = c\left(P_m/P_{cr}\right)^b \qquad \textbf{2.14}$$

where:

c, b = Constants obtained from the experimental data by plotting:

$\log\frac{P_{col}}{P_{cr}}$ verses $\log\left(\frac{P_m}{P_{cr}}\right)$. The slope of the curve is b and the y-intercept log c [**68**]

P_{col} = Collapse load of the plate

P_{cr} = Critical buckling load

P_m = Edgewise compression load

$$P_{col} = cP_m{}^{b} P_{cr}{}^{1-b} \qquad \textbf{2.15}$$

Equation 2.14 is the equivalent to Equation 2.15 and will be referred to as McKee Formula 1 in this document. The total BCS can then be computed by calculating P_{col} for each panel, by means of Equation 2.14 or 2.15, and then summing over all four panels. An alternate method is to multiply P_{col} by the width of the panel and then sum over all four panels. P_{cr} is calculated from the theory of buckling of plates. An estimate of this value is obtained through use of Equation 2.16.

$$P_{cr} = 12k_{cr}\sqrt{D_{11}D_{22}}/W^2 \qquad \textbf{2.16}$$

where:

k_{cr} = Buckling coefficient $= \left[\left(\frac{\pi^2}{12}\right)\left[\left(\frac{r^2}{n^2}\right)+\left(\frac{n^2}{r^2}\right)+2K\right]\right]$

$r = \left(\sqrt[4]{D_{11}D_{22}}\right)\left(d/W\right)$

n = Number of half-waves in the buckled panel in the direction of the applied load

$n = 1$ if $r \le \sqrt{2}$

$n = 2$ if $\sqrt{2} \le r \le \sqrt{6}$

$n = j$ if $\sqrt{j(j-1)} \le r \le \sqrt{j(j+1)}$

D_{11} = Flexural stiffness of board in the MD per unit width

D_{22} = Flexural stiffness of board in the CD per unit width

K = Plate parameter

Equation 2.16 is based on the assumption that the stresses in the panel remain elastic up to the point of buckling and that the corrugated board is modelled as a thin orthotropic plate. The buckling coefficient k_{cr} depends on the manner of support of the edges as well as the material properties and plate dimensions. McKee assumed, in this case, that edges were simply supported i.e. the plate is free to rotate about the edges, but the edges are constrained [**65**]. In addition, the flexural rigidities of the plate do not involve any failure properties. This would involve a correction for transverse shear effects within the plate. However, McKee ignored this effect as he felt it only contributed a small amount to the overall strength of the box.

McKee's original testing involved experimentally determining P_m and P_{col} and calculating P_{cr} using Equation 2.16. The constants, c and b, were approximated as 0.5 and 0.76, respectively. This semi-empirical approach to BCS calculations is only valid for boxes of conventional construction and size. Results of tests carried out by McKee showed that using his formula, the BCS of a box could be predicted to within 7-8% error of the actual BCS value. Hahn *et al.* found that the McKee formula produces fairly good results [**68**]. In addition, McKee proposed simplifications to his formula for easier use. His first simplification was to approximate the plate parameter K with a value of 0.5. The value of r was then approximated with a value of 1.17. Further simplifications involved treating all boxes as a square to avoid calculating P_{cr} for each individual panel. These three simplifications led to the following formula for total box load which will be referred to as McKee formula 2.

$$P = c(4\pi)^{2-2b} P_m{}^{b} (\sqrt{D_x D_y})^{1-b} Z^{2b-1} k^{1-b} \qquad \textbf{2.17}$$

McKee made further simplifications by approximating k^{1-b} with a value of 1.33. He stated that this simplification is only valid for boxes with d/z greater than 0.13. This simplification is thus applicable to most RSC boxes. This led to Equation 2.18 which will be referred to as McKee formula 3.

$$P = aP_m{}^{b} \left(\sqrt{D_x D_y}\right)^{1-b} Z^{2b-1} \qquad \textbf{2.18}$$

where:

a = 2.028

b = 0.76

McKee correlated flexural stiffness to edgewise compression which resulted in two further simplifications of his formula which will be refereed to as McKee formula 4 and 5, respectively [**65**].

$$P = 5.874 P_m T_b^{0.508} Z^{0.492} \quad \textbf{2.19}$$

$$P = 5.87 P_m \sqrt{T_b} \sqrt{Z} \quad \textbf{2.20}$$

2.4.5.1 Disadvantages of the McKee Formula

The disadvantages of the McKee formula are:

- The comparison of flexural rigidities versus edge compression values, based on the fact that both increase with basis weight, is incorrect [**76**]. This questions the reliability of both Equation 2.19 and 2.20 for box design.
- It does not take into account board failure, i.e. transverse shear effects, which limit its use for advanced box design.
- The theory is based only on elastic buckling [**37**]. For thicker board panels inelastic material response should be considered [**68**].
- It is only applicable to RSC style boxes where the length is not greater than three times the width and the perimeter is not bigger than seven times the depth [**61**].
- It is based on the bending characteristics of solid panels [**77**].
- It does not account for unbalanced board combinations [**77**].

- It does not take into account manufacturing factors such as gluing and crushing [77].
- It does not allow for box optimisation [77].

The McKee formula showed an error of 6.1% from box grades with average mechanical properties. In addition the use of non-RSC style boxes has raised issues as to the acceptability of this method with regard to box strength prediction. The Maltenfort equation shows much better sensitivity to box length and width effects than the McKee formula [**61**]. In addition the McKee formula only takes into account bending stiffness and ECS. As corrugated board is considered an orthotropic material, the influence of transverse shearing affects and material properties such as Poisson's ratio and tensile moduli should not be underestimated. In addition the use of non-linear material theory has shown to be more sensitive to different box styles and is consistent with the Maltenfort results [**60**]. This has led to a number of different methods for corrugated board and ultimately box strength predictions.

2.4.6 The Hahn *et al.* Method for Critical Buckling Load Calculation

An alternate method for the calculation of P_c, based on orthotropic plate theory and elastic buckling was used by Hahn *et al* [**68**]. The proposed formula is shown below:

$$N_{cr} = (\pi^2 \left[\frac{L^2 D_{11}}{W^4} + \frac{2(D_{12} + 2D_{66})}{W^2} + \frac{D_{22}}{L^2} \right] \qquad \textbf{2.21}$$

where:

$$D_{12} = \frac{Q_{11} T_b^3}{12} \text{ and } Q_{11} = \frac{E_{11}}{1 - \nu_{12}\nu_{21}}$$

$$D_{66} = \frac{Q_{66} T_b^3}{12} \text{ and } Q_{11} = G_{12}$$

D_{66} is the twist stiffness of the corrugated board and can also be approximated by Equation 2.22 [**68**]:

$$D_{66} = 0.354(D_{11}D_{22})^{\frac{1}{2}} \qquad \textbf{2.22}$$

It was found that this method had good correlation with experimental data and the panel collapse load predicted by the McKee formula [**68**].

2.4.7 Nyman and Gustafsson's Method for Critical Buckling Load Calculations

Nyman and Gustafsson derived an expression for the critical buckling load of corrugated board, based on a laminated composite plate model, under combined loading conditions [**28**,**36**,**78**]. The expression was based on a simplified laminated composite plate type model and is shown in shown in Equation 2.23.

$$\hat{N}_{cr} = \frac{G}{60l^2\lambda^2(f_2\alpha + 2l^2\varsigma\mu + l^2\chi)R} \qquad \textbf{2.23}$$

where:

$\hat{N}_{cr}$ = The critical load per unit length

$G = \sum_{i=1}^{33} g_i$

$R = \sum_{i=1}^{27} r_i$

l = Flute wavelength

λ = Half buckling wavelength

μ = 0 for uniaxial loading

μ = 1.005 for shear loading

ζ = Shear load

χ = CD load

α = MD load

The expressions for the coefficients f_2, g_i and r_i can be found in [**28**,**36**,**78**]. Using this analytical expression they determined that the buckling load of anisotropic plates is 56% lower than pure buckling predictions when transverse shearing effects are accounted for [**28**]. Using this relationship, a failure criterion was developed to incorporate failure of corrugated board that was based on material and structural failure. The criterion was compared to the Tsai-Wu criterion, commonly used for paper materials and found to have good correlation with experimental values. The developed theory can be used in finite element modelling techniques (FEM) to predict corrugated board failure [**78**]. It was stated that in pure bending, failure of corrugated board is dominated by structural failure of the board. This indicates the importance of transverse shear effects [**78**]. This method was similar to that used by Allanson and Svärd who used FEM to model corrugated panels using a linear elastic material model and failure criterion that took into account both material and structural failure to model the collapse load of corrugated panels [**5**]. The importance of transverse shear effects on the buckling load of corrugated panels was highlighted.

2.4.8 Nordstrand's Method for Critical Buckling Load Calculations

Nordstrand has stated that the critical buckling load of orthotropic plates is affected by the transverse shear rigidities of the board. The effect of transverse shear rigidities is that the critical buckling load decreases with boards exhibiting low transverse shear rigidities, particularly in the MD of the board. A panel compression rig was designed to apply loads to the panels with known boundary conditions i.e. simply supported. The out of plane displacement was measured at the centre of the panel versus compressive load. The object of the test was to obtain the critical buckling load of the panel. It was found that a discrepancy of between 15% - 20% exists between the theoretically calculated critical buckling, based orthotropic plate theory, and the experimentally determined value. This discrepancy was attributed to neglecting transverse shearing affects. It was also found that the collapse of the panels was

similar to the failure load predicted by the Tsai-Wu failure criterion [**63**]. This indicates that the final failure of the panels is triggered by material failure of one of the liners [**63**]. Nordstrand has derived an analytical expression for the critical buckling load of edge loaded orthotropic panels that includes transverse shear effects based on a laminated shear deformable orthotropic linear elastic plate model [**38**]. The expression derived for the critical buckling load per unit length for a square panel is [**38**]:

$$k = \left(\frac{L}{\pi}\right)^2 \frac{P_{y,crit}}{\sqrt{D_{11}D_{22}}} \qquad \textbf{2.24}$$

where:

L = plate length

k = buckling coefficient = $\lambda\zeta + 2\eta + \frac{1}{\lambda\zeta}$ for an orthotropic plate not including transverse shear.

where $\zeta = \sqrt{\frac{D_{11}}{D_{22}}}$

$$\eta = \frac{D_{12} + 2D_{66}}{\sqrt{D_{11}D_{22}}}$$

$$\lambda = \left(\frac{L}{mW}\right)^2$$

Nordstrand found that this solution to the critical buckling of orthotropic plates results in a more accurate solution with a deviation of less than 0.5% when compared to FEM analysis. However, there is still a discrepancy between this value and the experimentally determined values. This has been attributed to the difficulty in evaluating the critical buckling load from the experimental results due to non-linearity of the material [**38**,**63**].

2.4.9 Urbanik's Method for Box Strength Prediction

The original box compression strength formula derived by Maltenfort and McKee was based on the assumption of linear material behaviour. This model was used for strength prediction of square boxes. Urbanik has found that applying a non-linear material model to the postbuckling characterisation of corrugated board leads to a more accurate prediction of box strength and is more applicable to non-square boxes with varying width and depth [**37**]. Urbanik produced a theory for the MD strength of corrugated board. During the service life of a box it is not always loaded in the CD, but also end to end or side to side. This has resulted in researchers advocating the importance of both MD and CD paper strengths for the maximising of box strength [**67**]. The importance of this is due to the fact that boxes are designed to carry load in top to bottom compression i.e. CD loading and thus the MD properties may be neglected or suffer due to this optimisation. Buckling theory has been used to show the importance of corrugated liner stiffness. Urbanik has stated that in the CD corrugated board strength can be increased by 1.75 due to the use of a rigid liner and in the MD the strength can be increased by 4 times due to use of rigid liners [**67**]. In addition, Urbanik has derived equations for the postbuckling strength of corrugated board based on linear and non-linear material models.

2.4.9.1 Urbanik's Elastic Buckling Model

For an infinite linear material plate the critical buckling load is given by:

$$P_{cr} = \frac{4\pi^2 \sqrt{D_{11} D_{22}}}{W^2} \qquad \textbf{2.25}$$

The box compression strength P is then given by $\sum P_{col} W$

where:

$$\frac{P_{col}}{P_m} = c\left(\frac{P_{cr}}{P_m}\right)^b \qquad \textbf{2.26}$$

2.4.9.2 Urbanik's Non-Linear Material Model

The material behaviour of paper has been found to follow the stress strain relationship given by:

$$\sigma = c_1 \tanh\left(\frac{c_2}{c_1}\varepsilon\right) \qquad 2.27$$

where:

c_1 = Ultimate stress of the board

c_2 = Initial slope of the stress strain curve in the CD

Urbanik has found that modelling corrugated board as a non-linear material resulted in box compression estimations being more sensitive to box dimension changes [**37**]. For a non-linear material the box compression strength P can be calculated by:

$$P = \sum P_m \alpha (\theta_0 \hat{\sigma})^{\eta} \qquad 2.28$$

Saliklis and Urbanik performed FEM predictions using various box models and found that method of using the non-linear material model combined with elastic model and the shear modulus correction produced the best correlation with experimental data. This method is applicable to box geometry beyond the original strength models [**79**].

2.4.10 Homogenisation Techniques

Aboura *et al.* proposed the use of an analytical model based on classical laminate theory to analyse the elastic behaviour of corrugated board [**1**]. The proposed method uses the mechanical and geometrical properties of the flutings and facings to predict the homogenised elastic behaviour of a corrugated board structure. The results obtained from their analytical model were compared to the results obtained from their mechanical testing of not only the constituents, but also of the corrugated board. By

using this analytical model and their experimental results Aboura *et al.* were able to analyse the geometrical affect of corrugated board on the mechanical properties of the board. They found that E_{11} and the bending stiffnesses (D_{11}, D_{22}) are influenced by the total thick ness of the corrugated board whereas E_{22} is affected more by the fluting pitch. They further modelled corrugated board using two separate methods. The first is commonly used in the literature and is based on the constituent geometry and properties. The second method was a simplified model based on a homogenisation technique. It was found that the second method used was fairly accurate and 10 times faster than the conventional method. It produces a fast and effective method for analysing corrugated board panels in the preliminary and optimum design phases [**1**].

CHAPTER 3

DESIGN OF TESTING JIGS

During the course of this project three testing fixtures had to be designed. Of these fixtures, only one can be considered innovative and new, as the others adhered to the relevant standards for that particular testing method. In the following paragraphs the three designs will be discussed.

3.1 The MD Shear Stiffness Fixture

One of the major requirements of this project was to design an apparatus that could be used to perform the McKinlay MD shear test. In this regard it was required that the apparatus had to fit onto an existing universal testing machine. The apparatus had to be designed so that it could be used at the Centre for Materials Engineering and at Nampak R&D. This influenced the design as the two institutions had different universal testers.

3.1.1 The McKinlay Test

The details of the McKinlay test were obtained from United States Patent 4,958,522 [**40**]. The test method requires an apparatus for measuring the structural properties of corrugated board. It requires that a corrugated specimen be placed in two axially aligned jaws. The specimen is then subjected to a twisting force due to the rotation of one jaw with respect to the other. The force and the angle of deflection are then

measured. This data is then used to measure the structural property of the board i.e. the MD shear stiffness.

3.1.2 The Design Requirements of the MD Shear Fixture

The design requirements were for an apparatus that:

- Had to have two axially aligned jaws.
- The one jaw had to move relative to the other i.e. rotate under load.
- The load and angle of rotation of the specimen had to be measured and recorded.
- The torque required to cause a deflection had to be measured and recorded.
- The apparatus had to be used in a universal testing machine.
- The apparatus had to used at Nampak R&D due to the standard humidity and temperature requirements for the testing of corrugated board.

3.1.3 Conceptual Ideas

During the course of the design process five ideas were considered. These conceptual designs will be dealt with in the following paragraphs.

3.1.3.1 Conversion of a Universal Testing Machine into a Torsion Testing Machine

The first conceptual idea was to convert a standard universal testing machine into one that could carry out torque measurements. The primary part of this design was to replace the existing load cell within the machine with a torque cell. It would also be necessary to add a rotary component to the universal tester. This would be in the

form of a stepper motor or a hydraulic unit. It would then be necessary to convert the software used by the machine to record the relevant data and control the rig [**80**].

3.1.3.2 A Lever Arm System

The second conceptual idea was to have a lever arm of known distance attached to the crosshead of the universal tester through a coupling. The force required to cause a certain rotation could be recorded. As the length of the moment arm is known, the moment applied to the specimen could then be calculated. The lever arm would be attached to the shaft. The shaft would be attached to the grip, which would then rotate when the load was applied. The second grip would be axially aligned with the grip attached to the shaft, but would be permanently fixed. This would result in the test specimen, placed in the grips, being placed in torsion. A sketch of this idea is shown in Figure 3.1.

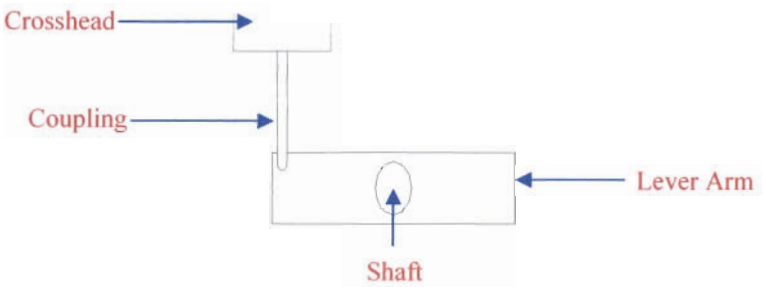

Figure 3.1: The second conceptual idea utilising a lever arm system to place the specimen in torsion.

3.1.3.3 A Rack and Pinion System

The third conceptual idea was to convert the vertical movement of the universal tester into rotation using a rack and pinion system. The rack would be attached to the crosshead of the universal tester. The rack would then be meshed to the pinion. The pinion in turn would be connected to a shaft on which the one grip is attached. The other grip would be axially aligned, but permanently fixed. The specimen would be placed in between the grips. As the crosshead moves up, the movement would be

resisted by the stiffness of the corrugated board resulting in a twisting moment being applied to the corrugated board specimen. A sketch of this idea is shown in Figure 3.2.

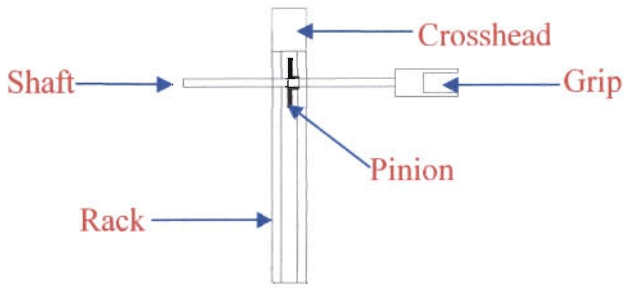

Figure 3.2: The third conceptual idea using a rack and pinion system to place the specimen in torsion.

3.1.3.4 A Pulley and Cable System

The fourth conceptual design idea was to have a lever arm of known distance attached to the crosshead of the universal tester through two pulleys and a steel wire. The lever arm would be connected to a shaft which would have a grip attached. The second grip would be axially aligned and permanently fixed. As the crosshead moves vertically the steel cable would apply a force to the lever arm, reduced through the pulleys. The lever arm would rotate and apply a moment to the shaft and the grip. This would result in a moment being applied to the specimen. A sketch of this idea is shown in Figure 3.3.

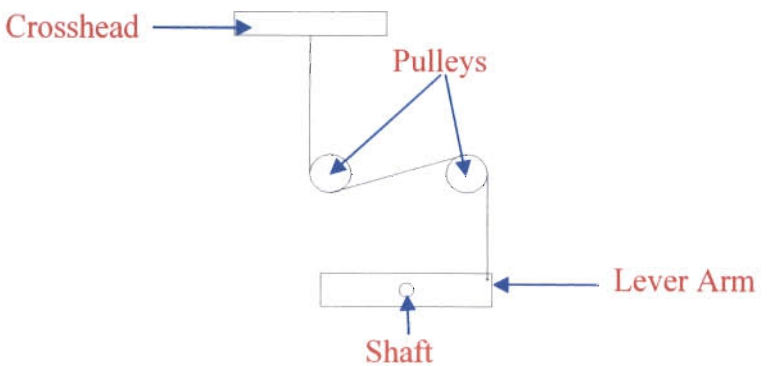

Figure 3.3: The fourth conceptual idea utilising a pulley and cable to place the specimen in torsion.

3.1.3.5 A Chain Drive System

This design was similar in concept to the rack and pinion design. However, instead of using a rack, a bicycle type chain and a sprocket would be used to convert the vertical movement of the crosshead into rotation. The bicycle chain would be attached to the crosshead. The chain would be meshed with a sprocket that would be attached to a shaft. The shaft would have one of the grips attached to it. The second grip would be axially aligned with the first grip, but permanently fixed. As the crosshead moves up, the chain applies a moment to the sprocket. This would result in the rotation of the shaft and grip with respect to the other grip. The corrugated specimen would therefore be placed in torsion.

3.1.4 Design Decision

The decision of which design to use was based on the design requirements in 3.1.2. Cost and ease of use also played a major part in the decision. All the designs mentioned will be discussed in the following paragraphs.

3.1.4.1 Conversion of a Universal Testing Machine into a Torsion Testing Machine

The conversion of a universal testing machine into a torsion testing machine would require a large amount of technical knowledge and work. The cost of a torsion load cell and rotary components alone would be substantial. In addition, the rig would need to be calibrated after the modifications had been made, which would result in an additional cost. Another major limitation was that the components could not be easily transferred to the Nampak R&D universal tester and thus components that would fit Nampak's rig would also need to be purchased. In addition, Nampak R&D did not want to permanently transform their tester into a torsion tester as they use their tester on a daily basis and it was not practical to try and remove load cells and other devices every time they wanted to measure tension or compression.

3.1.4.2 A Lever Arm System

The lever arm system appeared to be a very simple solution to the problem. However, due to the type of connection between the lever arm and the crosshead, the moment arm distance would change as the load was applied. This would significantly affect the test results. It was decided that the load should always be applied perpendicular to the lever arm or other rotation device to ensure that a uniform moment arm distance was maintained.

3.1.4.3 A Rack and Pinion System

The rack and pinion system was a simple solution to the problem. It would apply a moment to the shaft with the grip attached without the moment arm distance changing. In addition, it would also be fairly inexpensive and the manufacturing required would be kept to a minimum. However, the major concern with this design was the accuracy of the meshing between the pinion and the rack. It was felt that if a standard module gear was used, the rig would not be sensitive enough to accommodate the low loads that would be expected during the testing of the corrugated specimens. If this idea were to be used a half module or 0.8 module gear would need to be used.

3.1.4.4 A Pulley and Cable System

This idea would be more complicated than the two previous ideas as the load would be divided between the number of pulleys that were to be used. It was felt that this could result in inaccurate load readings during testing which would compromise the experiment. In addition, the pulley system would require more space than the previous design ideas. Due to the spatial limitations of the rig at Nampak R&D this would be undesirable.

3.1.4.5 A Chain Drive System

The chain drive system also appeared to be a simple solution to the problem. However, the limitation of this design was that it would require a very fine chain and sprocket to achieve the desired accuracy with respect to the load application. It was felt that this design idea would result in excessive noise during testing which would be an undesirable feature.

3.1.4.6 Concluding Remark

In conclusion it was felt that of all the design ideas, the rack and pinion design would be the most suitable. This was due to its ease of operation, the fact that it would require a minimum amount of machining, have a lower cost than all the other designs and also provide the accuracy which was required by the author.

3.1.5 Detail Design

The designed MD shear fixture is shown in Figure 3.4 and Figure 3.5. The design drawings can be found in *Appendix A*.

3.1.5.1 The Pinion of the MD Shear Fixture

The pinion used in this design was a Duracon 0.8 module gear with a 20° pressure angle purchased form RS Components [**81**]. It was decided to use a pinion with 80 teeth. This was the maximum number of teeth for this module gear. The reason for this choice was the fact that the author desired a gear diameter of 60mm or greater. This allows for a maximum moment to be applied to the shaft with a minimal load. The Duracon gear is injection moulded from a polyoxymethylene resin. This ensures that the gear has good mechanical, chemical and thermal properties [**82**]. A polymeric gear was chosen to reduce friction and wear between the rack and pinion.

As the crosshead of the universal tester moves vertically, the rack moves tangentially to the pinion which results in the subsequent rotation of the gear and shaft. The grip attached to the shaft rotates with this movement, placing the specimen in torsion. The moment applied to the specimen is dependent on the gear diameter and the force applied.

During manufacture the Duracon gear failed due to overload and it was necessary to replace the gear with a module 1 phosphor bronze gear. This would ensure that failure in overload would not occur and the pinion would still have good friction and wear properties in relation to the rack. The module was slightly higher than that previously required. However, the author felt that it would be sufficient for the test requirements.

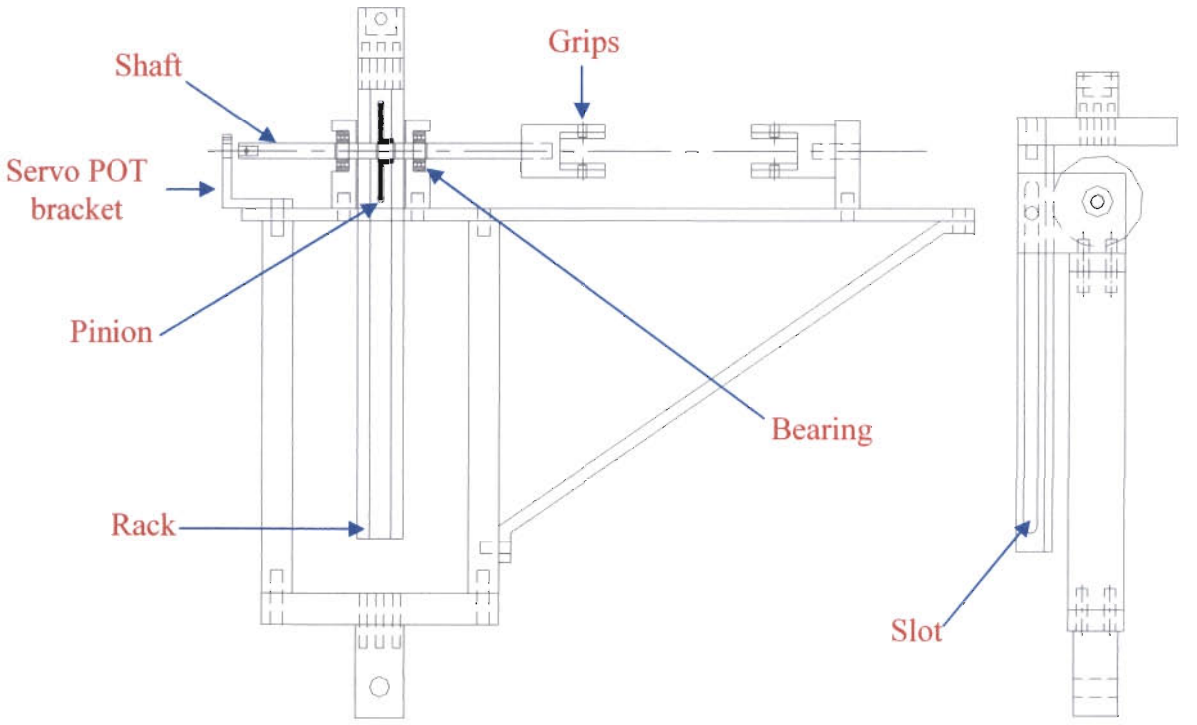

Figure 3.4: Design drawing of the MD shear fixture.

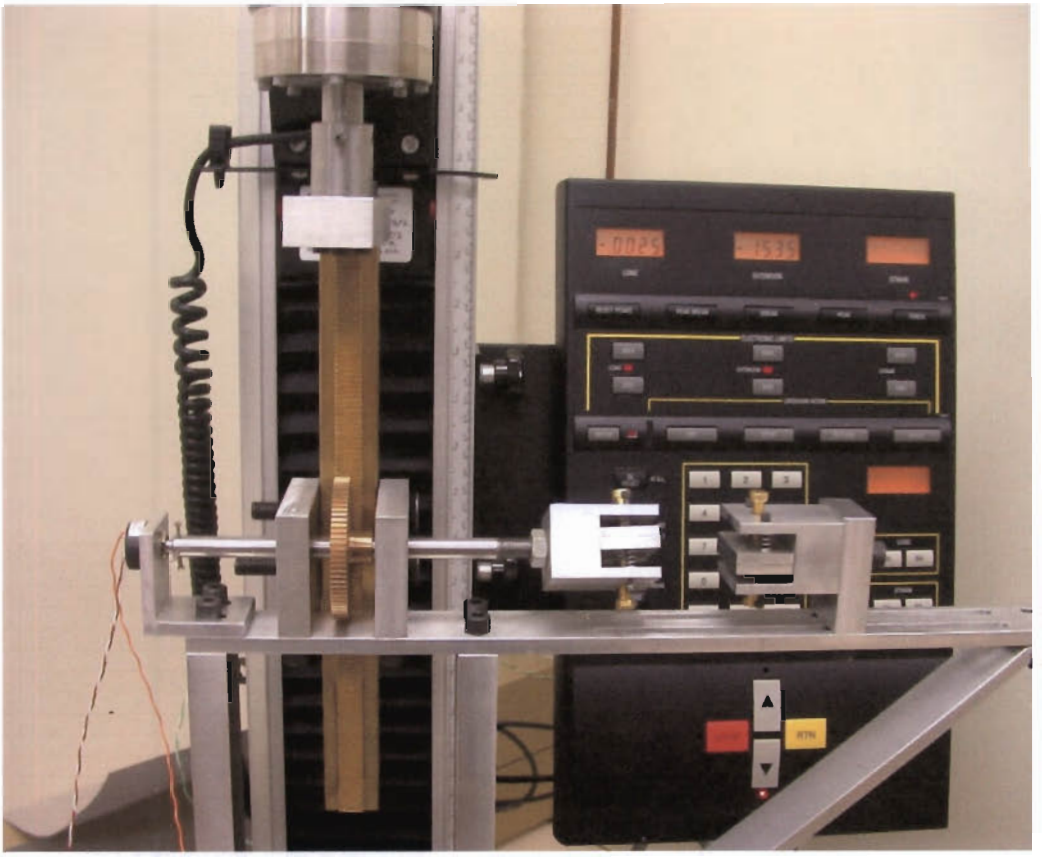

Figure 3.5: The MD shear fixture and peripheral instrumentation installed at Nampak R&D.

3.1.5.2 The Rack of the MD Shear Fixture

The rack was manufactured from brass. This was to ensure reduced friction and wear between the pinion and the rack. The rack was made long enough to ensure that during one test the gear would be allowed to complete two full rotations. This was due to the fact that the author was unsure of exactly what was considered to be a small angle of twist as mentioned by McKinlay [**40**]. The rack was attached to the cross head and would apply a tangential force to the gear as the crosshead moves upwards or downwards in the vertical plane. A slot was machined in the rack and a pin inserted into the bearing housing to ensure that the gear always moves tangentially to the pinion. The rack and pinion system is shown in Figure 3.6.

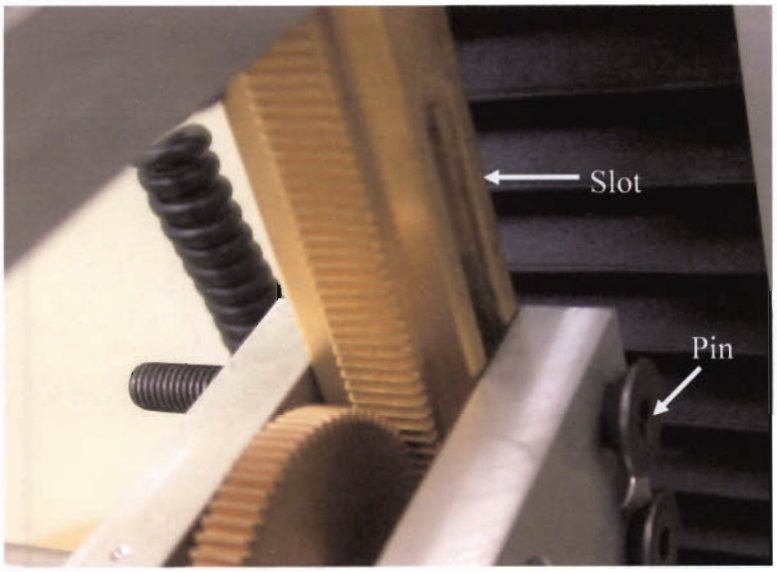

Figure 3.6: An enlarged view of the rack and pinion drive system.

3.1.5.3 The Shaft and Bearings of the MD Shear Fixture

The shaft was manufactured from stainless steel to reduce corrosion and had one threaded end to allow for the attachment of the grip. In addition, a hole was drilled through the shaft to allow for the attachment of the pinion. Recesses were machined into the shaft to allow the shaft to be fixed between the bearings through the use of circlips. The bearings were needed to ensure the smooth rotation of the shaft and to limit loads that could be induced due to resistance to rotation.

3.1.5.4 The Grips of the MD Shear Fixture

The grips, shown in Figure 3.7, were machined from aluminium. Originally the grip plates were only held by a single screw. However, after the initial trials, it was found that this situation allowed the specimen to rotate in the grips which was unacceptable. The grips were then modified to consist of extra stabiliser screws and springs to keep the grip plates parallel at all times as shown in Figure 3.7.

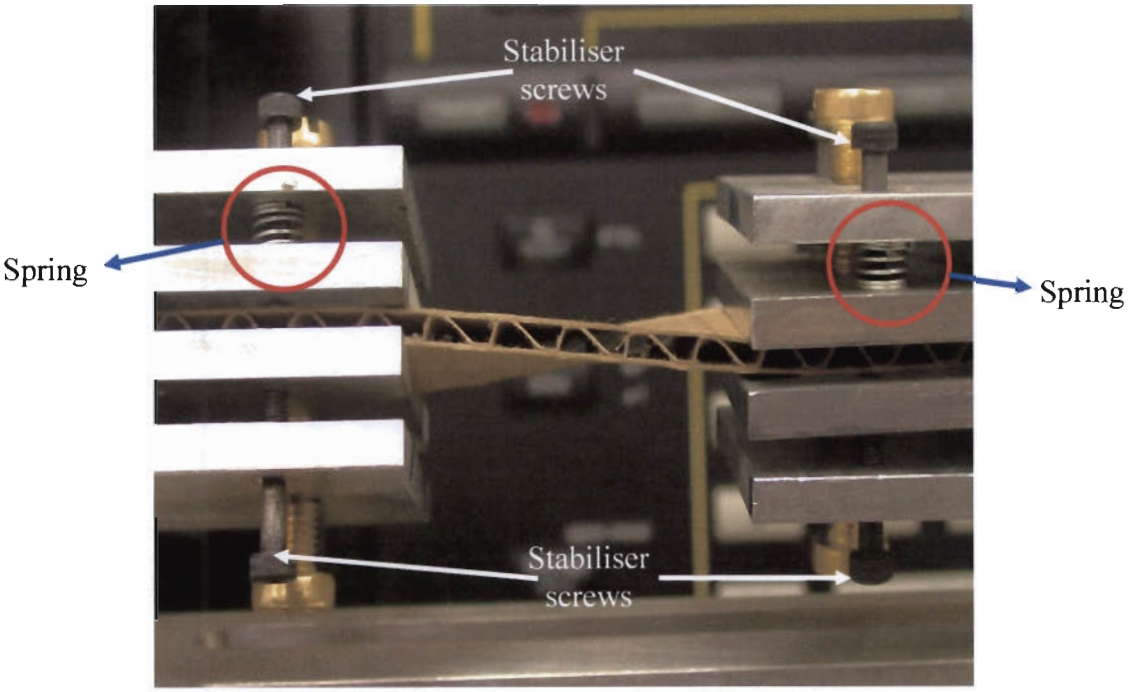

Figure 3.7: The modified grip system with extra screws and springs.

3.1.5.5 The Servo Potentiometer of the MD Shear Fixture

The total rotation of the shaft, and thus the corrugated specimen, had to be measured up to failure. It was decided that this could be achieved through the use of a servo potentiometer (servo POT). The servo POT would be mounted in a bracket shown in Figure 3.8. The shaft of the servo POT is inserted into the shaft and secured through three screws. This allows for the total rotation of the specimen in relation to the load and applied moment to be recorded electronically.

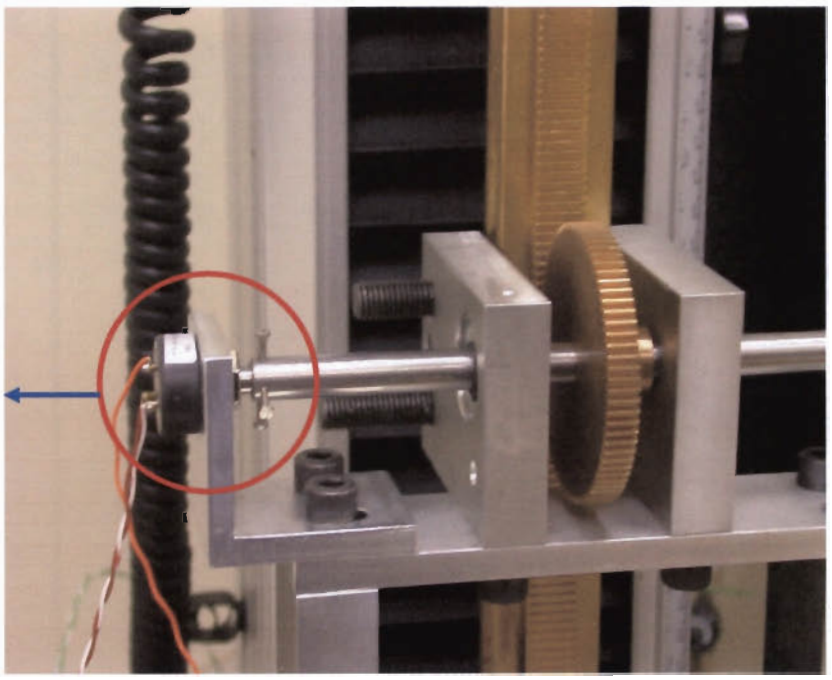

Figure 3.8: The servo potentiometer attached to the MD shear fixture shaft.

3.2 Block Shear Fixture

The block shear fixture was designed according to ASTM C 273-61, for shear properties in flatwise plane of flat sandwich constructions or cores [**41**].

3.2.1 The Block Shear Fixture Design Requirements

The block shear fixture had to be designed so that the line of action of the tensile force had to pass through the diagonal corners of the corrugated board specimen as shown in Figure 3.9. It was desirable to make the experimental process as easy as possible. Part of the problem with the ASTM C 273-61 test method, is the fact that the specimen needs to be glued to the surface of the plates. This requires the experimenter to glue the specimen to the plates, wait for the adhesive to set and then clean the plates before the next specimen can be tested. It was felt that this would be a tedious operation considering the number of specimens to be tested. In addition, this would be an unnecessary waste of time considering the possible use of this

method in a quality control situation i.e. in a research facility such as Nampak R&D. It was required that the method be easy to reproduce and be as time efficient as possible and that the displacement of the plates be measured, in-plane, relative to one another.

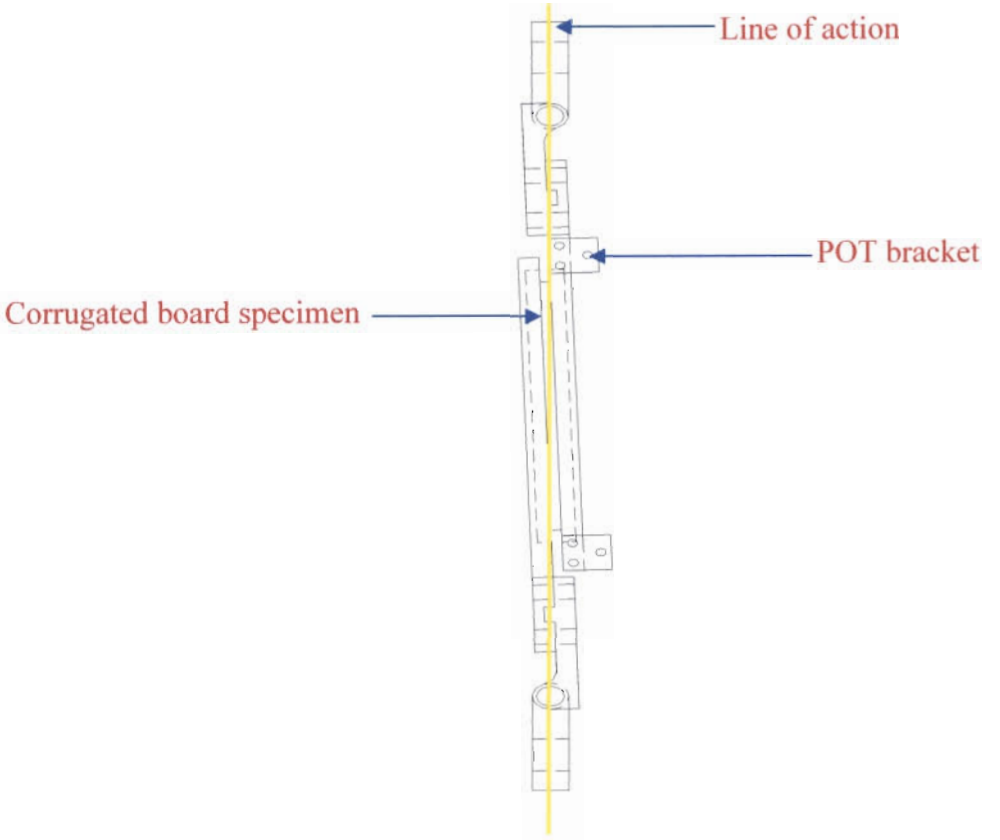

Figure 3.9: The side view design drawing of the block shear fixture.

3.2.2 The Detail Design of the Block Shear Fixture

The fixture design is shown in Figure 3.9. The complete design drawings are included in *Appendix B*. The fixture was manufactured out of aluminium to make it as light as possible to reduce the possibility of shearing the corrugated board specimens before the test had even begun. This was consistent with the fixture designed by Nordstrand and Carlsson [**19**]. The in-plane displacement of the plates, relative to one another, was measured using a slider potentiometer (**POT**) that would be attached to the brackets shown in Figure 3.9. The values of the displacement would be electronically recorded allowing the experimenter to plot the displacement

of the specimen as a function of the applied load. The slider POT was the perfect method to measure the plate displacement, as the slider POT records linear displacement and is cost effective as compared to more expensive measurement devices such as LVDT's. In addition, the slider POT gives good reliability, is robust, has a 50 000 cycle lifespan and a larger displacement of 100mm compared to about 30mm for a LVDT.

The plates of the block shear fixture were designed to allow for a wooden insert to be placed inside them. These wooden inserts would be fixed to the plates through the use of placement screws. This ensures that the inserts cannot be removed during the test and that the tensile load would be applied directly to the specimen. A plate is shown in Figure 3.10. The corrugated board specimen would be glued directly to the wooden inserts. This allows for all the specimens to be glued at the same time and consequently all the specimens could be tested in one session.

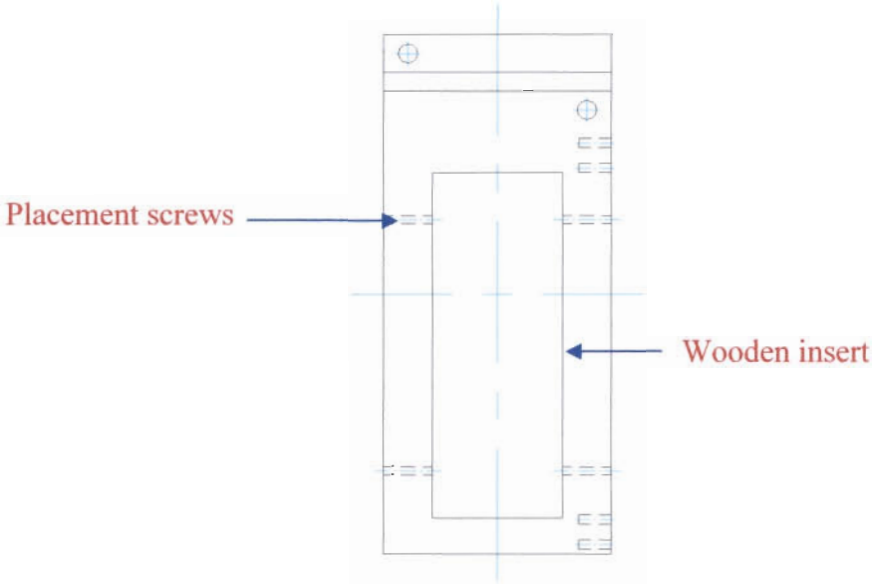

Figure 3.10: A block shear fixture plate with a recess to allow for the placement of the wooden inserts.

3.3 Bend Fixture

A bend fixture was designed according to ASTM C393-62 for the flexural properties of flat sandwich constructions [**83**]. In addition, Tappi Standards T 820 cm-00 and T 836 om-02 [**84,85**] were consulted for methods specific to the flexural testing of corrugated board.

3.3.1 Design Requirements for the Bend Fixture

The major requirement of the bend fixture is that it had to be able to be used for both 3-point and 4-point bend testing. This was important as both of these test methods were to be used in the experimental characterization of the corrugated board. The bend fixture needed to be designed so that the top loading platen would be fairly light to prevent damage of the board prior to testing. In addition, the size of the rollers was of concern, due the fact that smaller diameter rollers would result in localized crushing of the board in the areas of contact. This would affect the flexural results of the test. It was also desired to measure the mid-span deflection of the corrugated board specimens electronically to enable the plotting of the load deflection curves for each specimen.

3.3.2 The Detail Design of the Bend Fixture

The designed bend fixture can be seen in Figure 3.11 and Figure 3.12. The complete design drawings are included in *Appendix C*.

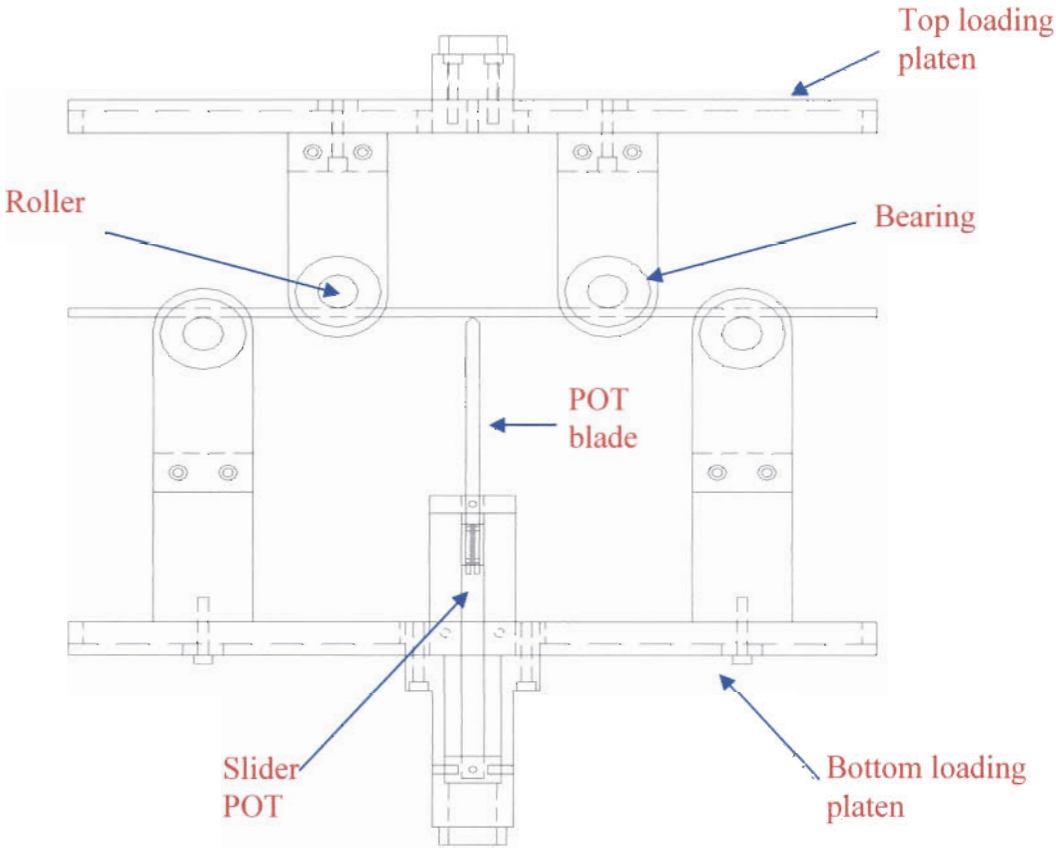

Figure 3.11: The front view design drawing of the bend fixture.

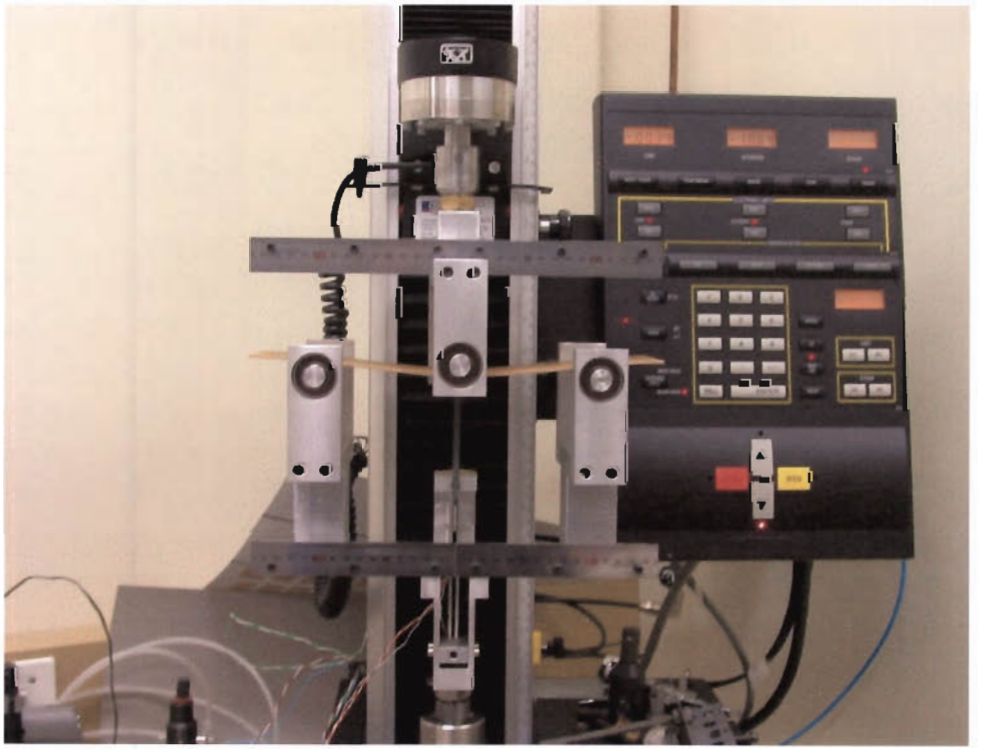

Figure 3.12: The bend fixture and peripheral instrumentation installed at Nampak R&D.

3.3.2.1 The Top Loading Platen of the Bend Fixture

The top loading platen was manufactured from aluminium. It was important to make the top platen as light as possible, but not sacrifice the rigidity of the platen as a whole. In addition, the cost of the fixture was to be kept to a minimum. T 820 cm-00 recommends the use of a magnesium alloy for this part of the design. It was felt that this would add unnecessary expense to the design and that the properties of aluminium were superior to that of the magnesium alloy.

3.3.2.2 The Rollers of the Bend Fixture

The diameter of the rollers was an important consideration. The Tappi standard T 820 cm-85 suggests a roller diameter of 3.18mm. It was felt that using this roller diameter would lead to premature board failure at the loading edge, considering the pitch of the corrugated board to be tested. The roller diameter used by Nordstrand and Carlsson was considered to be a better solution [**19**]. The rollers were designed to have a diameter of 15mm. These rollers also allow for the possibility of fitting a polymer collar over the roller should localised crushing occur. In addition, the rollers were mounted on bearings to allow the rollers to move with board deformation. This reduces the risk of localized crushing.

3.3.2.3 The Slider Potentiometer of the Bend Fixture

A bottom loading platen was designed to allow a slider POT to fit through the centre of the platen. The POT was mounted on a bracket allowing it to stand perpendicular to the plane of the board specimen. It was decided to use a slider POT for the deflection measurements as the slider POT is less expensive than an LVDT and has a greater travel. A nylon blade was glued to the slider POT to allow the measurement of the specimen's deflection.

CHAPTER 4

EXPERIMENTAL PROCEDURE

4.1 Testing Conditions

Due to the hygroscopic nature of paper, all specimens were conditioned and tested according to Tappi T 402 standard conditioning and testing atmospheres for paper, board, pulp handsheets and related products [**86**]. According to this standard, all corrugated board specimens were conditioned under 50.0% ± 2.0% relative humidity (RH) and 23.0 ± 1.0°C for 24 hours. These testing conditions must be used, as compression strength is very sensitive to moisture content. An increase of 1% moisture content can lead to a decrease in strength of about 8%. A 1% moisture increase is associated with a change in RH from 50% to 60%. Bending stiffness and tensile stiffness are also adversely affected by the moisture content [**58**].

4.2 Corrugated Board Sample Notation

The notations used for the various corrugated board samples tested are listed in Table 4.1. In Table 4.1 all the board combinations refer to virgin liner, except where otherwise stated. The notation used here will be used throughout this project. The first set of numbers refers to the liner grammage. The middle set of numbers refers to the fluting grammage and the letter refers to the flute profile. The notation VR after the first two sets of numbers refers to a board combination with one recycled liner and one virgin liner. The notation R after the first two sets of numbers refers to a board combination with recycled liners. The notation VU after the first two sets of numbers refers to a board combination with one virgin liner and one uniliner, where a uniliner

is a mixture of virgin and recycled fibre. The number set at the end refers to the year of manufacture. For example, 140-112B VR 04 refers to a board combination consisting of 140g/m² liners with a 112g/m² flute with a B type profile, with a virgin and a recycled liner, manufactured in 2004.

Block Shear Test	MD Shear Test	3-Point Bend Test	Corrugated Board Tensile Test	ECT Test	BCT Test
140-112B VR 04	140-112E 04	140-112E 04	140-112E 04	140-112E 04	140-112E 04
140-112C 03	140-112B 03	140-112B 03	140-112B 04	140-112B 03	140-112B 03
250-112B 03	140-112B 04	140-112B 04	140-112B VR 04	140-112B 04	140-112B 04
250-160C 03	140-112B VR 04	140-112B VR 04	140-112C R 04	140-112B VR 04	140-112B VR 04
	140-112C 03	140-112C 03	175-112B 04	140-112C 03	140-112C 03
	140-112C R 04	140-112C R 04	175-112C VU 04	140-112C R 04	140-112C R 04
	175-112B 04	175-112B 04	250-160B 04	175-112B 04	175-112B 04
	175-112C VU 04	175-112C VU 04	250-160C 04	175-112C VU 04	175-112C VU 04
	250-112B 03	250-112B 03		250-112B 03	250-112B 03
	250-160B 04	250-160B 04		250-160B 04	250-160B 04
	250-160C 03	250-160C 03		250-160C 03	250-160C 04
	250-160C 04	250-160C 04		250-160C 04	

Table 4.1: Corrugated board sample notation for all tests performed.

4.3 Block Shear Tests

Block shear testing was carried out to calculate the shear stiffness of the corrugated board specimens in the MD. This was necessary to compare the MD stiffness calculated form the block shear test to that recorded using the MD shear stiffness tester.

4.3.1 Specimens

Specimens for the block shear testing were designed according to ASTM Standard C 273-61 [**41**]. According to this standard, the width of the specimens must be more than twice the thickness and the length more than 12 times the thickness. Accordingly, it was decided to use specimens of the same dimension as used in the ECT, namely a rectangular specimen of dimensions 100mm ± 0.5mm by 25 mm ± 0.5mm in accordance with ISO 3037:1994(E) [**88**]. The board combinations tested are listed in Table 4.1.

4.3.2 Block Shear Test Procedure

A fixture for the block shear testing was designed according to ASTM Standard C 273-61 [**41**]. The design of this fixture is discussed in *Chapter 3*. The block shear specimens were glued to the wooden inserts using an epoxy-based adhesive. The fixture was attached to an Instron 4444 universal tester as shown in Figure 4.1.

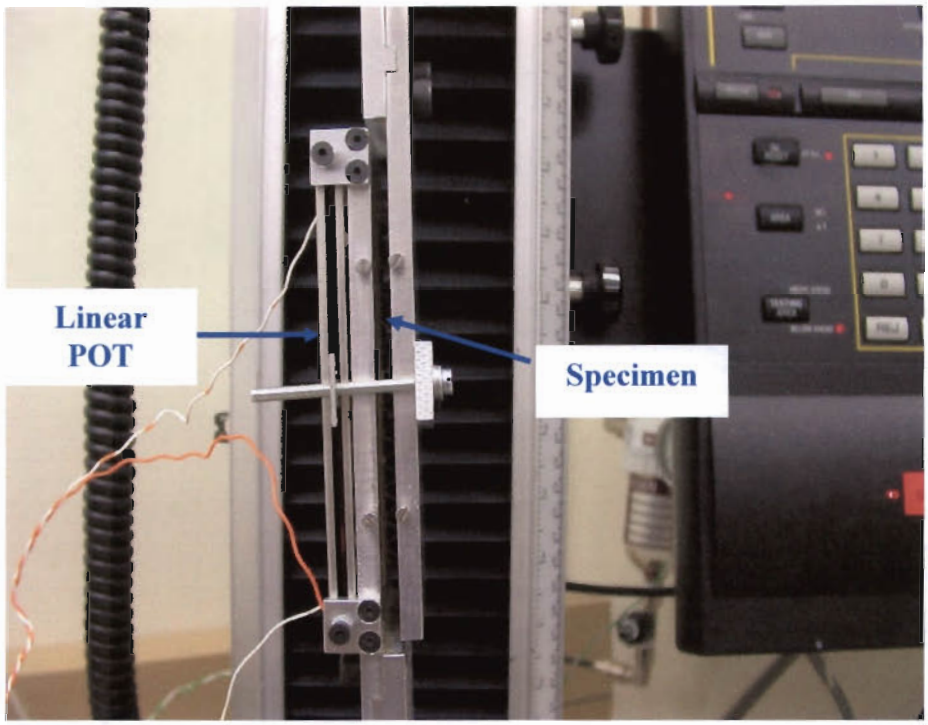

Figure 4.1: The block shear fixture during testing.

The specimens were conditioned and tested under the conditions laid out in Tappi T 402 at a crosshead speed of 3mm/min, as used by Nordstrand and Carlsson [**19,86**]. The load and relative plate displacement was recorded electronically using a DAQsi data logger. On completion of the test, the load versus displacement plot for the specimen was generated. The shear stress is calculated through use of Equation 4.1.

$$\tau = \frac{X}{LW} \qquad \textbf{4.1}$$

where:

τ = Shear stress
X = Load
L = Specimen length
W = Specimen width

The shear strain is calculated through the use of Equation 4.2.

$$\gamma = \frac{o}{T_b} \qquad \textbf{4.2}$$

where:

γ = Shear strain

o = Displacement of one plate relative to the other

T_b = Board caliper

The shear modulus of the specimen is then obtained by using Equation 4.3.

$$G = \frac{\tau}{\gamma} = \frac{X}{o}\frac{T_b}{LW} \qquad \textbf{4.3}$$

The value of X/o is obtained from the slope of the load displacement curve. On completion of the tests, the arithmetic mean, the standard deviation of the mean and the standard deviation of the sample were determined.

4.4 The MD Shear Test

MD shear testing was carried out to determine the stiffness of corrugated board in the MD. This is an important test method as it can be used in the processing of corrugated board to give an indication of board properties. The method consists of applying a twisting force to a corrugated board specimen.

4.4.1 MD Shear Test Specimens

Specimens for the MD shear testing were designed according to a patent compiled by McKinlay [**40**]. The specimen dimensions are the same dimensions as used in the ECT, namely a rectangular specimen of dimensions 100mm ± 0.5mm by 25 mm ± 0.5mm. Specimens were cut in the MD so that the width across the test piece did not vary more than 0.1mm in accordance with ISO 3037:1994(E) [**88**]. The board specimens tested are listed in Table 4.1.

4.4.2 The MD Shear Test Procedure

A fixture was designed to carry out the MD shear test according to United States Patent 4.958,522 [**40**]. The design of the fixture is discussed in *Chapter 3*. The fixture was attached to an Instron 4444 universal tester. All specimens were conditioned and tested according to Tappi T 402 [**86**]. The specimen is placed in the jaws of the testing device. A crosshead speed of 3mm/min was used to apply a load to the pinion of the testing device. During the test, the load, angle of twist and the applied moment (M) were electronically recorded using a DAQsi data logger. The M versus $K\vartheta$ graph was then plotted. The MD stiffness was then calculated using Equation 4.4.

$$M = K\vartheta S \qquad \textbf{4.4}$$

where:

K = $\frac{4a^3}{3L}$ where a is half the sample width and L the free length

M = Applied moment Nm.

S = MD stiffness

ϑ = Angle of rotation

On completion of the tests, the arithmetic mean, the standard deviation of the mean and the standard deviation of the sample were determined.

4.5 The 3-point Bend Tests

3-point bend tests were carried out to determine the flexural stiffness of corrugated board in the MD and CD. These values were then compared to the predicted values. The results of these tests are used in the calculations of the critical buckling load of orthotropic plates.

4.5.1 3-Point Bend Test Specimens

Specimens were cut to dimensions of 300mm by 100mm ± 0.25mm [**85**]. These dimensions are in accordance with ASTM C393-62 [**83**]. This allows for a span length of 200mm. The specimens were cut by Nampak Corrugated. The board combinations tested are listed in Table 4.1.

4.5.2 3-Point Bend Test Procedure

The specimens were conditioned and tested according to Tappi T 402 [**86**]. Prior to testing, the thickness of the specimen was measured using a digital calliper. Testing was carried in accordance with Tappi standards T 820 cm-00 and T 836 om-02 [**84**,**85**]. The tests were conducted at a crosshead speed of 3mm/min, as used by Nordstrand and Carlsson [**19**]. The testing was performed on an Instron 4444 universal tester with a specially designed test fixture (see *Chapter 3*). The specimens were loaded in 3-point bend with rollers of 15mm diameter. The centre span deflection of the specimen was measured using a linear POT. The outputs of load and centre span deflection were recorded using a DAQsi data logger. On completion of testing the load displacement curves for each specimen tested were plotted. The vertical deflection of a specimen under 3-point loading is given by Equation 4.5 [**19**,**34**].

$$\Delta = \left(\frac{XL^3}{48WD} \right) \qquad \textbf{4.5}$$

where:

D = flexural stiffness per unit width
X = Applied load
Δ = Centre span deflection
L = Span length
W = Specimen width

On completion of the tests, the arithmetic mean, the standard deviation of the mean and the standard deviation of the sample were determined.

4.6 Tensile Tests

During the course of this project, tensile tests of both the constituents of corrugated board and the corrugated board itself were tested. This section deals with the method used for testing the paper specimens and the method used for testing the corrugated board specimens.

4.6.1 Liner and Fluting Tensile Tests

Tensile tests of the liner and fluting were conducted in both the MD and CD. The moduli obtained were then used in the flexural rigidity predictions of the corrugated board panels as mentioned in *Chapter 2*.

4.6.1.1 Paper Tensile Specimens

The liner and fluting of all the board combinations manufactured in 2003 were tensile tested. The grades of paper tested were:

- 112g/m² Bayflute
- 140g/m² Kraft liner
- 160g/m² Bayflute
- 250g/m² Kraft liner

Nampak Corrugated commonly uses these paper grades. The specimens tested were from paper batches that had not been sent through the Corrugator. This means that the condition of the paper could be substantially different to the paper used in the

construction of corrugated board, as the paper will have been moistened and heated [**16**]. Specimens were cut in both the MD and CD to a width of 25 ± 1mm using a guillotine. The lengths of the specimens were cut to ensure that the specimens would have a span length of 180mm ± 5mm according to Tappi standard T 494 om-01 [**87**].

4.6.1.2 Paper Tensile Test Procedure

Tensile tests of the liners and fluting were carried out according to Tappi standard T 494 om-01 [**87**]. The tensile tests were performed on an Instron 4444 universal tester as shown in Figure 4.2. Prior to testing, the specimens caliper was measured using a digital micrometer. Specimens were conditioned and tested in accordance with Tappi T 402 [**86**]. The tests were carried out at a crosshead speed of 25 ± 5mm/min with a grip separation of 150mm. The load and displacement of the specimens was recorded electronically using the Instron software. The load versus displacement graphs and stress versus strain graphs were then recorded. The tensile moduli of the specimens were calculated from the slope of the stress strain curves. The arithmetic mean, the standard deviation of the mean and the standard deviation of the sample were then determined.

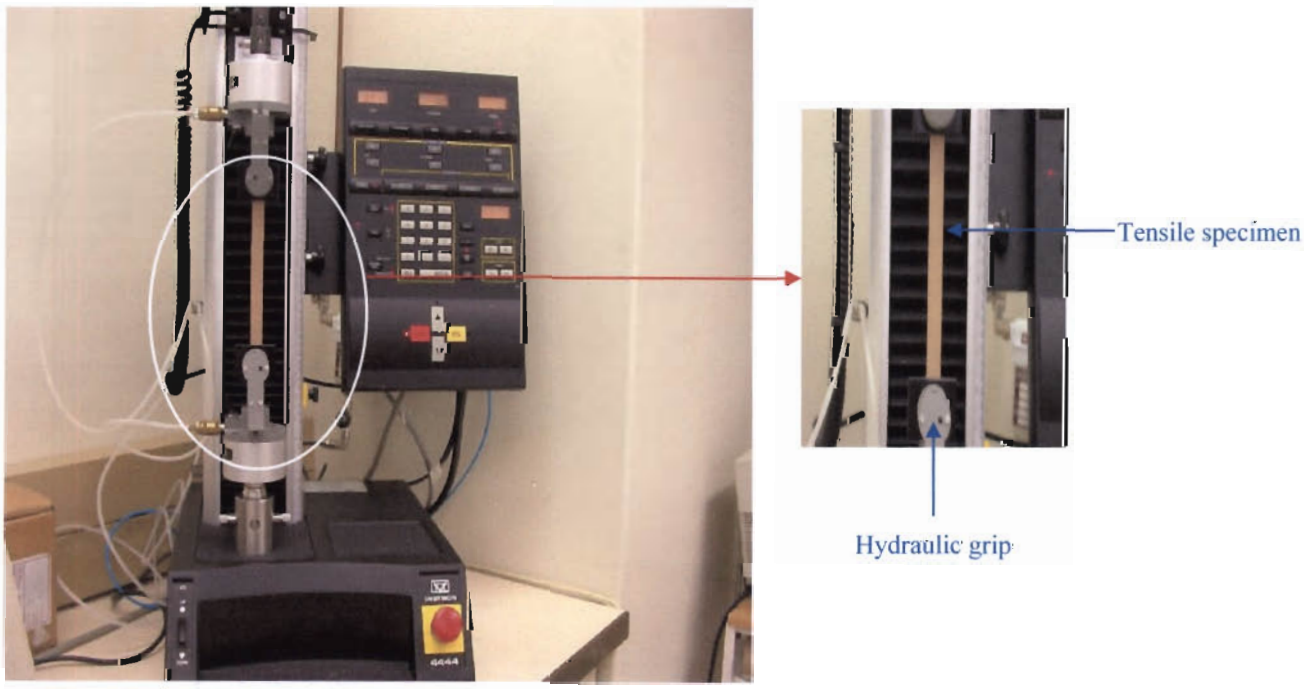

Figure 4.2: A tensile test being performed on an Instron 4444 universal tester at Nampak R&D.

4.6.2 Corrugated Board Tensile Tests

Tensile tests of corrugated board were conducted to measure the tensile modulus of the board in the MD and CD. This data would then be used in approximating bending stiffness and obtaining the constants needed for the box strength prediction method proposed by Urbanik [**37,61**].

4.6.2.1 Corrugated Board Tensile Specimens

The board combinations tested are listed in Table 4.1. The specimens were designed according to ISO type NF T51-034 and NF Q03-002 as used by Aboura *et al.* [**1**]. The specimen dimensions are shown in Figure 4.3.

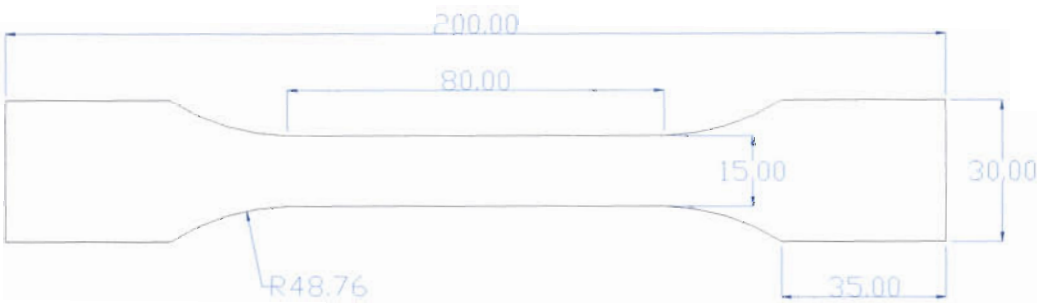

Figure 4.3: Corrugated board tensile specimen dimensions (mm).

To increase the rigidity of the specimen heads, Ampreg 20 epoxy resin was injected between the flutings. In addition, the skins of the specimen heads were coated with resin. This was considered necessary to protect the heads from damaged that could be caused by the gripping pressure of the hydraulic tensile grips resulting in incorrect data and premature failure. After initial trials, it was found that the reinforcement of the grip ends was unnecessary. This improved the speed and efficiency of the test method for an R&D situation. Nampak Corrugated cut the tensile specimens.

4.6.2.2 Procedure

Tensile tests, as shown in Figure 4.4, of corrugated board were carried out according to ISO type NF T51-034 and NF Q03-002 as used by Aboura *et al.* [**1**]. The tensile tests were carried out on an Instron 4444 universal tester. Prior to testing the caliper of the specimens was measured. Specimens were conditioned and tested in accordance with Tappi T 402 [**86**]. The tests were carried out at a crosshead speed of 3mm/min. The load versus displacement graphs and stress versus strain graphs were then recorded. The tensile moduli of the specimens were calculated from the slope of the stress strain curves. The arithmetic mean, the standard deviation of the mean and the standard deviation of the sample were determined.

Figure 4.4: A corrugated board tensile test being performed on an Instron 4444 universal tester at Nampak R&D.

4.7 The Edgewise Compression Test

During this project, ECT's of a number of board combinations were performed. The ECT results were used for box strength prediction using the McKee formula mentioned in *Chapter 2*. The ECT consists of subjecting a rectangular specimen to a load applied perpendicular to the flutes until failure occurs.

4.7.1 ECT Specimens

The dimensions of the specimens were 100mm ± 0.5mm, in the direction perpendicular to the flutes by 25 mm ± 0.5mm in the flute direction. Specimens were cut so that the width across the test piece did not vary more than 0.1mm in accordance with ISO 3037:1994(E) [**88**]. This ensured that the loading edge was straight, parallel and perpendicular to the surface of the board. In addition, the specimen had to be cleanly cut so that the flutes were not distorted and the edges of the specimen did not show any visible loose fibres or furriness [**88**]. The board combinations that were tested are listed in Table 4.1.

4.7.2 The ECT Procedure

All specimens were conditioned and tested in standard temperature and atmospheric conditions in accordance with Tappi T 402 [**86**]. Prior to testing, the dimensions of the specimens were measured using a calliper. The ECT was carried out on a Messmer 937 crush tester as shown in Figure 4.5 below. The tests were conducted at a crosshead speed of 12.5mm/min in accordance with ISO 3037:1994(E) [**88**]. The specimen was placed between the guide blocks of the crush tester. A load was then applied perpendicular to the flutes until failure occurred. The maximum load that the specimen sustained was then recorded. On completion of the test the edge crush resistance was determined using Equation 4.6.

$$R = \frac{F_{max}}{L} \quad \textbf{4.6}$$

where

R = Edgewise crush resistance in kN/m

F_{max} = Maximum applied load in N.

L = Specimen length

On completion the arithmetic mean, the standard deviation of the mean and the standard deviation of the sample were determined.

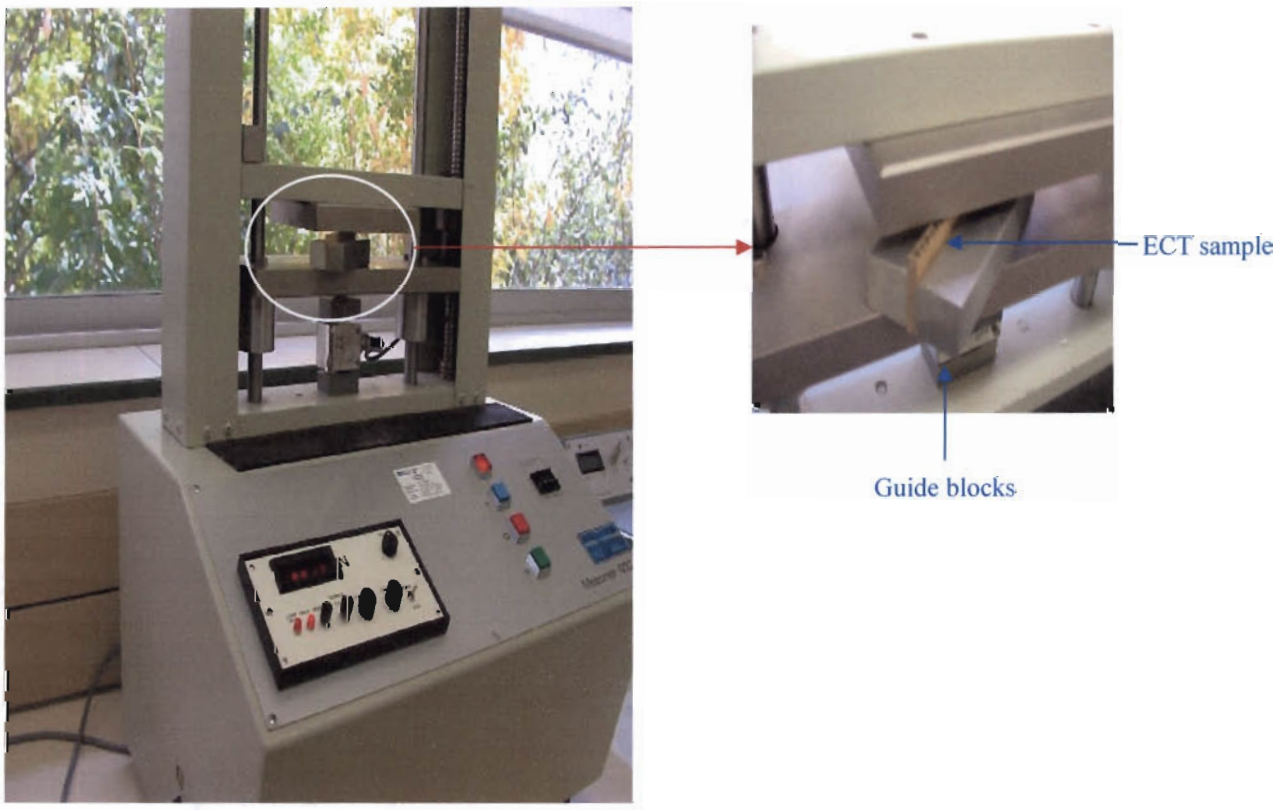

Figure 4.5: The Messmer 937 crush tester used to conduct ECT's.

4.8 The Box Compression Test

BCT's were carried out to measure the BCS of a box. This value was then compared to the values predicted by the McKee formula. During the test a corrugated cardboard box is placed between two parallel loading platens as shown in Figure 4.6a. The crosshead moves downwards in the vertical plane. This applies a compressive load to the box. The top loading platen is attached to a flexible coupling which allows the platen to move according to box deformation ensuring that a uniform load is applied at all times. This can be seen in Figure 4.6b.

Figure 4.6a: The BCT of a corrugated box.

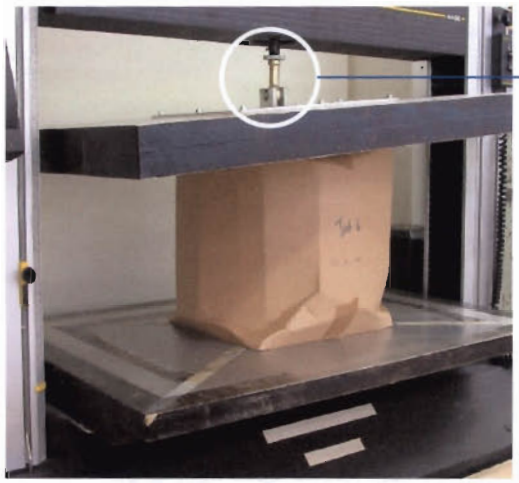

Figure 4.5b: Box failure during a BCT.

4.8.1 BCT Specimens

RSC boxes of dimensions 300x300x300mm and manufactured from various board combinations were supplied by Nampak Corrugated. The board combinations for the boxes tested are listed in Table 4.1.

4.8.2 BCT Procedure

BCT was performed according to Tappi standard T 804 0m-02 [**89**]. BCT was performed on an Instron 4466 universal tester as shown in Figure 4.6. Testing was

performed at a crosshead of 12.5mm/min as per Tappi Standard T 804 0m-02 [**89**]. Prior to testing the specimens were conditioned and tested according to Tappi T 402 [**86**]. The boxes were then sealed according to the Tappi standard using duct tape as shown in Figure 4.7 and Figure 4.8 [**89**].

Figure 4.7: Sealing of the inside flaps prior to BCT.

Figure 4.8: Sealing of the top flaps prior to BCT.

The dimensions of the specimens were recorded using a calliper. The crosshead displacement and load were electronically recorded using the Instron software. On completion of the test, the load versus displacement plot for the specimen was generated. The arithmetic mean, the standard deviation of the mean and the standard deviation of the sample were determined. Once the BCT's of a sample had been completed, the boxes were visually examined for areas of localized failure and deformation and photographed.

CHAPTER 5

RESULTS

The following chapter displays the results obtained from the experiments discussed in *Chapter 4* and the calculations that were performed using the data obtained. All error bars in this chapter will represent the high and low values of the samples tested. The results of all specimens tested have been included in *Appendix D*.

5.1 The Block Shear Test Results

Figure 5.1 shows a typical load displacement curve from the block shear testing of a 250-160C 03 board combination. The curve consists of an elastic phase followed by the compression of the fluting. An increased load follows until failure occurs. The ± values in Table 5.1 indicate the standard deviation of the mean. Block shear testing was performed on all samples listed in Table 4.1.

Sample	Modulus	SD	Stiffness	SD
	MPa	MPa	N/m	N/m
140-112B VR 04	1.8 ± 0.04	0.1	5275 ± 125	375
140-112C 03	1.3 ± 0.05	0.1	5094 ± 177	532
250-112B 03	2.6 ± 0.06	0.1	8310 ± 195	515
250-160C 03	2.2 ± 0.1	0.3	9092 ± 431	1219

Table 5.1: Block shear modulus and stiffness results. SD refers to standard deviation.

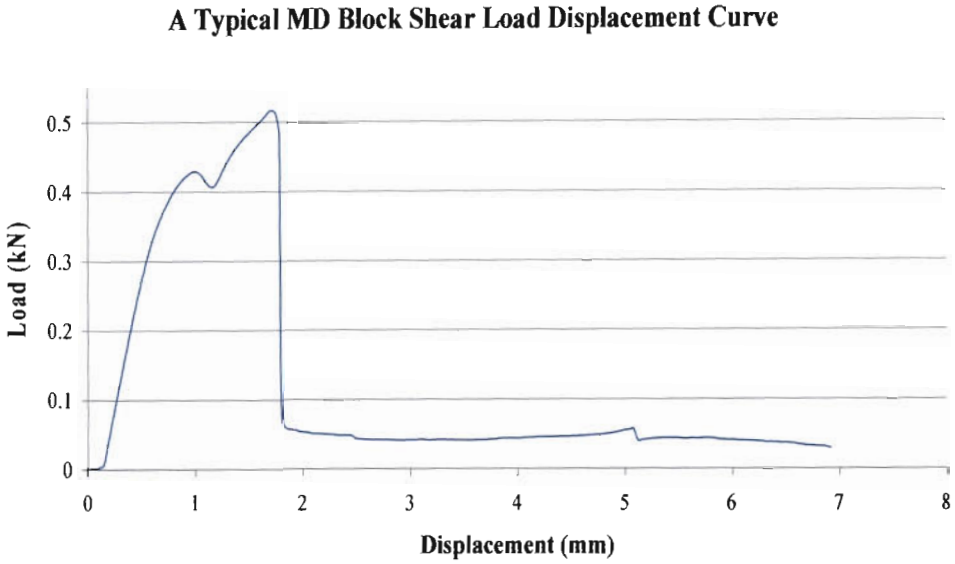

Figure 5.1: A typical MD block shear load displacement curve.

5.1.1 Block Shear Modulus Results

Between 7 and 9 specimens of each board combination were successfully tested. The average modulus and stiffness values of theses samples are shown in Table 5.1. Figure 5.2 shows the comparison of the various board combinations block shear moduli. The average moduli of the board combinations with a B flute profile are higher than the values exhibited by the board combinations with a C flute profile with the same liner grammage. On average, the board combinations with a B flute profile exhibit a 15-30% higher shear modulus than the board combinations with a C flute profile. The board combinations with 250g/m² liners are stiffer than the board combinations with 140g/m² liners. The 250-112B 03 board combination has a higher shear modulus than the 250-160C 03 board combination. This is interesting because the 250-160C 03 board combination has a heavier fluting than the 250-112B 03 board combination, namely 160g/m².

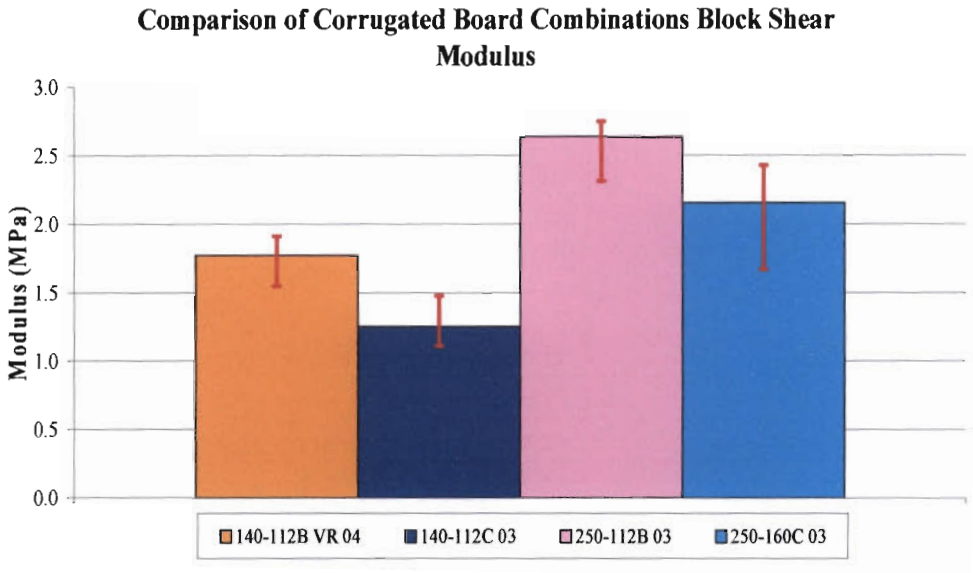

Figure 5.2: Comparison of average block shear modulus and data scatter.

5.1.2 Block Shear Stiffness Results

Figure 5.3 shows the comparison of the board combinations stiffness as measured by the block shear test. There is very little difference between the stiffness values of the 140-112B VR 04 sample and the 140-112C 03 sample. In addition, there appears to be no difference between the 250-112B 03 sample and the 250-160C 03 sample. The board combinations with the 250g/m² liners are, on average, stiffer than the board combinations with the 140g/m² liners.

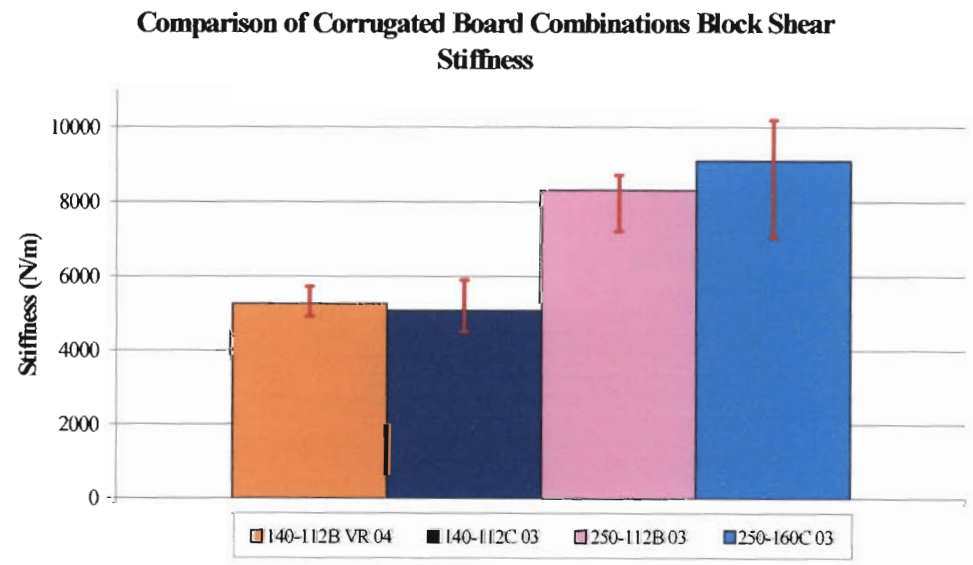

Figure 5.3: Comparison of the block shear stiffness of the corrugated board samples tested.

5.2 The MD Shear Test Results

Figure 5.4 shows a typical torque rotation curve. Only the initial linear portion of the curve is of interest for MD shear stiffness evaluations. The area of interest has been highlighted. Between 9 and 10 specimens were successfully tested for each board combination. Table 5.2 shows the average stiffness values of the samples tested as well as the standard deviation of the mean and the standard deviation of the samples. MD shear testing was performed on all samples listed in Table 4.1.

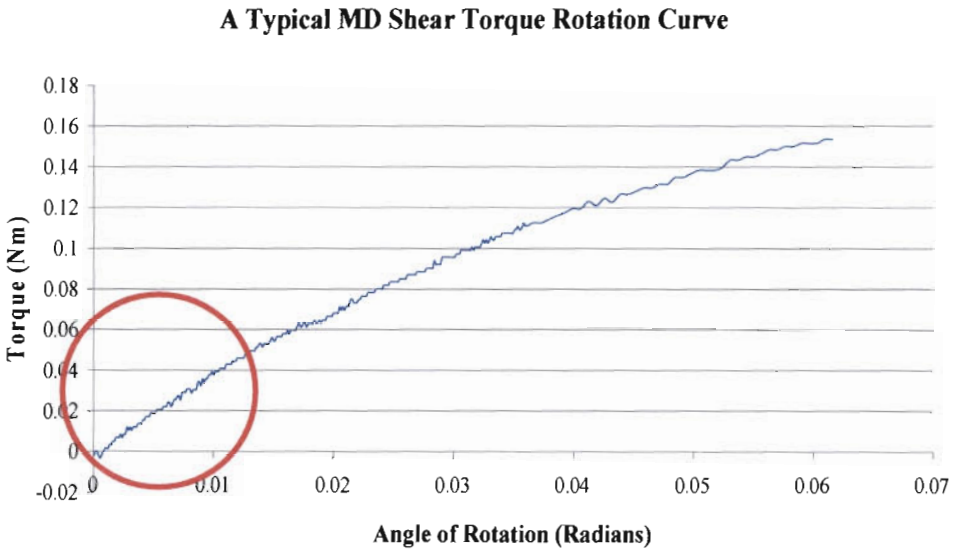

Figure 5.4: A typical MD shear torque rotation curve.

Sample	Stiffness	SD
	N/m	N/m
140-112E 04	2458 ± 15	244
140-112B 03	3937 ± 28	449
140-112B 04	4630 ± 19	283
140-112B VR 04	4806 ± 34	541
140-112C 03	3812 ± 14	221
140-112C R 04	4003 ± 17	264
175-112B 04	4097 ± 28	437
175-112C VU 04	4762 ± 25	392
250-112B 03	7435 ± 36	570
250-160B 04	5828 ± 39	619
250-160C 03	8694 ± 26	404
250-160C 04	6079 ± 34	530

Table 5.2: The average MD shear stiffness values for the samples tested.

5.2.1 MD Shear Stiffness Results for Board Samples with 140g/m² Liners

Figure 5.5 shows the shear stiffness of the 140-112E 04 i.e. the E flute profile sample was lower than all the other samples tested with 140g/m² liners. The board combinations manufactured in 2004 with a B flute profile had a slightly higher value than the B flute board manufactured in 2003. On average, the board with B flute was higher than the E and C flute board combinations. The board combinations with C flute show similar shear stiffness values, irrespective of the year of manufacture and the liner material.

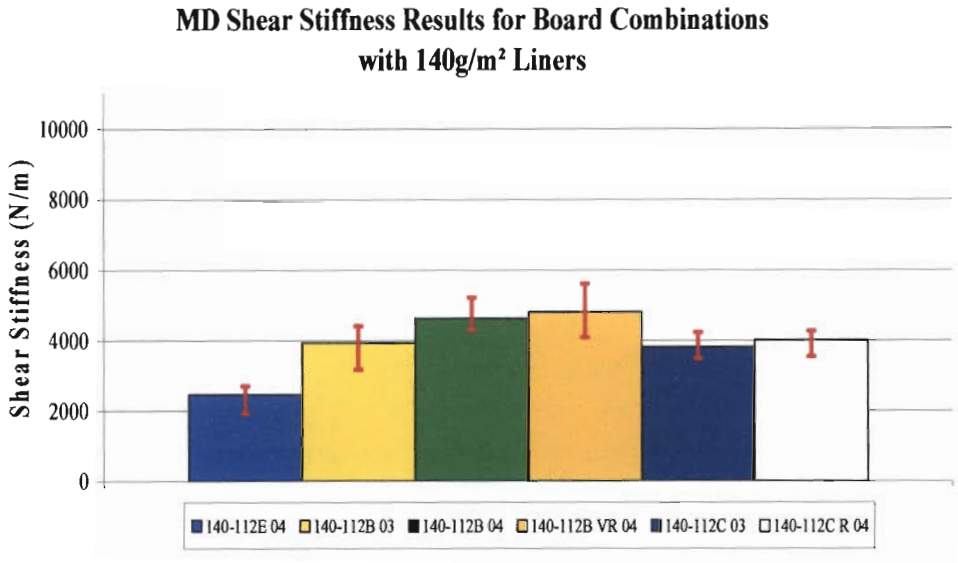

Figure 5.5: MD shear stiffness results for the board combinations tested with 140g/m² liners.

5.2.2 MD Shear Stiffness Results for Board Samples with 175g/m² and 250g/m² Liners

In Figure 5.6 the shear stiffness of the board combinations with 250g/m² liners were, on average, higher than the board combinations with 175g/m² liners. The 250-160C 03 board combination had the highest MD shear stiffness value of all the samples tested. It is interesting to note that the shear stiffness of the 175-112C VU 04 sample was slightly higher than the 175-112B 04 sample. In addition, the fact that the 250-112B 03 sample has a higher stiffness than the 250-160B 04 and the 250-160C 04 samples is of interest. It is noticed that there is very little stiffness difference between the 250-160B 04 and the 250-160C 04 samples.

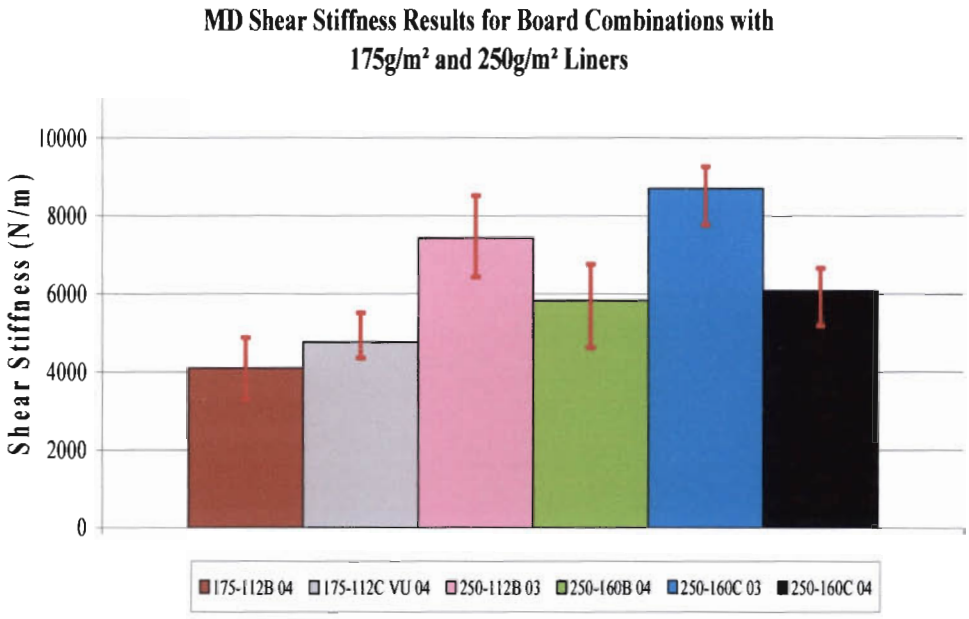

Figure 5.6: MD shear stiffness results for board combinations with 175g/m² and 250g/m² liners.

5.3 Correlation of the MD Shear Testing Method and the Block Shear Testing Method

Figure 5.7 shows the linear correlation between the shear stiffness values obtained through the MD shear test compared to the shear stiffness values obtained using the block shear test method. The coefficient of determination (R^2) is 0.97. This means that there is a 97% relationship between the two test methods. Only 3% of the variation in the MD shear values cannot be explained by the variation in the block shear values.

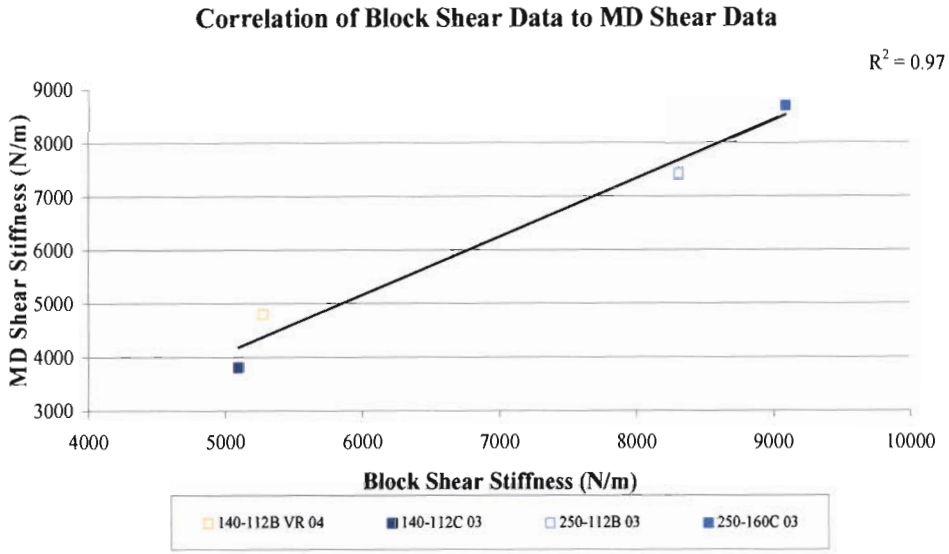

Figure 5.7: Correlation of MD shear values to block shear values for the same board combinations tested.

5.4 3-Point Bend Results

Figure 5.8 shows a typical load deflection curves for a 3-point bend test. The specimen tested in the MD is stiffer than the specimen tested in the CD. The CD specimen, however, fails at a higher load and exhibits a larger maximum deflection. 3-point bend testing was performed on all samples listed in Table 4.1.

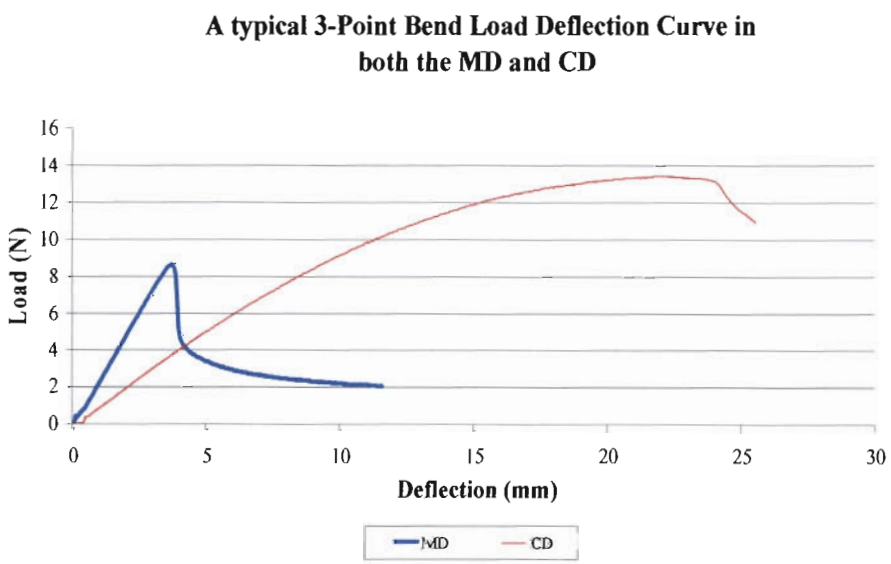

Figure 5.8: A typical MD and CD 3-point bend load deflection curve.

Table 5.3 and Table 5.4 show the average stiffness ± standard deviation of the mean and standard deviation of all the 3-point bend samples tested. The virgin up and virgin down comments in the sample names refers to the position of the virgin liner during testing. Virgin up refers to the virgin liner being in contact with the top roller during testing whereas virgin down refers to the virgin liner being in contact with the bottom rollers during testing.

Sample	Stiffness	SD
	Nm	Nm
140-112E 04	0.5 ± 0.01	0.0
140-112B 03	1.7 ± 0.02	0.1
140-112B 04	1.5 ± 0.01	0.0
140-112B VR 04 virgin down	1.5 ± 0.02	0.0
140-112B VR 04 virgin up	1.5 ± 0.01	0.0
140-112C 03	3.4 ± 0.04	0.1
140-112C R 04	3.2 ± 0.06	0.2
175-112B 04	2.5 ± 0.03	0.1
175-112C VU 04 virgin down	4.0 ± 0.06	0.2
250-112B 03	3.6 ± 0.05	0.2
250-160B 04	3.1 ± 0.06	0.2
250-160C 03	6.6 ± 0.06	0.2
250-160C 04	6.0 ± 0.04	0.1

Table 5.3: CD 3-point bend test results.

Sample	Stiffness	SD
	Nm	Nm
140-112E 04	0.9 ± 0.03	0.1
140-112B 03	4.3 ± 0.1	0.3
140-112B 04	3.3 ± 0.07	0.2
140-112B VR 04 virgin down	3.9 ± 0.09	0.3
140-112B VR 04 virgin up	4.0 ± 0.06	0.2
140-112C 03	5.0 ± 0.2	0.6
140-112C R 04	5.3 ± 0.13	0.4
175-112B 04	5.4 ± 0.12	0.4
175-112C VU 04 virgin down	6.1 ± 0.39	1.3
175-112C VU 04 virgin up	7.6 ± 0.18	0.6
250-112B 03	8.7 ± 0.3	1.0
250-160B 04	8.4 ± 0.07	0.2
250-160C 03	14.6 ± 0.2	0.7
250-160C 04	14.8 ± 0.28	0.9

Table 5.4: MD 3-point bend test results.

5.4.1 3-Point Bend Test Results for Samples with 140g/m² Liners

Figure 5.9 shows the comparison of the 3-point bend stiffness values for the board samples with 140g/m² liners tested in the CD. The 140-112E 04 board has an average stiffness of approximately 66% lower than the 140-112B 04 board. The 140-112B 03 board combination manufactured in 2003 has a 12% higher stiffness than its 2004 counterpart. The values of the 140-112B board grades manufactured in 2004 are very similar. The stiffness values of the 140-112C board combinations are higher than all the other samples tested with the average stiffness being 56% stiffer than the B flute board. The difference between the 140-112C board manufactured in 2003 and 2004 was minimal.

Figure 5.10 shows that the bending stiffness of the 140-112E 04 i.e. the E flute board combination, in the MD, is significantly lower (73%) than the B flute board combinations. The 140-112B 03 i.e. the board manufactured in 2003, has a 23% higher stiffness than the same board combination manufactured in 2004. The 140-112B VR 04 board has no stiffness difference when tested with the virgin liner down or up. In addition, the difference between the 140-112B 04 and the 140-112B VR 04 board stiffness is minimal. The board samples with C flute were stiffer than the other samples tested. There is no difference between the 140-112C 03 board and the 140-112C R 04 board.

When comparing Figure 5.9 and Figure 5.10, it can be seen that the samples tested in the MD are significantly stiffer than the samples tested in the CD. This is to be expected. The lower stiffness of the E-flute board compared to the B-flute board in both the MD and CD was consistent. The stiffness of the boards with the C flute is higher than the boards with B flute in both the CD and MD.

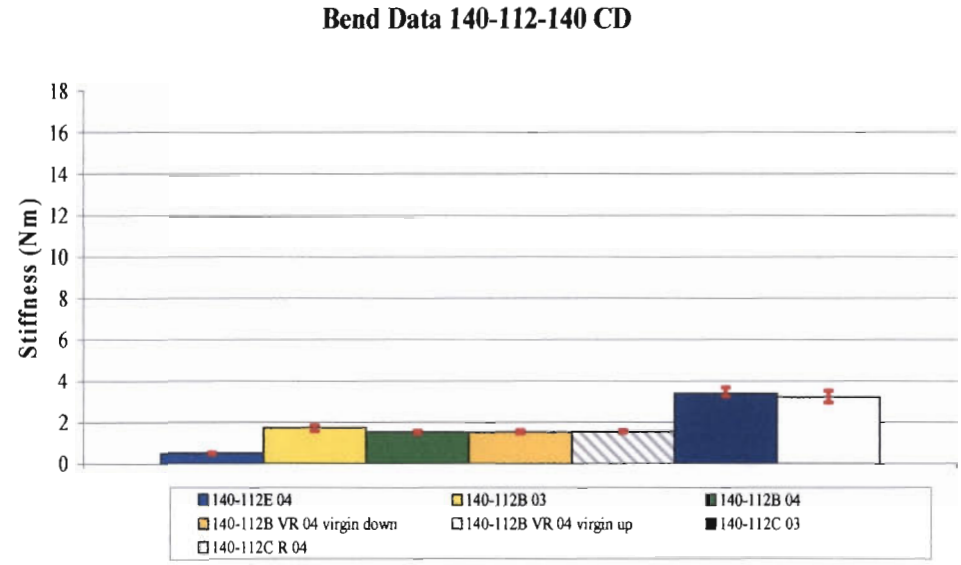

Figure 5.9: Comparison of bending stiffness of board samples with 140g/m² liners tested in the CD.

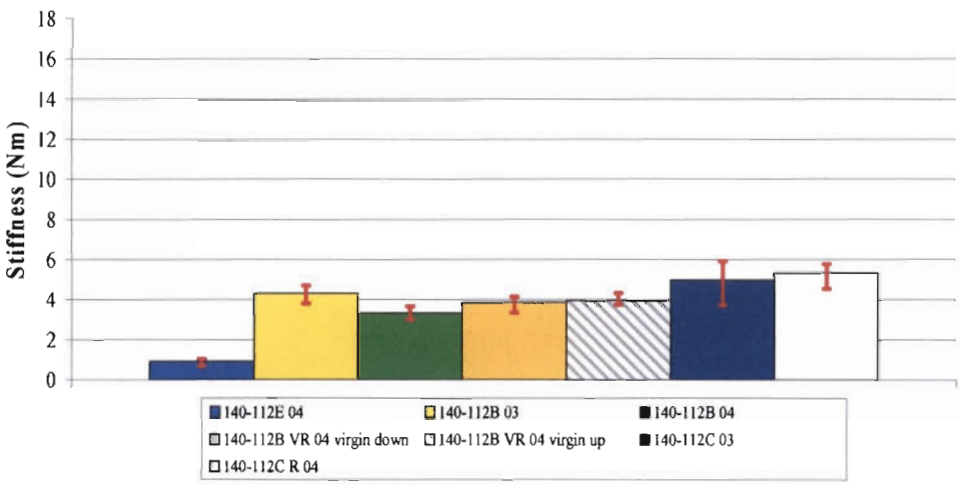

Figure 5.10: Comparison of bending stiffness of board samples with 140g/m² liners tested in the MD.

5.4.2 3-Point Bend Test Results for Samples with 175g/m² Liners

Figure 5.11 shows a comparison of the 175-112 samples tested in the CD. The bending stiffness of the 175-112C VU 04 sample was stiffer than the 175-112B 04 sample. The difference in stiffness between the B and C flute board is more pronounced in the CD than in the MD. The MD tested samples are stiffer than the CD

samples tested, which is expected. In addition, the stiffness of the 175g/m² liner board were stiffer than the 140g/m² liner in both the MD and the CD.

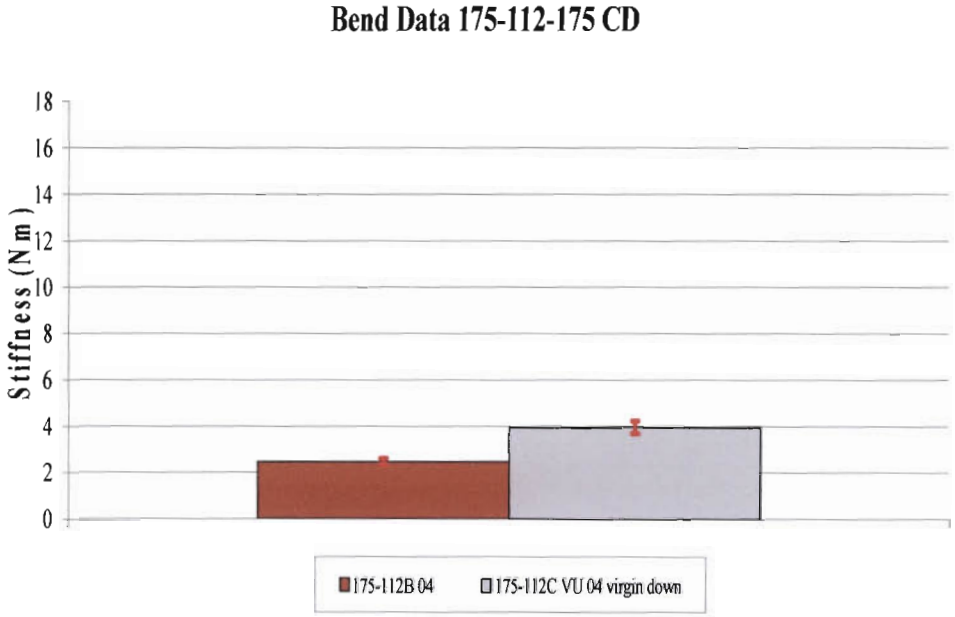

Figure 5.11: A comparison of the bending stiffness of board samples with 175g/m² liners tested in the CD.

Figure 5.12 shows a comparison between the bending stiffness of the board samples with 175g/m² liners tested in the MD. The 175-112B 04 board had a slightly lower stiffness than 175-112C VU 04 sample with the virgin liner facing down. There was a significant difference between the stiffness values of the 175-112C VU 04 board with the virgin liner in two different positions namely up and down. The sample tested with the virgin up was, on average, 20% stiffer.

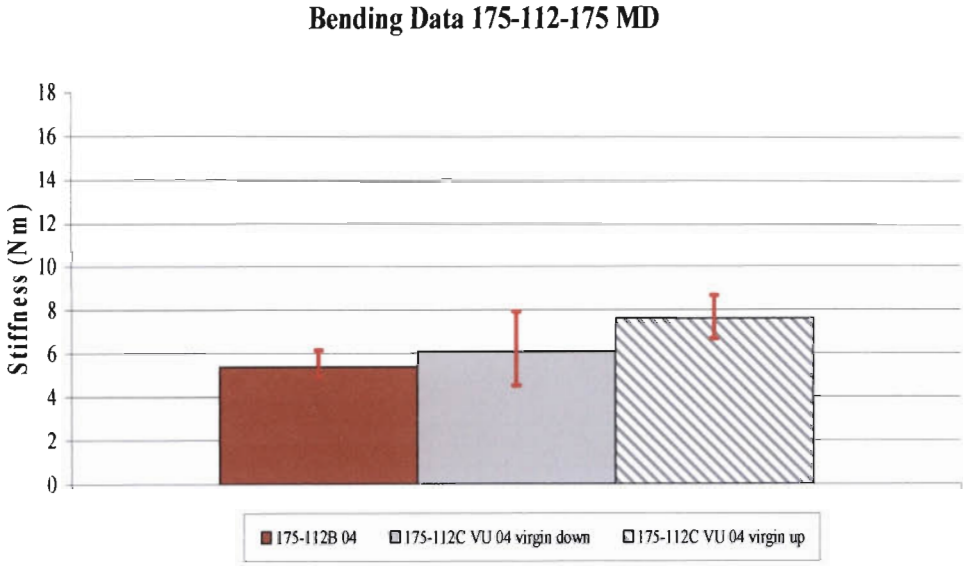

Figure 5.12: A comparison of the bending stiffness of board samples with 175g/m² liners tested in the MD.

5.4.3 3-Point Bend Test Results for Samples with 250g/m² Liners

Figure 5.13 shows a comparison between the board samples tested with 250g/m² liners in the CD. The board samples with B flute show very similar stiffness values. The C flute board samples are, on average, 45% stiffer than the B flute boards. The stiffness values of the C flute sample manufactured in 2003 is about 10% higher than the 2004 sample. Figure 5.14 shows a comparison between the board samples tested with 250g/m² liners in the MD. The board samples with B flute show no difference between them. The board samples with C-flute are about 40% stiffer than the board with B flute. There is no difference between the stiffness values of the C flute samples. The difference between the C flute and B flute board in the CD was consistent with the behaviour shown in the MD. The board samples with 250g/m² liners were stiffer than all of the previously mentioned samples in both the MD and the CD. This was also to be expected.

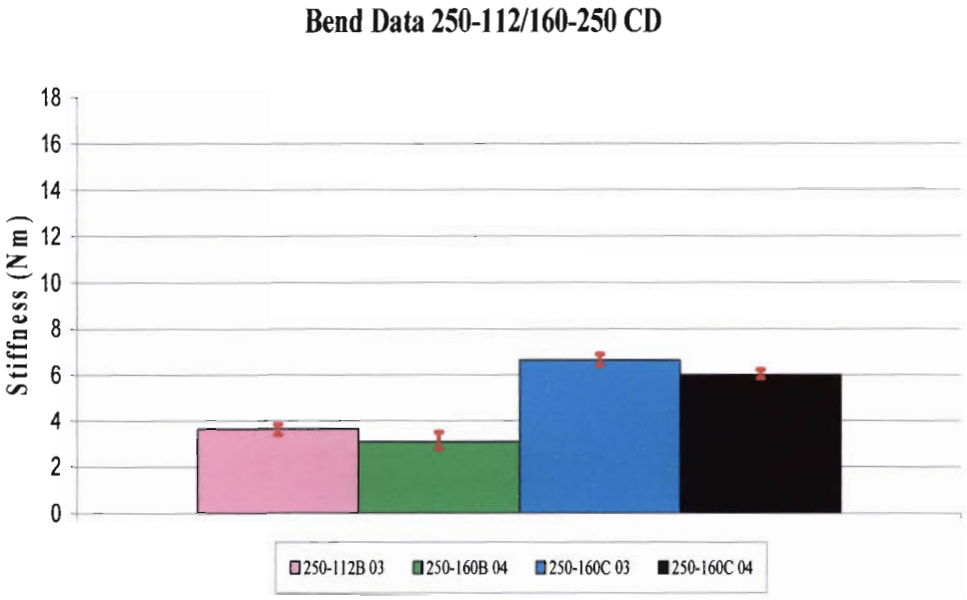

Figure 5.13: A comparison of the bending stiffness of board samples with 250g/m² liners tested in the CD.

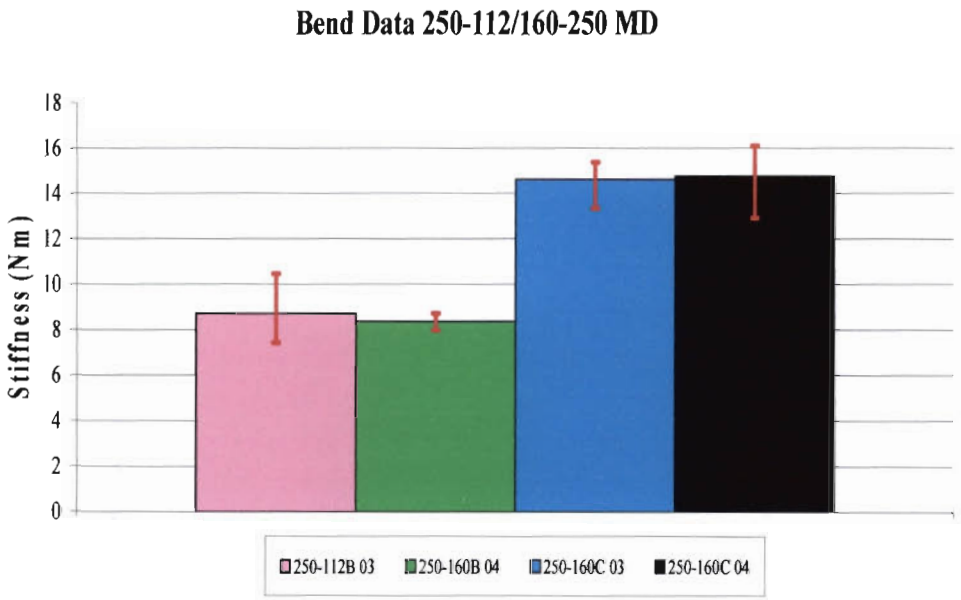

Figure 5.14: A comparison of the bending stiffness of board samples with 250g/m² liners tested in the MD.

5.5 Bending Stiffness Predictions

The bending stiffness of corrugated board was predicted using the Urbanik method discussed in 2.3.2.4. A homogenisation technique was also used to predict bending stiffness using Equation 2.8. In order to compute these predictions, the tensile stiffness of the liner and fluting of each board combination, as well as the board tensile moduli were needed. These results were obtained experimentally using the methods described in 4.2.1 and 4.2.2.

5.5.1 Liner Tensile Tests

A typical stress-strain curve for paper tested in the MD and CD is shown in Figure 5.15. Tensile tests were carried out on all the samples listed in Table 4.1. The stiffness and maximum load value of the paper is higher in the MD than in the CD, while the CD has a higher deformation to failure. The slope of the curves was obtained by a linear regression fit to the linear region of each curve. The average dimensions and stiffness values of the tensile tests of the fluting and liner are shown in Table 5.5.

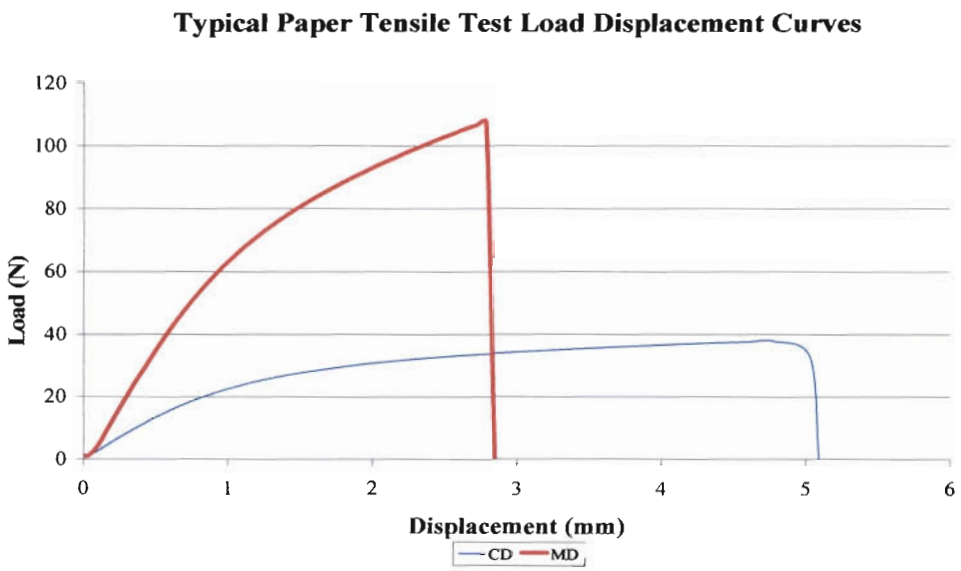

Figure 5.15: A typical paper tensile load displacement curve tested in the MD and CD.

CD				
Sample	**Stiffness kN/m**	**SD kN/m**	**Caliper mm**	**SD mm**
112g/m²	292 ± 4.3	14	0.168 ± 0.002	0.007
140g/m²	365 ± 6.8	21	0.212 ± 0.001	0.004
160g/m²	399 ± 6.7	21	0.235 ± 0.002	0.007
250g/m²	667 ± 6.4	20	0.382 ± 0.005	0.015
MD				
Sample	**Stiffness kN/m**	**SD kN/m**	**Caliper mm**	**SD mm**
112g/m²	714 ± 4.4	13	0.158 ± 0.003	0.008
140g/m²	1152 ± 14.4	46	0.222 ± 0.006	0.018
160g/m²	981 ± 10.9	35	0.246 ± 0.002	0.007
250g/m²	1968 ± 21.6	68	0.383 ± 0.006	0.019

Table 5.5: Experimental tensile results of the liners and fluting tested in the MD and CD.

Figure 5.16 shows the comparison of the tensile stiffness of paper tested in the CD. The tensile stiffness of the 250g/m² Kraft liners is substantially higher than the other paper grades tested. Figure 5.16 shows that there was very little difference in the average tensile stiffness of the 140g/m² and 160g/m², whereas the 112g/m² sample is about 20% lower. Figure 5.17 shows that the tensile stiffness of the 140g/m² Kraft liners is higher than the 160g/m² Bayflute in the MD. This is due to the recycled content of the Bayflute material. In addition, the tensile stiffness of the 250g/m² Kraft liners is higher than all the other samples tested, which was also to be expected. The results show that the paper tensile stiffness is related to the grammage and therefore the paper caliper.

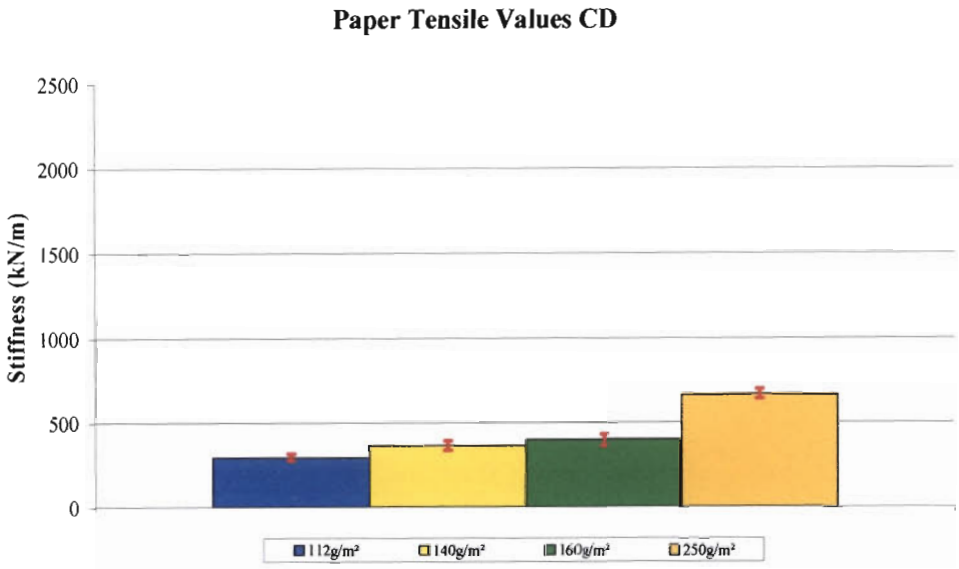

Figure 5.16: A comparison of the tensile stiffness of paper tested in the CD.

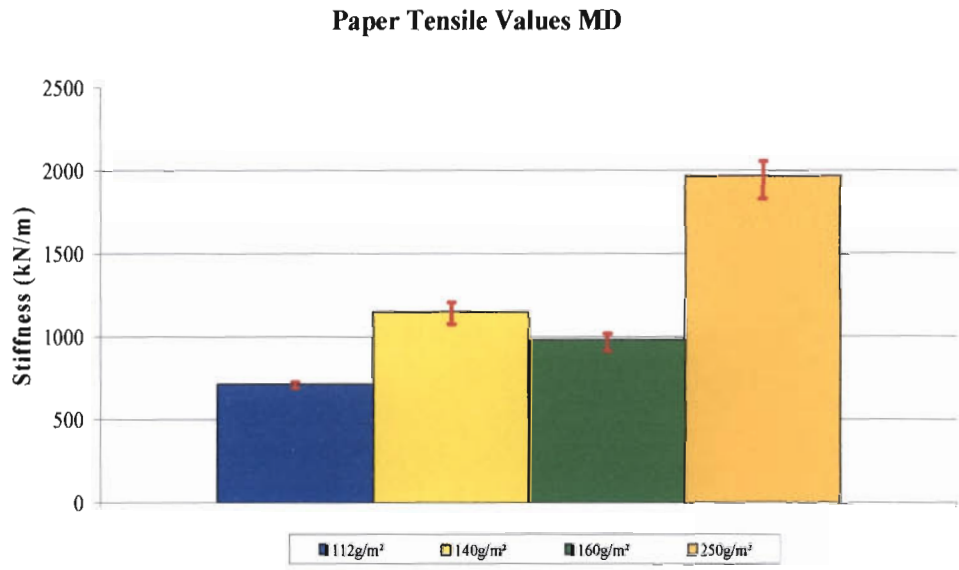

Figure 5.17: A comparison of the tensile stiffness of paper tested in the MD.

5.5.2 Stiffness Predictions Using Liner and Fluting Tensile Values

The bending stiffness of all the board combinations manufactured in 2003 was predicted using the formula mentioned in 2.3.2.4. The flute profile and geometric details of the board are shown in Table 5.6. Of these values β and Θ were calculated using the formula previously mentioned.

Flute	*H*	ß	*R*	*P*	*TF*	*Θ*
	mm	rad	mm	mm		rad
B	2.580	0.929	1.245	6.350	1.350	1.859
C	3.630	1.005	1.520	7.950	1.430	2.011
E	1.160	0.788	0.717	3.500	1.240	1.577

Table 5.6: Geometry and flute profile parameters of the different board combinations, where *R* is the tip radius, *TF* is the take-up factor, *P* is the flute pitch, *Θ* is the angle of wrap, *β* is $\theta/2$ and *H* is the pitch height.

The predicted values are shown in Table 5.7.

	MD	CD
Sample	Nm	Nm
140-112B 03	4.3	1.7
140-112C 03	8.6	4.1
250-112B 03	8.0	3.1
250-160C 03	14.7	6.9

Table 5.7: Predicted stiffness values using the Urbanik formula.

Figure 5.18 shows the correlation between the experimental data and the values predicted using the Urbanik formula for bending stiffness in the CD and MD. The predicted CD values have a coefficient of determination of 0.94 with the experimental bending stiffness values. The correlation between the MD experimental value and the predicted value is 83%.

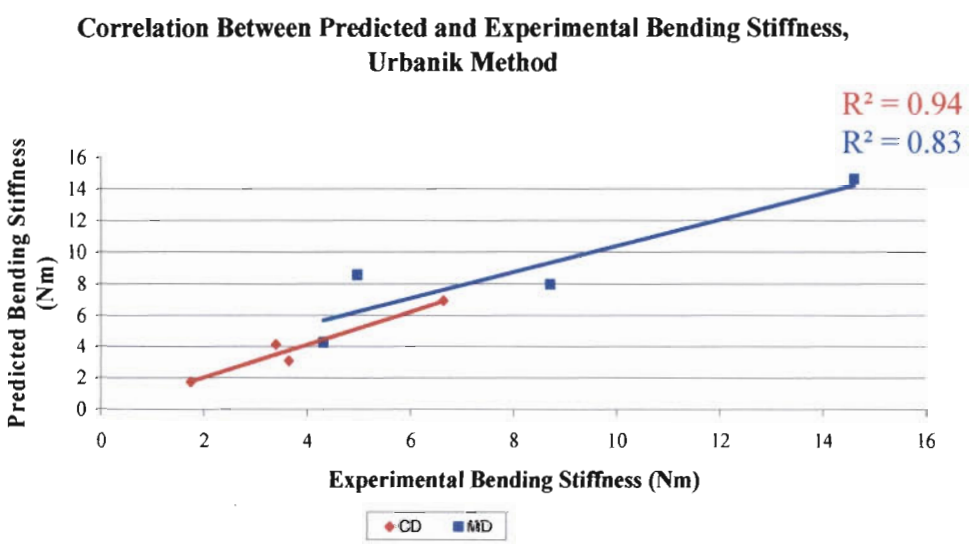

Figure 5.18: Correlation between experimental and predicted bending stiffness using the Urbanik method.

5.5.3 Combined Board Tensile Modulus

Figure 5.19 shows a typical load displacement curve of a balanced (the same liner on the top and bottom of the sandwich) corrugated board tensile test in the MD and CD. The MD is stiffer than the CD while the CD exhibits a larger deformation before material failure. All the samples listed in Table 4.1 were tested.

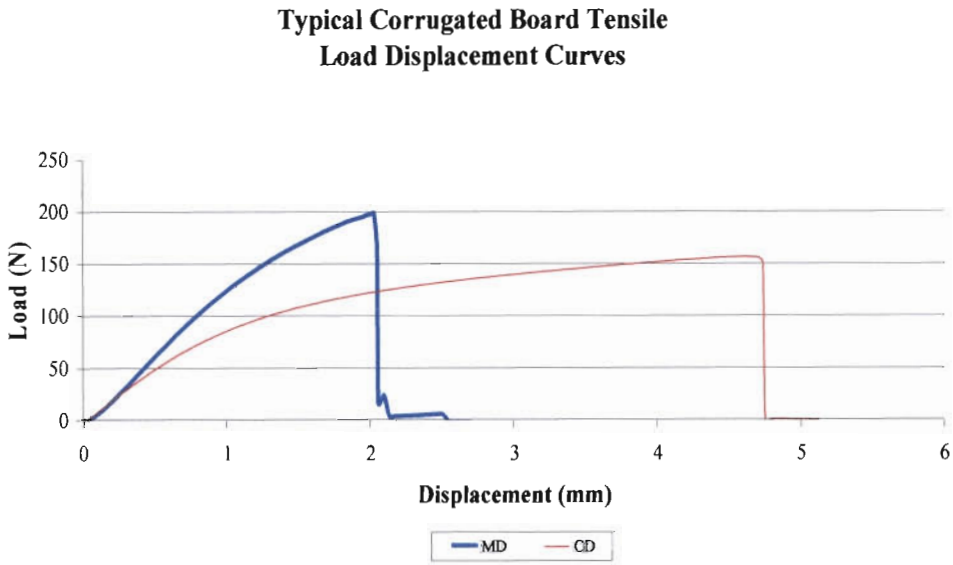

Figure 5.19: Load displacement curves of combined board tensile test in MD and CD.

Figure 5.20 shows a typical load displacement curve for an unbalanced board combination, namely a board with a virgin liner on one face and a uniliner on the other. The curve reaches a maximum value and then material failure occurs. This material failure is due to the uniliner failing. The load increases again. The virgin liner supports the increasing load until material failure. The maximum tensile values of the liners are similar. However, the maximum displacement and the strain to failure of the virgin liner is significantly higher than the uniliner. A similar failure pattern was noticed in some of the 140-112C R 04 board specimens as shown in Figure 5.21.

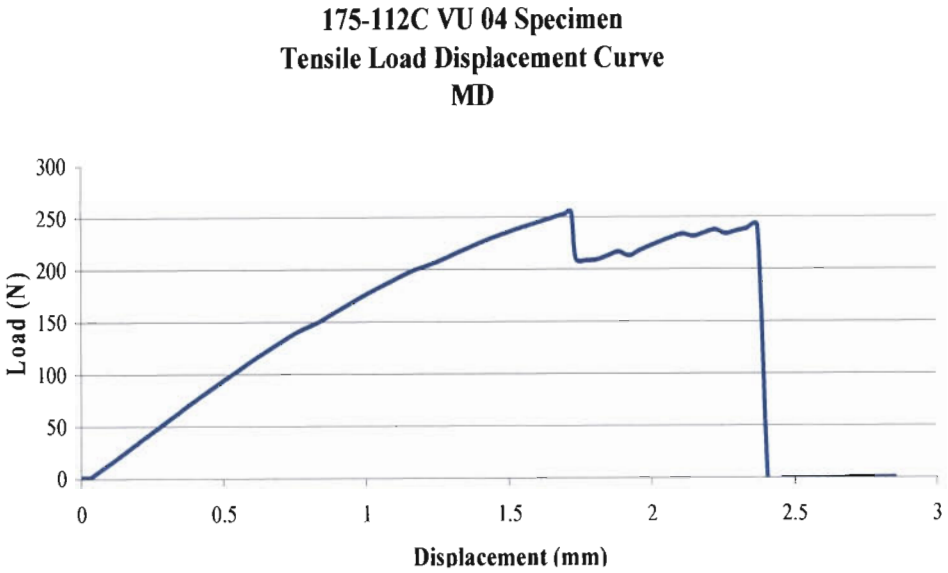

Figure 5.20: A typical load displacement curve for an unbalanced board combination.

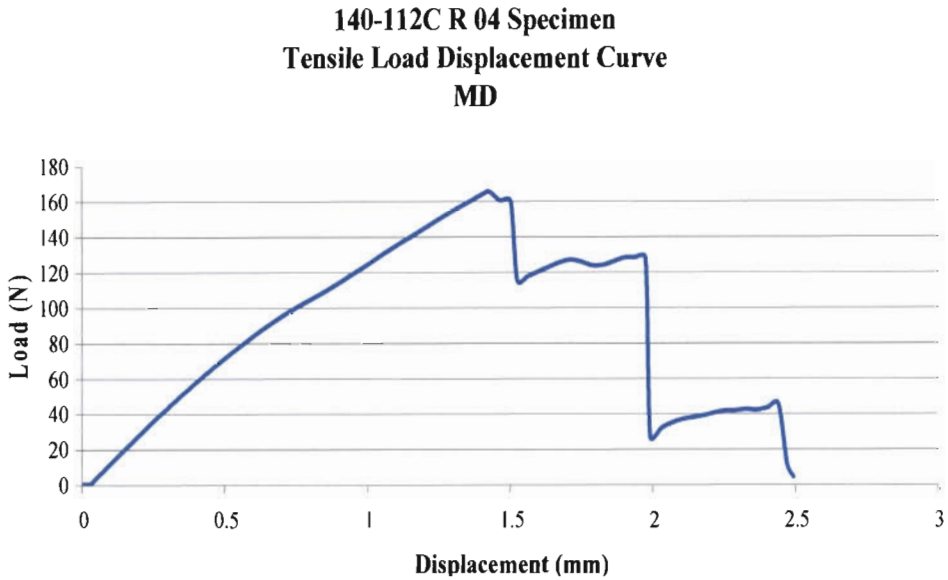

Figure 5.21: Tensile load displacement curve of a 140-112C R 04 board specimen.

The tensile modulus of the board was obtained from a linear regression fit to the linear portion of the load displacement curves and the geometry of the specimens. The area of the specimens was approximated by the thickness of the liners and fluting taken as the average caliper values from 5.5.1. The average values, standard deviation and standard error of all samples tested are shown in Table 5.8.

Figure 5.22 shows the comparison of all the board sample moduli in the CD. The corrugated board samples with 140g/m² liners all exhibited similar tensile moduli.

The board samples with 175g/m² liners had tensile moduli slightly higher than the samples with 140g/m liners. The board samples with 250g/m² liners had the highest tensile moduli, but only slightly higher than the 175g/m² board samples. The board samples with virgin material had tensile moduli that were consistent with their virgin counterparts.

CD		
Sample	**Modulus MPa**	**SD MPa**
140-112E 04	916 ± 12.6	60
140-112B 04	906 ± 8.4	45
140-112B VR 04	916 ± 16.0	75
140-112C R 04	879 ± 25.2	119
175-112B 04	1137 ± 21.7	102
175-112C VU 04	1019 ± 24.4	115
250-160B 04	1180 ± 29.4	139
250-160C 04	1217 ± 20.2	90
MD		
Sample	**Modulus MPa**	**SD MPa**
140-112E 04	1489 ± 23.2	125
140-112B 04	1096 ± 15.3	72
140-112B VR 04	1436 ± 38.4	172
140-112C R 04	1123 ± 43.6	205
175-112B 04	1510 ± 30.5	136
175-112C VU 04	1556 ± 39.3	185
250-160B 04	2018 ± 18.5	83
250-160C 04	2081 ± 34.4	154

Table 5.8: Tensile data of all corrugated board samples tested in the MD and the CD.

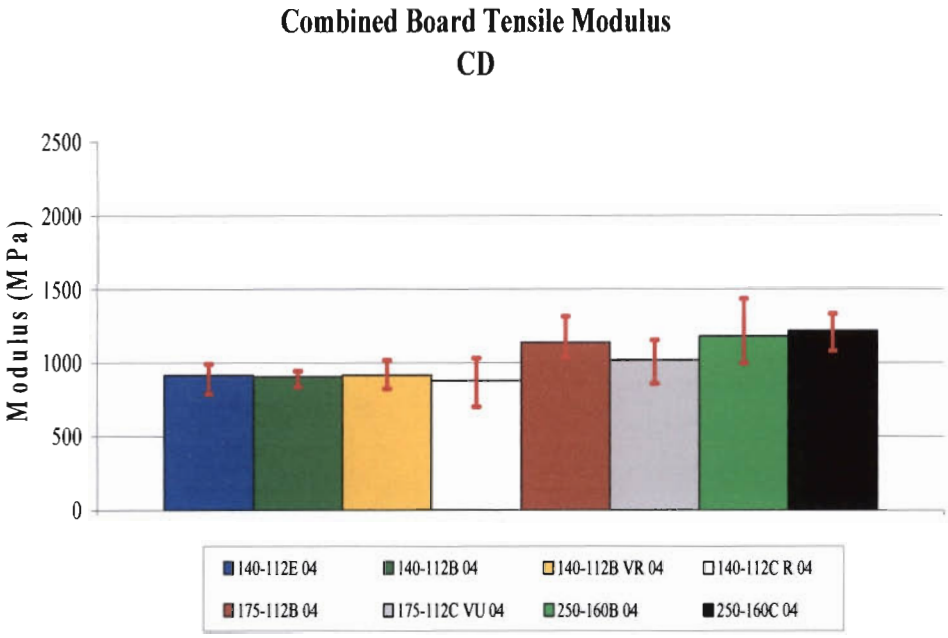

Figure 5.22: Comparison of all corrugated board tensile moduli in the CD.

Figure 5.23 shows the comparison of the board combination tensile moduli in the MD. These results showed more scatter in the sample behaviour than the results for the tensile tests conducted in the CD. The board samples with 140g/m² showed that the 140-112E 04 board and the 140-112B VR 04 board had similar moduli. This value was higher than the moduli exhibited by the 140-112B 04 and 140-112C R 04 board samples. The tensile moduli of the board samples with 175g/m² liners were fairly similar. These values were also very similar to the values exhibited by the 140-112E 04 board and the 140-112B VR 04 board samples. The board samples with 250g/m² liners had significantly higher tensile moduli than the other samples tested. The values of the 250-160B 04 and the 250-160C 04 samples were very similar. It is noted that the board samples with recycled content exhibited a larger data scatter than their virgin counterparts. As expected, the tensile moduli, in the MD, of all samples was higher than the value measured in the CD.

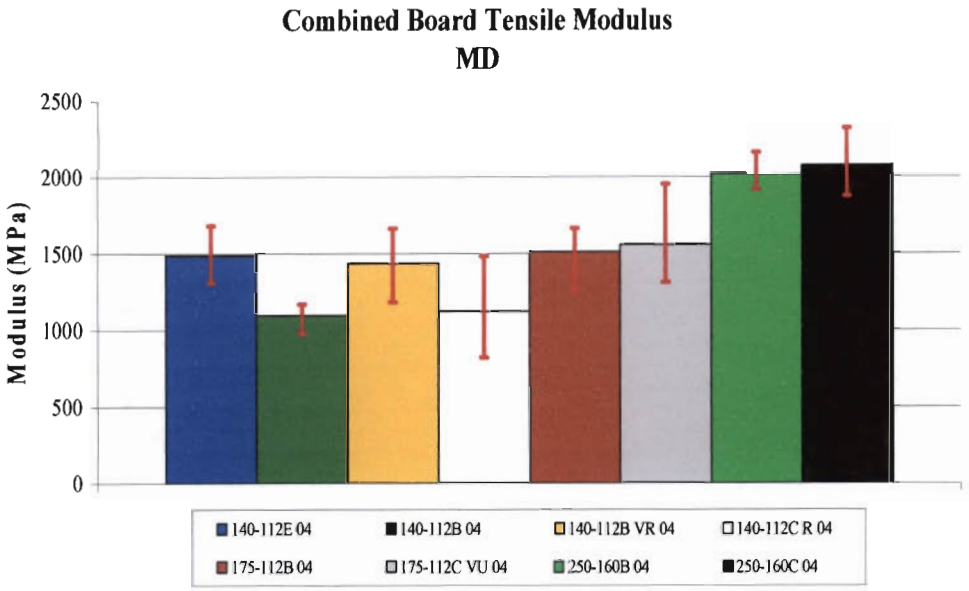

Figure 5.23: Comparison of all corrugated board tensile moduli in MD.

5.5.4 Correlation between Experimental Data and Predicted Bending Stiffness Value Using the Homogenisation Method

Bending stiffness predictions were performed using the combined board combinations tensile moduli stated in the previous section. A simple homogenisation method was used to predict the stiffness. The board was assumed to be a solid and the moment of inertia was approximated by the method mentioned in 2.3.2.4. The predicted values using the homogenisation method are shown in Table 5.9.

Sample	MD	CD
	Nm	Nm
140-112E 04	0.5	0.3
140-112B 04	2.2	1.9
140-112B VR 04	2.9	1.9
140-112C R 04	5.5	4.7
175-112B 04	2.9	2.4
175-112C VU 04	8.0	5.2
250-160B 04	5.0	2.9
250-160C 04	12.2	7.3

Table 5.9: Predicted stiffness values in the MD and the CD using a homogenisation method.

Figure 5.24 shows the correlation between the experimentally determined bending stiffness values and the values predicted using the homogenisation method. The correlation between the CD values is 95%. The correlation between the MD values is 83%.

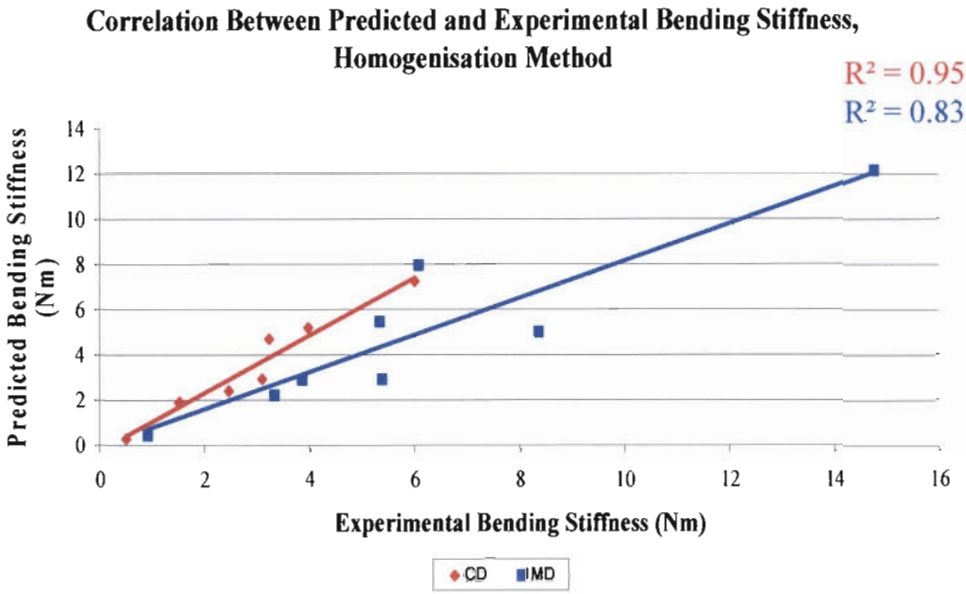

Figure 5.24: Correlation between experimental and predicted bending stiffness using a homogenisation method.

5.6 ECT Results

ECT testing was performed on all the board samples listed in Table 4.1. The average values, standard deviation of the mean and standard deviation of the samples tested are shown in Table 5.10.

Sample	ECS	SD
	kN/m	kN/m
140-112E 04	5.3 ± 0.11	0.4
140-112B 03	4.6 ± 0.04	0.1
140-112B 04	4.9 ± 0.08	0.3
140-112B VR 04	4.8 ± 0.06	0.2
140-112C 03	4.5 ± 0.03	0.1
140-112C R 04	5.2 ± 0.05	0.2
175-112B 04	5.5 ± 0.13	0.5
175-112C VU 04	5.9 ± 0.06	0.2
250-112B 03	7.7 ± 0.06	0.2
250-160B 04	7.7 ± 0.04	0.2
250-160C 03	8.0 ± 0.08	0.1
250-160C 04	7.7 ± 0.03	0.1

Table 5.10: ECS values of all the board samples tested.

5.6.1 ECT Results for Board Samples with 140g/m² Liners

Figure 5.25 shows a comparison of the ECT data of the board samples with 140g/m² liners tested. The ECS values for the samples are all fairly consistent. The ECS of the 140-112E 04 and 140-112C R 04 board samples were slightly higher than the other samples tested.

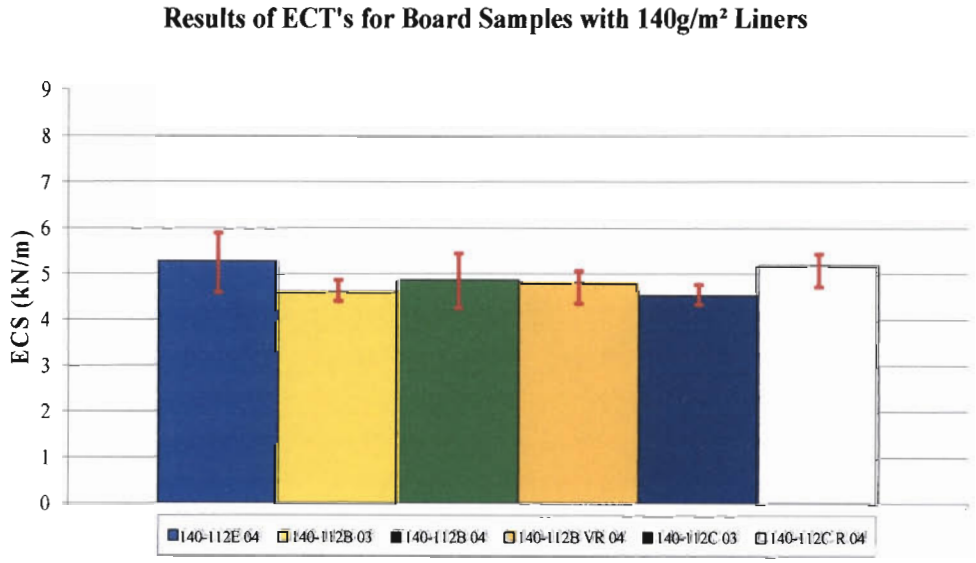

Figure 5.25: Comparison of ECS values for board samples with 140g/m² liners.

5.6.2 ECT Results for Board Samples with 175g/m² Liners

Figure 5.26 shows the comparison of the ECS values of board samples with 175g/m² liners. The ECS values of the two samples are consistent with one another, which is expected.

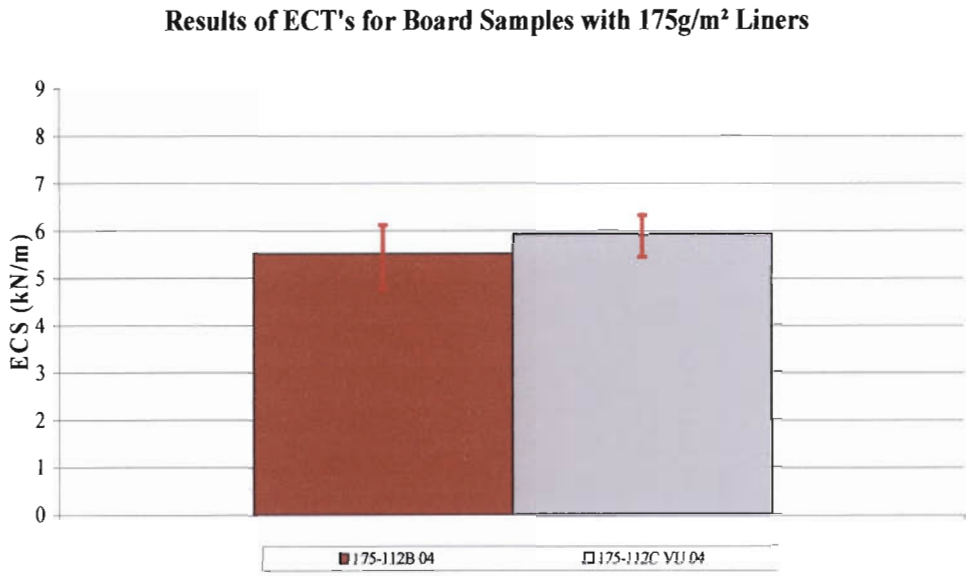

Figure 5.26: Comparison of ECS values for board samples with 175g/m² liners.

5.6.3 ECT Results for Board Samples with 250g/m² Liners

Figure 5.27 shows the comparison of board samples with 250g/m² liners. The board samples with 250g/m² liners had the highest ECS values of all the samples tested. The ECS values of the samples shown in Figure 5.27 are all similar.

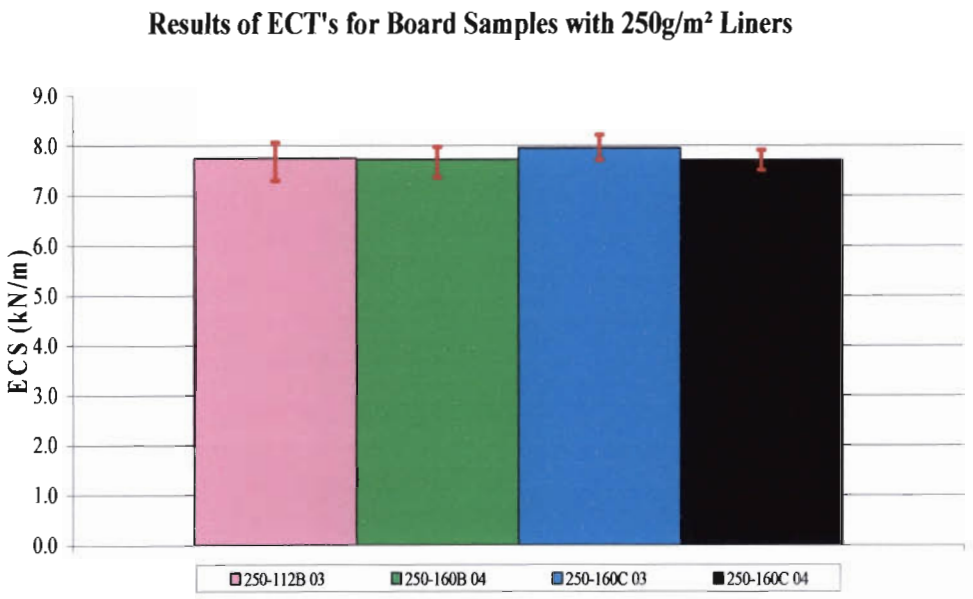

Figure 5.27: Comparison of ECS values for board samples with 250g/m² liners.

5.7 BCT Results

BCT's were performed on all the samples listed in Table 4.1. During the BCT the majority of boxes failed in a global buckling type failure as shown in Figure 5.28. In addition, the corners act as stress concentrations and often experienced compression type failure as shown in Figure 5.29. Material failure near the corners and edges of the boxes sometimes occurred. Examples of this are shown in Figure 5.30. In one or two cases the glue line of the boxes failed. These tests were excluded from the data later presented in this section. Examples are shown in Figure 5.31. In addition, cross-sectional photos of the buckled sections of corrugated board were taken to investigate the failure mechanisms that occurred. Figure 5.32 shows that, during buckling, corrugated boards undergo transverse shearing. Transverse shearing is often accompanied by bending and localized buckling as shown in Figure 5.33. The results of all the BCT's are shown in Table 5.11.

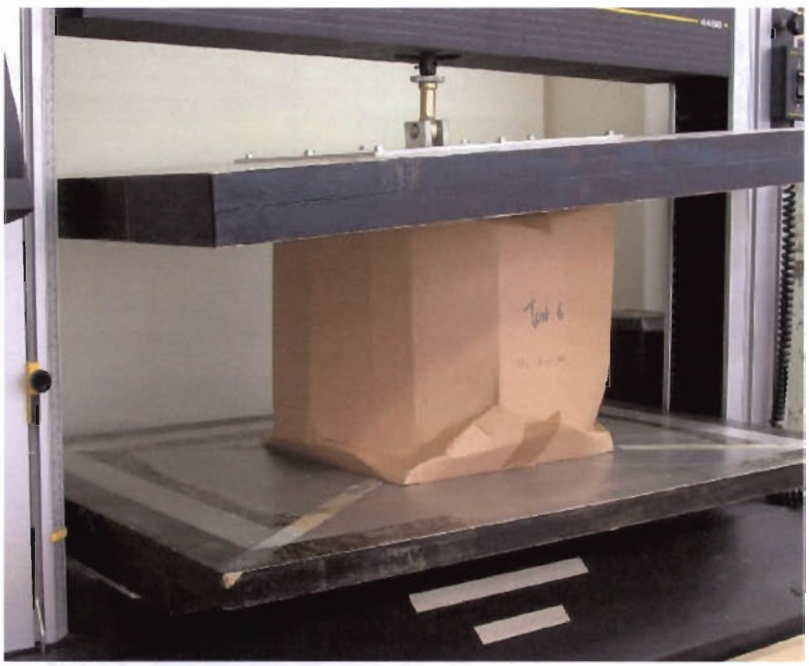

Figure 5.28: Global buckling of corrugated box during a BCT.

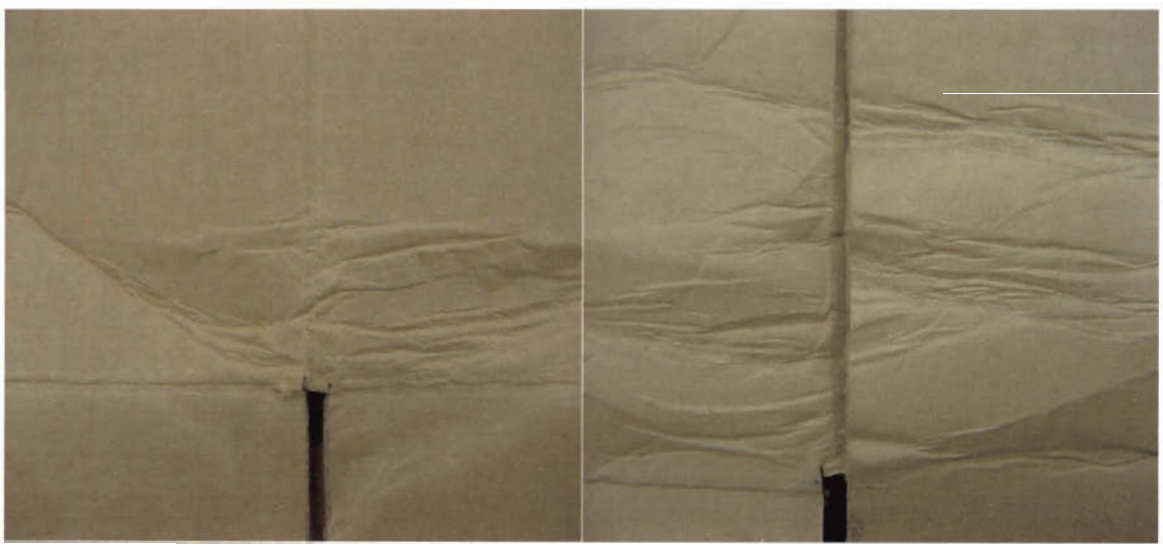

Figure 5.29: Compression of a box corner due to a BCT.

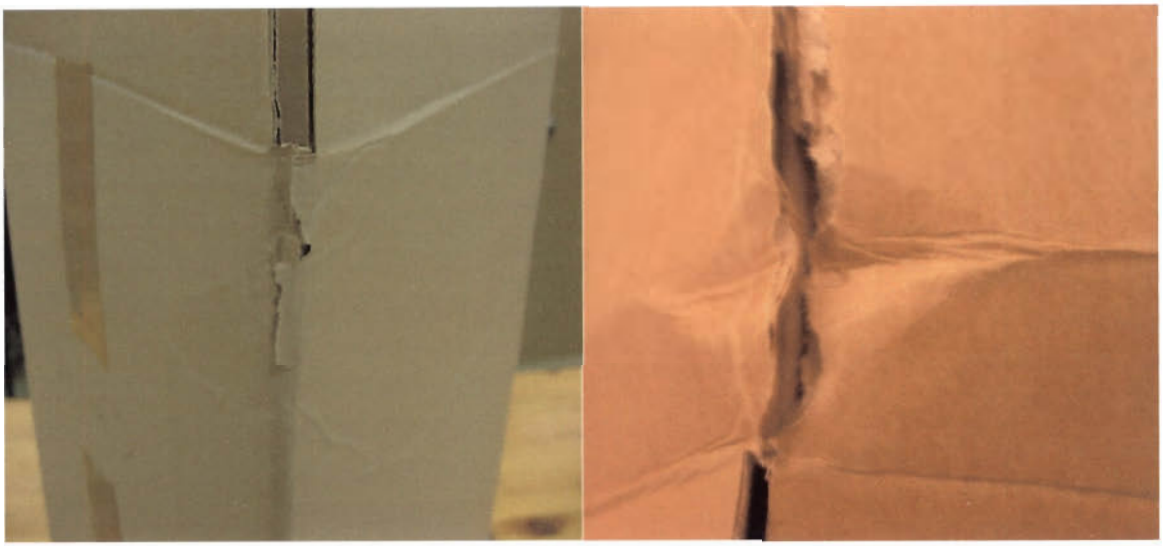

Figure 5.30: Liner material failure during a BCT.

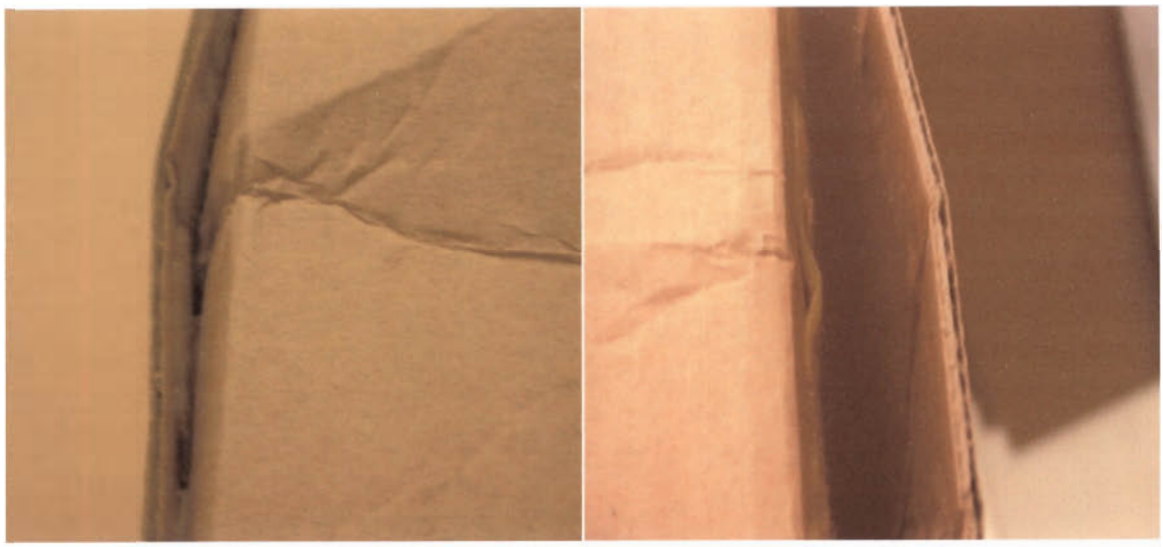

Figure 5.31: Glue line failure of corrugated board during a BCT.

Figure 5.32: Cross-section of a buckled panel showing transverse shearing.

Figure 5.33: Cross-section of a panel showing bending, localised buckling and transverse shearing.

Sample	Load	SD
	kN	kN
140-112E 04	1.28 ± 0.03	0.10
140-112B 03	2.38 ± 0.04	0.15
140-112B 04	2.44 ± 0.05	0.17
140-112B VR 04	2.12 ± 0.06	0.20
140-112C 03	2.36 ± 0.04	0.13
140-112C R 04	2.93 ± 0.09	0.25
175-112B 04	2.74 ± 0.07	0.21
175-112C VU 04	3.34 ± 0.09	0.28
250-112B 03	4.29 ± 0.06	0.23
250-160B 04	3.57 ± 0.06	0.03
250-160C 04	5.31 ± 0.11	0.33

Table 5.11: BCS data for all board combinations tested.

5.7.1 BCT Results for Board Samples with 140g/m² Liners

In Figure 5.34, the BCS of the 140-112E 04 sample was substantially lower than the other samples tested with this grammage liner. The values of the board samples with B flute were fairly similar. The 140-112C R 04 board sample had a higher BCS than all the other samples. It was significantly higher than the 140-112C 03 sample which was similar to the B flute board values.

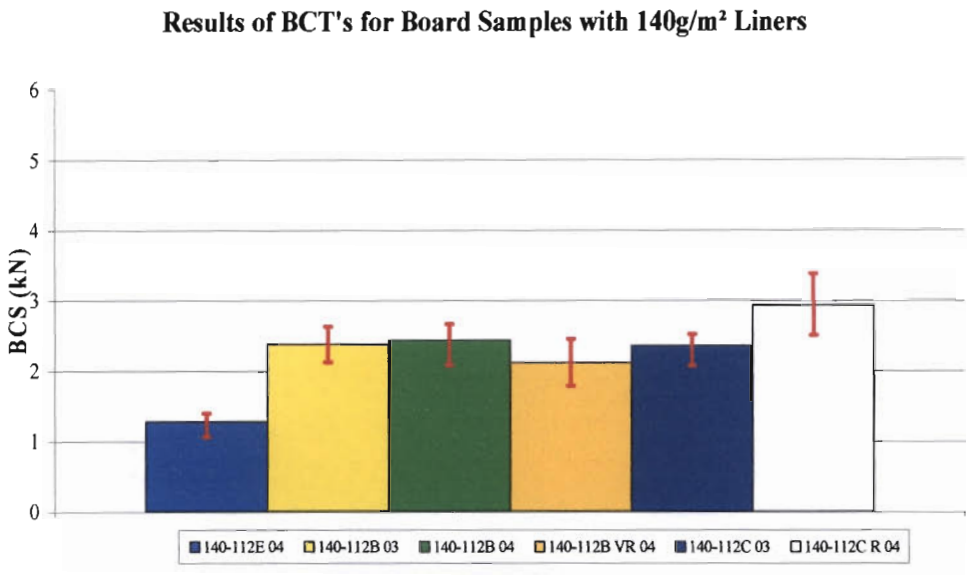

Figure 5.34: BCT results for board samples with 140g/m² liners.

5.7.2 BCT Results for Board Samples with 175g/m² Liners

Figure 5.35 shows a comparison of the average BCS values of the board samples with 175g/m² liners. The board with the C flute had a slightly higher BCS than the B flute board. This value was also higher than the board samples with 140g/m² liners. The board with B flute had a similar BCS to the 140-112C R 04 sample.

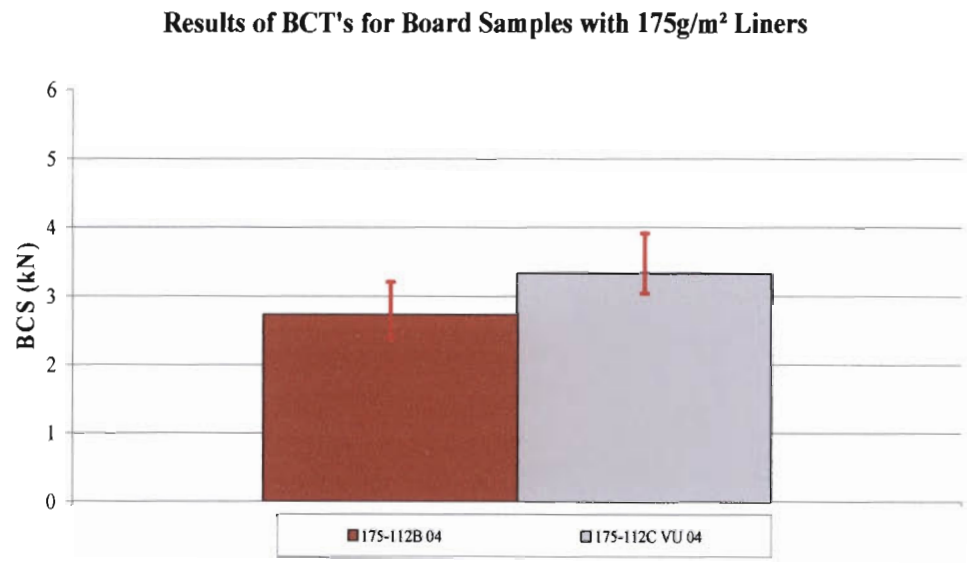

Figure 5.35: BCT results for 175-112 board combinations.

5.7.3 BCT Results for Board Samples with 250g/m² Liners

Figure 5.36 shows the BCS values for the board samples with 250g/m² liners. The BCS value of the 250-112B 03 board sample was higher than the 250-160B 04 sample. In addition, the BCS of the 250-160C 04 board sample was significantly higher than the BCS of the B flute boards. All the board samples with 250g/m² liners were higher than the previously mentioned samples BCS's.

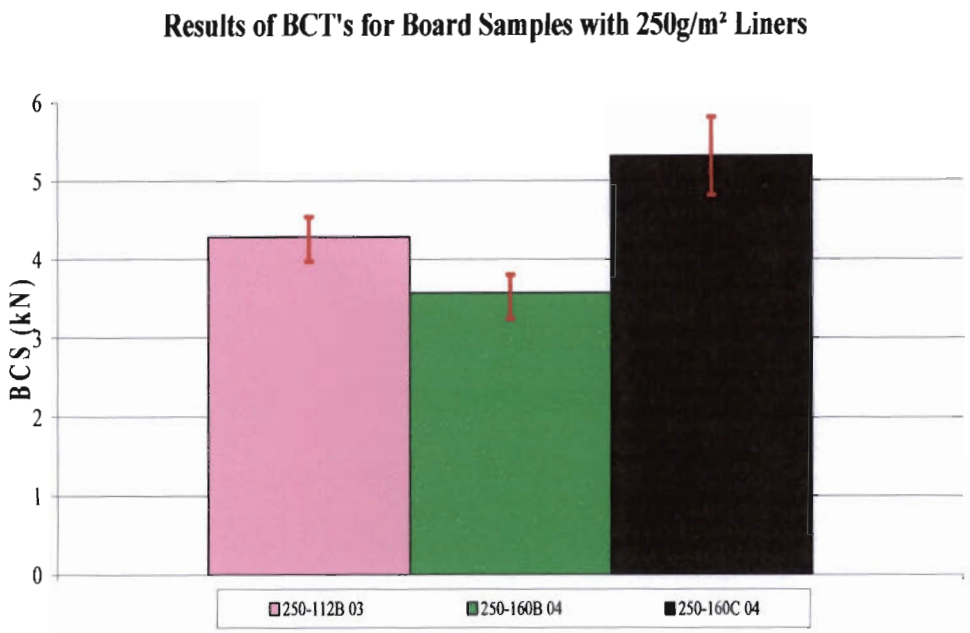

Figure 5.36: BCT results for 250-112/160-250 board combinations.

5.8 Box Strength Predictions Using the McKee Formulae

The BCS values of the boxes tested were predicted using the formulae mentioned in 2.4.4. The predicted values were then compared to the experimental values. Where applicable, the values were predicted using experimental bending stiffness values and the same calculations were then repeated with predicted bending stiffness values. For convenience, the correlation of the predicted values with the experimental BCS values has been plotted on the same set of axis for each prediction method.

5.8.1 Predicted Values Using the McKee Formula 1 and the Nordstrand Formula for Critical Buckling Load

Table 5.12 shows the predicted BCS values using the McKee formula 1 and the Nordstrand method for the critical buckling load of orthotropic plates not including transverse shear affects.

Sample	Predicted Bending Stiffness	Experimental Bending Stiffness
	Predicted BCT Value (N)	**Predicted BCT Value (N)**
140-112E 04	1668	1922
140-112B 03	2356	2358
140-112B 04	2450	2366
140-112B VR 04	2457	2364
140-112C 03	2848	2685
140-112C R 04	3203	2955
175-112B 04	2861	2926
175-112C VU 04	3654	3426
250-112B 03	4023	4173
250-160B 04	3909	4020
250-160C 04	4850	4691

Table 5.12: Predicted BCS values using the McKee formula 1 and the Nordstrand method for the critical buckling load.

Figure 5.37 shows a comparison of the experimental BCS values compared to the predicted BCS values. The correlation between the experimental values and the predicted values, using predicted stiffness values, is 95%. The correlation between the experimental BCS values and the predicted values, using experimental bending stiffness values, is 94%.

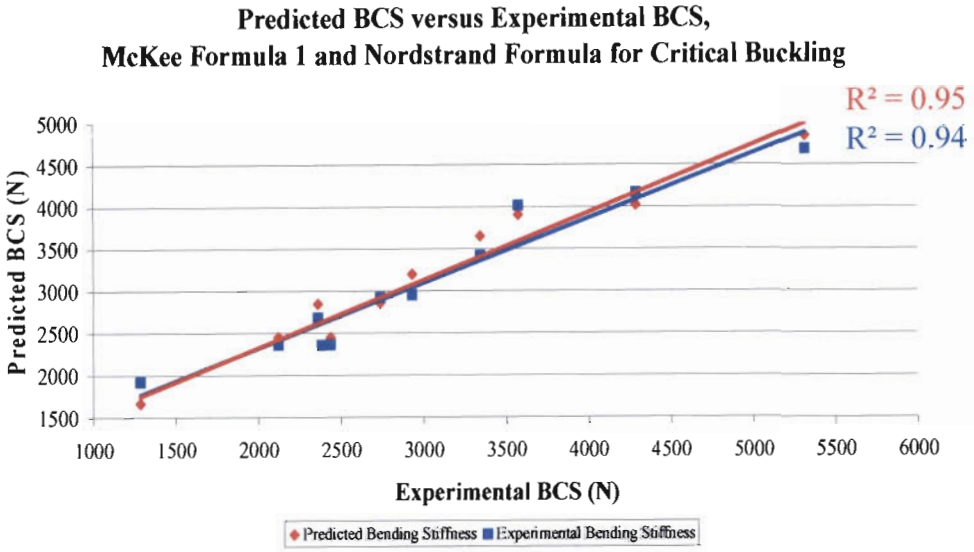

Figure 5.37: Correlation between the experimental BCS and predicted BCS using the McKee formula 1 and Nordstrand's method for calculating the critical buckling load of orthotropic plates.

5.8.2 Predicted BCS Values Using the McKee Formula 1 and the Hahn *et al.* Formula for Critical Buckling Load

Table 5.13 shows the predicted BCS values using the McKee formula 1 and the Hahn *et al.* method for the critical buckling load of orthotropic plates, not including transverse shear affects.

Sample	Predicted Bending Stiffness	Experimental Bending Stiffness
	Predicted BCT Value (N)	**Predicted BCT Value (N)**
140-112E 04	1369	1597
140-112B 03	2024	2027
140-112B 04	1948	2008
140-112B VR 04	2004	2038
140-112C 03	2401	2183
140-112C R 04	2544	2432
175-112B 04	2281	2482
175-112C VU 04	2985	2797
250-112B 03	3475	3574
250-160B 04	3229	3490
250-160C 04	3998	4031

Table 5.13: Predicted BCS values using the McKee formula 1 and the Hahn *et al.* formula for critical buckling load of orthotropic plates.

Figure 5.38 shows a comparison between the experimental BCS values and the predicted BCS. The correlation between the experimental values and the predicted values, using predicted stiffness values, is 95%. The correlation between the experimental BCS values and the predicted values, using experimental bending stiffness values, is 94%.

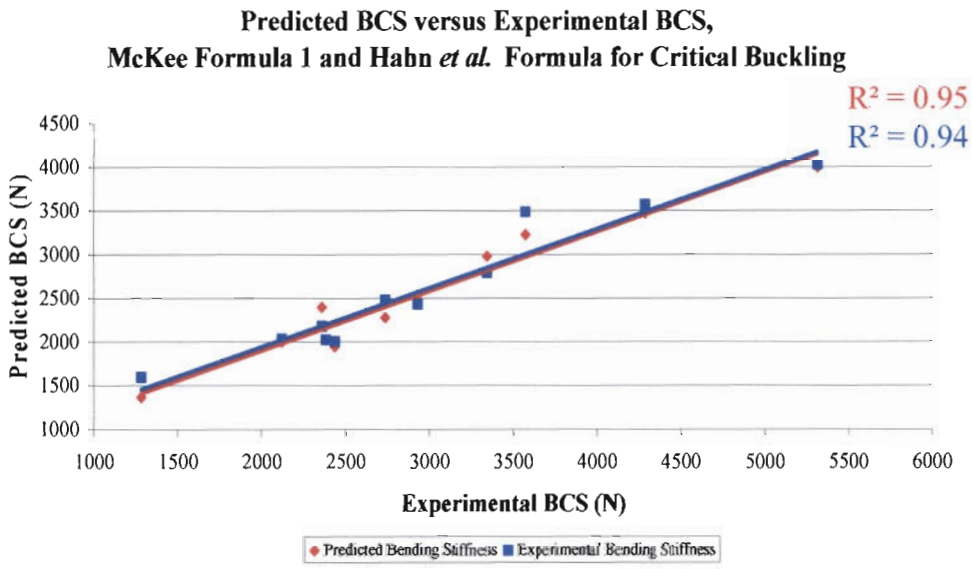

Figure 5.38: Correlation between the experimental BCS and predicted BCS using the McKee formula 1 and the Hahn *et al.* method for calculating the critical buckling load of orthotropic plates.

5.8.3 Predicted BCS Values Using the McKee Formula 1 and the McKee Formula for Critical Buckling Load

Table 5.14 shows the predicted BCS values using the McKee formula 1 and the McKee formula for the critical buckling load of orthotropic plates, not including transverse shear affects.

Sample	Predicted Bending Stiffness	Experimental Bending Stiffness
	Predicted BCT Value (N)	**Predicted BCT Value (N)**
140-112E 04	1374	1500
140-112B 03	1888	1890
140-112B 04	1881	1906
140-112B VR 04	1906	1915
140-112C 03	2251	2033
140-112C R 04	2384	2262
175-112B 04	2156	2297
175-112C VU 04	2801	2612
250-112B 03	3212	3329
250-160B 04	3001	3225
250-160C 04	3807	3809

Table 5.14: Predicted stiffness values using the McKee formula 1 and the McKee formula for critical buckling load of orthotropic plates.

Figure 5.39 shows the correlation between the predicted BCS and experimental BCS. The correlation between the experimental values and the predicted values, using predicted stiffness values, is 96%. The correlation between the experimental BCS values and the predicted values, using experimental bending stiffness values, is 94%.

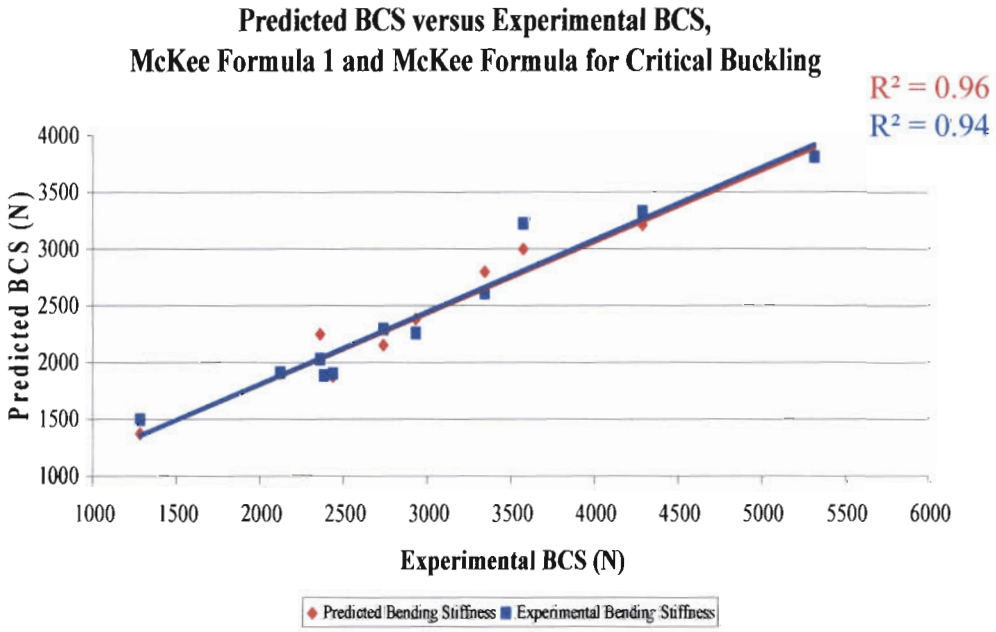

Figure 5.39: Correlation between the experimental BCS and predicted BCS using the McKee formula 1 and the McKee formula for calculating the critical buckling load of orthotropic plates.

5.8.4 BCS Predictions Using the McKee Formula 2

Table 5.15 shows the predicted BCS values using the McKee formula 2. As with the other formulae previously mentioned, the calculations were performed for experimental and predicted bending stiffness values.

Sample	Predicted Bending Stiffness	Experimental Bending Stiffness
	Predicted BCT Value (N)	**Predicted BCT Value (N)**
140-112E 04	1283	1494
140-112B 03	1880	1883
140-112B 04	1831	1871
140-112B VR 04	1879	1892
140-112C 03	2240	2048
140-112C R 04	2391	2278
175-112B 04	2144	2313
175-112C VU 04	2799	2623
250-112B 03	3224	3323
250-160B 04	3023	3234
250-160C 04	3744	3745

Table 5.15: Predicted BCS values using the McKee formula 2 and experimental and predicted bending stiffness values.

Figure 5.40 shows a comparison between the predicted BCS and experimental BCS. The correlation between the experimental values and the predicted values, using predicted stiffness values, is 95%. The correlation between the experimental BCS values and the predicted values, using experimental bending stiffness values, is 94%.

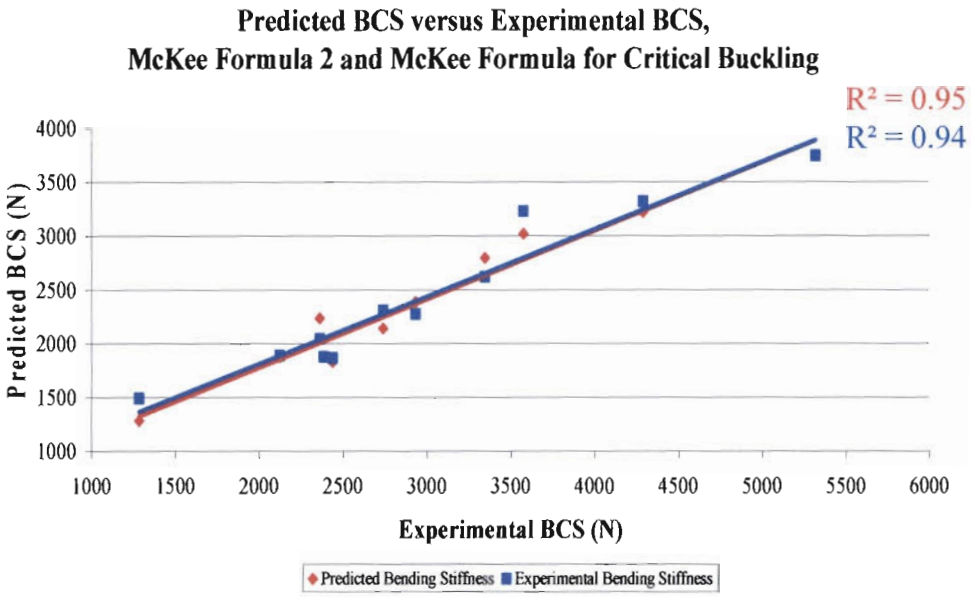

Figure 5.40: Correlation between the experimental BCS and predicted BCS using the McKee formula 2 and the McKee formula for calculating the critical buckling load of orthotropic plates.

5.8.5 BCS Predictions Using the McKee Formula 3

Table 5.16 shows the predicted BCS values using the McKee formula 3. As with the other formulae previously mentioned, the calculations were performed for experimental and predicted bending stiffness values.

Sample	Predicted Bending Stiffness	Experimental Bending Stiffness
	Predicted BCT Value (N)	**Predicted BCT Value (N)**
140-112E 04	1177	1371
140-112B 03	1726	1728
140-112B 04	1680	1717
140-112B VR 04	1724	1736
140-112C 03	2056	1879
140-112C R 04	2194	2091
175-112B 04	1967	2122
175-112C VU 04	2568	2407
250-112B 03	2959	3049
250-160B 04	2774	2968
250-160C 04	3436	3437

Table 5.16: Predicted BCS values using the McKee formula 3 and experimental and predicted bending stiffness values.

Figure 5.41 shows the correlation between the experimental BCS values and the predicted BCS values. The correlation between the experimental values and the predicted values, using predicted stiffness values, is 95%. The correlation between the experimental BCS values and the predicted values, using experimental bending stiffness values, is 94%.

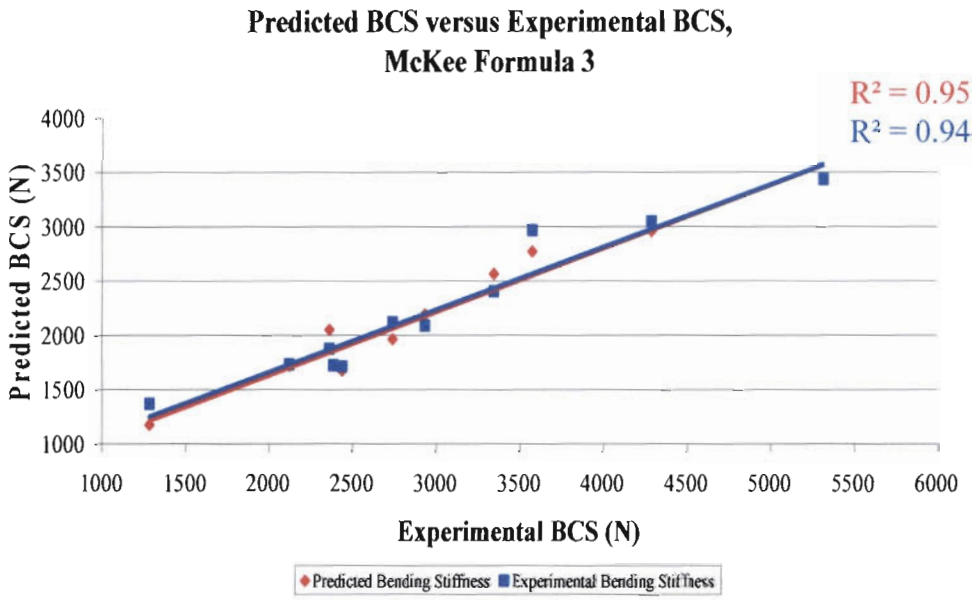

Figure 5.41: Correlation between the experimental BCS and predicted BCS using the McKee formula 3.

5.8.6 BCS Predictions Using the McKee Formula 4 and 5

Table 5.17 shows the predicted BCS values using McKee formula 4 and 5. The formulae do not require any bending stiffness data. Figure 5.42 shows the comparison of experimental BCS versus predicted BCS using the McKee formula 4 and 5. Using the McKee formula 4, the correlation between the experimental and predicted value is 94%. Using the McKee formula 5, the correlation between the experimental and predicted BCS values is 94%.

Sample	McKee Formula 4	McKee Formula 5
	Predicted BCT Value (N)	**Predicted BCT Value (N)**
140-112E 04	1264	1332
140-112B 03	1521	1595
140-112B 04	1611	1690
140-112B VR 04	1589	1666
140-112C 03	1754	1835
140-112C R 04	2014	2107
175-112B 04	1839	1928
175-112C VU 04	2292	2398
250-112B 03	2632	2759
250-160B 04	2641	2768
250-160C 04	3057	3197

Table 5.17: Predicted BCS values using the McKee formula 4 and 5.

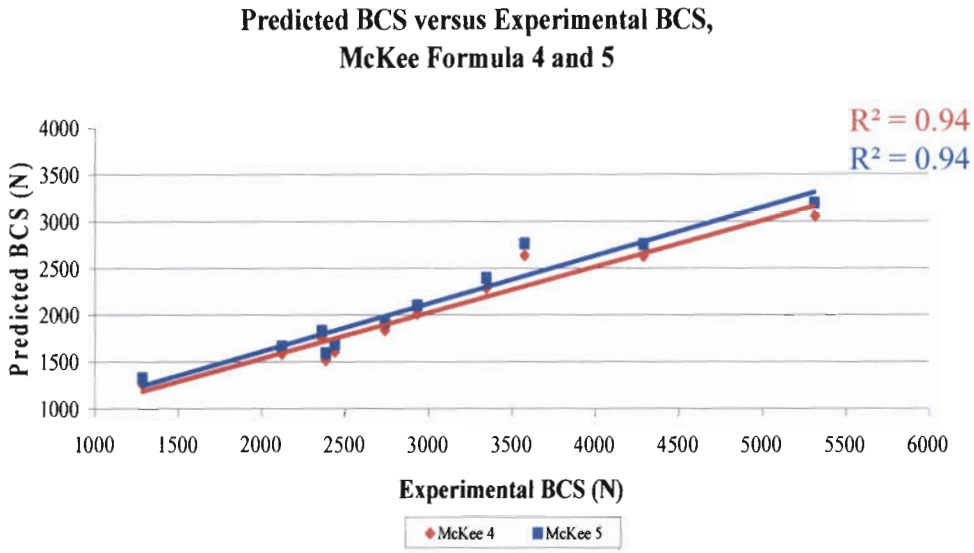

Figure 5.42: Correlation between the experimental BCS and predicted BCS using the McKee formula 4 and the McKee formula 5.

5.9 Urbanik Non-linear Material Model

Table 5.18 shows the predicted BCS values using the Urbanik non-linear material model and predicted and experimental bending stiffness data. The elasticity constant c_1 was recorded during the combined board tensile tests and therefore only BCS predictions of the board combinations that were tensile tested have been performed.

Sample	C_1	Predicted Stiffness Values	Experimental Stiffness Values
	MPa	**Predicted BCS (N)**	**Predicted BCS (N)**
140-112E 04	39.5	1763	2071
140-112B 04	18.6	2874	2937
140-112B VR 04	14.4	2839	2858
140-112C R 04	20.0	3703	3544
175-112B 04	21.8	3511	3777
175-112C VU 04	21.0	4531	4279
250-160B 04	29.2	4999	5331
250-160C 04	44.2	6824	6825

Table 5.18: Predicted BCS values using the Urbanik non-linear material model and predicted and experimental bending stiffness values.

Figure 5.43 shows a comparison between the experimental and predicted BCS values calculated using Urbanik's non-linear material model. The correlation between the experimental values and the predicted values, using predicted stiffness values, is 98%. The correlation between experimental BCS values and the predicted values, using experimental bending stiffness values, is 96%.

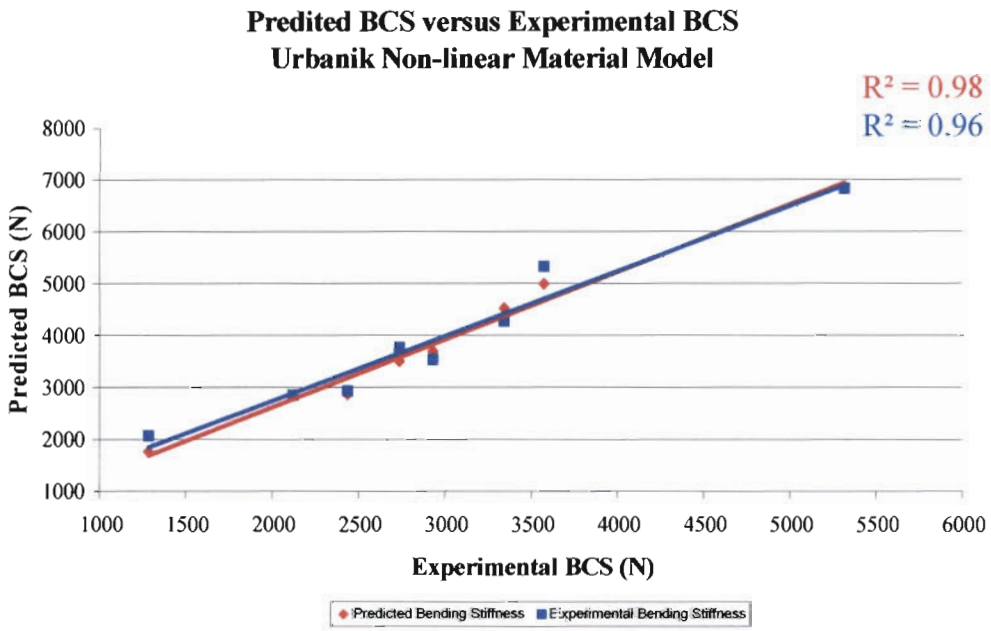

Figure 5.43: Correlation between the experimental BCS and predicted BCS using Urbanik's non-linear material model.

CHAPTER 6

DISCUSSION

The following chapter deals with the discussion of the results in *Chapter 5*. This chapter will be divided into three sections. The first section will deal with the test fixtures designed, particularly the MD shear stiffness fixture. The next section will discuss the material and structural properties that affect the properties of corrugated board and boxes. Finally, the different box strength methods will be discussed.

6.1 Test Fixture Design and Accuracy

6.1.1 The Block Shear Fixture

As mentioned in 3.2, the block shear fixture was modified to make the method as easy and time efficient as possible, without sacrificing the accuracy of the method. This was to be achieved through the use of wooden inserts. It was thought that by having multiple inserts, a full set of specimens for each board combination could be glued prior to testing, so that when the tests were performed, time would not be wasted by needing to clean the block shear plates and glue the specimen after each test had been performed. However, a large amount of time was consumed by screwing the wooden inserts into place so that they were held as firmly as possible. In addition, the inserts had to be unscrewed at the end of each test. This was time consuming. In some circumstances the screws holding the inserts caused the wooden inserts to shear. These test results were unacceptable.

The results from the block shear test were of the same magnitude as the results stated by Aboura *et al.* and Nordstrand *et al.* [**1**,**19**]. In addition, the load deflection plots were similar to the load deflection plots found in the literature. This indicates that the block shear moduli measured in this project are consistent with those found in the literature. It is felt that the use of inserts for block shear testing can lead to a more optimised test method. However, the inserts would need to be manufactured from a metal rather than wood. In addition, a more acceptable method of fastening the inserts to the fixture would need to be investigated to ensure the speed of the testing procedure. This could be achieved through the use of magnets.

6.1.2 The MD Shear Stiffness Fixture

The MD shear test method proved to be easier to perform than the block shear test. In addition, the fact that there was no lengthy gluing or cleaning procedures involved saved a substantial amount of time. However, due to manufacturing problems there was a small amount of interference between the rack and pinion of the designed fixture. It is felt that through a better manufacturing process and through the use of a lower module rack and pinion these interference problems can be minimized. In addition, the length of the rack need not be so long in any future MD shear fixtures. The rack was originally made long as the author was unsure of exactly what was meant by a small angle of twist [**40**]. The preliminary load torsion tests that were performed to establish a baseline for the loads that were expected, were substantially higher than those recorded during testing. This is also an indication that a finer module rack and pinion could be used. In addition, the grips that were used, whilst accurately twisting the specimens, are not suitable for fast and regular testing in an R&D environment and should be replaced by pneumatic grips. It is felt that better and more consistent results could be obtained through using bigger samples than those stated by McKinlay [**40**]. The literature does not provide any numerical evidence as to a preferred strain rate. The strain rate affects the speed at which the tests can be performed and thus in an R&D environment there is a need to optimise the method to achieve the best possible results.

The results from the MD shear testing had a 0.97 coefficient of determination when compared with the block shear results. This indicates that the two test methods have a good correlation. In addition, there is a 90% confidence level with the stiffness values calculated using this test method as shown in Table 6.1. This indicates that the MD shear fixture is working correctly and accurately. In addition, it has a high reproducibility. As a result, this method can be used for calculating the MD shear stiffness of corrugated board. However, the major limitation of this test is that it is only valid for the MD. Further research should be conducted to investigate the application of this method for the measurement of the CD transverse shear stiffness.

Sample	Value	Confidence
	N/m	
140-112E 04	2458 ± 141.2	90%
140-112B 03	3937 ± 260.5	90%
140-112B 04	4630 ± 175.6	90%
140-112B VR 04	4806 ± 313.8	90%
140-112C 03	3812 ± 128.3	90%
140-112C R 04	4003 ± 153.0	90%
175-112B 04	4097 ± 253.3	90%
175-112C VU 04	4762 ± 227.3	90%
250-112B 03	7435 ± 330.3	90%
250-160B 04	5828 ± 359.1	90%
250-160C 03	8694 ± 234.3	90%
250-160C 04	6079 ± 307.2	90%

Table 6.1: The level of confidence associated with the MD shear stiffness values.

6.2 Properties Affecting Corrugated Board and Box Strength

6.2.1 Effect of Paper Grammage

The tensile stiffness of the liner and fluting exhibited the behaviour expected. The tensile stiffness of the liners and fluting tested showed that the higher the paper

grammage, the higher the tensile stiffness in a given direction. This behaviour was consistent with the combined board tensile tests. However, this trend was not consistent when virgin paper was compared to recycled paper. The 140g/m² virgin liner had a higher MD stiffness than the 160g/m² Bayflute (which has a recycled content), but a lower CD stiffness. This is mainly due to the assumed reduced fibre length in the 160g/m² Bayflute sample due to the recycling process.

It is evident from the MD shear testing that the grammage of the paper used, affects the transverse shear stiffness. In general, the boards with heavier fluting grammage had higher transverse shear stiffness than the board with the lighter fluting. This behaviour was reinforced by the block shear test results. However, there were exceptions. The 250-112B 03 board had a higher stiffness than all the other boards with 112g/m² liners and this behaviour is assumed to be due to the year in which it was manufactured and its associated peculiarities. In addition, this board combination had a higher stiffness than the two board combinations with 160g/m² liners manufactured in 2004. This behaviour could be due to the stiffness of the liners or differences in the manufacturing process. These differences could be due to factors such as:

- Changes in the adhesive used
- Moisture effects
- Different pressures during manufacture
- Damage during manufacture
- Different paper properties

In general, the board combinations manufactured with the heavier paper grammage, namely the boards manufactured with 250g/m² liners and 160g/m² fluting, had higher bending stiffness in both the MD and the CD. It is also evident that the board combinations with the higher grammage liners and the lighter 112g/m² fluting had higher bending stiffness than the boards with the same fluting and lighter liners. The

250-112B 03 and the 175-112B 04 boards showed anomalous behaviour. The 175-112B board had a lower CD stiffness than the 140-112C board, but had a slightly higher average MD stiffness. This indicates that flute height could have a greater effect on bending stiffness than paper grammage as the CD tensile modulus of the 175-112B 04 board was higher than the 140-112C R 04 board. The 250-112B 03 board had a higher bending stiffness in both the MD and CD than the 250-160B 04 board. This was unexpected as the 250-160B 04 board has a heavier fluting. The differences can only be attributed to the fact that one board was manufactured in 2003 and the other in 2004. This board combination showed the same trends in the shear stiffness results. This reinforces the fact that there could have been differences in the manufacturing process.

The ECT results showed that the boards with a heavier paper grammage have a higher ECS than the boards with a lower grammage paper. The BCT results showed the same behaviour as the other test methods discussed. The boxes with heavier paper grammage had higher BCS values than those with smaller paper grammage. In addition, the 250-112B 03 boxes had a higher BCS than the 250-160B 04 boxes which is consistent with the other test results.

6.2.2 Effect of Fibre Alignment

The fibre alignment direction, i.e. the MD or CD, plays an important role in strength design. The MD strength and stiffness of the paper and board tested was higher than the CD strength for all of the test methods. It would appear that board combinations with recycled content have a reduced strength difference between the CD and MD and an increased scatter in the strength values. The literature states that the transverse shear stiffness of corrugated board is higher in the CD than in the MD **[1,19]**. However, it raises an important question as to whether boxes could be made stronger by orientating the box sides with the MD up. The bending stiffness of board in the MD is substantially higher than the CD, however the ECS and transverse shear values are higher in the CD than the MD. These two factors would dominate any advantage the bending stiffness could add to a box of this nature.

6.2.3 Effect of Flute Height

The flute height affects the transverse shear stiffness of corrugated board. This was expected considering the reports of this in the literature [**18,19,39**]. The lowest MD shear stiffness was exhibited by the 140-112E 04 board combination. The 140-112C board combinations had a lower stiffness than the 140-112B board combinations. This was expected considering the results shown in the literature and the block shear results. It indicates that the distance of separation of the facings plays an important role in transverse shear stiffness and modulus. The 175-112B 04 board had a lower stiffness than the 175-112C VU 04 board. This result was not expected due to the trends shown in the literature and the results of the 140-112 board combinations. The only possible explanation is due to a change in the manufacturing conditions for the two boards, or the fact that the uniliner plays a significant role in the MD stiffness of the board. However, there is at present no data to substantiate this and it is assumed that the difference is more likely due to the manufacturing process.

The board combinations with 250g/m² liners showed some interesting MD shear results. The 250-112B 03 board showed a higher stiffness than the 250-160B 04 and 250-160C 04 boards. In addition, the stiffness of the 250-160B 04 board was slightly lower than the 250-160C 04 board combination manufactured in the same year. The 250-160C 03 board had a higher stiffness than any of the previously discussed results. These results are indicative of the fact that, even though it is assumed that the separation of the faces plays an important role in transverse shear stiffness of corrugated board, there are other effects and mechanical properties that are also influencing these results. The effect of the actual manufacturing process cannot be underestimated and is stated as an important influence in the literature [**18,19,39**]. However, it must be noted that these tests were performed on corrugated board prior to secondary operations and there is no indication on how post board operations such as cutting and printing may affect transverse shear properties and ultimately box strength. The fact that the MD shear method can detect differences in stiffness between the same board combinations, indicates that this method has possible applications as a quality control method.

The bending stiffness of corrugated board is strongly influenced by the separation of the faces. This, in turn, is related to the height of the flute, which is determined by the flute profile, with the C flute having the highest flute height and E flute the lowest. As expected, the board combinations with C flute had higher stiffness than the board combinations with B flute with the same liner material. The 140-112E 04 board showed the lowest bending stiffness value in both the MD and CD. Due to the low flute height this result was expected. As expected, the 175-112C VU 04 board exhibited a higher bending stiffness than the 175-112B 04 board in both the MD and CD. The 175-112B 04 board had lower CD stiffness than the 140-112C boards and a similar MD stiffness values. In terms of the units of measurement it appears that the flute height is more dominant in affecting bending stiffness than paper grammage. This is evident considering that the 140-112C R 04 board with the recycled content has a higher stiffness in the CD even though it has a lower paper grammage than the 175-112B 04 board. The bending stiffness of the board combinations with 250g/m² liners exhibited the behaviour expected; with the board combination with C flute having higher stiffness in both the MD and CD than the B flute board combinations. However, the fact that the 250-112B 03 board had a significantly higher bending stiffness than the 250-160B 04 board in both the MD and CD was consistent with the other test methods used.

Flute height also affected the ECS values. Generally, the board with the higher flute height exhibited larger ECS values. This is consistent with the literature, which states that boards with low slenderness values have good compression properties [**64**]. However, there were a number of exceptions to this rule, namely the 140-112E 04, 140-112C 03 and the 250-160C 04 boards. It is thought that the 140-112E 04 boards' high ECS has to do with the failure mechanism of this board type which is strongly influenced by the flute profile. The 140-112C 03 board had a lower ECS which is thought to be related to the manufacturing process. This is reinforced by the fact that the MD bending stiffness of this board was lower than the 140-112C R 04 board. The fact that the 250-112B 03 board had a similar ECS to the 250-160B 04 board was interesting as it was not consistent with the other test results already described.

As expected, the boxes with the C flute profile had higher BCS than the boxes with B flute. The exceptions to this were the 140-112C 03 boxes and the 175-112B 04 boxes. The 140-112C 03 boxes had a lower BCS than the 140-112C R 04 boxes. This was consistent with the MD bending stiffness results and the transverse shear results. This is attributed to the year of manufacture i.e. the manufacturing process, as theoretically it was expected that the 140-112C R 04 boxes would have a lower BCS due the recycled nature of the liners. The 175-112B 04 boxes had lower BCS than the 140-112C R 04 board. The 175-112B 04 board had a slightly higher MD bending stiffness and transverse shear value, but a substantially lower CD bending stiffness which could account for this.

6.2.4 Effects of Virgin vs. Recycled Paper

The use of virgin and recycled paper in the board construction had an effect on the board properties. It appears that the liner properties have no affect on the MD shear stiffness of corrugated board. The 175-112B 04 board had a slightly lower stiffness than the 175-112C VU 04 board manufactured with a uniliner. This result was not expected due to the trends shown in the literature and the results of the 140-112 board combinations. The only possible explanation is due to a change in the manufacturing conditions for the two boards, or the fact that the uniliner plays a significant role in the MD stiffness of the board. However, there is at present no data to substantiate this and it is assumed that the difference is more likely due to the manufacturing process.

The combined board tensile modulus of the 140-112B VR 04 board had a higher modulus than the 140-112B 04 board in both the MD and the CD. This result explains why the bending stiffness of the board with recycled liners had higher bending stiffness than its virgin counterpart manufactured in the same year. The 140-112C R 04 board with recycled liners had a lower modulus than the 140-112C 03 board in both the MD and CD. This was expected considering the fact that the recycled fibres would be shorter than the virgin fibres. The CD modulus of the 175-112B 04 board is slightly higher than the 175-112C VU 04 board, while the MD tensile modulus of the 175-112C VU 04 board was higher than the 175-112B 04

board in the MD. This result was not expected due to the fact that the 175-112C VU 04 board consists of a uniliner with virgin and recycled paper.

The 140-112B VR 04 board showed a higher bending stiffness than the 140-112B 04 board, but had lower stiffness than the board manufactured in 2003 in the MD. Its CD value was similar to the 2004 board, but still lower than the 2003 board. Assuming similar manufacturing conditions, the only difference between the 140-112B board combinations manufactured in 2004 was the fact that the one had a recycled liner. Therefore the only reason for the difference in the bending stiffness would be related to the mechanical properties of the liners. The 140-112C R 04 board had a higher MD bending stiffness than the same combination manufactured in 2003. As expected, the 175-112C VU 04 board exhibited a higher bending stiffness than the 175-112B 04 board in both the MD and CD. What was of particular interest with this board combination, was the bending stiffness results with the virgin liner in different orientations i.e. up and down. It was noted that the bending stiffness with the uniliner facing down was about 20% higher. This was deemed to be a significant difference for a simple reversal of the board orientation.

The ECT values of the 140-112B board combinations were all fairly consistent. This indicates that the recycled liner used in the 140-112B VR 04 board had similar compression properties to the virgin material. This was expected, as recycling will tend to affect tensile properties more than the compressive properties due to the reduction of fibre length in the recycling process. The 140-112C R 04 board had a substantially higher ECT value than its virgin counterpart. This indicates that the recycled paper may have had better mechanical properties than the virgin liners. This assumption is reinforced by the fact that the transverse shear stiffness of the 140-112C R 04 board was higher than the 2003 board combination. The ECT values of the 175-112 board combinations were fairly similar with the C flute board having a slightly higher ECT value which once again indicates that the uniliner may have better mechanical properties than the virgin material.

6.2.5 Effect of Board Structure

The bending stiffness results showed that the structure of the board i.e. the position of the liners, in an unbalanced board combination can affect the properties of the board and ultimately the BCS of a box. This was highlighted by the 175-112C VU 04 board. When tested with the uniliner down this board had a higher bending stiffness than when tested with the uniliner up. Typically, the box would be manufactured with the uniliner on the inside face of the box. As this orientation has substantially lower bending stiffness than with the uniliner down, the box could be made substantially stronger by just reversing the box orientation. This increased strength could be achieved at no extra cost.

6.3 Board and Box Strength Predictions

6.3.1 Bending Stiffness Predictions

Two different methods were used to predict the bending stiffness of corrugated board. The Urbanik method had an 83% correlation with the experimental values in the MD and a 94% correlation with the CD experimental values. This was a good correlation. The homogenization method also had good correlation with the experimental values. A 95% correlation with the CD value and an 83% correlation with the MD values was found. Comparing these values to the Urbanik method it is felt that the Urbanik method produces a more accurate prediction method as it incorporates the whole flute profile, not just the face separation. The correlation between the experimental and predicted values may produce better values if a 4-point bend test method is used. The reason for this is that this method is based on the pure bending properties of corrugated board, while it is recognised that the 3-point bend test does not lead to a state of pure bending and has inherent transverse shear effects that would influence the results [**19**,**34**,**48**]. In addition, the Urbanik MD correlation may be improved if the effect of the fluting is included.

6.3.2 Box Strength Predictions

Figure 6.1 shows the comparison of all the BCS predictions using McKee formula 1 and Urbanik's formula. Even though the Urbanik formula and the McKee formula 1, using Nordstrand's formula for critical buckling load, shows the best correlation with the experimental values, it can be seen that these methods over-predict experimental BCS which is undesirable from a design point of view. Table 6.2 shows that the Urbanik formula always over-predicts, whereas the McKee formula 1 using Nordstrand's formula for critical buckling load over-predicts for the boxes with lower BCS values. The original McKee formula 1 and the McKee formula 1 using Hahn *et al.* critical buckling, under-predict the experimental BCS which is suitable for a design situation. These predictions are accurate for the lower box strength combinations, but become less accurate as the box strength increases.

All the methods tend to over-predict the strength of the E flute boxes. It is felt that both these prediction methods can be improved through the use of transverse shear data in both the MD and CD and through the use of experimental Poisson's ratios. In addition, the constants in the McKee formula 1 can be solved from experimental critical buckling loads which would also improve the predictions. It appears that a method should be investigated that accurately predicts box strength for all box combination strengths. Figure 6.2 shows the BCS predictions using only the McKee formulae. For all the box combinations, the McKee formulae under-predicts box strength, except for the E flute boxes. This is consistent with the other methods already discussed.

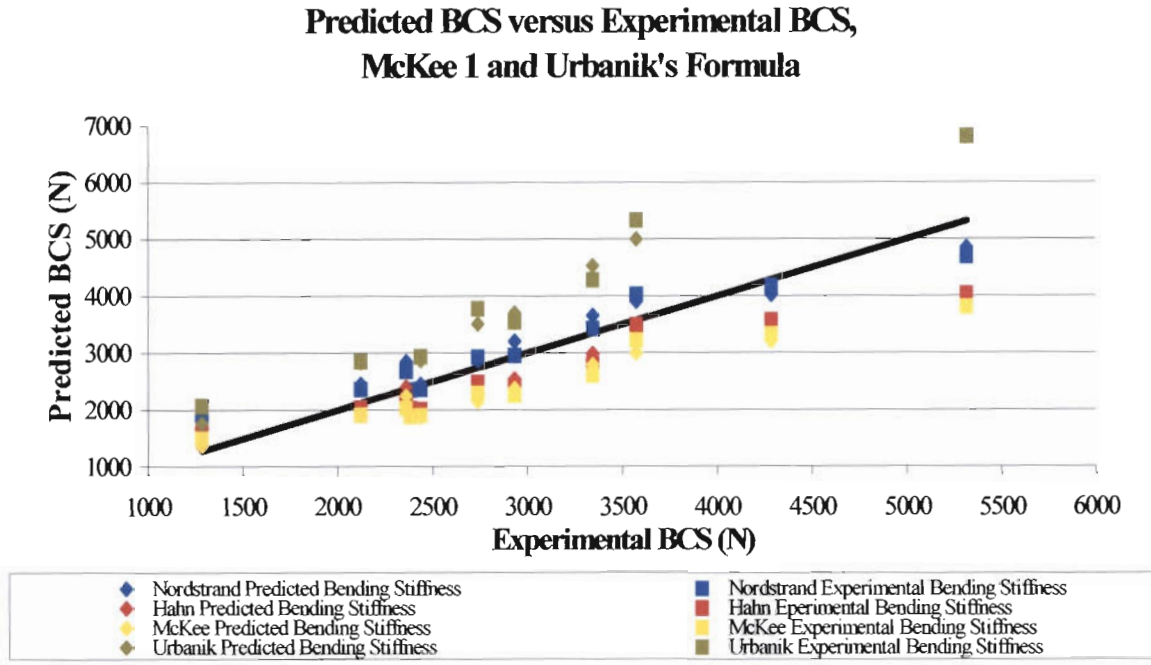

Figure 6.1: Comparison of BCS prediction methods using McKee 1 and Urbanik's formula.

BCS Prediction Method	Slope	Constant	R^2
Urbanik (Predicted)	1.30	14	0.98
Urbanik (Experimental)	1.25	241	0.96
McKee 1 & Nordstrand (Predicted)	0.81	713	0.95
McKee 1 & Nordstrand (Experimental)	0.77	775	0.94
McKee 1 & Hahn et al (Experimental)	0.68	590	0.95
McKee 1 & Hahn et al (Predicted)	0.68	538	0.94
McKee 1 (Experimental)	0.64	542	0.94
McKee 1 (Predicted)	0.63	55	0.96
McKee 2 (Predicted)	0.64	509	0.95
McKee 2 (Experimental)	0.63	561	0.94
McKee 3 (Predicted)	0.58	467	0.95
McKee 3 (Experimental)	0.57	515	0.94
McKee 5	0.51	589	0.94
McKee 4	0.49	556	0.94

Table 6.2: Correlation between experimental BCS and predicted BCS and slope of trend lines values for all prediction methods.

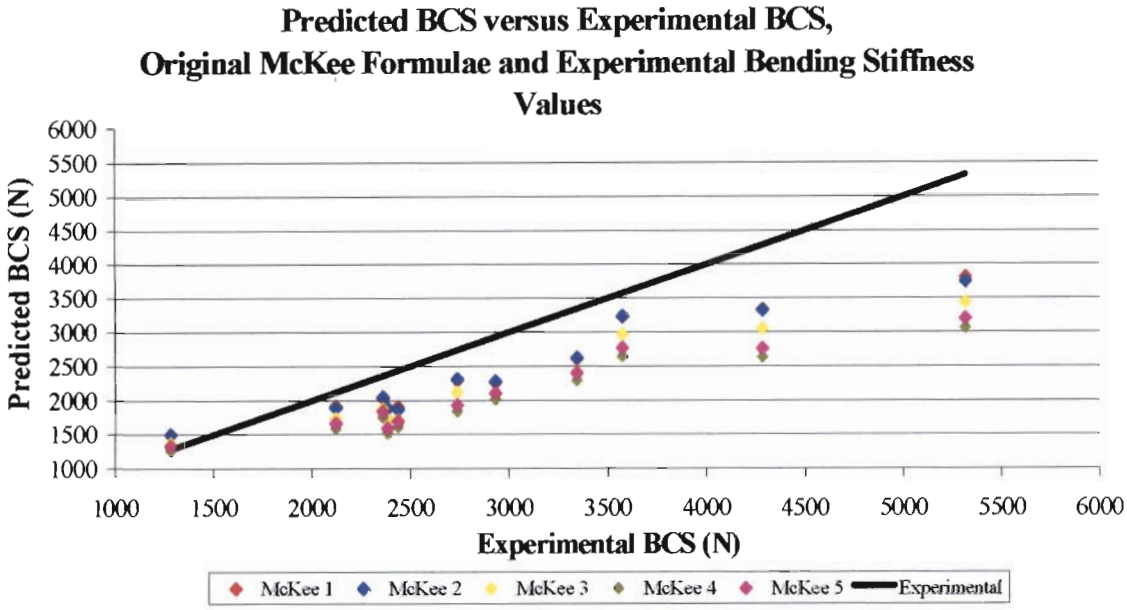

Figure 6.2: BCS predictions using the McKee formulae.

All the BCS prediction methods used in this project have good correlations with the experimental values, despite some of the methods over-predicting the experimental values. However, what is particularly important is the ability to accurately predict the BCS of a box from paper properties. This enables the designer to be able to accurately determine the strength of a box from paper properties and thus avoid the cumbersome experimental and trial part of box optimisation. This project has proved that we can perform accurate BCS predictions from paper properties. A schematic of this process is shown in Figure 6.3. In the schematic the dotted lines refer to optional inputs. The blue blocks represent data that was predicted in this project, but could be experimentally obtained to improve the model accuracy. The ECT data can be experimentally obtained, or predicted if a suitable model can be found.

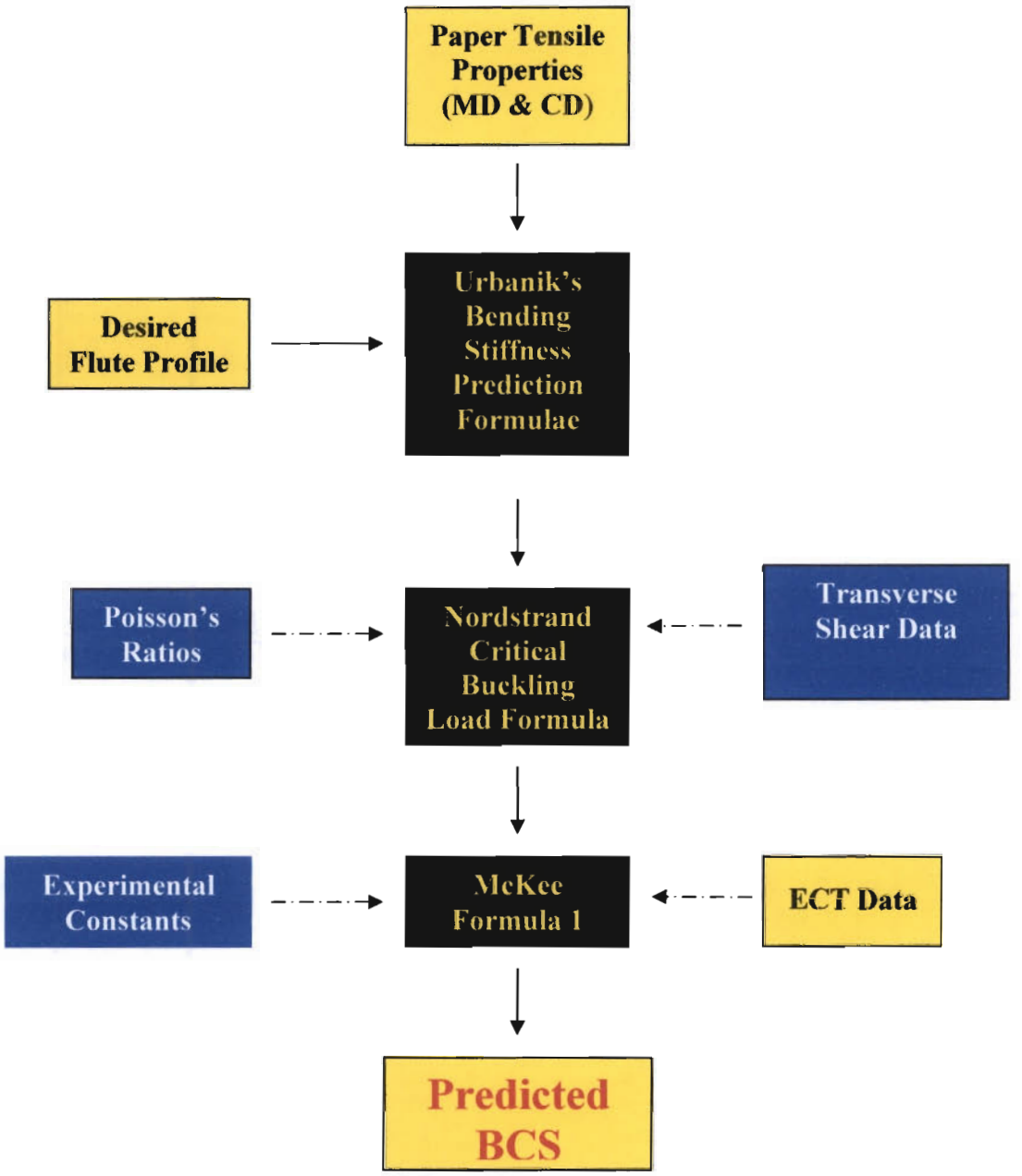

Figure 6.3: Flow chart of the BCS prediction method.

CHAPTER 7

CONCLUSIONS

The following chapter states the conclusions that can be drawn from the results shown in *Chapter 5* and the discussion of these results in *Chapter 6*.

7.1 The MD Shear Fixture

- The design of the MD shear fixture was shown to have been very successful. The apparatus successfully records the load required to twist a specimen and the angle of twist experienced by the specimen for a given load. The fixture is relatively easy to install on a Universal Tensile Testing Machine.

7.2 Evaluation of the MD Shear Test Method

- The MD shear test method produces excellent results when compared to the block shear test results. It was shown that a 97% correlation could be found between the block shear test and MD shear results. In addition, the method is very sensitive to slight changes in board combinations, relating to manufacturing and construction differences. This means that the fixture can be used as a quality control apparatus. The MD shear method proved to be easier to perform than the block shear test method. However, the test speed and specimen size need to be optimised for future use in an R&D environment.

7.3 Factors Affecting BCS

- The results have shown that box compression strength (BCS) is influenced by transverse shear stiffness, bending stiffness in the MD and the CD and the edge compression strength (ECS) values of the board. It is apparent that the boxes with high BCS generally have high shear stiffness, bending stiffness and ECS values. The relative weighting of these properties, with relation to box strength, is not known. From the research conducted, it appears that the bending stiffness of the board in both the MD and CD is one of the dominant factors affecting BCS. It is concluded that the MD shear stiffness influences the bending stiffness of corrugated board.

- In addition to mechanical properties, this research has also found that the structure of the board i.e. the facing separation or fluting type, plays a dominant role in the strength properties.

- The research has shown that the shear stiffness, bending stiffness and ECS are dependent on the quality of the paper used in the manufacture of the corrugated board. The use of recycled liners introduces more scatter in the data and reduces the difference between the MD and CD properties. Higher paper grammage boards leads to increased BCS values.

- The experimental results have shown that the boards manufactured in different years have substantially different properties. This could be due to variance in the paper used or differences in the manufacturing process. Other contributing factors could be due to varying moisture contents of the boards or an aging of the cellulosic fibres.

7.4 Box Strength Predictions

- All of the prediction methods used in this project have shown good correlation with the experimental values. Of these methods, the McKee formula 1 with Nordstrand's formula for critical buckling of orthotropic plates and Urbanik's formula are the most accurate. Urbanik's formula is possibly more useful as it can be used for the BCS prediction of non-square boxes.

- More accurate BCS predictions can be obtained by incorporating MD shear data and experimental Poisson's ratios into the prediction models. In addition, experimental critical buckling loads should be measured to obtain the formulae constants.

- Box strength predictions were successfully performed from liner tensile data using predicted bending stiffness values and ECT data. This is an important design method. It can be improved through using a method for predicting ECT values, resulting in accurate box strength predictions from only liner and fluting properties.

7.5 Evaluation of Test Methods

- The block shear test method is not suitable for quick data recovery in an R&D environment. Improvements on this method could be made, but it is felt that it will still be slow and tedious.

- The MD shear method is much easier to perform and more user friendly.

- The MD shear test method needs to be extended to measure the properties in the CD and also to be evaluated for its applicability for triple-wall board combinations.

- The 3-point bend method is useful as an evaluation method as it incorporates transverse shearing in its stiffness results.

- For modelling purposes and strength predictions, better prediction results would be obtained through the use of 4-point bend test results.

CHAPTER 8

FUTURE WORK

This project has highlighted a number of areas that should be investigated to improve our understanding of corrugated board and the factors that affect BCS. These areas are discussed below.

8.1 The MD Shear Test

The MD shear test method should be studied in more detail with the aim of establishing whether only transverse shear stiffness is being measured or whether other board properties are influencing the results. In addition, the method should be extended for CD testing and triple-wall board testing.

8.2 The Effect of Recycled Paper

The effect of recycled paper on board stiffness is an area that has received very little research. The effect of paper properties on the strength of boxes should be investigated to improve box strength design.

8.3 The Effect of Processing Variables

The effect of processing variables on corrugated board mechanical properties needs to be investigated and incorporated into box strength predictions. This should include the variables such as die-cutting and printing.

8.4 Improved Box Strength Design

An improved method of box strength design should be undertaken. This would involve FEM modelling of corrugated board. It should try to include processing variables and the effect of using unbalanced board combinations. In addition, the model should incorporate the effects of the liner flute interface and box flaps on box strength. This would involve an improved modelling technique, especially where the liner flute interface is involved.

REFERENCES

1. Aboura Z, Talbi N, Allaoui S and Benzeggah ML, *Elastic behavior of corrugated cardboard: experiments and modeling*, Composite Structures, Vol. 63; 2004, pp. 53-62.
2. Ndimande B, *Packaging industry in South Africa*, [Online] Available: http//strategis.ic.gc.ca/epic/internet/inimr-ri.nsf/en/gr110893e.html [2004, September 9]
3. Loubser G, *South Africa*, Boxboard Containers International, 2000, [Online] Available: http://boxboard.com/ar/boxboard_south_africa/index.htm [2004, September 9].
4. Johansson K; Glasenapp A and Teleman O, *Lean, intelligent and moisture resistant corrugated board, A conceptual memorandum on sustainable growth.* Packforsk, Stockholm, 2002.
5. Allansson A and Svärd B, *Stability and collapse of corrugated board; Numerical and experimental analysis*, Lund University, Masters Dissertation, Sweden, 2001.
6. FEFCO. [Online] Available:http://www.fefco.org [2004, September 9].
7. *The first hundred years*, [Online] Available: http://langstoncorp.com/leader.htm [2004, September 9].
8. *The history of corrugated board*, Forum Wellpappe Austria, [Online] Available: http://www.wellpappe.at/wellpappe_english/frames_flash/frame_sitemap.html. [2004, September 9].
9. *What is paper cardboard and how did it come about*, The Source. [Online] Available:http://lowprice4u.com/TheSource/TheSource.asp?PageID=258 [2004, September 9].
10. McKinlay AH, *Transport packaging*, Richard Warrington, USA, 1998.
11. Fromm L and Vermillion RJ, *A study of ESD corrugated.* [Online] Available:http://www.packaging.hp.com/misc/Presentation/AHPStudy.pdf [2004, September 28]
12. Xia QS, Boyce MC and Parks DM, *A constitutive model for the anisotropic elastic-plastic deformation of paper and paperboard*, International Journal of Solids and Structures, Vol. 39, 2002, pp. 4053–4040.
13. Luo S, Suhling JC, Considine, JM and Laufenberg TL, *The bending stiffness of corrugated board*, Mechanics of Cellulosic Materials, ASME, Vol. 36, 1992, pp. 15-26.
14. *Types of corrugated board*, GDV. [Online] Available:http://www.tis-gdv.de/tis_e/verpack/papier/wp_arten/wp_arten.htm [2004, September 9].
15. *Fiberboard and paperboard containers*, Departments of the Army, Navy and Air Force, and the Defence Logistics Agency, [Online] Available: http://155.217.58.58/cgi-bin/atdl.dll/fm/38-701/ch2.htm [2004, September 9].
16. Kline JE, *Paper and paperboard: Manufacturing and converting fundamentals*, Miller Freeman Publications Inc., San Francisco, 1982.

17. Urmanbetova A, *Terminology on paper & pulp: Types of paper and containerboard, containerboard grades and tests*, 2001.
18. McKinlay PR, *Analysis of the strain field in a twisted sandwich panel with application to determining the shear stiffness of corrugated fibreboard*, Products of paper-making, 10th Fundamental Research Symposium, Vol. 1, 1993, pp. 575-599.
19. Nordstrand TM and Carlsson LA, *Evaluation of transverse shear stiffness of structural core sandwich plates*, Composite Structures, Vol. 37, 1997; pp. 145-153.
20. Gilchrist AC, Suhling JC and Urbanik TJ, *Nonlinear finite element modeling of corrugated board*, Mechanics of Cellulosic Materials, Vol. 85, 1999, pp. 101-106.
21. *Advantages*. Federation of Corrugated Box Manufacturers of India, [Online]. Available: http://www.fcbm.org/technology/advantages.htm [2004, September 9].
22. Rahman AA; Urbanik TJ and Mahamid M, *Transient nonlinear analysis of moisture flow through a corrugated fiberboard*, Department of Civil Engineering and Mechanics, University of Wisconsin-Milwaukee. [Online] Available: http://www.ce.washington.edu/em03/proceedings/papers/210.pdf [2004, September 28].
23. Urbanik TJ, *Strength criterion for corrugated fiberboard under long –term stress*, Tappi Journal, Vol. 81, No. 3, 1998, pp. 33-37.
24. Stenberg N, *Mechanical properties in the thickness direction of paper and paperboard*, Licentiate Thesis, Department of Solid Mechanics, Royal Institute of Technology, Sweden, 1999.
25. Conpac Group, [Online] Available: http://www.conpacgroup.com/corrugated.htm [2004, September 9].
26. Nordstrand TM, Carlsson LA and Allen HG, *Transverse shear stiffness of structural core sandwich*, Composite Structures, Vol. 27, 1994, pp. 317-329.
27. Nyman U, *Strength design analysis of corrugated boar,* Lund University., Sweden, 2000.
28. Nyman U and Gustafsson J, *Local buckling of corrugated board facings*, Lund University, Sweden, 1999.
29. Jones RM, *Mechanics of Composite Materials*, McGraw-Hill, Kogakusha, Tokyo, 1975.
30. Baum GA, Brennan DC and Habeger CC, *Orthotropic elastic constants of paper*, Tappi Journal, Vol. 64, 1981, pp. 97-101.
31. Mann RW, Baum GA and Habeger CC. *Determination of all nine orthotropic elastic constants for machine-made paper*, Tappi Journal, Vol. 63, 1980, pp. 163-166.
32. Beldie L, *Implementing a constitutive model for paperboard in abaqus and experiments on paperboard packages*, Lund University Sweden, 2001.
33. Stenberg N, *On the out-of-plane mechanical behaviour of paper materials*, Department of Solid Mechanics, Royal Institute of Technology, Stockholm, 2002.
34. Allen HG, *Analysis and design of structural sandwich panels*, Pergamon Press, Oxford, 1969.
35. Saliklis EP, Urbanik TJ and Tokyay B, *Bilinear modelling of cellulosic orthotropic nonlinear materials*, Journal of Pulp and Paper Science, Vol. 29, No. 12, 2003, pp. 407-411.

36. Nyman U and Gustafsson J, *Buckling of long orthotropic plates including high–order transverse shear*, Lund University, Sweden, 2004.
37. Urbanik TJ, *Linear and nonlinear material effects on postbuckling strength of corrugated containers*, Mechanics of Cellulosic Materials, ASME, Vol. 77, 1997, pp. 93-99.
38. Nordstrand TM, *On buckling loads for edge-loaded orthotropic plates including transverse shear*, Composite Structures, Vol. 65, 2004, pp. 1-6.
39. McKinlay PR, *A method for calculating the transverse shear stiffness of corrugated board, measured in the machine direction*, 3rd International Conference on Sandwich Constructions, Vol. 1, 1995, pp. 449-461.
40. McKinlay PR, Amcor Limited, United Stated Patent 4.958,522, September 25, 1990.
41. ASTM Standard, *ASTM C 273-61, Standard test method for shear properties in flatwise plane of flat sandwich constructions or sandwich cores*, 1993, Annual Book of ASTM Standards, pp. 5-8.
42. Sawyer JPG, Jones R and McKinlay PR, *An experimental description of the response of paper*, Composite Structures, Vol. 36, 1996, pp. 101-111.
43. Hung SC and Suhling JC, *Rate dependent pure shear behaviour of linerboard*, 3rd International Symposium, Moisture and Creep Effects on Paper, Board and Containers, 1997, pp. 69-84.
44. Vorakunpinij A, Coffin DW and Habeger CC, *A new device for measuring tensile and compressive creep in paper*, Experimental Techniques, 2004, pp. 43-48.
45. Koran Z, *The bending stiffness of paperboard*, Corrugated Containers Conference, 1988. pp. 49-56.
46. Whitsitt WJ, *Papermaking factors affecting box properties*, Corrugated Containers Conference, 1988, pp 57-63.
47. De Ruvo A, Fellers C and Engman C, *The influence of raw material and design on the mechanical performance of boxboard*, Svensk Papperstidning, Vol. 18, 1978, pp. 557-566.
48. McKee RC, Gander JW and Wachuta JR, *Flexural stiffness of corrugated board*, Paperboard Packaging, 1962, pp. 111-120.
49. *Bending stiffness of paper and board*, [Online] Available:http://pygar`g.ps.umist.ac.uk/ianson/paper_physics/Bending_Stiffness.html [2004, September 9].
50. Urbanik TJ, *Effect of relative humidity on the optimum flute shape for corrugated fibreboard*, 4th International symposium on moisture and creep effects on paper, board and containers, E.F.P.G, 1999.
51. Urbanik TJ, *Effect of corrugated flute shape on fibreboard edgewise crush strength and bending stiffness*, Journal of Pulp and Paper Science, Vol. 27, No. 10, 2001, pp. 27-43.
52. Hearn EJ, *Mechanics of materials*, Butterworth Heinemann, Oxford, 1997.
53. Koning JW and Moody RC, *Predicting flexural stiffness of corrugated fibreboard*, Tappi Corrugated Containers Conference Proceedings, 1971.
54. McKee RC, Gander JW and Wachuta JR, *Edgewise compression strength of corrugated board*, Paperboard Packaging, 1961, pp. 70-76.

55. Longtin S, *ECT from a user's perspective*, Hewlett-Packard Company, 2003.
56. Jiménez MA and Liarte E, *Simulation of the edge crush test of corrugated paperboard using ABAQUS*, ABAQUS User's Conference, 2003.
57. Fellers C, *Edgewise Compression Strength of Paper*, Handbook of mechanical and physical testing of paper and paperboard, 1983, pp. 349-383.
58. Markström H, *Testing methods and instruments for corrugated board*, Lorentzen and Wettre, Sweden, 1988. Translated by Bristows Engelska Språktjänst.
59. Westerlind BS and Carlsson LA, *Compressive response of corrugated board*, Tappi Journal, 1992, pp. 145-154.
60. Urbanik TJ, *Effect of paperboard stress-strain characteristics on strength of singlewall corrugated fibreboard*, Research paper, Forest Products Laboratory, 1981.
61. Urbanik TJ, *Review of buckling mode and geometry effects on postbuckling strength of corrugated containers*, ASME, 1996.
62. Renman M, *Test fixture for eccentricity and stiffness of corrugated board*, Sage Social Science Collections, Vol.36, 1996, pp. 262-268.
63. Nordstrand TM, *Analysis and testing of corrugated board panels into the post-buckling regime*, Composite Structures, Vol. 63, 2004, pp. 189-199.
64. Nordstrand TM, *Parametric study of the post-buckling strength of structural core sandwich panels*, Composite Structures, Vol. 30, 1995, pp. 441-451.
65. McKee RC, Gander JW, Wachuta JR, *Compression strength formula for corrugated boxes*, Paperboard Packaging, 1969, pp. 149-159.
66. Beldie L, *Paperboard packages exposed to static loads – finite element modelling and experiments*, Lund University, Sweden, 2001.
67. Urbanik TJ, *Machine direction strength theory of corrugated fibreboard*, American Society for Testing and Materials, 1996.
68. Hahn EK, De Ruvo A, Westerlind BS and Carlsson LA, *Compressive strength of edge-loaded corrugated board panels*, Sage Social Science Collections, 1992, pp. 259-265.
69. Patel P, Nordstrand TM and Carlsson LA, *Local buckling and collapse of corrugated board under biaxial stress*, Composite Structures, Vol. 39, 1997, pp. 93-110.
70. Leake C, *Measuring Corrugated Box Performance*, Corrugated Containers Conference, 1987, pp. 27-31.
71. Rahman AA and Abubakr S, *Adhesive in the buckling failure of corrugated fiberboard: A finite element investigation*, ANSYS Conference, Simulating Real Life: Software with No Boundaries, Vol. 1, 1998, pp. 533-539.
72. Nordstrand TM, Blackenfeldt M and Renman M, *A strength prediction model for corrugated board containers*, SCA Research, Sweden., 2003.
73. Timoshenko S and Woinowsky-Krieger S, *Theory of plates and shells*, McGraw Hill, New York, 1959.
74. Timoshenko S, *Theory of elastic stability*, McGraw Hill, New York, 1936.

75. Urbanik TJ and Saliklis EP, *Finite element corroboration of buckling phenomena observed in corrugated boxes*, Wood and Fiber Science, Vol. 35, No. 3, 2003, pp. 322-333.
76. Du Plooy ABJ, *Comments on some publications regarding the prediction of corrugated box compression strengths*, Division of Processing and Chemical Manufacturing Technology, CSIR, Pretoria, 1988.
77. McKinlay PR and Bennet PG, *Box compression prediction – beyond McKee*, 8th ICCA Conference, 1987.
78. Nyman U and Gustafsson J, *Material and structural failure criterion of corrugated board facings*, Lund University, Sweden, 2000.
79. Urbanik TJ and Saliklis EP, *Comparison of postbuckling model and finite element model with compression strength of corrugated boxes*, Progress in Paper Physics, 2002.
80. http://isb.ri.ccf.org/biomch-1/archives/biomch-1-1996-09/00125.html
81. *RS International Electronic Catalogue*, RS Components, 2003.
82. *Polyplastics*, [Online]. Available: http://www.polyplastics.com [2004, September 9].
83. ASTM Standard, *ASTM C 393-62 Standard test method for flexural properties of flat sandwich constructions,* Annual Book of ASTM Standards, 1993, pp. 22-24.
84. Tappi Standard, *T 820 cm-00, Flexural stiffness of corrugated board*, Tappi, 2000.
85. Tappi Standard, *T 836 cm-02, Bending stiffness, four point method*, Tappi, 2002.
86. Tappi Standard, *T 402 sp-98, Standard conditioning and testing atmospheres for paper, board, pulp handsheets, and related products*, Tappi, 1998.
87. Tappi Standard, T 494 om-01, *Tensile properties of paper and paperboard (using constant rate of elongation apparatus)*, Tappi 2001.
88. ISO 3037, *Corrugated fiberboard – Determination of edgewise crush resistance (Unwaxed edge method)*, International Standard, 1994.
89. Tappi Standard, *T 804 om-02, Compression test of fiberboard shipping containers*, Tappi 2002.

Appendix A

MD Shear Fixture

Side View

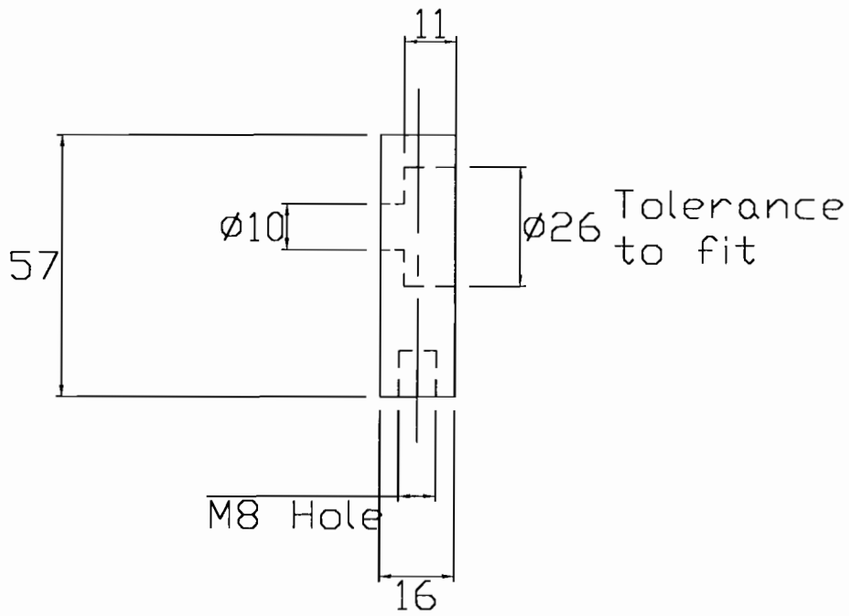

Front View

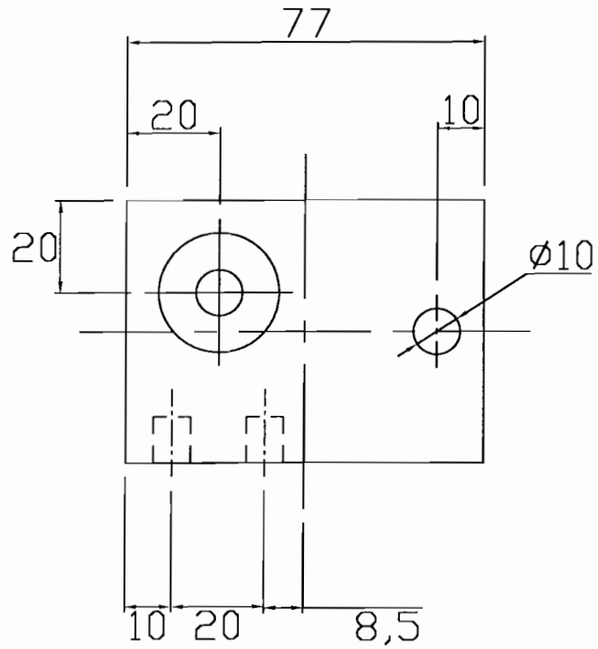

Part no: 1a	Description: Right Bearing Housing	Material: Aluminium AISI 6261	No of: 1
University of Cape Town Department of Mechanical Engineering Centre for Materials Engineering			
Title: Stiffness Tester			
Dimensions in millimetres (mm)	Scale: 2 to 3	Date: 19/08/03	Sheet: 1 of 18
Tolerance unless otherwise stated 0.01	Drawing By: John Jones		Drawing no: 1

Front View

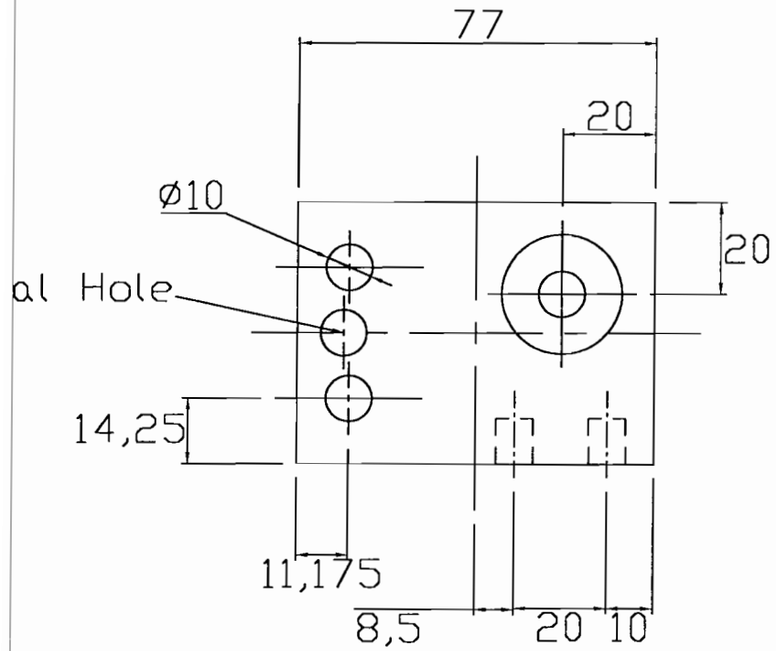

Side View

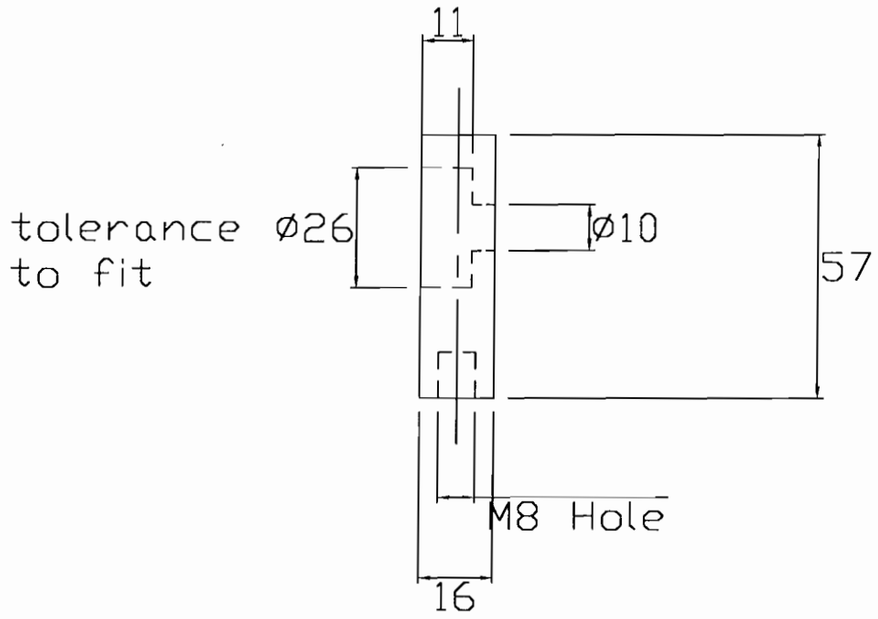

Part no: 1b	Description: Left Bearing Housing	Material: Aluminium AISI 6261	No of: 1
University of Cape Town Department of Mechanical Engineering Centre for Materials Engineering			
Title: Stiffness Tester			
Dimensions in millimetres (mm)	Scale: 2 to 3	Date: 19/08/03	Sheet: 2 of 18
Tolerance unless otherwise stated 0.01	Drawing By: John Jones		Drawing no: 2

Side View

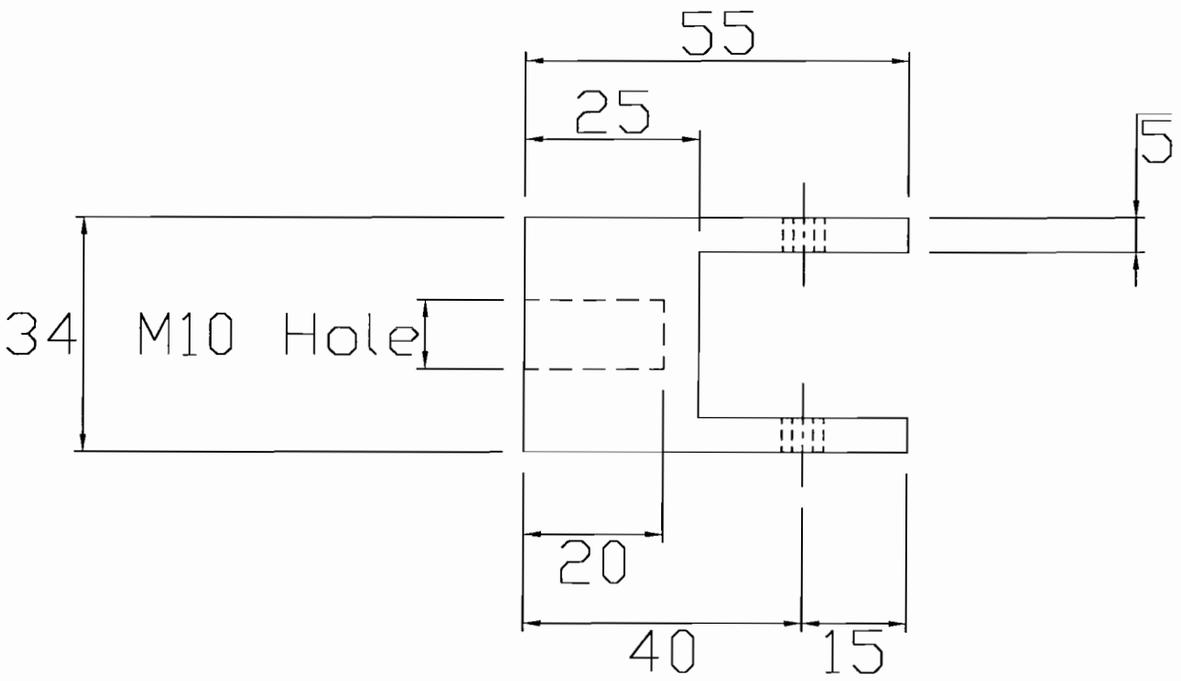

Front View

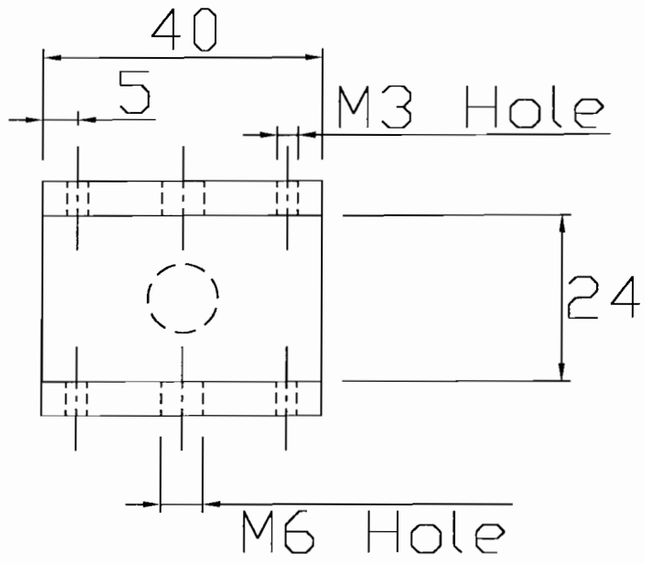

Part no: 2	Description: Grip	Material: Aluminium AISI 6261	No of: 2
University of Cape Town Department of Mechanical Engineering Centre for Materials Engineering			
Title: Stiffness Tester			
Dimensions in millimetres (mm)	Scale: 1 to 1	Date: 19/08/03	Sheet: 3 of 18
Tolerance unless otherwise stated 0.01	Drawing By: John Jones		Drawing no: 3

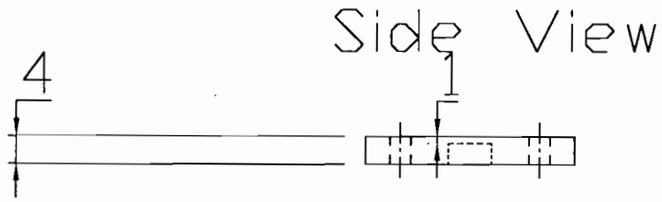

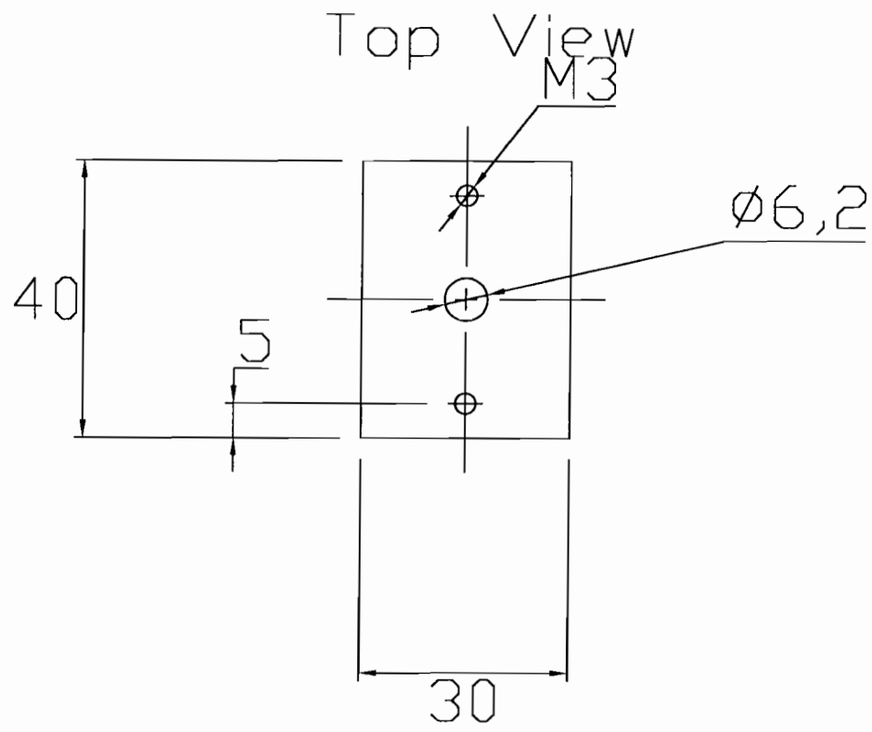

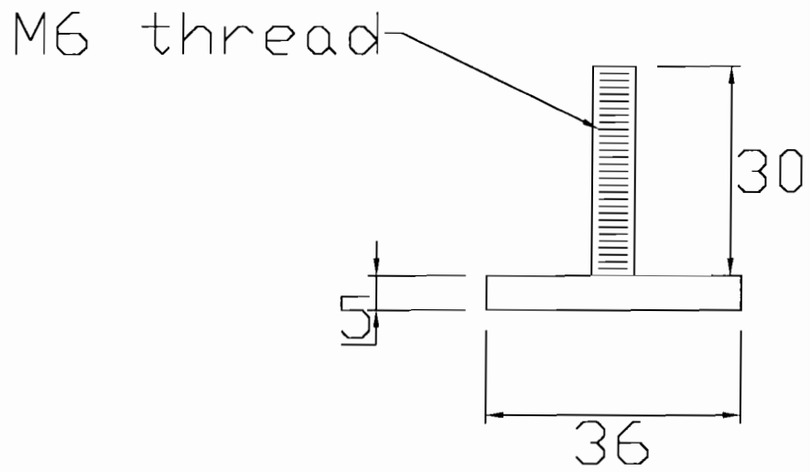

	Part no: 3	Description: Grip Plate & Pin	Material: Aluminium AISI 6261	No of: 4
	University of Cape Town Department of Mechanical Engineering Centre for Materials Engineering			
	Title: Stiffness Tester			
Dimensions in millimetres (mm)	Scale: 1 to 1	Date: 19/08/03	Sheet: 4 of 18	
Tolerance unless otherwise stated 0.01	Drawing By: John Jones		Drawing no: 4	

Front View

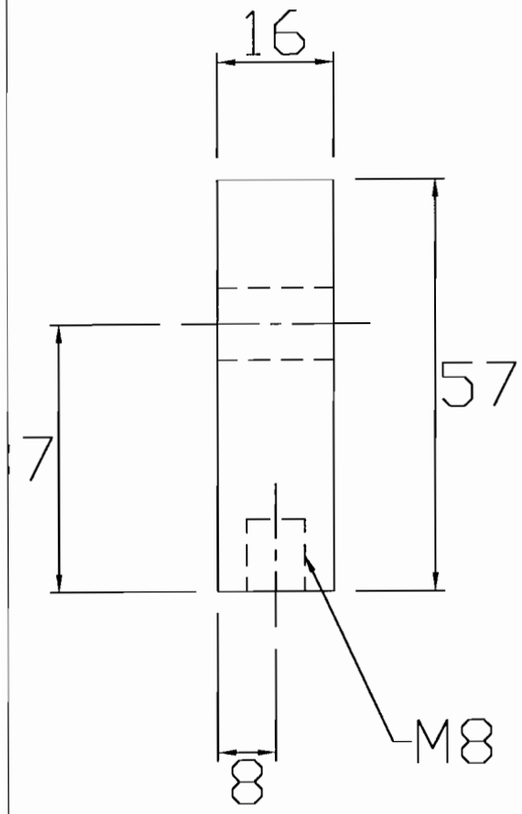

Front View

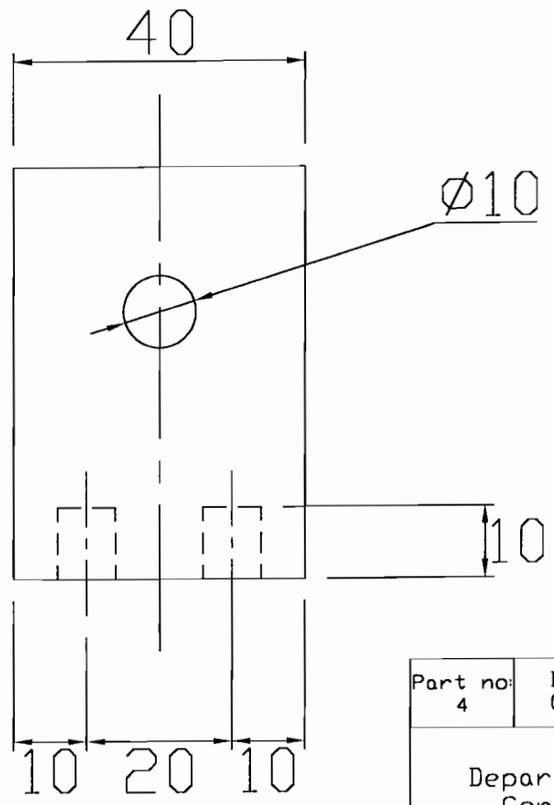

Part no: 4	Description: Grip Holder	Material: Aluminium AISI 6261	No of: 1

University of Cape Town
Department of Mechanical Engineering
Centre for Materials Engineering

Title:
Stiffness Tester

Dimensions in millimetres (mm)	Scale: 1 to 1	Date: 19/08/03	Sheet: 5 of 18
Tolerance unless otherwise stated 0.01	Drawing By: John Jones		Drawing no: 5

Side View

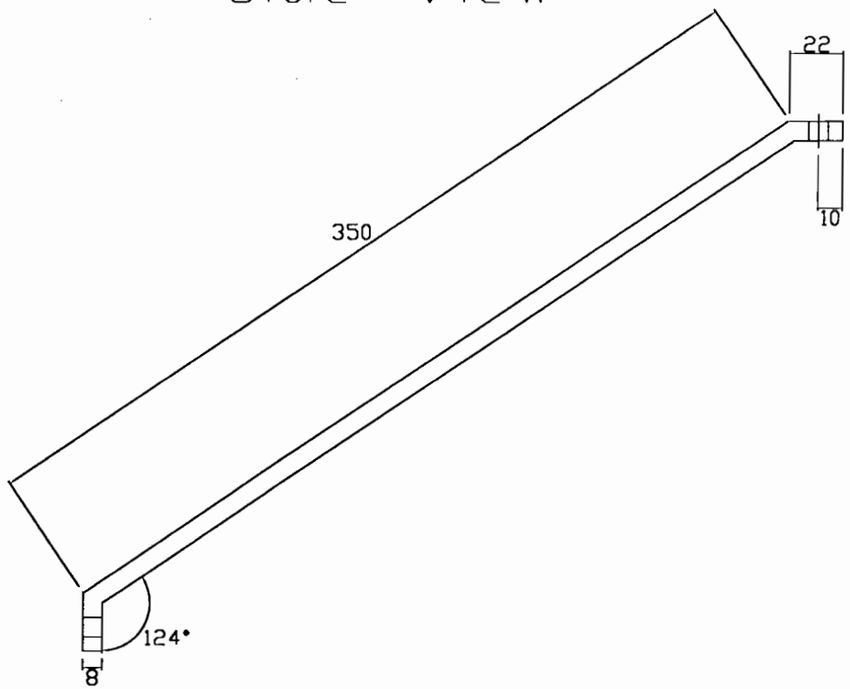

Front View

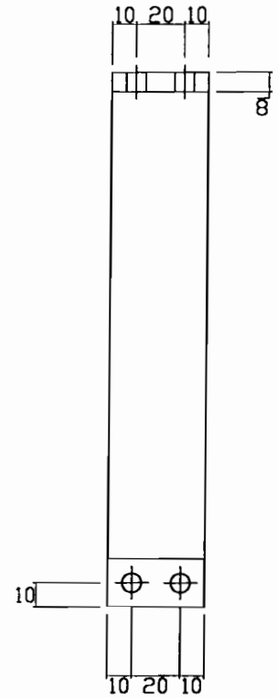

Part no: 5	Description: Angled Support	Material: Aluminium AISI 6261	No of: 1

University of Cape Town
Department of Mechanical Engineering
Centre for Materials Engineering

Title:
Stiffness Tester

Dimensions in millimetres (mm)	Scale: 1 to 3	Date: 19/08/03	Sheet: 6 of 18
Tolerance unless otherwise stated 0.01	Drawing By: John Jones		Drawing no: 6

Side View

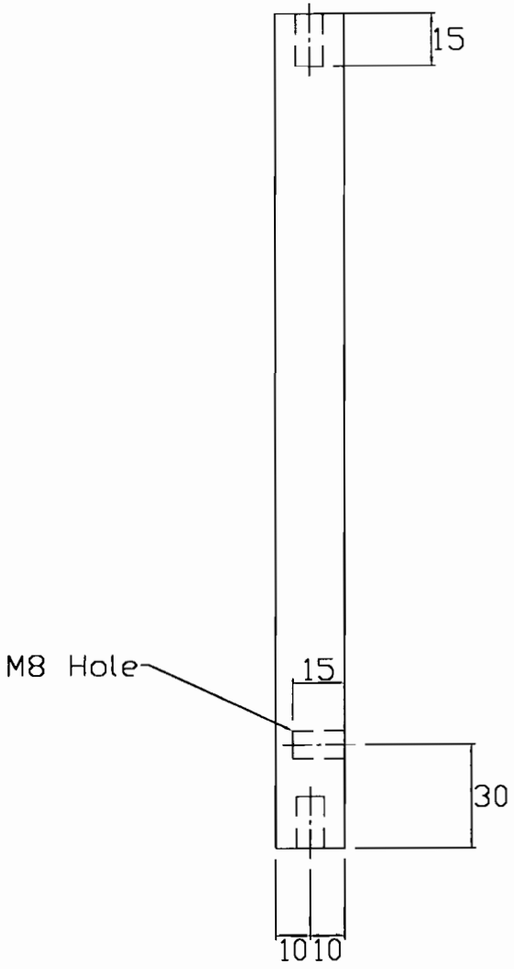

Front View

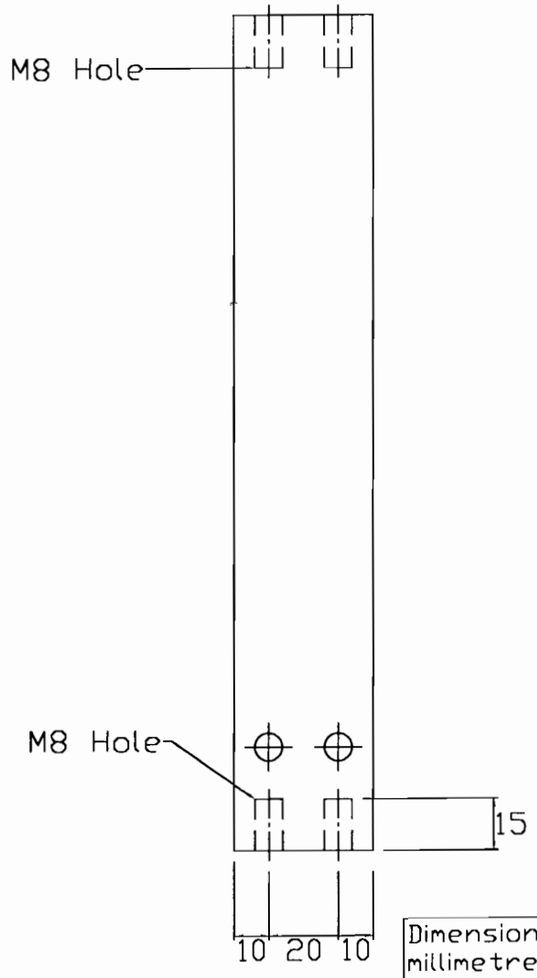

Part no: 6a	Description: Right Support	Material: Aluminium AISI 6261	No of: 1

University of Cape Town
Department of Mechanical Engineering
Centre for Materials Engineering

Title:
Stiffness Tester

Dimensions in millimetres (mm)	Scale: 1 to 2	Date: 19/08/03	Sheet: 7 of 18
Tolerance unless otherwise stated 0.01	Drawing By: John Jones		Drawing no: 7

Side View

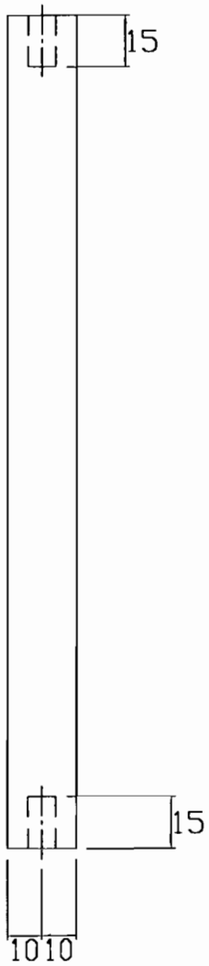

Front View

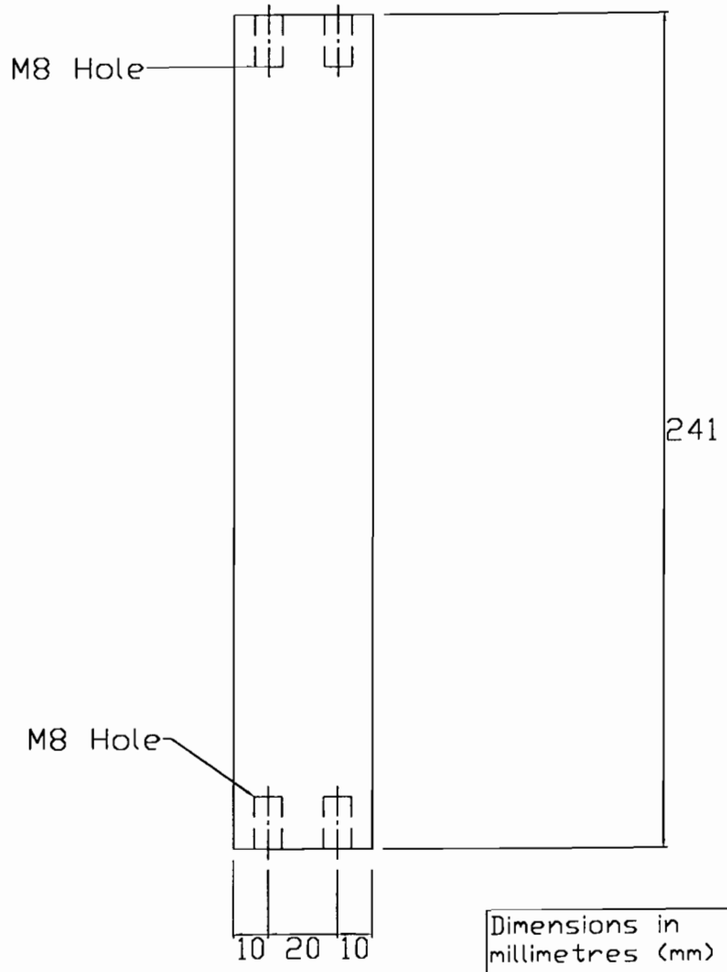

Part no: 6b	Description: Left Support	Material: Aluminium AISI 6261	No of: 1

University of Cape Town
Department of Mechanical Engineering
Centre for Materials Engineering

Title:
Stiffness Tester

Dimensions in millimetres (mm)	Scale: 1 to 2	Date: 19/08/03	Sheet: 8 of 18
Tolerance unless otherwise stated 0.01	Drawing By: John Jones		Drawing no: 8

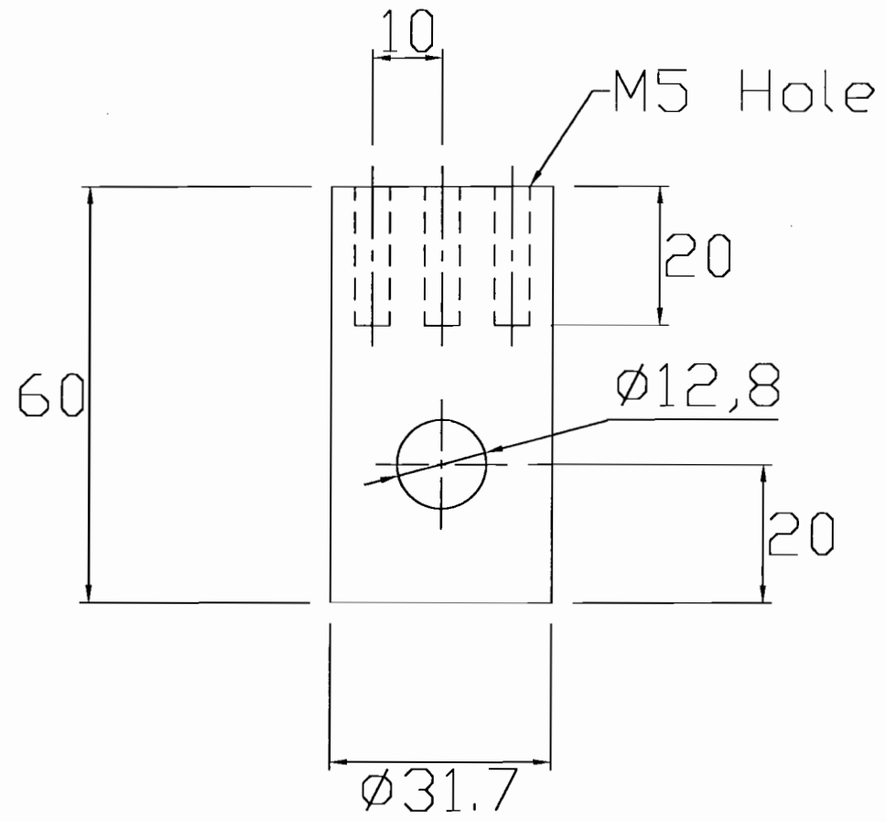

Side View

Top View

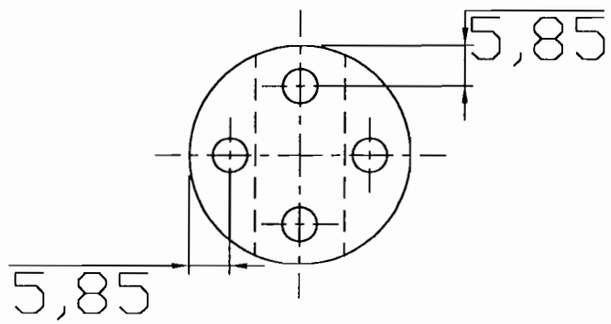

Part no: 7	Description: Bottom Connection	Material: Aluminium AISI 6261	No of: 1
University of Cape Town Department of Mechanical Engineering Centre for Materials Engineering			
Title: Stiffness Tester			
Dimensions in millimetres (mm)	Scale: 1 to 1	Date: 19/08/03	Sheet: 9 of 18
Tolerance unless otherwise stated 0.01	Drawing By: John Jones		Drawing no: 9

Side View

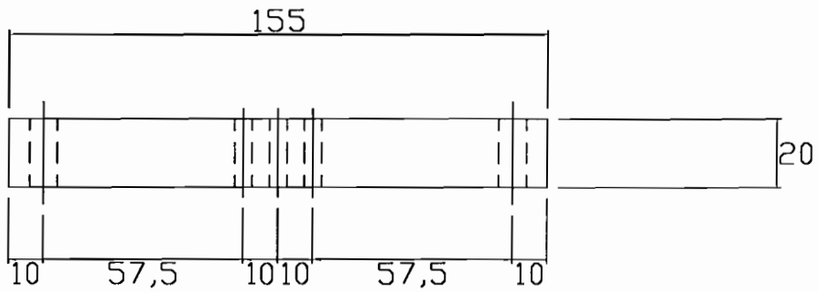

Top View

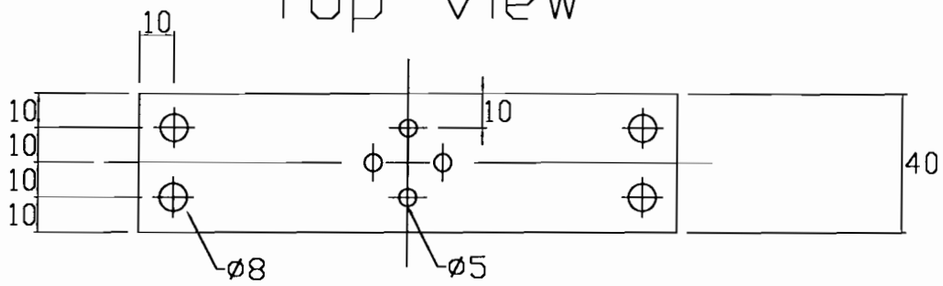

Part no: 8	Description: Bottom Plate	Material: Aluminium AISI 6261	No of: 1
University of Cape Town Department of Mechanical Engineering Centre for Materials Engineering			
Title: Stiffness Tester			
Dimensions in millimetres (mm)	Scale: 1 to 2	Date: 19/08/03	Sheet: 10 of 18
Tolerance unless otherwise stated 0.01	Drawing By: John Jones		Drawing no: 10

Front View

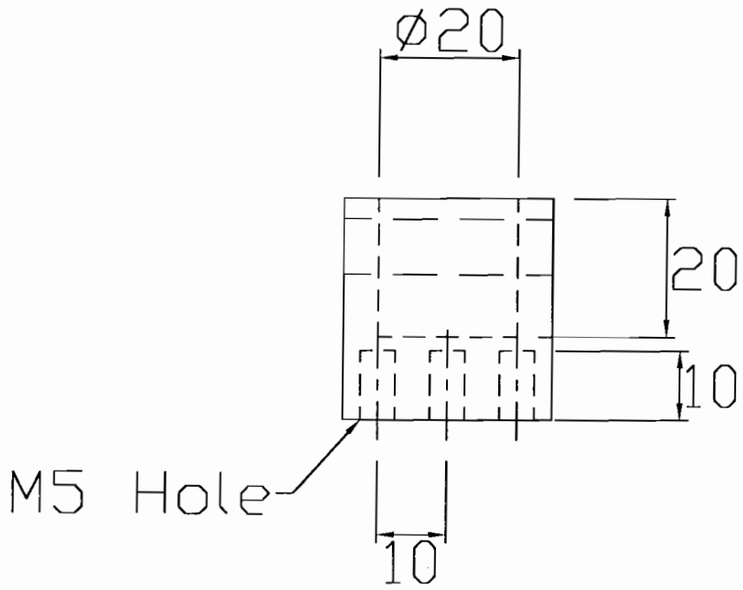

Side View

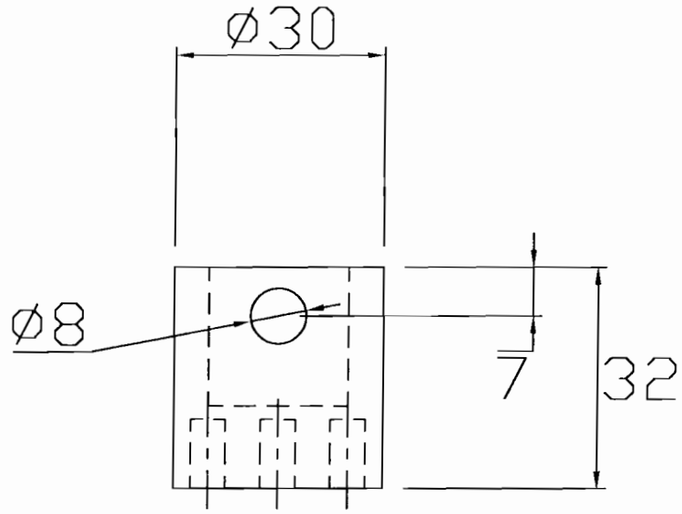

Top View

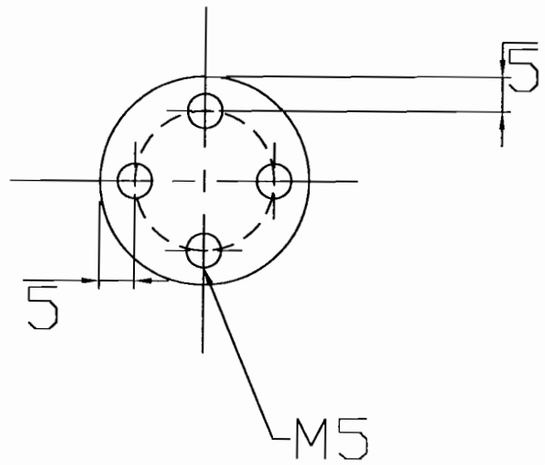

Part no: 9	Description: Top Connection	Material: Aluminium AISI 6261	No of: 1

University of Cape Town
Department of Mechanical Engineering
Centre for Materials Engineering

Title:
Stiffness Tester

Dimensions in millimetres (mm)	Scale: 1 to 1	Date: 19/08/03	Sheet: 11 of 18
Tolerance unless otherwise stated 0.01	Drawing By: John Jones		Drawing no: 11

Top View

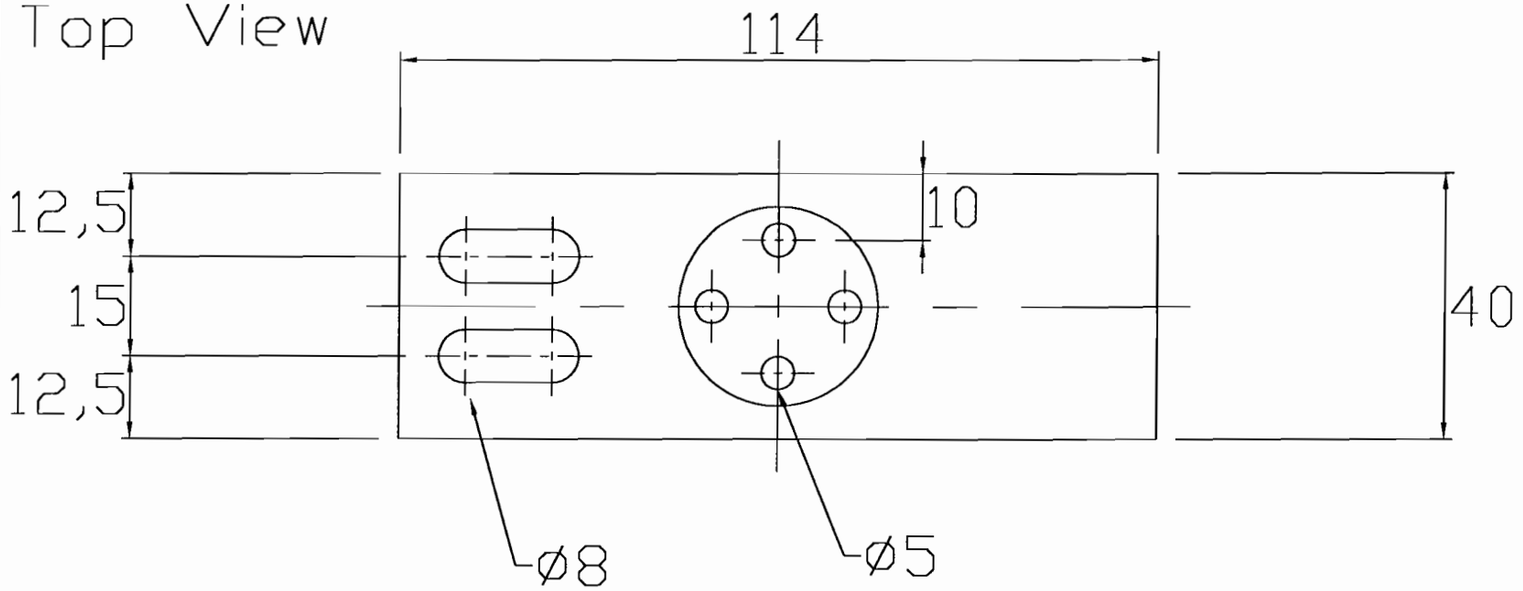

Side View

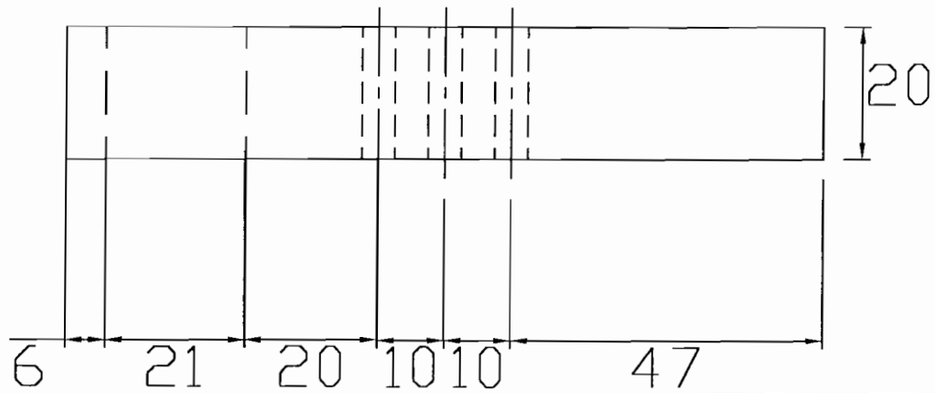

Part no: 10	Description: Top Plate	Material: Aluminium AISI 6261	No of: 1
University of Cape Town Department of Mechanical Engineering Centre for Materials Engineering			
Title: Stiffness Tester			
Dimensions in millimetres (mm)	Scale: 1 to 1	Date: 19/08/03	Sheet: 12 of 18
Tolerance unless otherwise stated 0.01	Drawing By: John Jones		Drawing no: 12

Side View

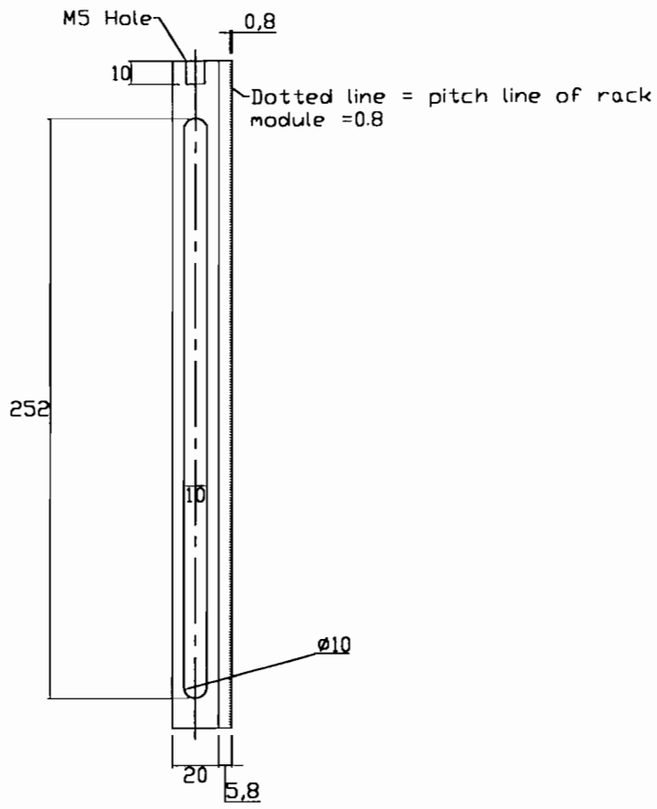

Front View

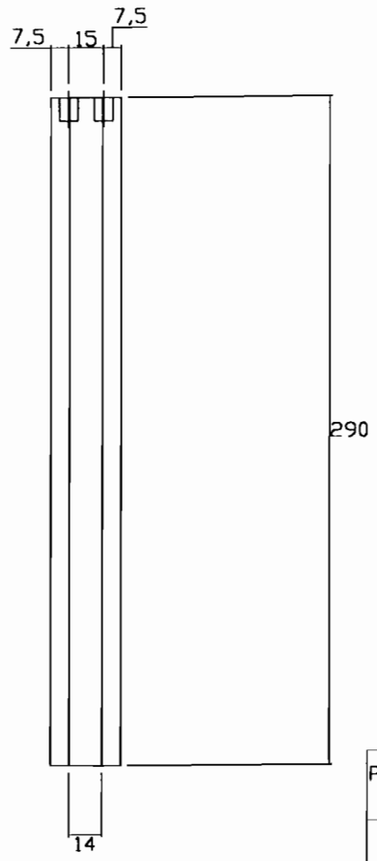

Pin

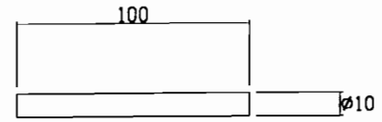

Approximate Circular Pitch = 2.52mm, cut teeth to mesh with duracon gear.

Part no: 11	Description: Rack	Material: Brass	No of: 1
University of Cape Town Department of Mechanical Engineering Centre for Materials Engineering			
Title: Stiffness Tester			
Dimensions in millimetres (mm)	Scale: 1 to 3	Date: 19/08/03	Sheet: 13 of 18
Tolerance unless otherwise stated 0.01	Drawing By: John Jones		Drawing no: 13

All Holes Countersunk

Side View

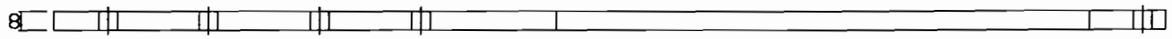

Top View

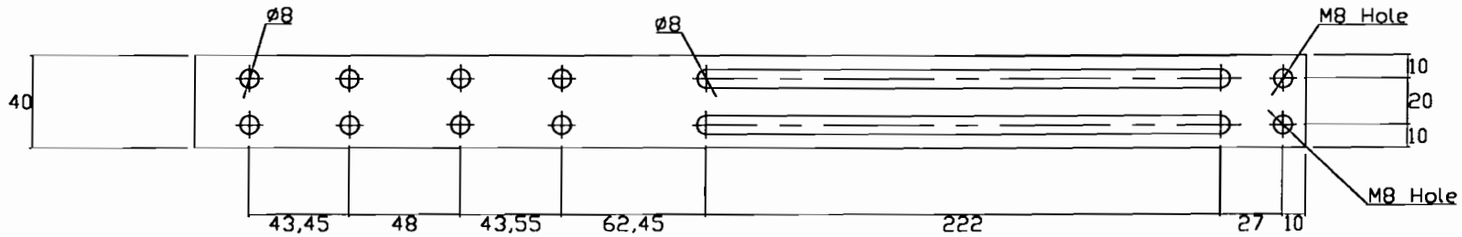

Part no: 12	Description: Base Plate	Material: AISI 431	No of: 1
University of Cape Town Department of Mechanical Engineering Centre for Materials Engineering			
Title: Stiffness Tester			
Dimensions in millimetres (mm)	Scale: 1 to 3	Date: 19/08/03	Sheet: 14 of 18
Tolerance unless otherwise stated 0.01	Drawing By: John Jones		Drawing no: 14

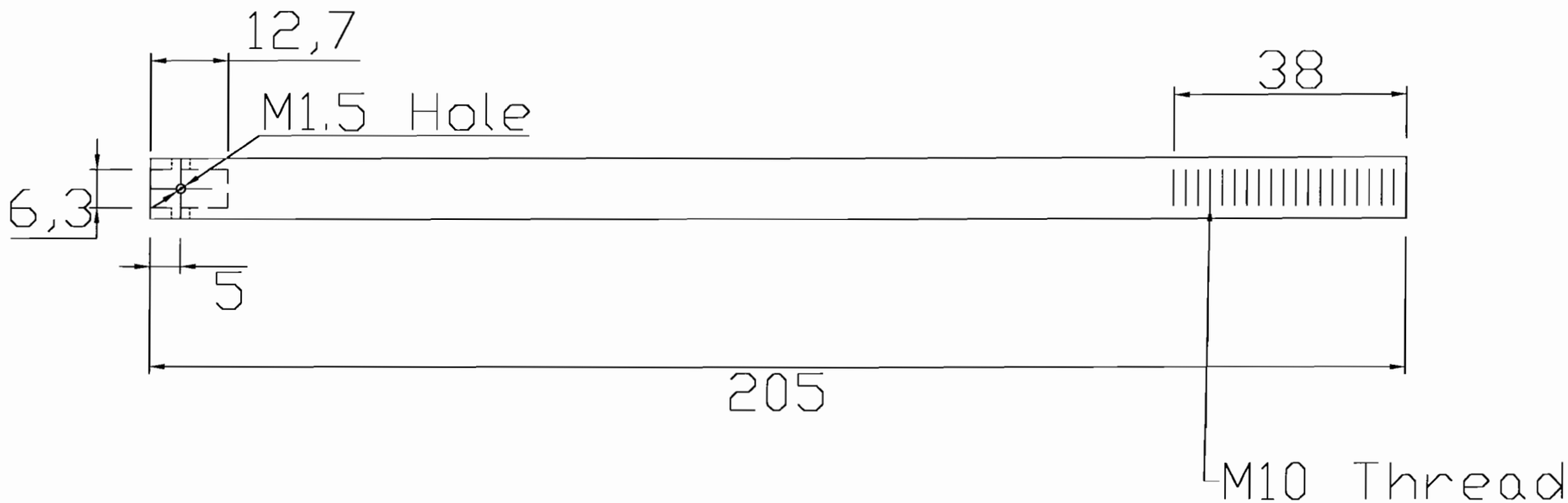

Part no: 13	Description: Shaft	Material: Stainless Steel	No of: 1

University of Cape Town
Department of Mechanical Engineering
Centre for Materials Engineering

Title:
Stiffness Tester

Dimensions in millimetres (mm)	Scale: 1 to 1	Date: 19/08/03	Sheet: 15 of 18
Tolerance unless otherwise stated 0.01	Drawing By: John Jones		Drawing no: 15

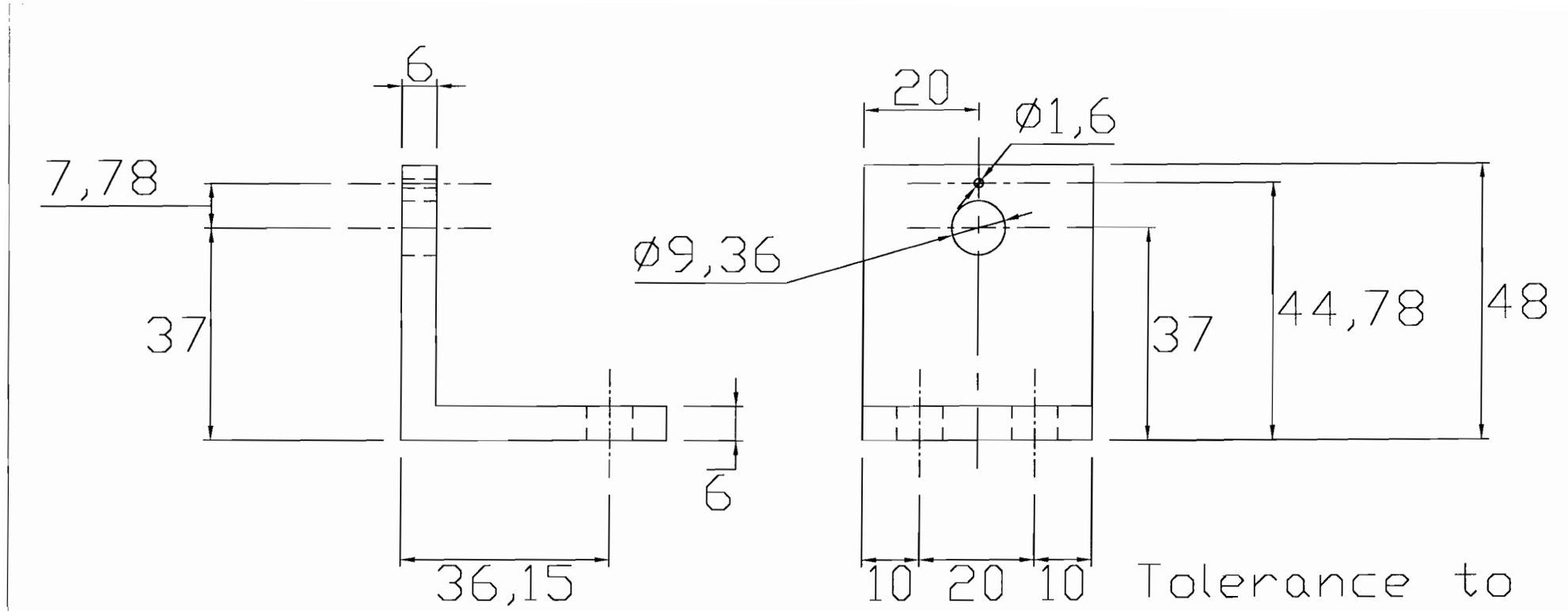

Part no: 14	Description: Servo POT Bracket	Material: Aluminium AISI 6261	No of: 1
University of Cape Town Department of Mechanical Engineering Centre for Materials Engineering			
Title: Stiffness Tester			
Dimensions in millimetres (mm)	Scale: 1 to 1	Date: 19/08/03	Sheet: 16 of 18
Tolerance unless otherwise stated 0.01	Drawing By: John Jones		Drawing no: 16

Assembly - Side View

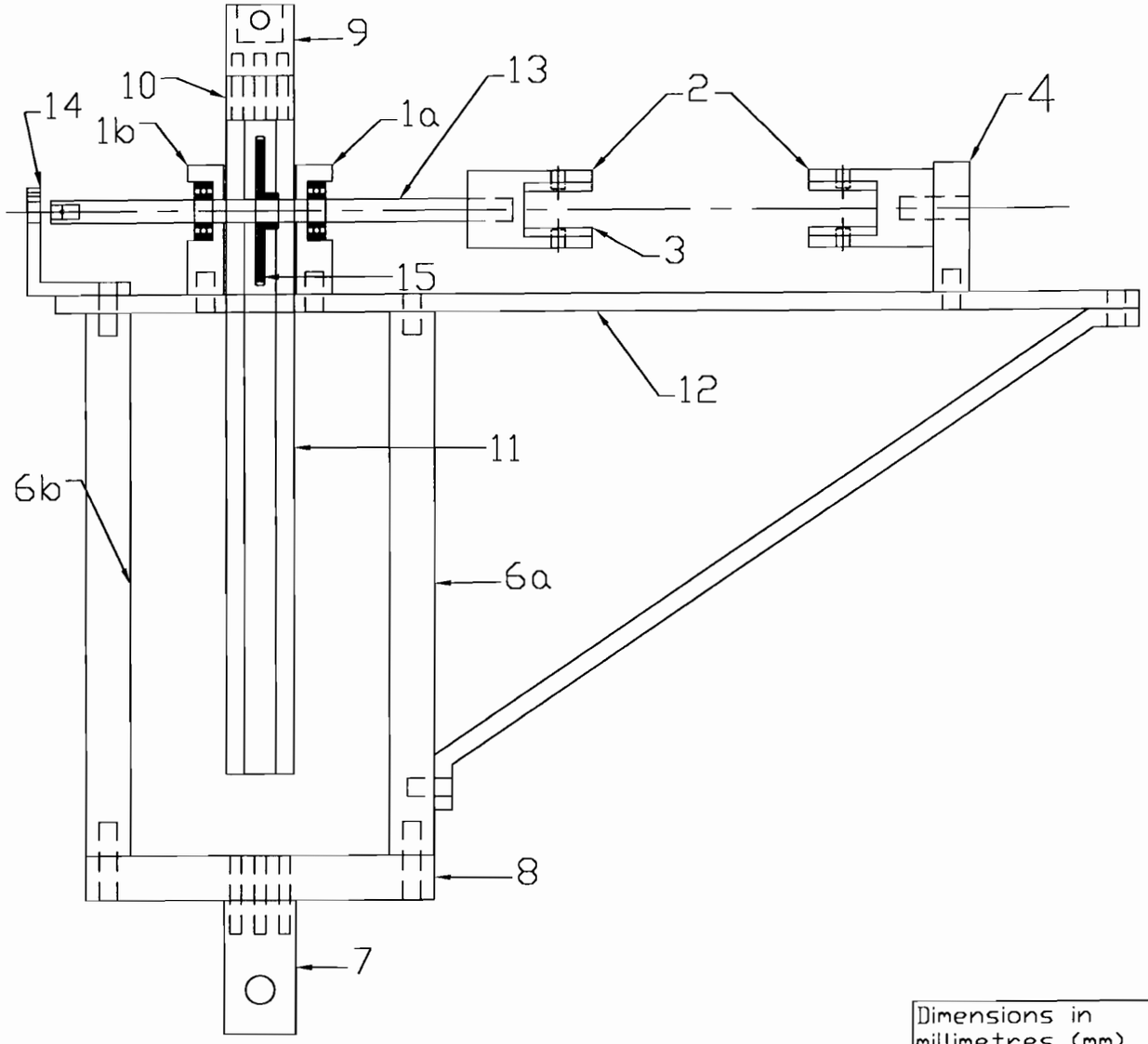

Part no:	Description:	Material:	No of:
19	M1.5 Bolt		3
18	M3 Bolt		8
17	M5 Bolt		8
16	M8 Bolt		16
15	Gear	Phosphour Bronze	1
14	Servo POT Bracket	Aluminium AISI 6261	1
13	Shaft	Stainless Steel	1
12	Base Plate	Aluminium AISI 6261	1
11	Rack	Brass	1
10	Top Plate	Aluminium AISI 6261	1
9	Top Connection	Aluminium AISI 6261	1
8	Bottom Plate	Aluminium AISI 6261	1
7	Bottom Connection	Aluminium AISI 6261	1
6b	Left Support	Aluminium AISI 6261	1
6a	Right Support	Aluminium AISI 6261	1
5	Angled Support	Aluminium AISI 6261	1
4	Grip Holder	Aluminium AISI 6261	1
3	Grip Plate	Aluminium AISI 6261	4
2	Grip	Aluminium AISI 6261	2
1b	Left Bearing Housing	Aluminium AISI 6261	1
1a	Right Bearing Housing	Aluminium AISI 6261	1

University of Cape Town
Department of Mechanical Engineering
Centre for Materials Engineering

Title:
Stiffness Tester

Dimensions in millimetres (mm)	Scale: 1 to 3	Date: 19/08/03	Sheet: 17 of 18
Tolerance unless otherwise stated 0.01	Drawing By: John Jones		Drawing no: 17

Assembly - Front View

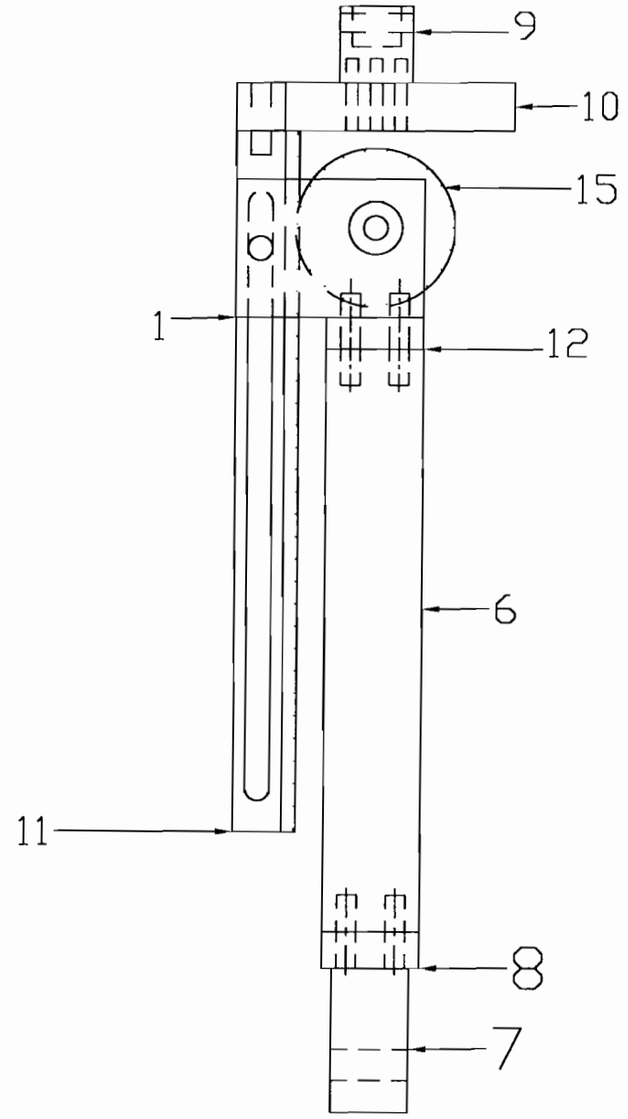

Part no:	Description:	Material:	No of:
19	M1.5 Bolt		3
18	M3 Bolt		8
17	M5 Bolt		8
16	M8 Bolt		16
15	Gear	Phosphour Bronze	1
14	Servo POT Bracket	Aluminium AISI 6261	1
13	Shaft	Stainless Steel	1
12	Base Plate	Aluminium AISI 6261	1
11	Rack	Brass	1
10	Top Plate	Aluminium AISI 6261	1
9	Top Connection	Aluminium AISI 6261	1
8	Bottom Plate	Aluminium AISI 6261	1
7	Bottom Connection	Aluminium AISI 6261	1
6b	Left Support	Aluminium AISI 6261	1
6a	Right Support	Aluminium AISI 6261	1
5	Angled Support	Aluminium AISI 6261	1
4	Grip Holder	Aluminium AISI 6261	1
3	Grip Plate	Aluminium AISI 6261	4
2	Grip	Aluminium AISI 6261	2
1b	Left Bearing Housing	Aluminium AISI 6261	1
1a	Right Bearing Housing	Aluminium AISI 6261	1

University of Cape Town
Department of Mechanical Engineering
Centre for Materials Engineering

Title:
Stiffness Tester

Dimensions in millimetres (mm)	Scale: 1 to 3	Date: 19/08/03	Sheet: 18 of 18
Tolerance unless otherwise stated 0.01	Drawing By: John Jones		Drawing no: 18

Appendix B

Block Shear Fixture

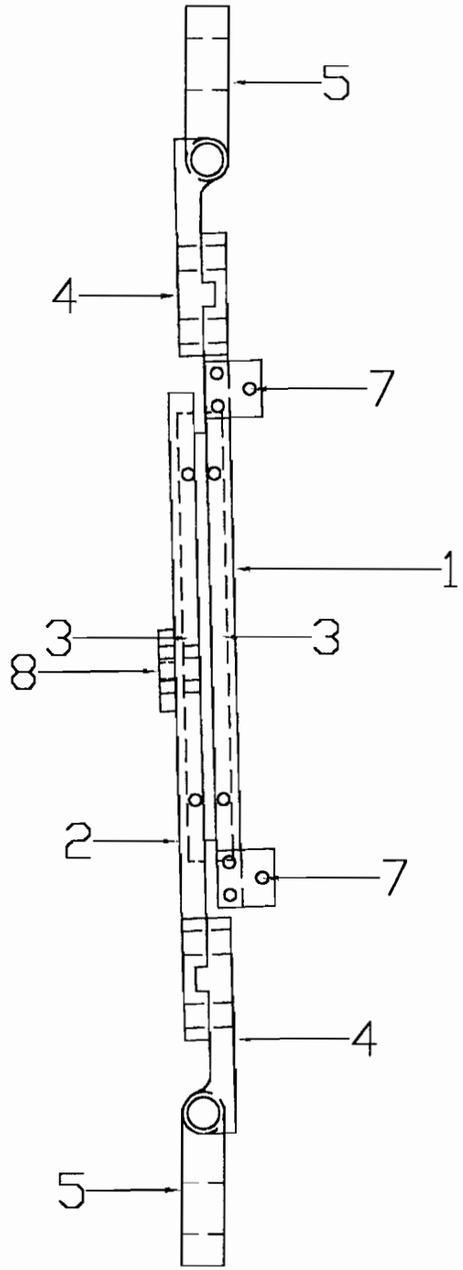

Part no:	Description:		No of:
10	M3 Machine Head Screw		13
9	M6 Machine Head Screw		4
8	Pin Holder	Aluminium AISI 6261	1
7	PDT Holder	Aluminium AISI 6261	2
6	Load Cell Connection	Aluminium AISI 6261	1
5	Swivel	Aluminium AISI 6261	2
4	Connection	Aluminium AISI 6261	2
3	Insert	Pine Ply	
2	Back Plate	Aluminium AISI 6261	1
1	Front Plate	Aluminium AISI 6261	1

University of Cape Town
Department of Mechanical Engineering
Centre for Materials Engineering

Title:
Block Shear Rig

Dimensions in millimetres (mm)	Scale: 2 to 3	Date: 05/08/03	Sheet: 1 of 9
Tolerance unless otherwise stated 0.01	Drawing By: John Jones		Drawing no: 1

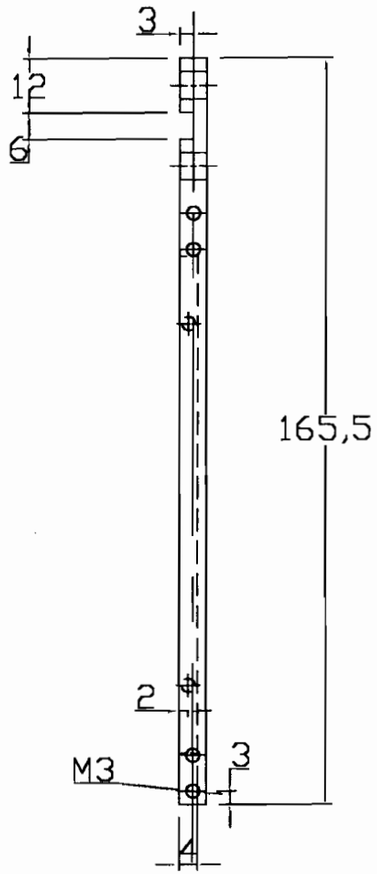

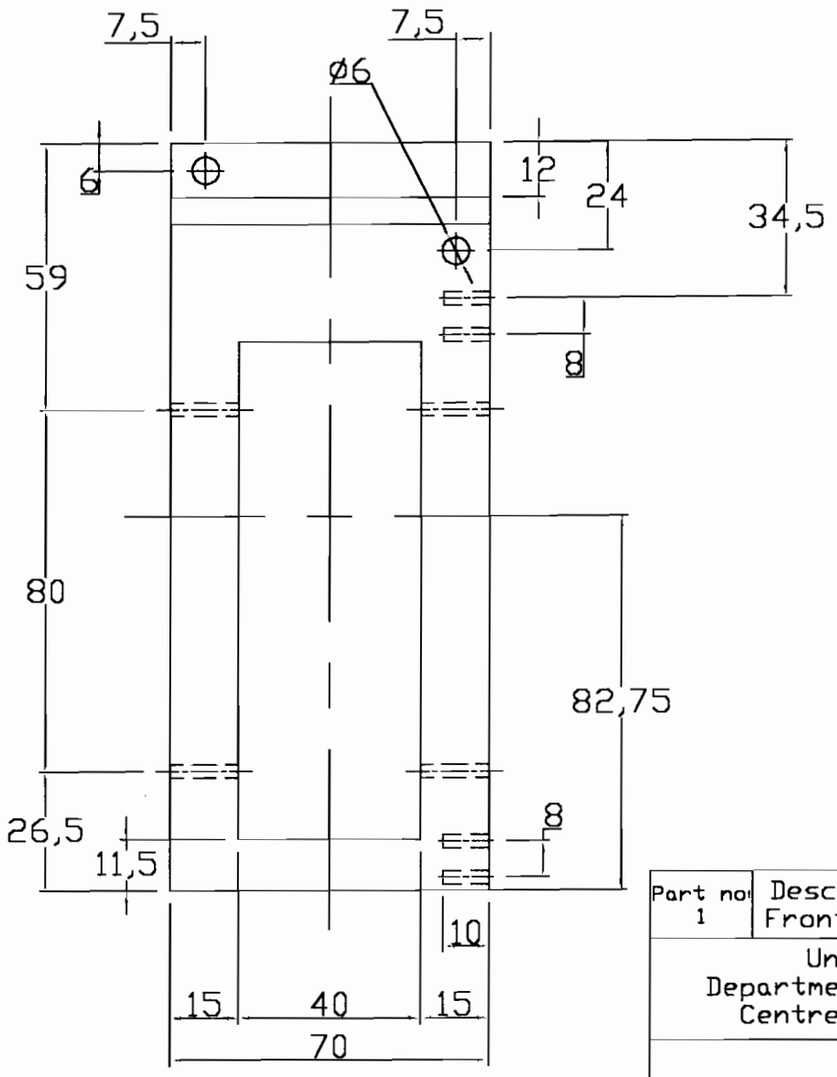

Part no: 1	Description: Front Plate	Material: Aluminium AISI 6261	No of: 1

University of Cape Town
Department of Mechanical Engineering
Centre for Materials Engineering

Title:
Block Shear Rig

Dimensions in millimetres (mm)	Scale: 2 to 3	Date: 05/08/03	Sheet: 2 of 9
Tolerance unless otherwise stated 0.01	Drawing By: John Jones		Drawing no: 2

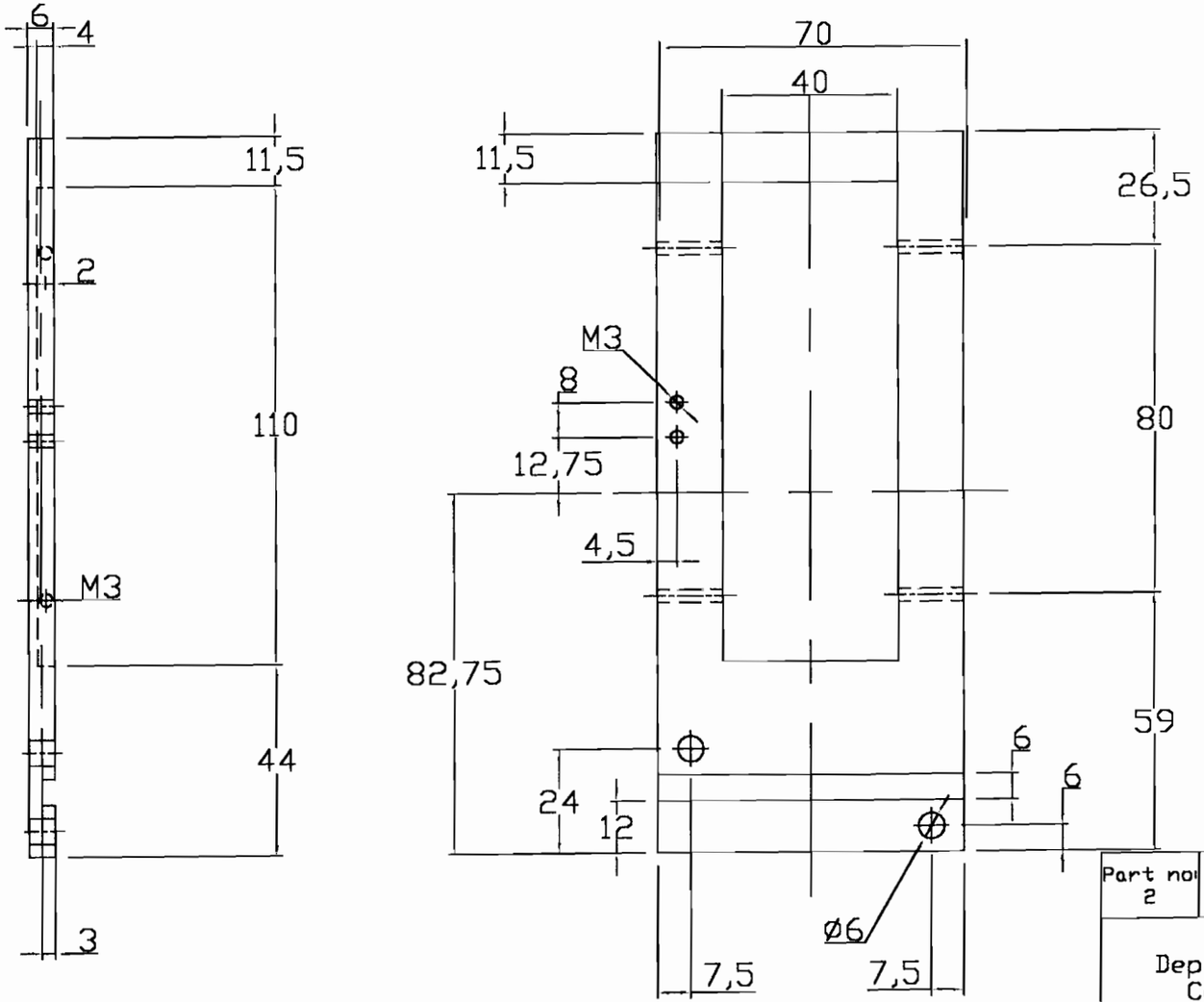

Part no: 2	Description: Back Plate	Material: Aluminium AISI 6261	No of: 1

University of Cape Town
Department of Mechanical Engineering
Centre for Materials Engineering

Title:
Block Shear Rig

Dimensions in millimetres (mm)	Scale: 2 to 3	Date: 05/08/03	Sheet: 3 of 9
Tolerance unless otherwise stated 0.01	Drawing By: John Jones		Drawing no: 3

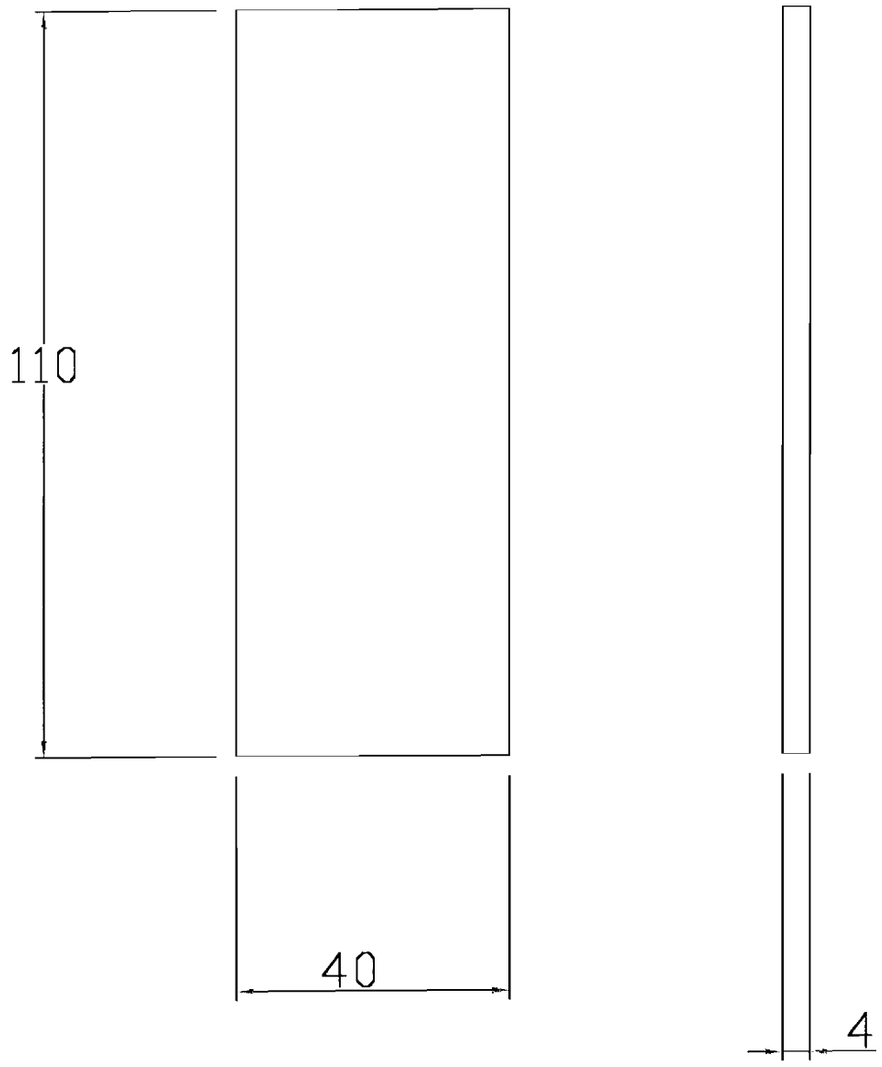

Part no: 3	Description: Insert	Material: Wood	No of: 12

University of Cape Town
Department of Mechanical Engineering
Centre for Materials Engineering

Title:
Block Shear Rig

Dimensions in millimetres (mm)	Scale: 1 to 1	Date: 05/08/03	Sheet: 4 of 9
Tolerance unless otherwise stated 0.01	Drawing By: John Jones		Drawing no: 4

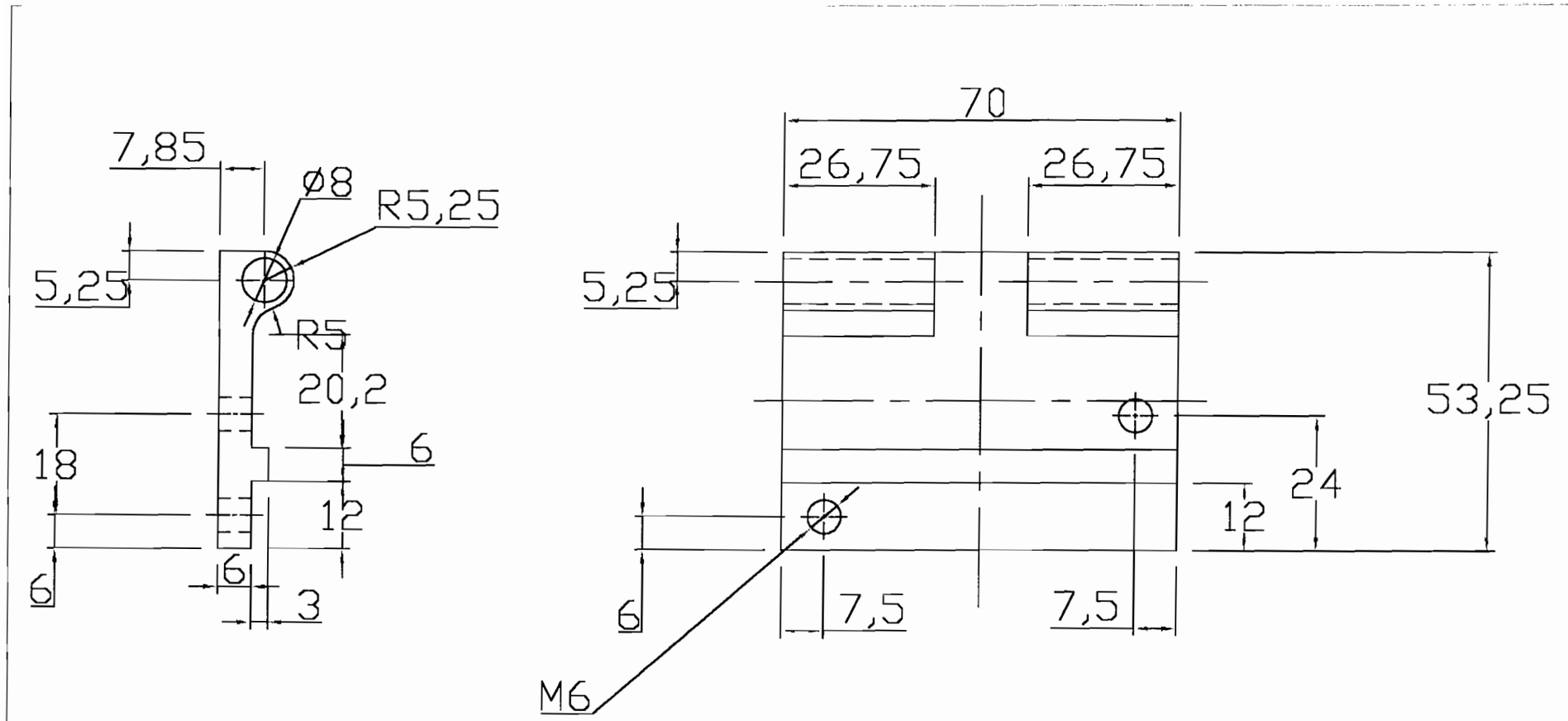

Part no: 4	Description: Connection	Material: Aluminium AISI 6261	No of: 2
University of Cape Town Department of Mechanical Engineering Centre for Materials Engineering			
Title: Block Shear Rig			
Dimensions in millimetres (mm)	Scale: 1 to 1	Date: 05/08/03	Sheet: 5 of 9
Tolerance unless otherwise stated 0.01	Drawing By: John Jones		Drawing no: 5

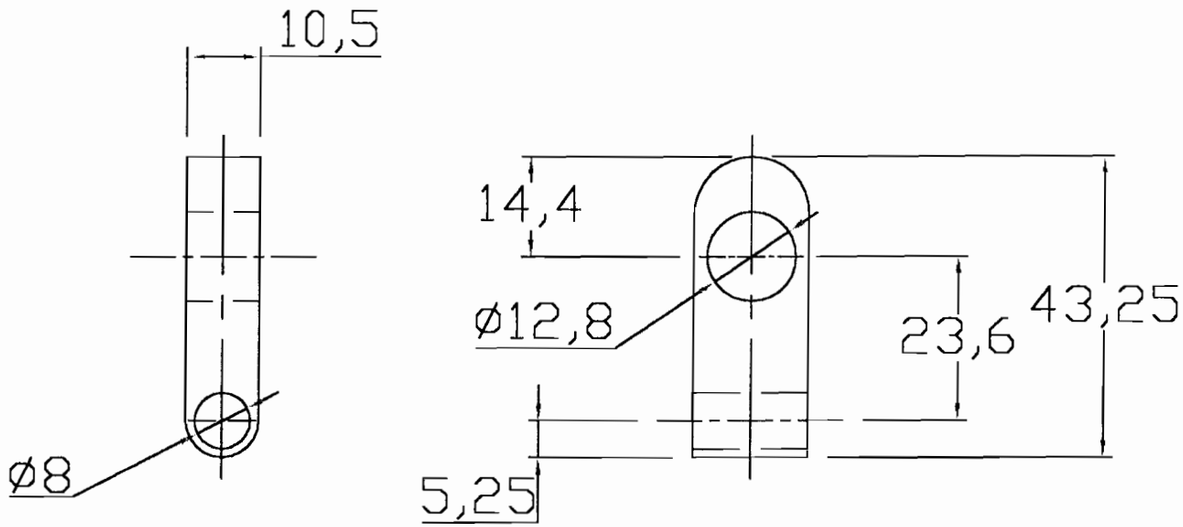

Part no: 5	Description: Swivel	Material: Aluminium AISI 6261	No of: 2
University of Cape Town Department of Mechanical Engineering Centre for Materials Engineering			
Title: Block Shear Rig			
Dimensions in millimetres (mm)	Scale: 1 to 1	Date: 05/08/03	Sheet: 6 of 9
Tolerance unless otherwise stated 0.01	Drawing By: John Jones		Drawing no: 6

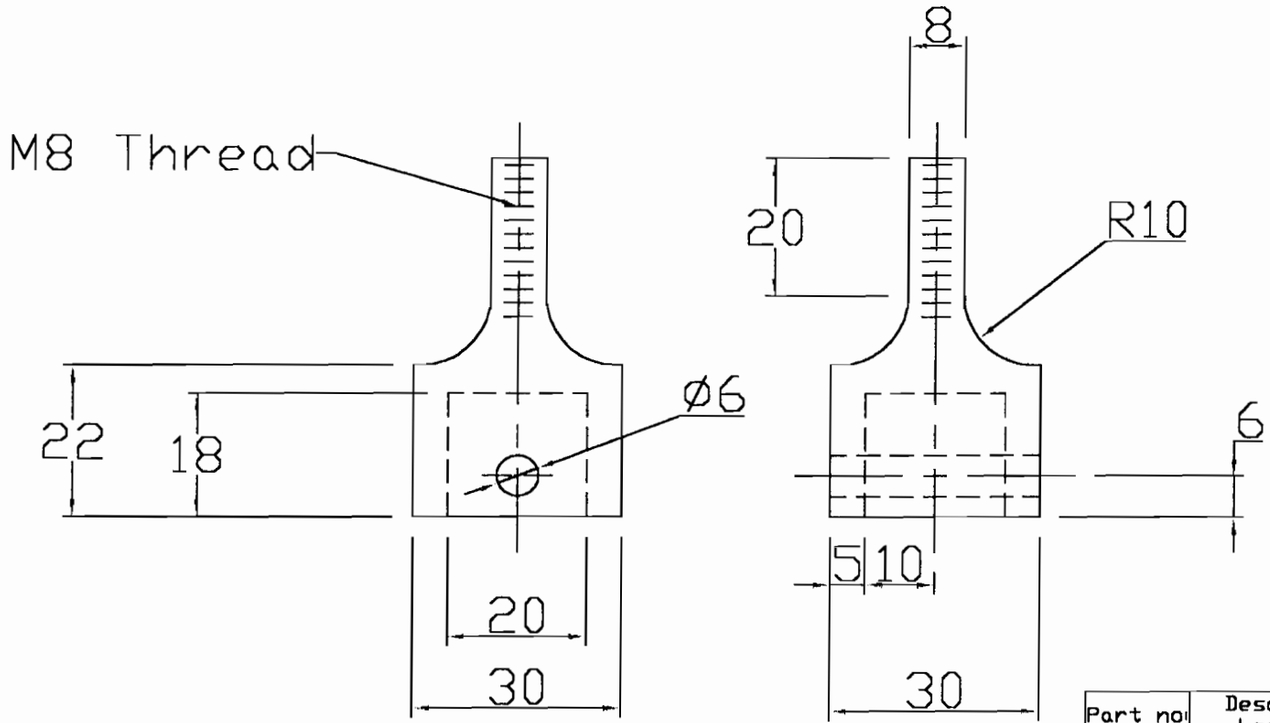

Part no: 6	Description: Load Cell Connection	Material: Aluminium AISI 6261	No of: 1
University of Cape Town Department of Mechanical Engineering Centre for Materials Engineering			
Title: Block Shear Rig			
Dimensions in millimetres (mm)	Scale: 1 to 1	Date: 05/08/03	Sheet: 7 of 9
Tolerance unless otherwise stated 0.01	Drawing By: John Jones		Drawing no: 7

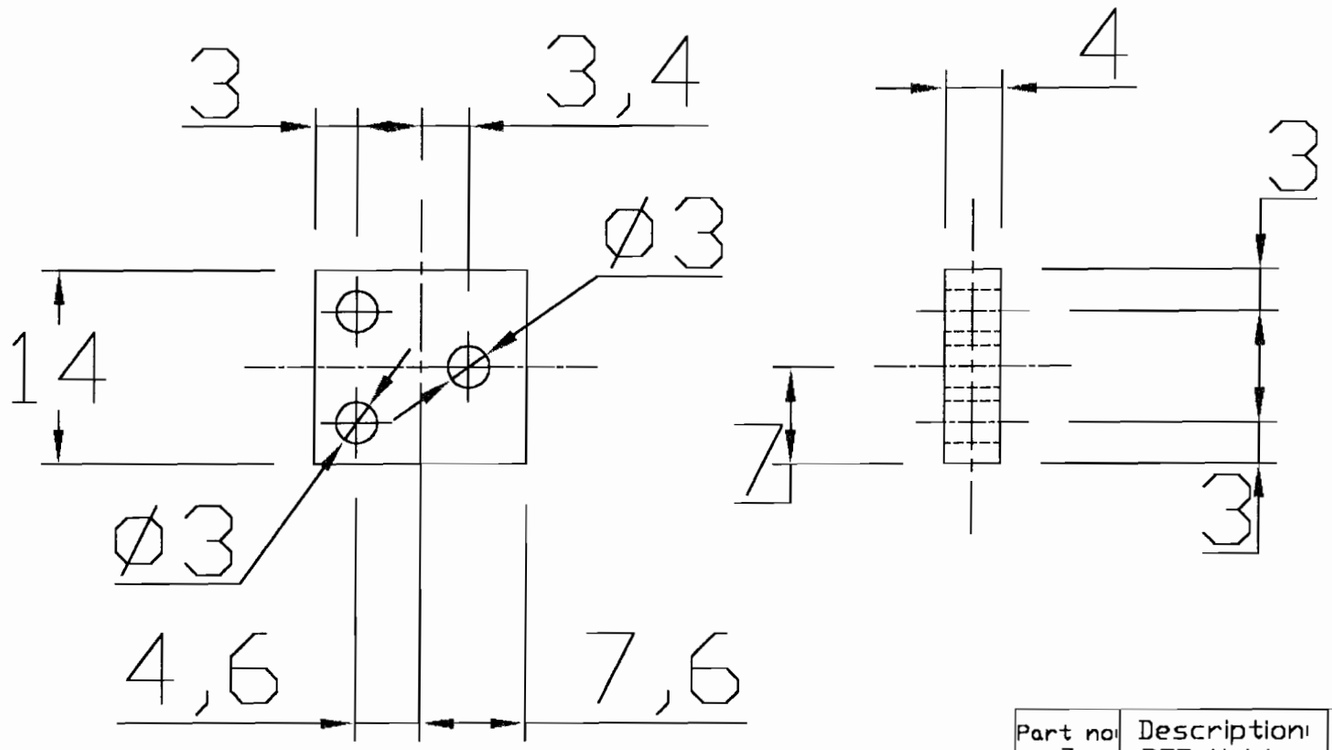

Part no: 7	Description: PDT Holder	Material: Aluminium AISI 6261	No of: 2
University of Cape Town Department of Mechanical Engineering Centre for Materials Engineering			
Title: Block Shear Rig			
Dimensions in millimetres (mm)	Scale: 2 to 1	Date: 05/08/03	Sheet: 8 of 9
Tolerance unless otherwise stated 0.01	Drawing By: John Jones		Drawing no: 8

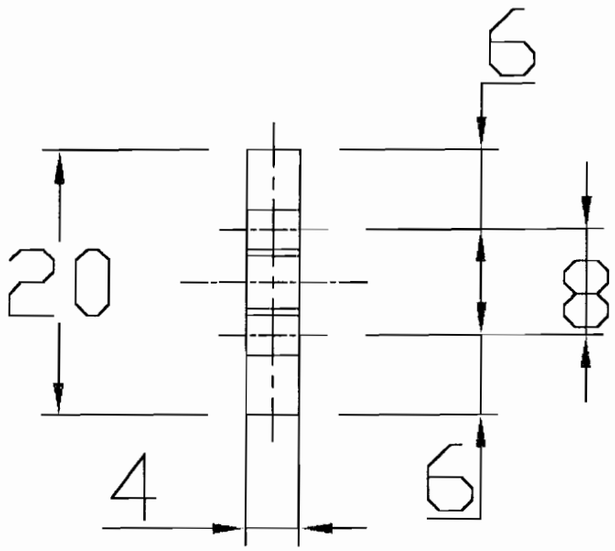

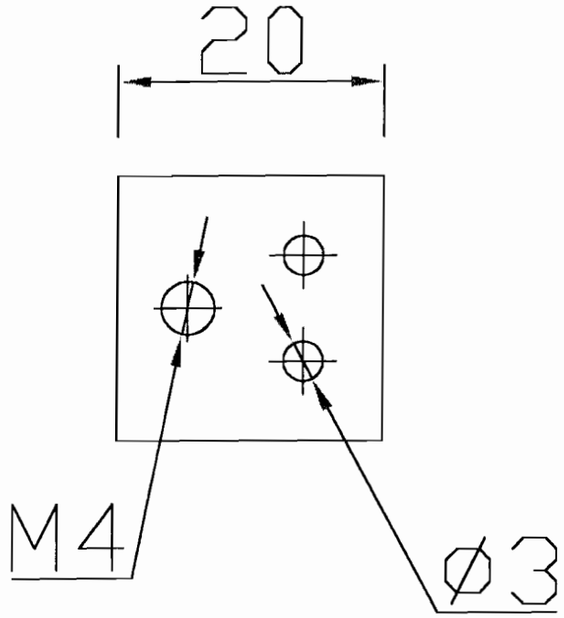

Part no: 8	Description: Pin Holder	Material: Aluminium AISI 6261	No of: 1
University of Cape Town Department of Mechanical Engineering Centre for Materials Engineering			
Title: Block Shear Rig			
Dimensions in millimetres (mm)	Scale: 2 to 1	Date: 05/08/03	Sheet: 9 of 9
Tolerance unless otherwise stated 0.01	Drawing By: John Jones		Drawing no: 9

Appendix C

3-Point Bend Fixture

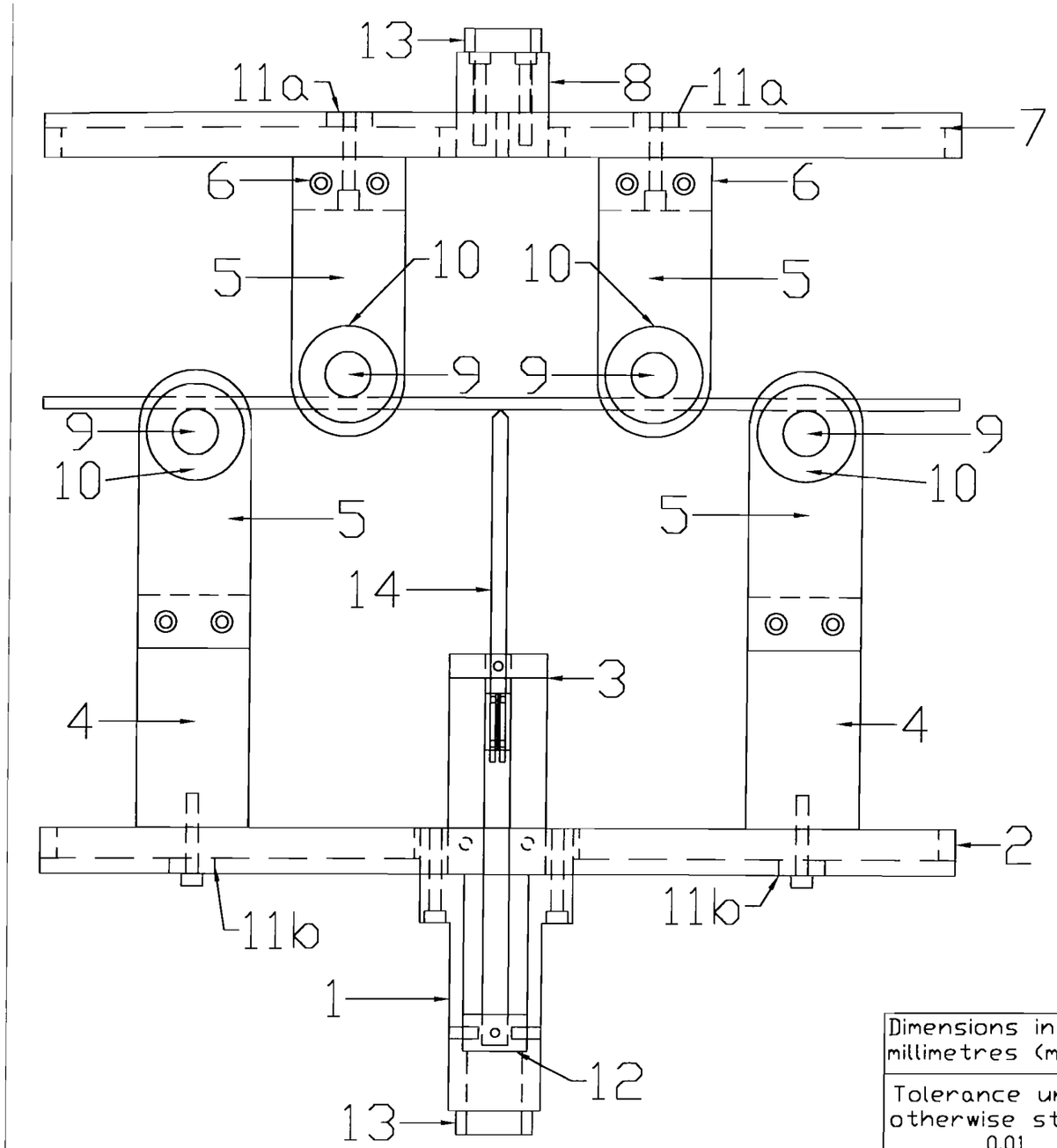

Part no.	Description: Full Assembly Side view	Material:	No of:
14	PDT Blade	Nylon	1
13	Lock Washer	Stainless Steel M300	2
12	PDT Spacer	Stainless Steel M300	1
11	Slide Bracket	Aluminium AISI 6261	4
10	Bearing	SKF 6002	8
9	Roller	Aluminium AISI 6261	4
8	Top Connection	Stainless Steel M300	1
7	Top Plate	Aluminium AISI 6261	1
6	Top Support	Aluminium AISI 6261	2
5	Roller Housing	Aluminium AISI 6261	8
4	Bottom Support	Aluminium AISI 6261	2
3	PDT Bracket	Aluminium AISI 6261	1
2	Base Plate	Aluminium AISI 6261	1
1	Base Connection	Stainless Steel M300	1

University of Cape Town
Department of Mechanical Engineering
Centre for Materials Engineering

Title:
3/4 point bend

Dimensions in millimetres (mm)	Scale: 1 to 2	Date: 10/09/03	Sheet: 1 of 20
Tolerance unless otherwise stated 0.01	Drawing By: John Jones		Drawing no: 1

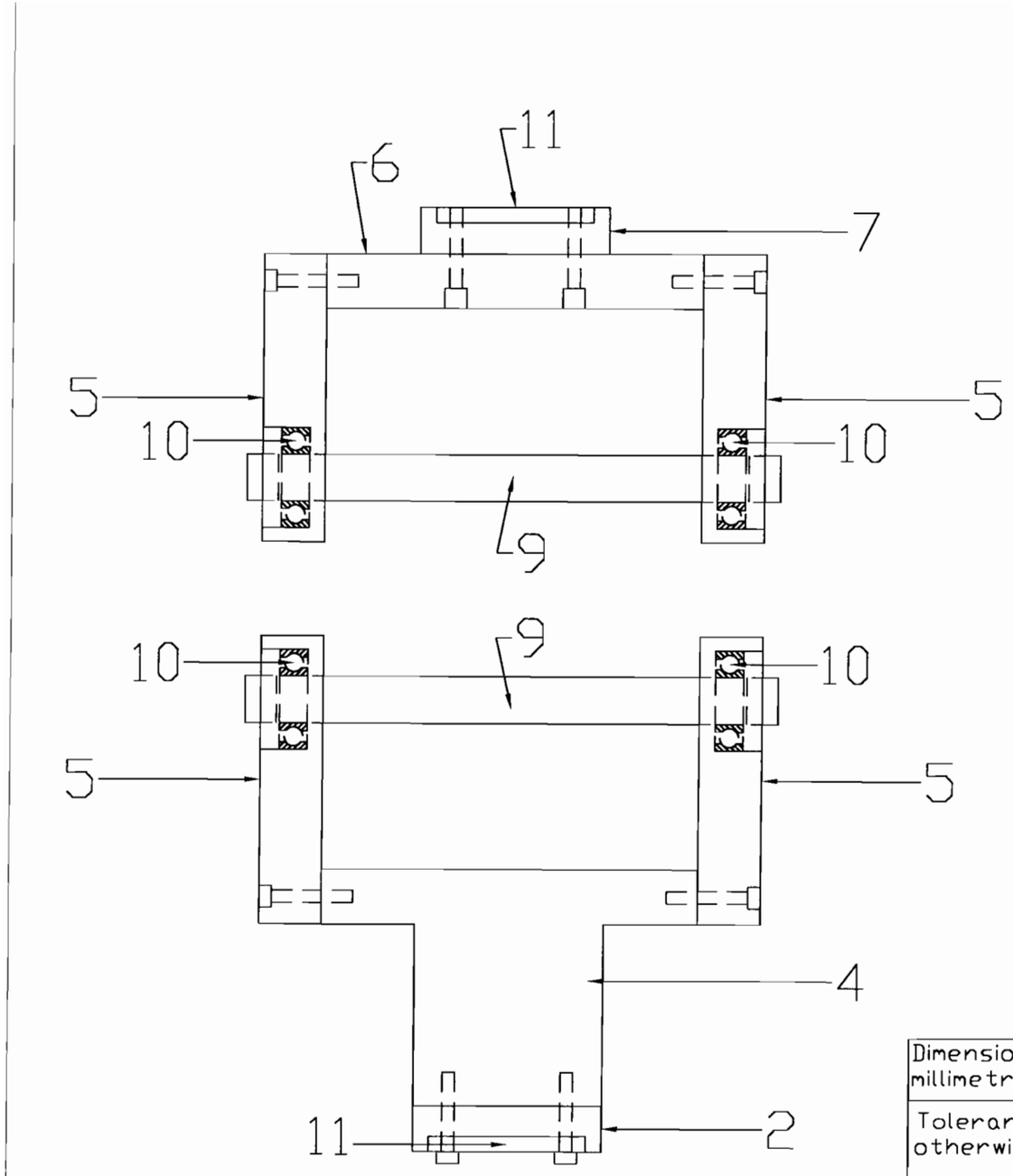

11	Slide Bracket	Aluminium AISI 6261	2
10	Bearing	SKF 6002	8
9	Roller	Aluminium AISI 6261	4
7	Top Plate	Aluminium AISI 6261	1
6	Top Support	Aluminium AISI 6261	2
5	Roller Housing	Aluminium AISI 6261	4
4	Bottom Support	Aluminium AISI 6261	2
2	Base Plate	Aluminium AISI 6261	1
Part no.	Description: Sub - Assembly Front View	Material:	No of:

University of Cape Town
Department of Mechanical Engineering
Centre for Materials Engineering

Title:
3/4 point bend

Dimensions in millimetres (mm)	Scale: 1 to 2	Date: 10/09/03	Sheet: 2 of 20
Tolerance unless otherwise stated 0.01	Drawing By: John Jones		Drawing no: 2

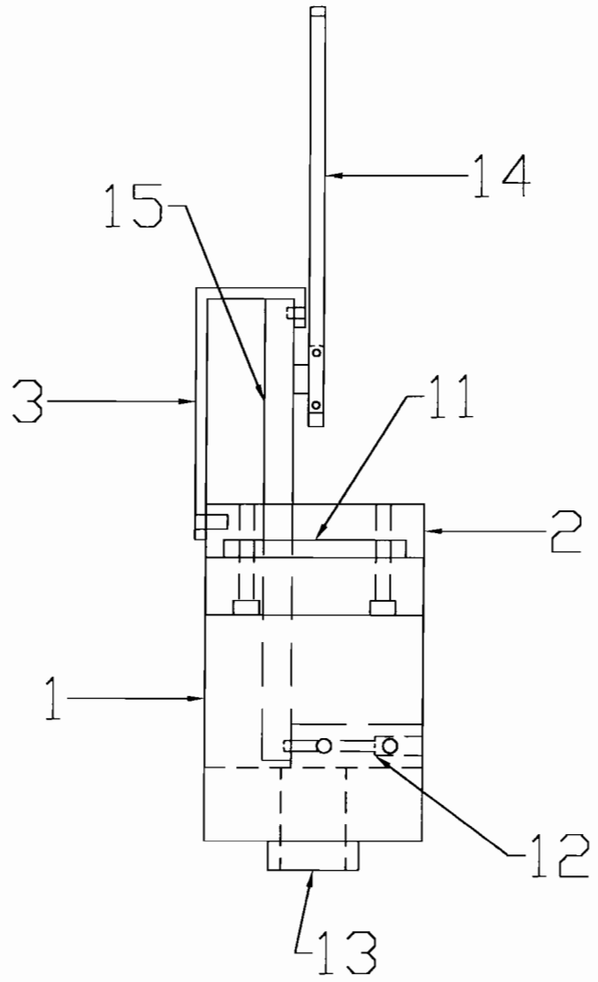

15	POT		
14	POT Blade	Nylon	1
13	Lock Washer	Stainless Steel M300	2
12	POT Spacer	Stainless Steel M300	1
11	Slide Bracket	Aluminium AISI 6261	4
3	POT Bracket	Aluminium AISI 6261	1
2	Base Plate	Aluminium AISI 6261	1
1	Base Connection	Stainless Steel M300	1
Part no.	Description: POT Assembly Front view	Material:	No of:

University of Cape Town
Department of Mechanical Engineering
Centre for Materials Engineering

Title:
3/4 point bend

Dimensions in millimetres (mm)	Scale: 1 to 2	Date: 10/09/03	Sheet: 3 of 20
Tolerance unless otherwise stated 0.01	Drawing By: John Jones		Drawing no: 3

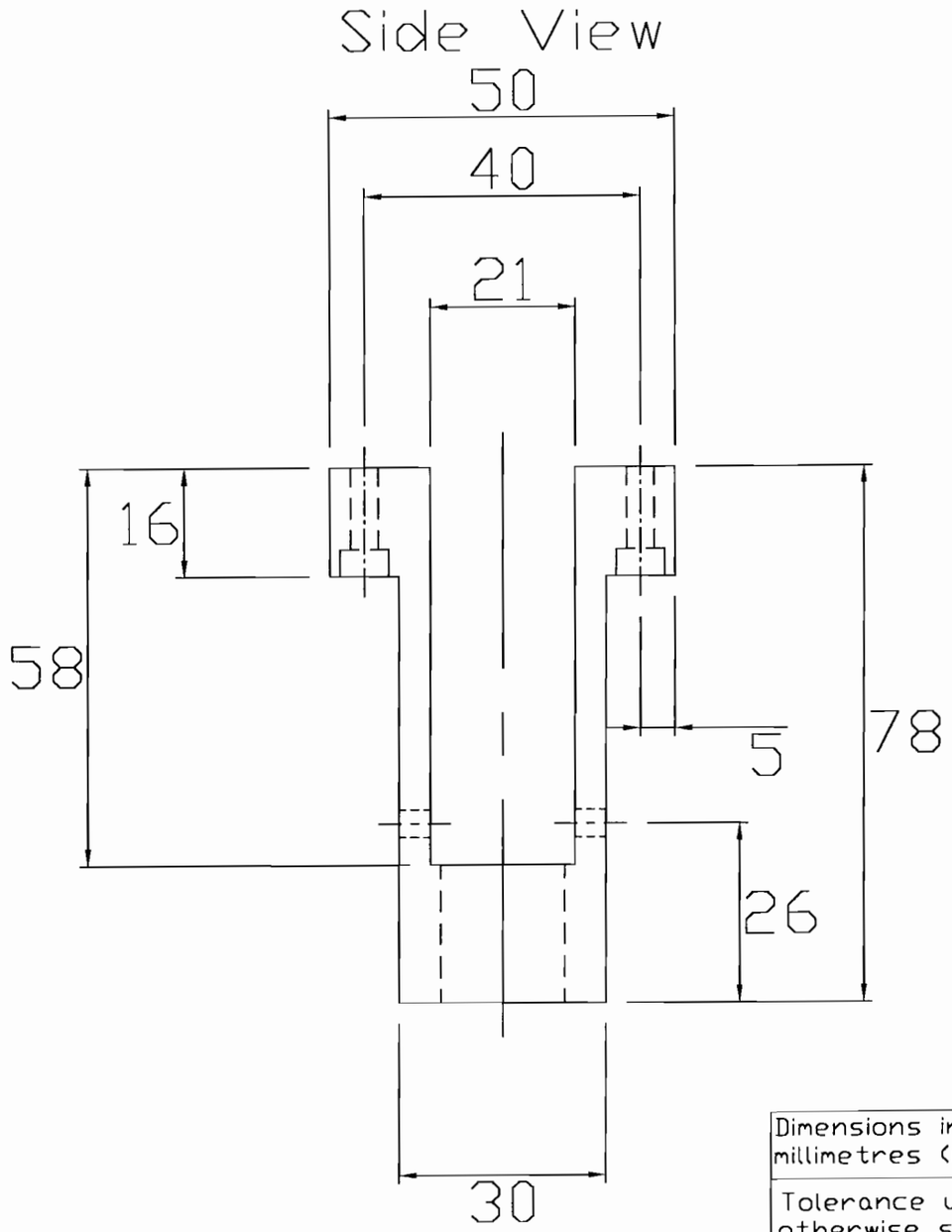

Part no:1	Description: Base Connection	Material: Stainless Steel M300	No of: 1
University of Cape Town Department of Mechanical Engineering Centre for Materials Engineering			
Title: 3/4 point bend			
Dimensions in millimetres (mm)	Scale: 1 to 1	Date: 10/09/03	Sheet: 4 of 20
Tolerance unless otherwise stated 0.01	Drawing By: John Jones		Drawing no: 4a

Front View

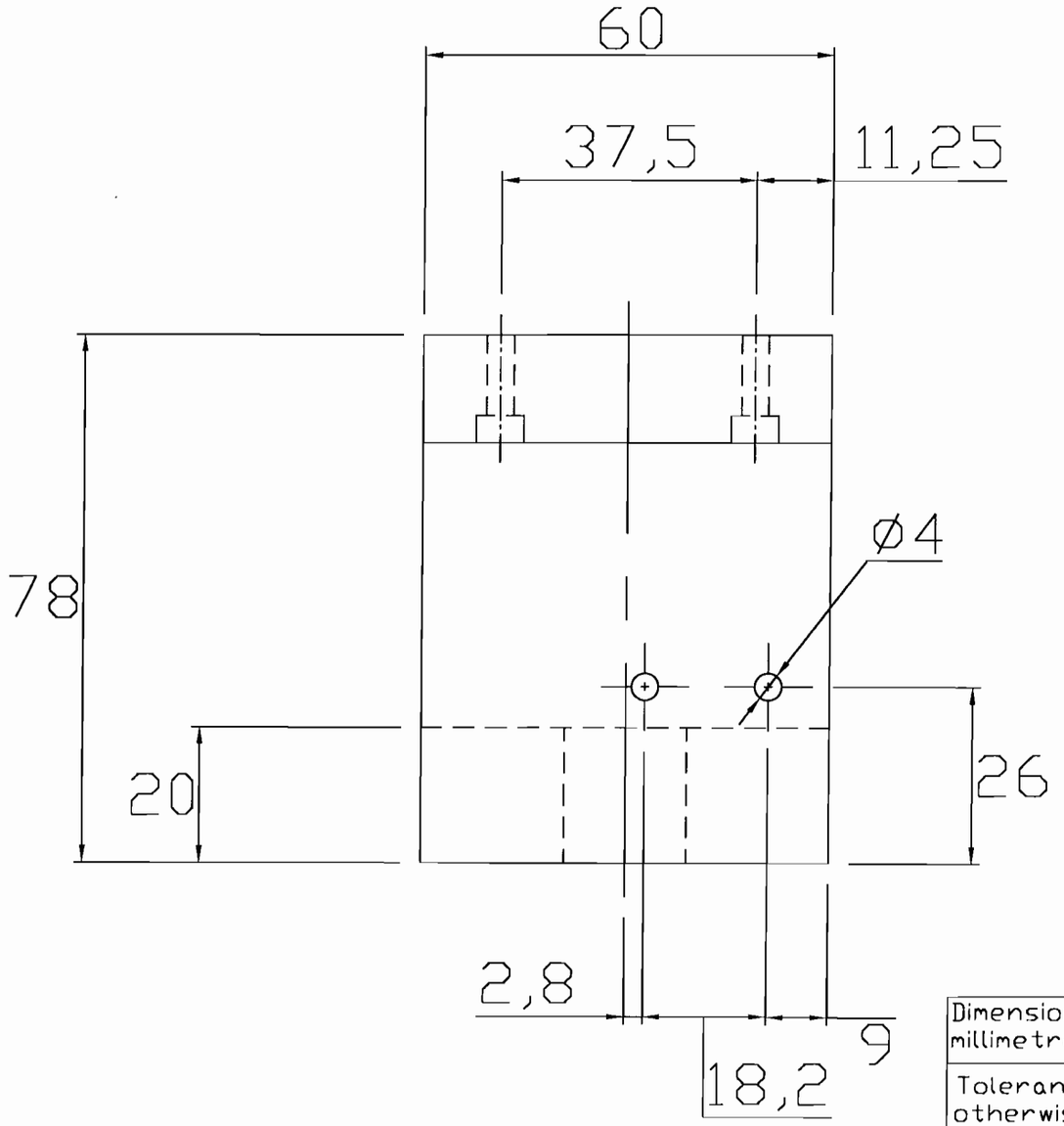

Part no:1	Description: Base Connection	Material: Stainless Steel M300	No of: 1
University of Cape Town Department of Mechanical Engineering Centre for Materials Engineering			
Title: 3/4 point bend			
Dimensions in millimetres (mm)	Scale: 1 to 1	Date: 10/09/03	Sheet: 5 of 20
Tolerance unless otherwise stated 0.01	Drawing By: John Jones		Drawing no: 4b

Bottom View

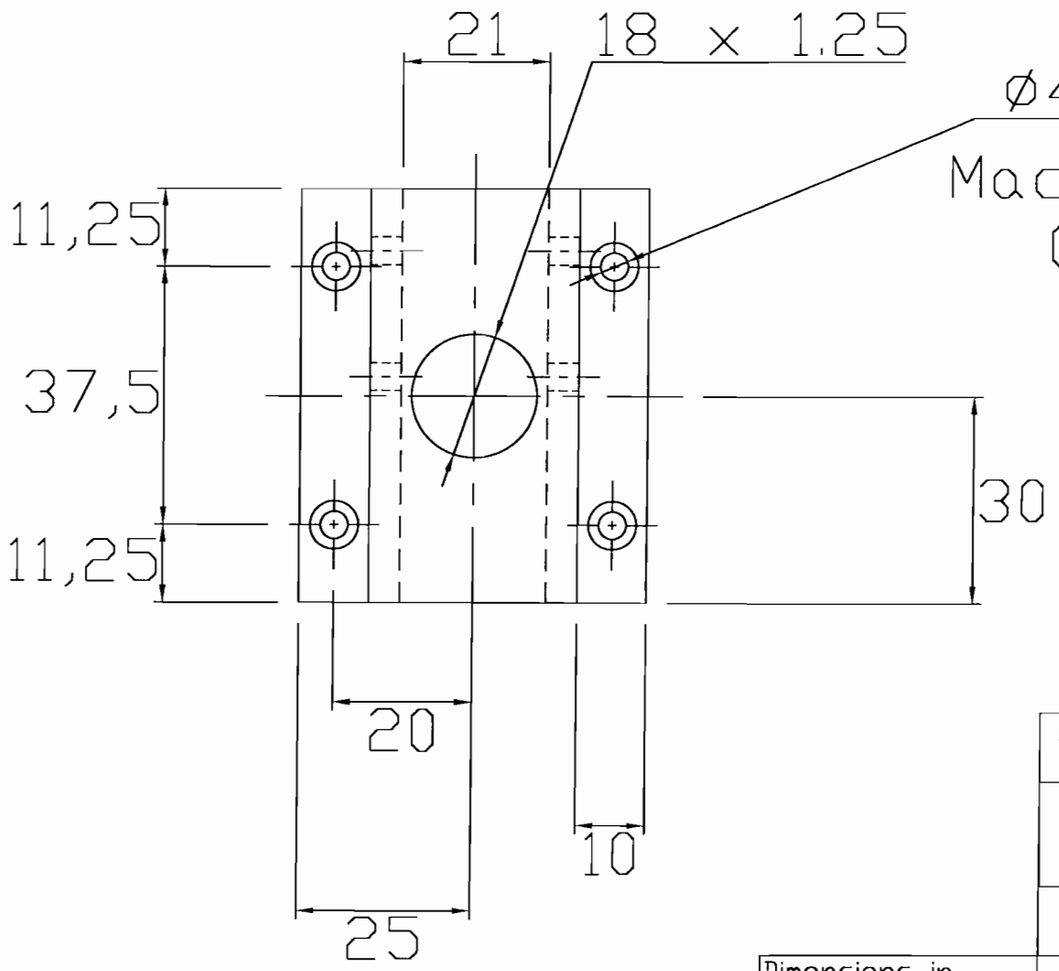

Part no:1	Description: Base Connection	Material: Stainless Steel M300	No of: 1
University of Cape Town Department of Mechanical Engineering Centre for Materials Engineering			
Title: 3/4 point bend			
Dimensions in millimetres (mm)	Scale: 1 to 1	Date: 10/09/03	Sheet: 6 of 20
Tolerance unless otherwise stated 0.01	Drawing By: John Jones		Drawing no: 4c

Bottom View

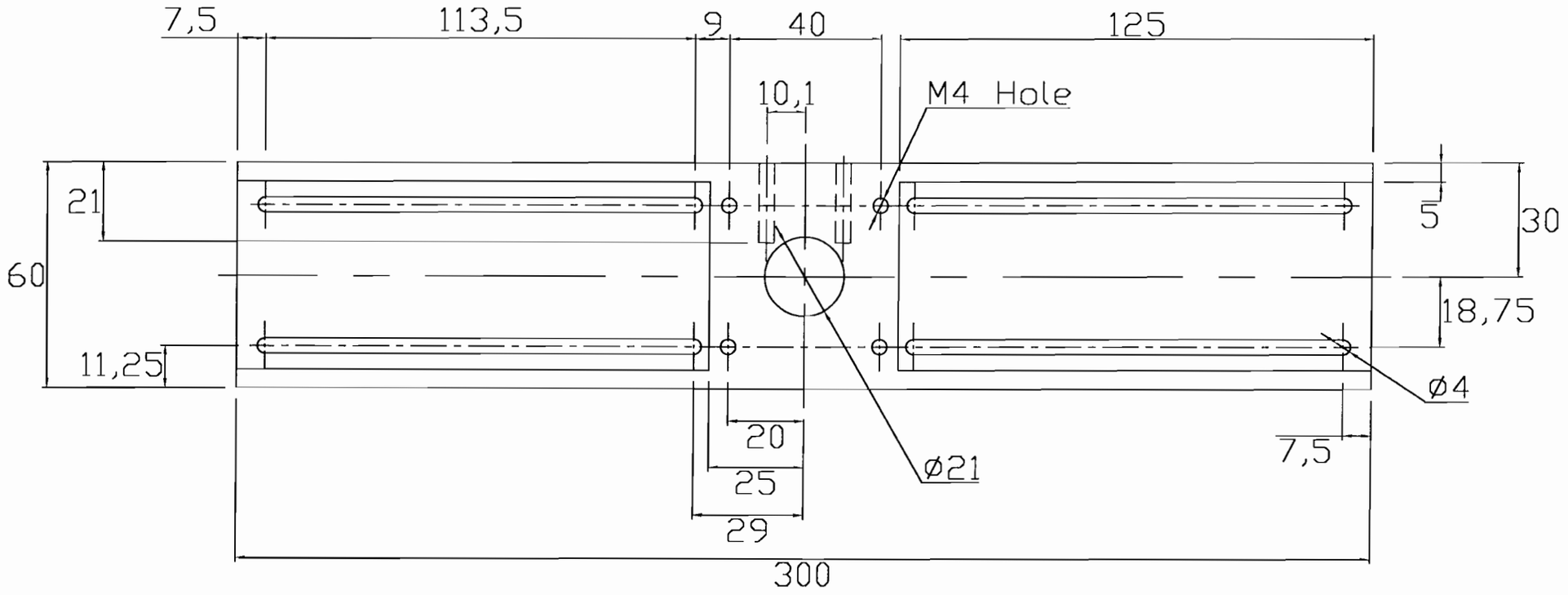

Part no: 2	Description: Base Plate	Material: Aluminium AISI 6261	No of: 1

University of Cape Town
Department of Mechanical Engineering
Centre for Materials Engineering

Title:
3/4 point bend

Dimensions in millimetres (mm)	Scale: 2 to 3	Date: 10/09/03	Sheet: 7 of 20
Tolerance unless otherwise stated 0.01	Drawing By: John Jones		Drawing no: 5a

Side View

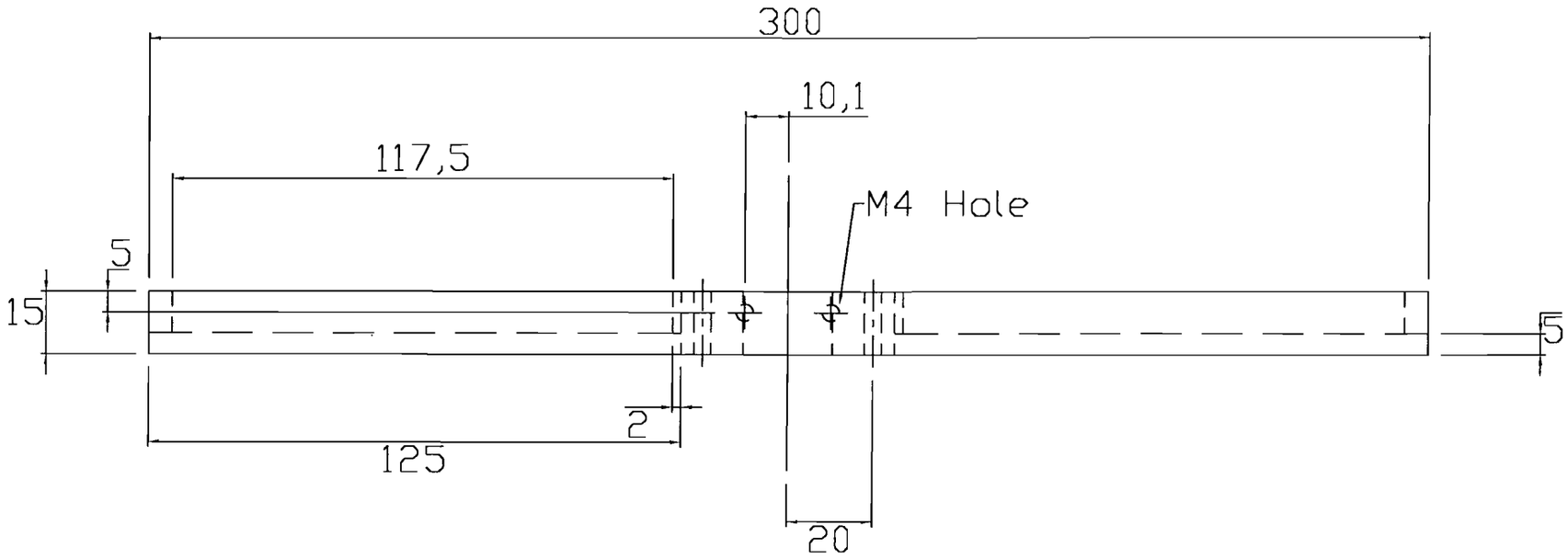

Part no: 2	Description: Base Plate	Material: Aluminium AISI 6261	No of: 1
University of Cape Town Department of Mechanical Engineering Centre for Materials Engineering			
Title: 3/4 point bend			
Dimensions in millimetres (mm)	Scale: 2 to 3	Date: 10/09/03	Sheet: 8 of 20
Tolerance unless otherwise stated 0.01	Drawing By: John Jones		Drawing no: 5b

Side View

Ø3,Flat Head Screw Countersunk

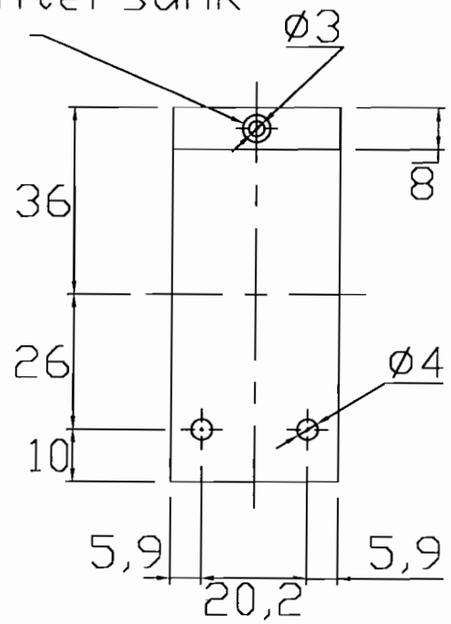

Front View

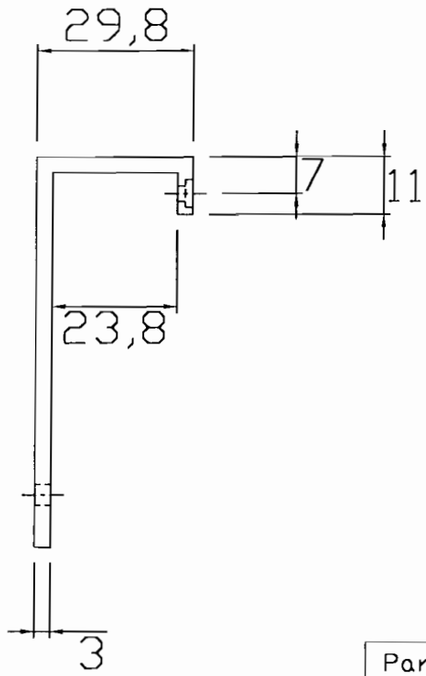

Part no: 3	Description: PDT Bracket	Material: Aluminium AISI 6261	No of: 1
University of Cape Town Department of Mechanical Engineering Centre for Materials Engineering			
Title: 3/4 point bend			
Dimensions in millimetres (mm)	Scale: 1 to 1	Date: 10/09/03	Sheet: 9 of 20
Tolerance unless otherwise stated 0.01	Drawing By: John Jones		Drawing no: 6

Front View

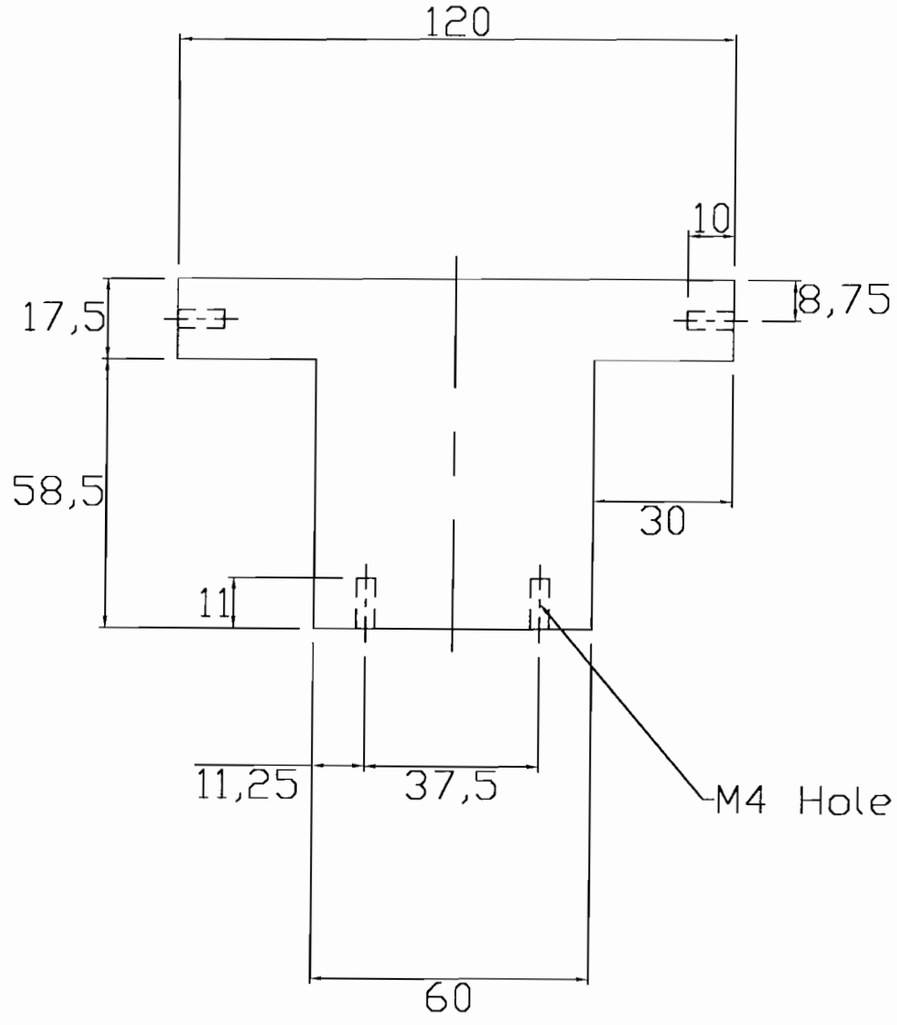

Side View

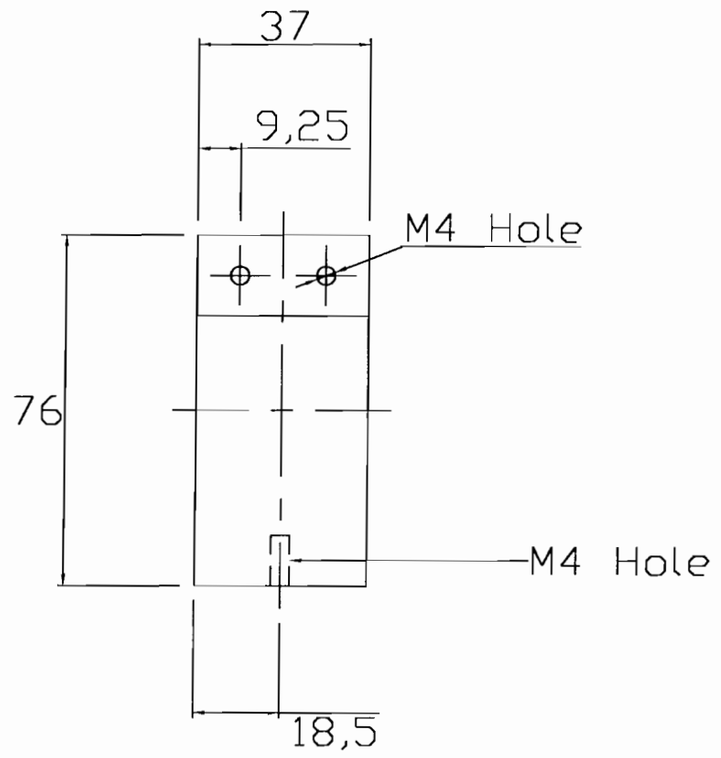

Part no: 4	Description: Bottom Support	Material: Aluminium AISI 6261	No of: 2
University of Cape Town Department of Mechanical Engineering Centre for Materials Engineering			
Title: 3/4 point bend			
Dimensions in millimetres (mm)	Scale: 2 to 3	Date: 10/09/03	Sheet: 10 of 20
Tolerance unless otherwise stated 0.01	Drawing By: John Jones		Drawing no: 7

Front View

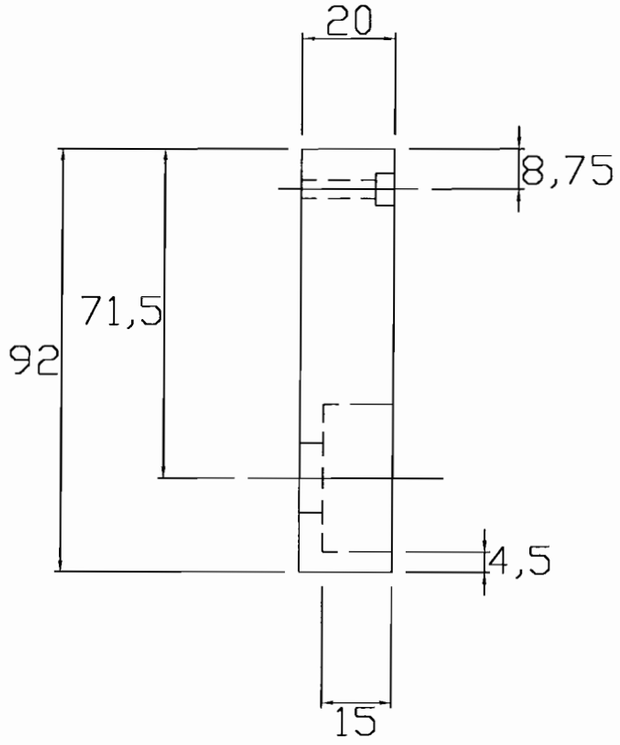

Side View

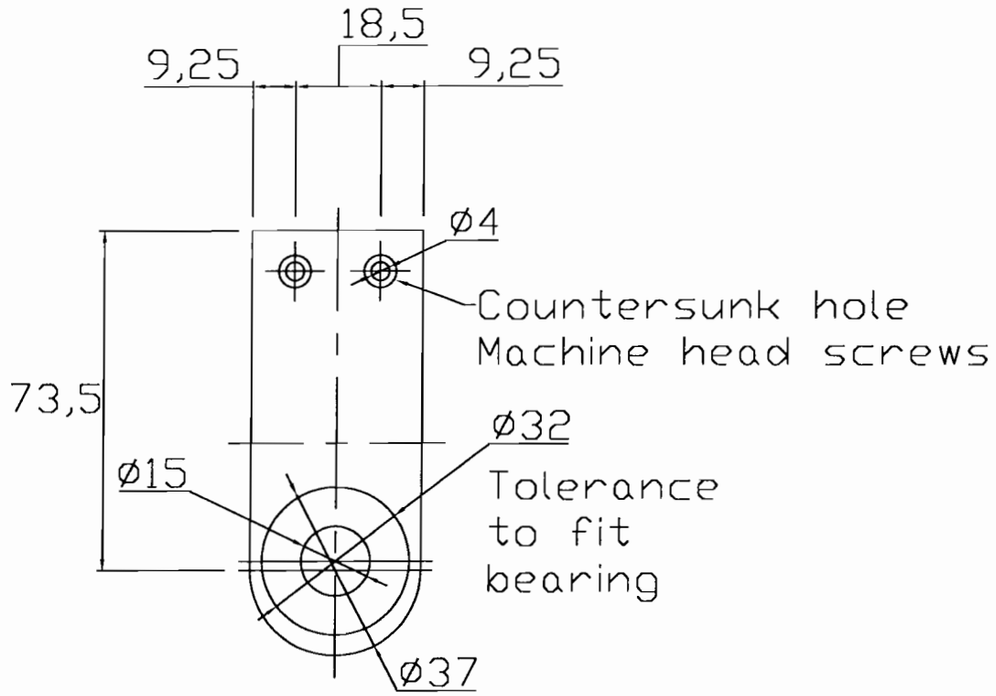

Part no: 5	Description: Roller Housing	Material: Aluminium AISI 6261	No of: 8
University of Cape Town Department of Mechanical Engineering Centre for Materials Engineering			
Title: 3/4 point bend			
Dimensions in millimetres (mm)	Scale: 2 to 3	Date: 10/09/03	Sheet: 11 of 20
Tolerance unless otherwise stated 0.01	Drawing By: John Jones		Drawing no: 8

Side View

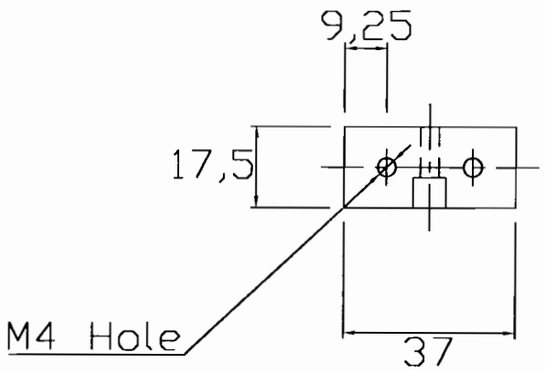

Front View

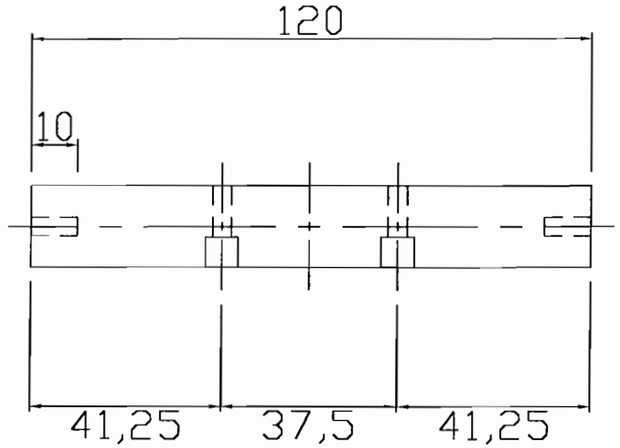

Bottom View

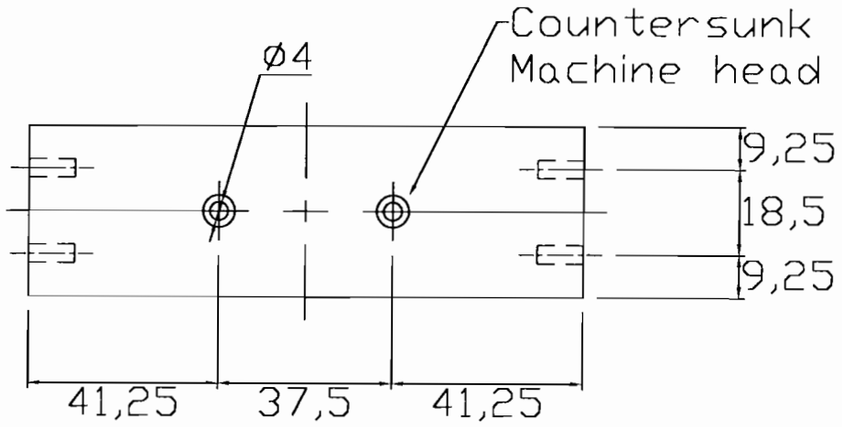

Part no: 6	Description: Top Support	Material: Aluminium AISI 6261	No of: 2
University of Cape Town Department of Mechanical Engineering Centre for Materials Engineering			
Title: 3/4 point bend			
Dimensions in millimetres (mm)	Scale: 2 to 3	Date: 10/09/03	Sheet: 12 of 20
Tolerance unless otherwise stated 0.01	Drawing By: John Jones		Drawing no: 9

Top View

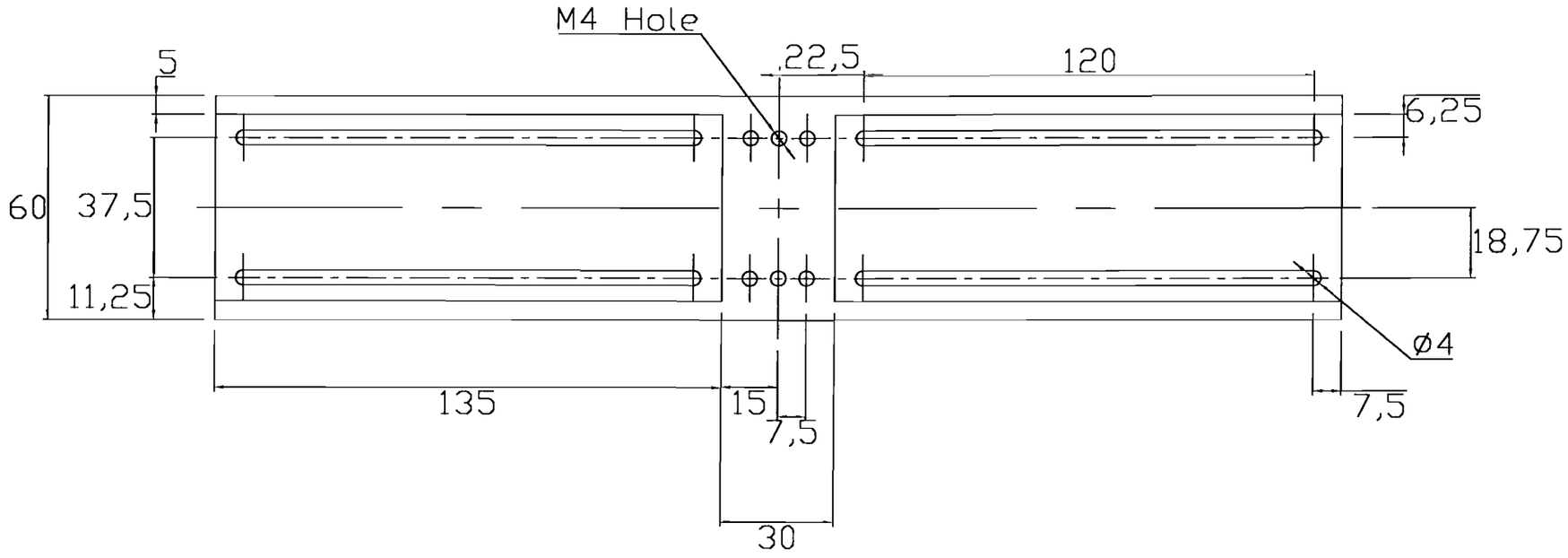

Part no: 7	Description: Top Plate	Material: Aluminium AISI 6261	No of: 1

University of Cape Town
Department of Mechanical Engineering
Centre for Materials Engineering

Title:
3/4 point bend

Dimensions in millimetres (mm)	Scale: 2 to 3	Date: 10/09/03	Sheet: 13 of 20
Tolerance unless otherwise stated 0.01	Drawing By: John Jones		Drawing no: 10a

Side View

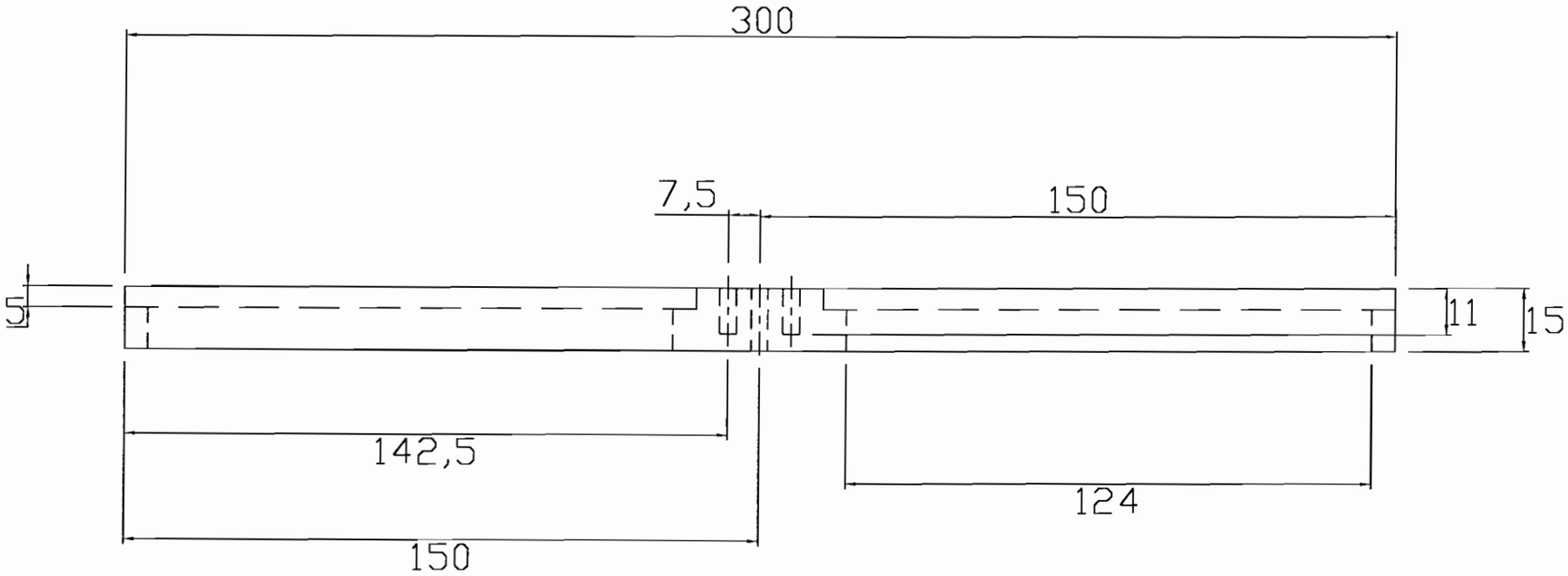

Part no: 7	Description: Top Plate	Material: Aluminium AISI 6261	No of: 1

University of Cape Town
Department of Mechanical Engineering
Centre for Materials Engineering

Title:
3/4 point bend

Dimensions in millimetres (mm)	Scale: 2 to 3	Date: 10/09/03	Sheet: 14 of 20
Tolerance unless otherwise stated 0.01	Drawing By: John Jones		Drawing no: 10b

Top View

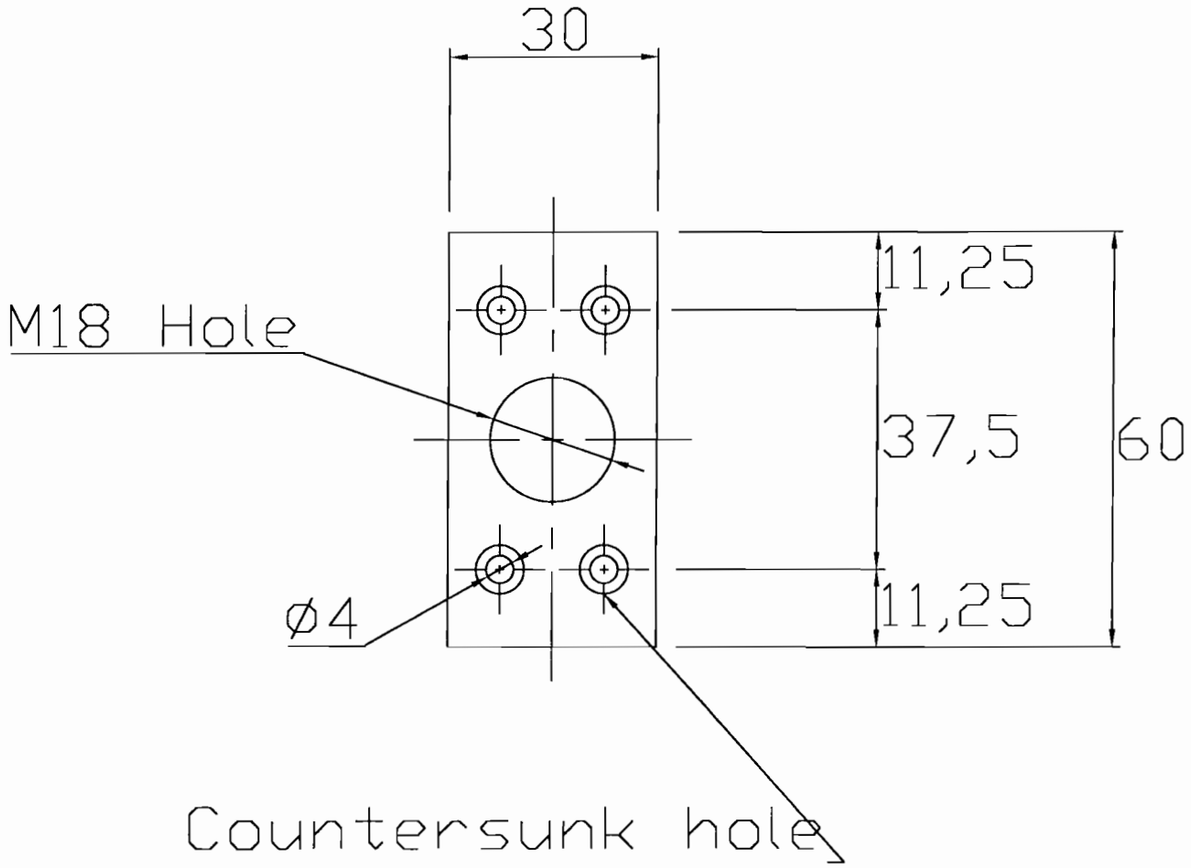

Countersunk hole
Machine head screws

Side View

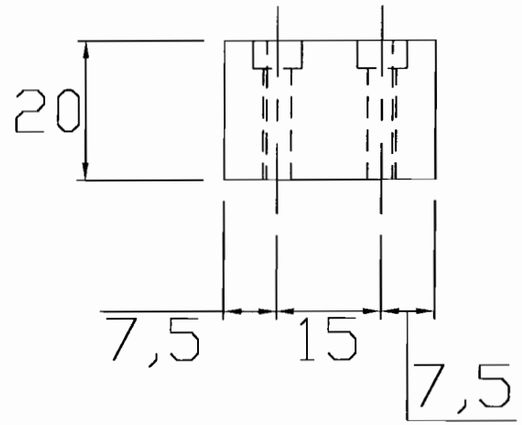

Part no: 8	Description: Top Connection	Material: Stainless Steel M300	No of: 1
University of Cape Town Department of Mechanical Engineering Centre for Materials Engineering			
Title: 3/4 point bend			
Dimensions in millimetres (mm)	Scale: 1 to 1	Date: 10/09/03	Sheet: 15 of 20
Tolerance unless otherwise stated 0.01	Drawing By: John Jones		Drawing no: 11

Front View

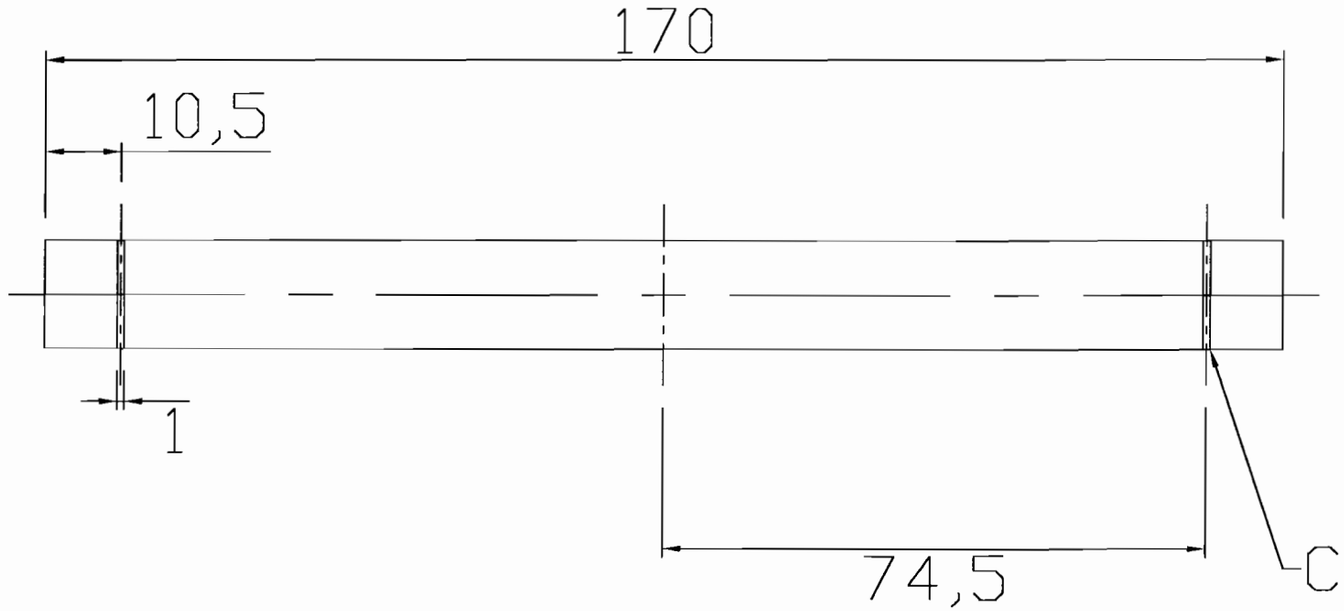

Side View

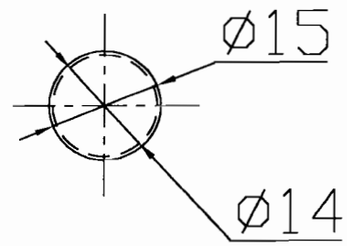

Part no: 9	Description: Roller	Material: Aluminium AISI 6261	No of: 4
University of Cape Town Department of Mechanical Engineering Centre for Materials Engineering			
Title: 3/4 point bend			
Dimensions in millimetres (mm)	Scale: 1 to 1	Date: 10/09/03	Sheet: 16 of 20
Tolerance unless otherwise stated 0.01	Drawing By: John Jones		Drawing no: 12

Top View

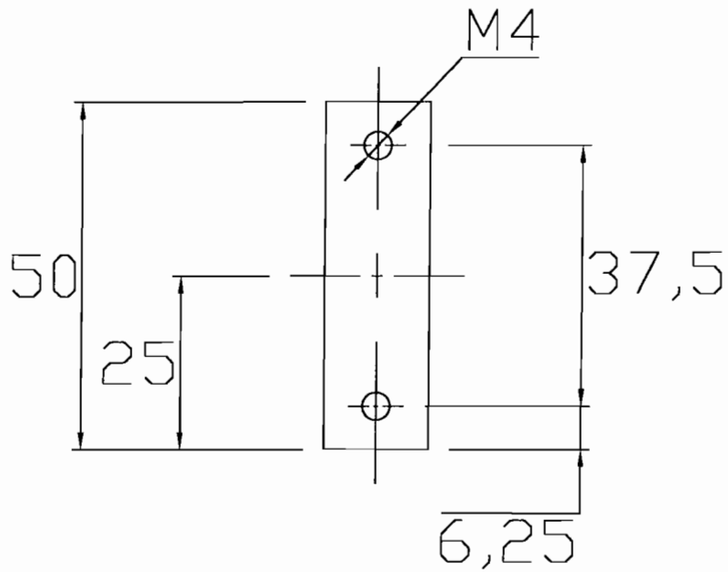

Side View

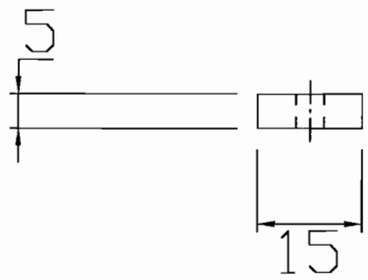

	Part no: 11	Description: Slide Bracket	Material: Aluminium AISI 6261	No of: 4
	University of Cape Town Department of Mechanical Engineering Centre for Materials Engineering			
	Title: 3/4 point bend			
Dimensions in millimetres (mm)	Scale: 1 to 1	Date: 10/09/03	Sheet: 17 of 20	
Tolerance unless otherwise stated 0.01	Drawing By: John Jones		Drawing no: 13	

Front View

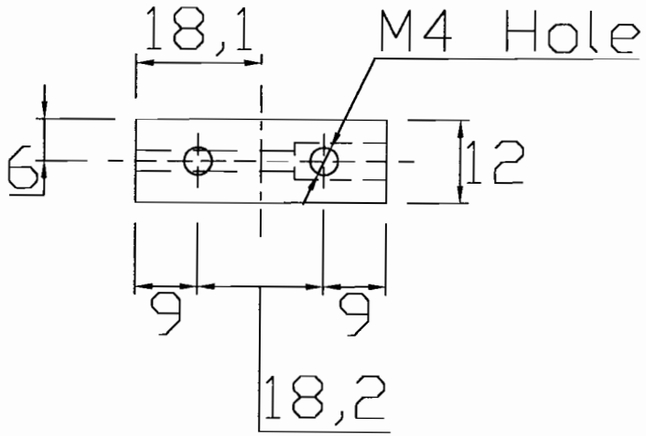

Top View

ø3
Machine Head Bolt
Countersunk

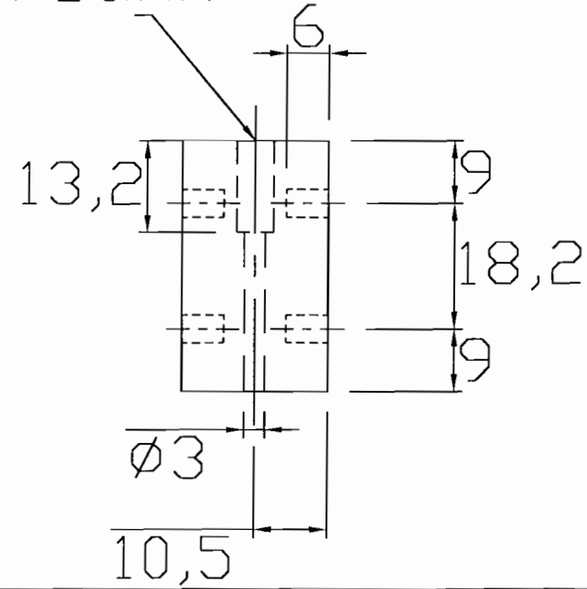

Part no: 12	Description: PDT Spacer	Material: Aluminium AISI 6261	No of: 1
University of Cape Town Department of Mechanical Engineering Centre for Materials Engineering			
Title: 3/4 point bend			
Dimensions in millimetres (mm)	Scale: 1 to 1	Date: 10/09/03	Sheet: 18 of 20
Tolerance unless otherwise stated 0.01	Drawing By: John Jones		Drawing no: 14

Top View

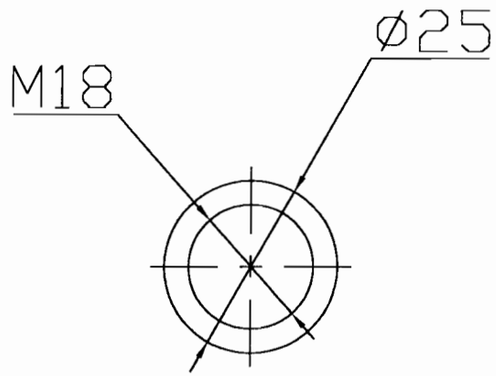

Side View

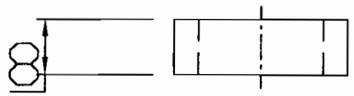

	Part no: 13	Description: Lock Washer	Material: Stainless Steel M300	No of: 2
	University of Cape Town Department of Mechanical Engineering Centre for Materials Engineering			
	Title: 3/4 point bend			
Dimensions in millimetres (mm)	Scale: 1 to 1	Date: 10/09/03	Sheet: 19 of 20	
Tolerance unless otherwise stated 0.01	Drawing By: John Jones		Drawing no: 15	

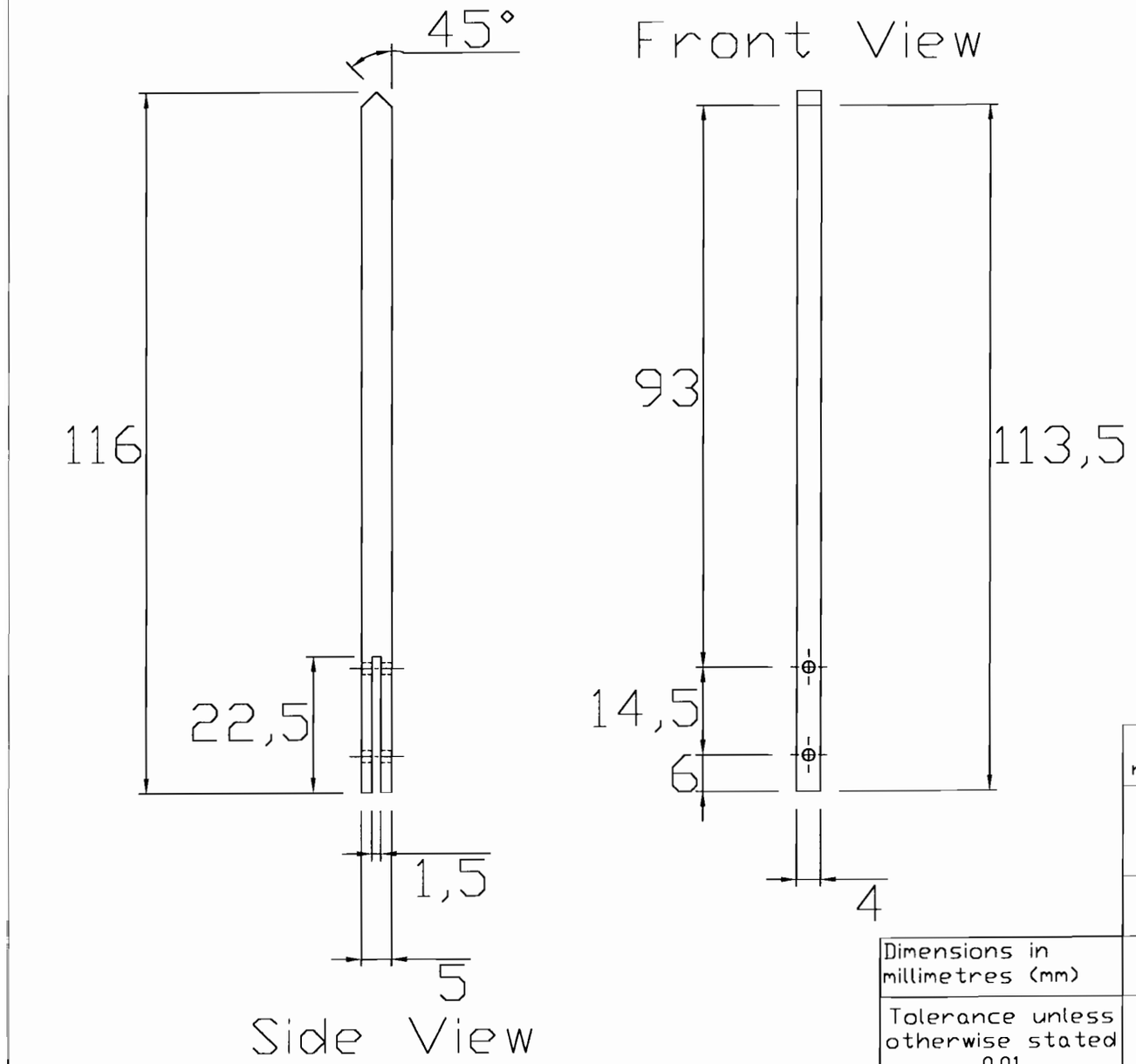

Part no: 14	Description: PDT Blade	Material: Nylon	No of: 1
University of Cape Town Department of Mechanical Engineering Centre for Materials Engineering			
Title: 3/4 point bend			
Dimensions in millimetres (mm)	Scale: 1 to 1	Date: 10/09/03	Sheet: 20 of 20
Tolerance unless otherwise stated 0.01	Drawing By: John Jones		Drawing no: 16